TRANSFER LENGTH IN PRESTRESSED SELF-CONSOLIDATING CONCRETE

Except where reference is made to the work of others, the work described in this thesis is my own or was done in collaboration with my advisory committee. This thesis does not include proprietary or classified information.

Jesse Shane Swords

Certificate of Approval:

Anton K. Schindler
Gottlieb Assistant Professor
Civil Engineering

Robert W. Barnes
Associate Professor, Chair
Civil Engineering

Mary L. Hughes
Assistant Professor
Civil Engineering

Stephen L. McFarland
Dean
Graduate School

TRANSFER LENGTH IN PRESTRESSED SELF-CONSOLIDATING CONCRETE

Jesse Shane Swords

A Thesis

Submitted to

the Graduate Faculty of

Auburn University

in Partial Fulfillment of the

Requirements for the

Degree of

Master of Science

Auburn, Alabama
December 16, 2005

TRANSFER LENGTH IN PRESTRESSED SELF-CONSOLIDATING CONCRETE

Jesse Shane Swords

____
Signature of Author

____
Date of Graduation

VITA

Jesse Shane Swords, son of Jesse Bedford Swords and Debbie (Sutherland) Swords, was born July 6, 1980, in Charlotte, North Carolina. He graduated from East Mecklenburg High School in Charlotte, North Carolina, in 1998. He graduated from Auburn University with a Bachelor of Civil Engineering degree in 2003. He entered the Graduate School at Auburn University in August, 2003 to seek the degree of Master of Science in Civil Engineering (Structures).

THESIS ABSTRACT

TRANSFER LENGTH IN PRESTRESSED SELF-CONSOLIDATING CONCRETE

Jesse Shane Swords

Master of Science, December 16, 2005
(B.C.E., Auburn University, 2003)

238 Typed Pages

Directed by Robert W. Barnes

Over the years much research into the transfer lengths of prestressed beams cast with conventional-slump concrete has been performed, but very little has been done in regard to beams cast with self-consolidating concrete (SCC). Currently, expressions for predicting transfer length of prestressed specimens in the ACI and AASHTO building codes are based on conventional-slump concrete. An experimental study was performed to determine the effects that SCC would have on transfer length. Currently, expressions for predicting transfer length of prestressed specimens in the ACI and AASHTO building codes are based on conventional-slump concrete. Thirty-six concentrically prestressed concrete specimens were cast and used to measure transfer lengths. One conventional-slump mixture and four different SCC mixtures were tested. The SCC mixtures were made up of a high- and low-strength mixture for each type of mineral admixture, Class C fly ash or ground-granulated blast furnace slag. The high-strength mixtures had

compressive strengths at prestress transfer ranging from 8,700 to 9,700 psi. The low-strength SCC mixtures and the conventional-slump concrete varied from 5,000 to 6,250 psi at prestress transfer. It was found that prestressed specimens cast with SCC had transfer lengths 14% longer on average than prestressed beams cast with conventional-slump concrete. The transfer lengths on the cut ends were significantly longer than those on the dead ends of the specimens. Transfer lengths were found to be indirectly proportional to the square-root of the concrete compressive strength. It was also observed that the transfer length growth stabilized within the first week after prestress transfer.

An analysis of all transfer lengths from the current study was done to evaluate the adequacy of the ACI 318, AASHTO Standard, and AASHTO LRFD equations and other proposed equations in predicting transfer length. It was determined that the ACI 318, AASHTO Standard, and AASHTO LRFD equations for transfer length do not adequately predict transfer length for prestressed specimens cast with SCC or conventional concrete. These expressions predict shorter transfer lengths then were actually measured.

ACKNOWLEDGEMENTS

The author would like to thank Dr. Robert Barnes for his assistance with the collection and analysis of the transfer length data. The author would also like to thank Dr. Anton Schindler for his assistance in the development of SCC mixtures. The financial support provided by the Alabama Department of Transportation is greatly appreciated. Assistance with the mixture process from Charles Bell of Twin City Concrete in Auburn, Alabama and the help provided with the experimental design and prestressing strand from Dwain Hamby of Sherman Prestress in Pelham, Alabama are greatly appreciated. The author would like to thank Degussa and Cresset Chemical Company for their generous donations to this study. Graduate Research Assistants James Roberts, Nadim Farhat, Kelly Levy, Jason Meadows, and the concrete lab technician Billy Wilson contributed a lot of time and effort to this investigation. Their hard work is greatly appreciated.

Style manual or journal used The Chicago Manual of Style, 14th Edition

Computer software used Microsoft Word 2000

TABLE OF CONTENTS

LIST OF TABLES

LIST OF FIGURES

CHAPTER 1

INTRODUCTION

1.1 BACKGROUND

Many structures are supported by pretensioned concrete elements. Bridges, parking decks, and flooring systems are some of the structures that contain these type of elements. For many years in the precast, pretensioned industry, vibration has been used to consolidate the fresh concrete in these prestressed elements. Though it has been used successfully for casting, several problems exist with this conventionally consolidated concrete. One of the major problems with the use of vibrated concrete is the high amount of labor needed for consolidation. Noise pollution emitted by the mechanical vibrators results in many health concerns (Skarendahl 2003). Even after the costly vibration, many voids are present on the surfaces of the prestressed elements when the forms are stripped; thus, laborers are needed to patch the unwanted voids, which can be very time consuming. In an industry where methods for increasing productivity without sacrificing performance are always being investigated, a concrete that does not need any external vibration and can easily fill heavily congested forms is a definite improvement in the state of practice.

Developed in Japan in the 1980s, self-consolidating concrete (SCC) is a highly flowable, non-segregating concrete that consolidates under its own weight. As a result, the use of vibration (internal or external) is not required. Although this technology is fairly new to North America, many bridges and buildings have been constructed with SCC in Japan and Europe since the 1990's. Precast industries in the United States have begun to use SCC in components of concrete structures. Because of its high flowability, resistance to segregation, and inherent workability, the interest in SCC has risen tremendously in the last few years. This is especially the case in elements that are highly congested with reinforcing steel and therefore difficult to vibrate effectively. Many prestressed elements must have numerous prestressing tendons spaced on a two-inch grid with a high content of stirrups, especially in the anchorage zone. It is vital that the concrete in this area be well consolidated, or bond loss in the anchorage zone could occur.

The use of SCC can decrease production costs by lowering the labor required (Skarendahl 2003). Since no vibration is needed, workers operating this machinery would not be required. Another benefit of SCC is its ability to produce smoother surfaces than that produced with conventional-slump concrete. With fewer surface voids, less labor would be needed to patch these surfaces, resulting in a further decrease in cost. Because SCC has the ability to encapsulate all reinforcement and fill forms without external aid, total production time decreases while performance may increase (Skarendahl 2000).

With so many beneficial qualities of SCC, there has been a recent push to increase its use in the precast, pretensioned industry. But, like any new technology, investigations are required to develop confidence in the performance of prestressed elements that are cast with this new material. One of the biggest unknowns is how well SCC bonds to the prestressing steel in the anchorage zone. This is a concern since SCC is created by reducing the amount of coarse aggregate and increasing the amount of fine material relative to more conventional-slump concrete mixtures. Does the increase in the fine to coarse aggregate ratio result in longer transfer lengths than in prestressed members cast with conventionally consolidated concrete? This and many other questions should be answered before SCC achieves widespread implementation in prestressed elements.

1.2 OBJECTIVES

The Alabama Department of Transportation (ALDOT) has sponsored an investigation into the use of SCC in prestressed concrete bridge girders. The primary objective of the portion of this study described in this thesis was to examine how transfer lengths in prestressed specimens cast with SCC mixtures compare to transfer lengths in specimens cast with a conventional-slump concrete mixture commonly used for casting prestressed concrete bridge girders.

All the specimens in this study were pretensioned with 0.5-in. “oversized” prestressing strand and were designed to emulate many of the concentrically prestressed specimens that were tested prior to development of the transfer length design expressions that have been used in American practice for the past forty years. Using the data generated in this study, a rational means for predicting transfer lengths was also investigated.

A secondary objective of this study was the evaluation of the ability to accurately predict transfer lengths by using strand draw-in measurements.

1.3 SCOPE

This research study consisted of an investigation of the transfer lengths of thirty-six concentrically prestressed concrete specimens. Initial and long-term transfer lengths measurements were performed on all specimens in the study. Corresponding draw-in measurements were performed at the same time intervals. The mixing, fabrication, and measurements were performed in the Structural Engineering Laboratory of the Auburn University Department of Civil Engineering.

One conventional mixture and four different SCC mixtures were tested. The SCC mixtures were made up of a high- and low-strength mixture for each type of mineral admixture, Class C fly ash or ground-granulated blast-furnace (GGBF) slag. The high-strength mixtures had compressive strengths at prestress transfer ranging from 8,700 to 9,700 psi. The low-strength SCC mixtures and the conventional-slump concrete mixture varied from 5,000 to 6,250 psi at prestress transfer. Six specimens were cast for each mixture. Included in each set of six, were three specimens prestressed with a single strand, and three specimens prestressed with two strands spaced at two inches on center. Due to an air content that exceeded the ALDOT-specified maximum on the first attempt, the high-strength, fly ash mixture was cast twice; test data from both of these specimen sets are included in this thesis.

1.4 ORGANIZATION OF THESIS

Chapter 2 provides information regarding the history and development of SCC. This chapter contains a brief summary of factors that contribute to the fresh and hardened properties of SCC, and the different testing procedures for determining these properties. Code provisions related to transfer length and past research studies that have influenced these provisions are also presented in Chapter 2. Chapter 3 discusses the details and procedures for constructing the experimental test specimens. Transfer length results are presented and discussed in Chapter 4. Comparisons among the different mixtures and a means of best predicting the transfer lengths from this data are discussed in this chapter. Chapter 4 also discusses the effects that concrete compressive strength, release method, and time have on transfer length. The results from draw-in measurements corresponding to the measured transfer lengths are presented in Chapter 5. A summary of the study and relevant conclusions are presented in Chapter 6.

1.5 NOTATION

Since there are several design codes used for precast, pretensioned concrete design in North American practice, the notation employed in the *AASHTO LRFD Bridge Design Specifications* (2004) is used for terms throughout this thesis. A list of these terms and the symbols adopted by other codes for the same meaning can be found in Appendix F of this thesis.

CHAPTER 2

REVIEW OF KNOWLEDGE REGARDING SCC AND PRESTRESS TRANSFER BOND

2.1 INTRODUCTION

In this literature review, a background of self-consolidating concrete (SCC), SCC testing procedures, and special properties of SCC will be discussed. This chapter also includes a review of literature pertaining to relevant research topics associated with transfer lengths of fully bonded strands in prestressed concrete. An introduction to transfer lengths, code provisions for transfer lengths of fully bonded strands, transfer bond theory, and bond of SCC to steel reinforcement will be discussed in this chapter.

2.2 SELF-CONSOLIDATING CONCRETE

In concrete structures, all designs are based on the assumption that there will be adequate bond between the concrete and reinforcement. To ensure that there will be a good bond between the two materials, quality construction practices are of the highest priority. With conventional-slump vibrated concrete, careful placement and thorough vibration is needed to encapsulate reinforcement bars and completely fill formwork. In the 1980's, researchers in Japan noticed an increase in deficient structures due to a lack of quality construction practices and poor concrete placement by unskilled laborers. To help resolve the durability issues of concrete structures attributed to poorly placed concrete, Professor Hajime Okamura at the University of Tokyo developed a concrete that could consolidate under its own weight and would not require vibration. With the elimination of vibration, the problems of unskilled labor and poor concrete placement were greatly reduced. This concrete became known as self-compacting concrete, or as it is referred to in North America, self-consolidating concrete (Okamura and Ouchi 1999).

With the aid of gravity alone, SCC has the ability to fill formwork and encapsulate reinforcing bars while maintaining homogeneity (Skarendahl 2000). There has been a large increase in the construction of high-performance structures. Increasing structural demands often lead to increased reinforcement volumes. It can be very difficult to consolidate traditional vibrated concrete in these areas of reinforcement congestion. Complexities with cast-in-place and precast structures containing very congested reinforcement cages, small spacing between reinforcement bars, and tight cover between the reinforcement and formwork can all be mitigated through the use of SCC.

According to RILEM Report 23 from Technical Committee 174 (Skarendahl 2000), there are three main characteristics that fresh SCC must have:

1. **Filling Ability**: The capability of the concrete to completely fill the formwork and encapsulate reinforcement without external assistance.
2. **Resistance to Segregation**: The ability to keep particles suspended, thus maintaining homogeneity during mixing, transportation, and casting.
3. **Passing Ability**: The ability of the concrete to flow through tightly spaced obstacles without blocking of aggregate particles.

A mixture can be referred to as SCC only if all of these characteristics are present.

From its conception in the middle of the 1980s, SCC has been increasing in research and use in large-scale projects each year. From the late 1980's to the mid 1990s, the awareness of SCC outside of Japan was very limited. This was due mainly to large Japanese construction companies wanting to keep their knowledge of SCC secret to maintain commercial advantage (Bartos 2000). An application of great significance for the development of SCC was the casting of the Akashi-Kaikyo suspension bridge. The anchorages of this Japanese suspension bridge were cast with SCC, and the construction time was decreased from 2.5 to 2 years (Petersson 2000).

Around the middle to late 1990s, research and development in Sweden began taking place for the use of SCC in engineered applications (Petersson 2000). By 1998, the first full bridge project was carried out, thus verifying the use of SCC in a bridge application. By the turn of the century, many different countries from all over the world began to take part in the development of SCC. This rapid growth in interest in concrete that consolidates under its own weight was fueled by numerous positive features that the technology possesses. Reduced manpower for casting, healthier working environments, shorter construction times, increased confidence in the quality of cast structures, and improved final product performance are some of the many positive features that led to SCC acquiring such attention (Skarendahl 2003). Another positive quality of SCC is its ability to produce smoother surfaces than that of vibrated concrete. With fewer surface voids, less labor is needed to patch these surfaces, resulting in a decrease in cost.

Not only has there been ongoing interest for use of SCC for cast-in-place construction; a push for SCC use in the precasting industry is now taking place (Skarendahl 2003). Compared with normal vibrated concrete, the use of SCC in precasting reduces high noise levels (mainly associated with vibratory equipment from the consolidation process), decreases the amount of labor needed for casting, and thereby reduces costs. Because of the decreases in production cost, noise levels, and the health problems associated with the operation of vibration equipment, it is likely that the use of SCC in this sector will increase tremendously in the years to come.

Conventional-slump portland cement concrete has been in use since the early 19th century; on the other hand, SCC has been in existence for less than twenty years. Because SCC is such a new technology compared to conventional-slump concrete, testing procedures have yet to be standardized. Since there are so many different worldwide agencies that are involved in the development of SCC, standardization is of great importance so the supplier and engineer can agree on performance quantification. Organizations such as ASTM and RILEM are currently addressing these issues.

2.3 PROPERTIES OF FRESH SCC

"Workability" is a term used to describe the deformation and flow properties of fresh concrete during casting and finishing operations. Not only does workability reflect the ability of a concrete to resist segregation, but the term also describes how well the fresh concrete will perform in different site conditions. SCC differs from conventional-slump concrete because of its filling ability, resistance to segregation, and passing ability. In order to determine how well these properties will act in diverse site conditions, several testing procedures have been developed to address the workability of SCC. While some procedures were developed to determine individual properties, it is important to remember that all three of the characteristics are some what interdependent. The ability of SCC to fill the forms is dependent on its resistance to segregation and its ability to pass through congested areas. This is why most of the testing procedures actually reflect more than one property. The slump flow test, L-Box, and J-Ring are the test methods that will be discussed in this section.

2.3.1 THE SLUMP FLOW TEST

The ability of SCC to flow large distances horizontally under its own self-weight is what sets it apart from conventional-slump concrete. Even though there is no standardized testing to date for SCC, the most widely recognized test method is the slump flow test. The slump flow is used to evaluate the horizontal free flow of SCC in the absence of obstructions (Ramsburg 2003). Since there are no obstructions present in the test, many argue that it is not representative of practical concrete construction (PCI 2003). However, it is generally stated that this test gives a good indication of the filling ability and can be used to assess the consistency of the mixture of SCC from batch to batch (PCI 2003). During the slump flow test, the viscosity and the segregation (stability) of the mixture can also be determined. The viscosity is quantified using the T-50 test. In this test, the time that it takes for the concrete to flow to a diameter of 20 inches (50 cm, hence T-50) during the slump flow test is measured. The degree of segregation is quantified by assigning a Visual Stability Index (VSI).

The slump flow test is based on ASTM C143, the test method for determining slump of conventional-slump concrete. To start the slump flow test, a slump cone is placed in the center of a moist non-absorptive base plate and filled completely to the top (without rodding). After striking off the top of the cone and removing any SCC from around the bottom, the cone is raised to allow the SCC to flow out freely. After the SCC has stopped flowing, the diameter of the slump patty is measured in two mutually perpendicular directions. The mean of the two measured diameters is recorded as the slump flow. This procedure is described in detail in the *Interim Guidelines for the Use of Self-Consolidating Concrete in Precast/Prestressed Concrete Institute Member Plants* (PCI 2003). The slump cone can be filled in the normal upright or inverted position with very little difference in the outcome of the test (Ramsburg 2003). For this research, the slump cone was inverted, and the slump test was performed on a Plexiglas base plate. The slump flow test setup can be seen in Figure 2-1.

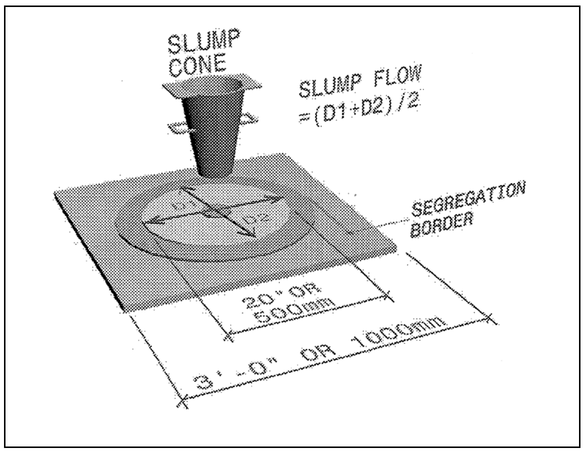

Figure 2-1: Inverted Slump Cone Method (PCI 2003)

The T-50 time and the VSI can be assessed during the slump flow test. In order to determine the T-50 time, a stopwatch is started when the slump cone is lifted vertically and stopped when the SCC reaches a 20-in. (50-cm) circle. The recorded time is the T-50 time, and it is considered as a secondary indication of flowability (PCI 2003). The VSI, which is determined by visual inspection, numerically describes the segregation of the mixture in 0.5 increments. By examining the slump flow patty, a rating of 0 to 3.0 is assigned to the mixture depending on certain criteria. PCI (2003) concludes that viewing fresh SCC in a wheelbarrow or mixer should be part of the process in determining the VSI rating. Table 2-1 has a listing of the ratings and associated criteria for the VSI rating.

Table 2-1: Visual Stability Index (VSI) Rating (PCI 2003)

Rating	Criteria
0	No evidence of segregation in slump flow patty or in mixer drum or wheelbarrow.
1	No mortar halo or aggregate pile in the slump flow patty but some slight bleed or air popping on the surface of the concrete in the mixer drum or wheelbarrow
2	A slight mortar halo (< 3/8 in.) and/or aggregate pile in the slump flow patty and highly noticeable bleeding in the mixer drum and wheelbarrow
3	Clear segregation evidenced by a large mortar halo (> 3/8 in.) and/or large aggregate pile in the center of the concrete patty and a thick layer of paste on the surface of the resting concrete in the mixer drum or wheelbarrow.

2.3.2 THE L-BOX TEST

One of the appealing features of SCC is its ability to flow through tight spaces; however, in some instances blocking may occur with certain mixtures. The term blocking refers to coarse aggregate particles in the SCC that, instead of flowing through an opening, collide and form a bridge that prevents the free flow of the remaining concrete. To see how well a mixture of SCC will flow through an obstructed path, the L-Box test can be performed. This test procedure uses an apparatus, shown in Figure 2-2, which has a vertical segment and a horizontal segment that together form the shape of an ‘L’. A movable gate that has several vertical reinforcing bars on the other side separates the two segments. The vertical segment is filled with SCC, and after waiting for one minute, the gate is lifted, and the concrete flows into the horizontal segment. When the flow has stopped, the height of the SCC at the end of the horizontal segment (H2) is expressed as a proportion of that remaining in the vertical segment (H1). This blocking ratio (H2/H1) is an indication of the passing ability of the concrete (PCI 2003).

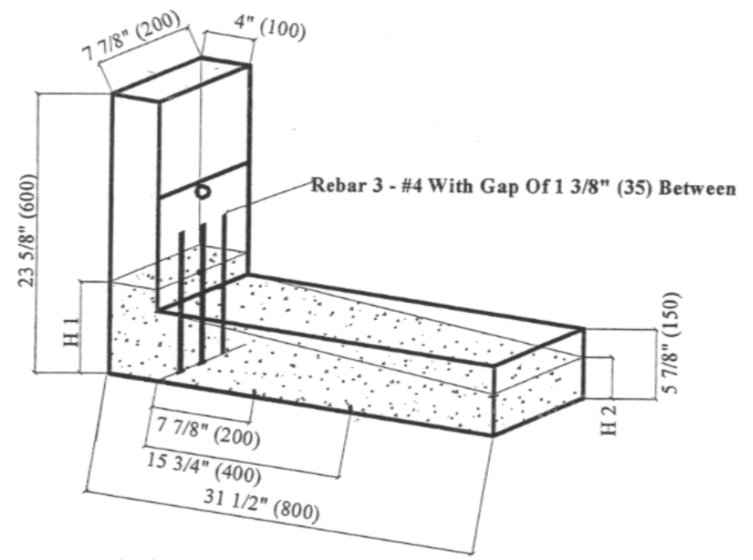

Note: mm units in parentheses

Figure 2-2: L-Box Test Apparatus (PCI 2003)

This has become another widely used test procedure for SCC. Both the slump flow test and the L-Box measure the deformation capacity of the concrete to an extent. The slump flow test evaluates the two-dimensional flowability with no obstructions present, and the L-Box evaluates the one-dimensional flowability through obstructions under directionally restrained conditions. It has been concluded that the L-Box is a representative test for modeling how the SCC will perform during casting (Petersson 2000).

2.3.3 J-RING TEST

Another test used for determining the passing ability of SCC is the J-Ring test. The equipment consists of an open steel circular ring that has holes drilled to accept vertical reinforcing bars. The vertical bars are attached to a baseplate. For this research, a

Plexiglas base plate was used. The ring has a diameter of 12 inches and a height of 4 inches. The spacing between the vertical bars can vary depending on the application for which the SCC will be used. As a general rule, the bars should be spaced at three times the maximum aggregate size for normal applications (PCI 2003). Typical J-Ring dimensions are shown in Figure 2-3.

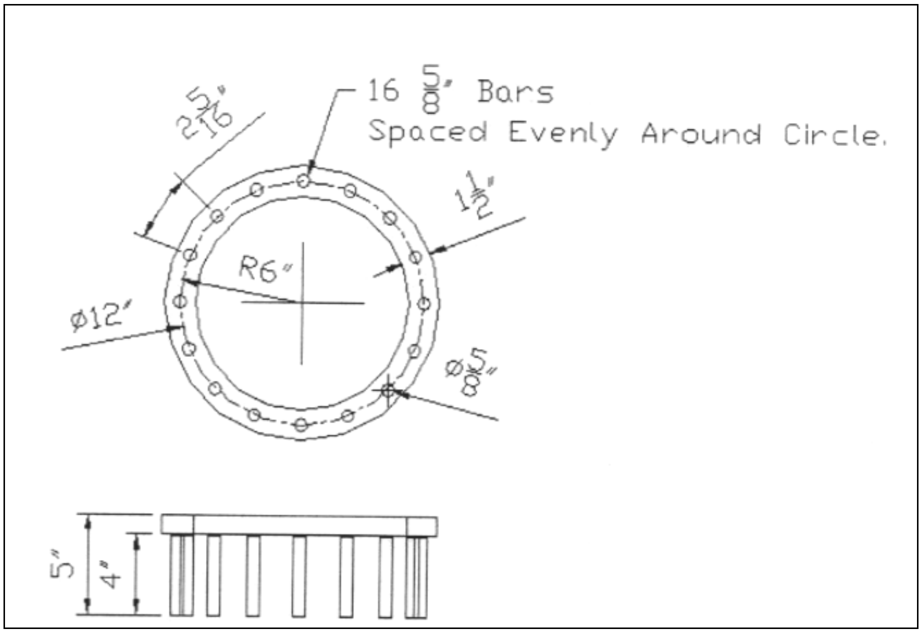

Figure 2-3: Diagram of the J-Ring Apparatus (ASTM Draft 2004)

To perform the J-Ring test, the base plate and slump cone are moistened and placed on a level surface. An inverted slump cone is placed in the center of the J-Ring and filled to the top with SCC. After the cone is raised and the SCC stops flowing, the diameter of the concrete is measured in two mutually perpendicular directions. The average of the two diameters is then compared to the corresponding value from the slump flow test. The greater the difference between the two values, the lower the passing ability of the SCC mixture. This difference between the slump flow value and the J-Ring value can be used to assign a rating for the passing ability; this procedure is summarized in Table 2-2. The slump cone can be upright or inverted, but must be positioned consistently for both tests.

Table 2-2: J-Ring Passing Ability Rating (ASTM Draft 2004)

Difference between Slump Flow and J-Ring Flow	**Passing Ability Rating**	**Remarks**
$0 \leq X \leq 1$ inch	0	No visible blocking
$1 < X \leq 2$ inches	1	Minimal to noticeable blocking
$X > 2$ inches	2	Noticeable to extreme blocking

2.4 PROPERTIES OF HARDENED SCC

When a concrete structure is being designed, the engineer must know the expected properties of the hardened concrete. The safety of the occupants of the structure depends on how well the concrete reaches its designed hardened property values. It has been shown that the hardened properties of SCC are comparable to, if not better than, conventional-slump concrete (Skarendahl 2000). Most of this has to do with the improved microstructure achieved by SCC. When conventional-slump concrete is vibrated, water has a tendency to localize around the surfaces of the coarse aggregate, thus forming weak interfacial zones throughout the concrete (Neville 1996). Since there is no need for external consolidation, SCC has stronger interfacial zones; as a result, the microstructure is denser and hardened properties are improved.

Because of the improved microstructure, it has been determined that the compressive strength for SCC is higher than that of vibrated concrete with the same water-to-cementitious materials ratio (Tragardh 1999). The stiffness or modulus of elasticity, of SCC has been presumed to be lower than that of conventional-slump concrete. This assumption comes from the fact that SCC has a lower aggregate volume fraction than that of conventional-slump concrete. Another factor that can influence the stiffness of SCC is its higher sand-to-aggregate ratio, which helps with stability and passing ability. Su et al. (2002) concluded that the elastic modulus of SCC is not significantly affected by these parameters. Gibbs and Zhu (1999) also concluded that the stiffness of SCC is at the same level as of normal concrete at comparable compressive strengths. Another hardened property of SCC is its tensile strength. The failure of concrete in tension is governed by microcracking, associated particularly with the interfacial regions between the mortar and the aggregate particles. Because compressive strength is the principal material property that is measured for hardened concrete, the relationship between tensile and compressive strength is typically used for comparisons (Mindess et al. 2003). This relationship of the tensile strength to the compressive strength has been recorded as equal for SCC and conventional-slump concrete (Gibbs and Zhu 1999).

There are many parameters that affect shrinkage and creep deformations. Creep refers to an increase in strain due to a sustained load. Drying shrinkage represents the strain caused by the loss of water from the hardened concrete (Mindess et al. 2003). The amount and size of aggregate in concrete is one of the main factors that affect drying shrinkage. The drying shrinkage of concrete will be less than that of pure paste because of the restraining influence of the aggregate (Mindess et al. 2003). Given that SCC contains lower volumes of aggregate and higher paste volumes than conventional-slump concrete, increased shrinkage has been predicted. Some groups have reported a larger drying shrinkage for SCC when compared to conventional-slump concrete, while some have observed it to be less (Skandrehl 2000). Persson (1999) reports that both the creep and shrinkage for SCC was comparable to creep and shrinkage for conventional-slump concrete of equal strengths. Shrinkage and creep are two very important properties that affect the behavior of prestressed concrete; therefore, they are relevant to this research.

2.5 TRANSFER LENGTH IN PRETENSIONED MEMEBERS

Bond between concrete and steel reinforcement may well be one of the most important, and sometimes overlooked, properties in the design of concrete structures. For any type of concrete member, sufficient anchorage from bond is necessary to ensure that the member will behave in service as designed. Flexure, shear and, torsion are all forces that can be applied to a member resulting in stresses that must be accounted for with a required amount of reinforcement. After determining the amount of reinforcement needed, checks have to be made to ensure that there will be satisfactory anchorage in the locations needed to resist these stresses. Failure to make these checks could result in the collapse of a structure injuring many occupants.

In precast, pretensioned members, bond along a straight line of the prestressing tendon is what causes anchorage for the tendon (Barnes et al. 1999). Because the pretensioned tendons transfer their force all the way up to the ultimate strength of the member to the concrete by bond, a certain bonded distance is needed beyond all critical sections to allow adequate bond to develop between the concrete and prestressing strands. This required bonded distance is called the development length. In pretensioned members, the development length is made up of two components: transfer length and flexural bond length. These two components that make up the development length when a member is loaded to its ultimate strength are shown in Figure 2-4.

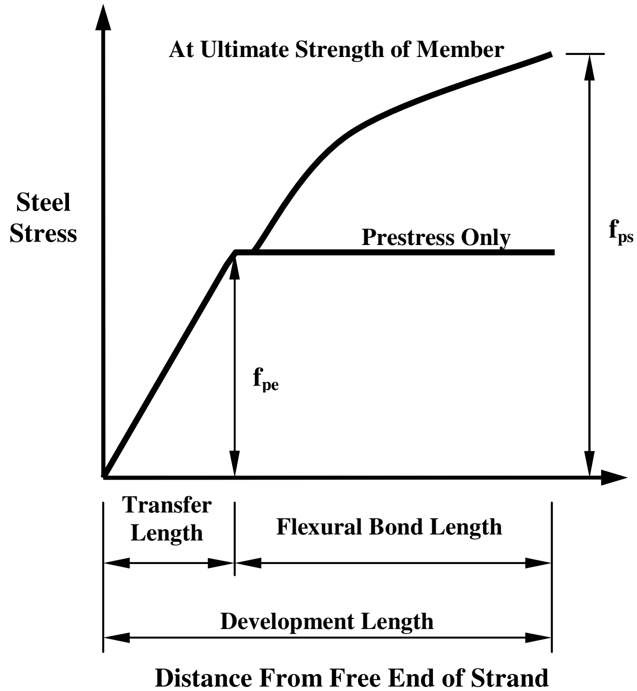

Figure 2-4: Development of Steel Stress in a Pretensioned Member

The transfer length, l_t, is the distance from the end of a member over which the effective prestress, f_{pe}, is fully developed in the prestressing tendon by bond. This stress, f_{pe}, is the effective stress in the prestressing strand after all losses (elastic shortening, concrete shrinkage, concrete creep, and steel relaxation) have occurred. The flexural bond length is the bonded length needed beyond the transfer length to develop the stress in the strand at the ultimate strength of the member, f_{ps}. This thesis will focus on the transfer length portion of the development length.

Transfer lengths are an important part of the design of a prestressed concrete element. Some of the most critical portions of a prestressed beam are the end regions, which make up the anchorage zones. Stresses in the anchorage zone can only be accurately predicted with an accurate estimation of the transfer length. Accurate estimates of the transfer length are also critical for determining the shear capacity of beam end regions, which are usually subjected to the largest shear demand. If the transfer length is not accurately estimated, the anchorage zone may have too little shear reinforcement to resist flexure-shear cracking and web-shear cracking (Simmons 1995). Knowledge of the amount of stress in the steel and concrete at a certain location in the anchorage zone is vital for designing a safe pretensioned beam.

2.6 DESIGN PROVISIONS FOR TRANSFER LENGTHS OF FULLY BONDED STRANDS

The equations that are presented in the current codes are used to determine the total strand development length to be used in design. Since first being introduced in the 1963 ACI Building Code, ACI 318-63, the development length equation was later adopted by the AASHTO Standard Specifications and the AASHTO LRFD Specifications (Tabatabai and Dixon 1995). These development length equations can be separated into two components: transfer length and the flexural bond length. The transfer length portion of these equations for fully bonded strands and the relevant research that led to the development of these equations will be discussed in this section.

2.6.1 ACI AND AASHTO CODES AND COMMENTARY

Currently, the relevant equations for the transfer length as a part of the development of prestressing strands are found in Section 12.9 of the ACI Building Code Provisions (ACI 318-05), Section 9.28 of the AASHTO *Standard Specifications for Highway Bridges* (AASHTO 2002), and Article 5.11.4 of the *AASHTO LRFD Bridge Design Specifications* (AASHTO 2004). Although the equations are fairly similar, these organizations use different notations. Because of a push by the Federal Highway Administration (FHWA) to use the AASHTO LRFD Specification, the notation used by this code is used throughout this thesis.

In Article 12.9.1 of ACI 318-05, the development length of seven-wire strand, in inches, in a pretensioned concrete member is given by Equation 12-2 as

$$l_d = \left(\frac{f_{pe}}{3000}\right)d_b + \left(f_{ps} - f_{pe}\right)d_b \qquad \textbf{\textit{Equation 2-1}}$$

where stresses f_{ps} and f_{pe} are reported in psi and the strand diameter, d_b, is reported in inches. Since Equation 2-1 can be broken up into two parts, the equation for the transfer length is

$$l_t = \frac{f_{pe}}{3000}d_b \qquad \textbf{\textit{Equation 2-2}}$$

In the commentary R12.9.1.1 of ACI 318-05, it goes on to state that the expressions for transfer length and flexural bond length are based on the research by Hanson and Kaar (1959); Kaar, LaFraugh, and Mass (1963), and Kaar and Magura (1965). Their research included tests of members prestressed with clean, ¼-in., 3/8-in., and 1/2-in. diameter strands having an f_{ps} of 250 ksi. Except for the value of 3 (ksi) instead of 3000 (psi) used in the denominator, the transfer length equation in Article 9.28.1 of the AASHTO Standard Specifications is the same as the ACI equation. Until recently, the denominators had the same value of 3 (ksi). The AASHTO Standard Specifications do not give any detail on how this equation was developed.

The equation for the transfer length in the AASHTO LRFD Specifications is different. According to Article 5.11.4.1, the prestress force in the strand increases linearly along the transfer length, which should be taken as $60d_b$, and the development length should be taken as specified in Article 5.11.4.2. There are two different equations for the development length in this article. The first expression, Equation 5.11.4.2-1, is stated as

$$l_d \geq \kappa\left(f_{ps} - \frac{2}{3}f_{pe}\right)d_b$$ ***Equation 2-3***

where κ is a multiplier equal to 1.6 for precast, prestressed beams, d_b is in inches, and f_{ps} and f_{pe} are expressed in ksi. Equation 2-3 is very similar to the development length equations given by ACI 318-05 and the AASHTO Standard Specifications, except for the κ multiplier. Article C5.11.4.2 of the commentary states the addition of this multiplier resulted from an October 1998 FHWA memorandum which accurately reflects the worst-case characteristics of strands shipped prior to 1997. The next expression, Equation 5.11.4.2-2, for determining an alternative development length in Article 5.11.4.2 is stated as

$$l_d \geq \frac{4f_{pbt}d_b}{f_c^{'}} + \frac{6.4\left(f_{ps} - f_{pe}\right)}{f_c^{'}}d_b + 10$$ ***Equation 2-4***

where f_{bpt} is the stress in the prestressing steel immediately prior to transfer. All stresses (f_{bpt}, f_{ps}, f_{pe}, and the concrete compressive strength, f'_c) are expressed in ksi, and d_b is expressed in inches. This expression was developed at the FHWA Turner-Fairbanks research facility. Susan Lane used the data from her research and many other previous studies to develop conservative expressions for both transfer length and flexural bond length that were combined to form Equation 5.11.4.2-2 (Lane 1998). The transfer length equation that she developed is incorporated within Equation 2-4, and is expressed as

$$l_t = 4\frac{f_{pbt}}{f_c^{'}}d_b - 5$$ ***Equation 2-5***

Since there were very few data points from members with concrete compressive strengths over 10,000 psi, the value of f'_c should not exceed 10 ksi in this equation (Lane 1998). A similar statement is provided in the commentary of Article 5.11.4.2.

Expressions for the transfer length are also contained in the shear provisions of the ACI Code and AASHTO Specifications. When determining the amount of reinforcement needed to adequately resist shear forces in the end region of a member, Section 11.4.4 of ACI 318-05 states that the transfer length is assumed to be 50 strand diameters for prestressing strand. The commentary for this section explains that since the stress of the strand varies linearly from zero stress at the end of a member to the maximum stress, this reduced prestress force in the transfer length must be accounted for (ACI 318-05). There is no reference to the origin of this assumed length; however, it is worth noting that 50 strand diameters equals the transfer length obtained from Equation 2-2 when the effective prestress, f_{pe}, is 150 ksi—a common value at the time these expressions first appeared in the relevant specifications.

The shear provisions of the AASHTO Standard Specifications are very similar to ACI 318-05 shear provisions. In the AASHTO LRFD Specifications, there is no other equation for the transfer length in the shear provisions. Article 5.8.2.3 just refers back to Article 5.11.4 for determining the transfer length (60 strand diameters).

2.6.2 BACKGROUND RESEARCH RELEVANT TO THE CODE PROVISIONS

The Commentary of Section 12.9.1.1 of ACI 318-05 and Commentary of Article 5.11.4.2 of the AASHTO Standard Specifications cite references for the basis of their expressions involving transfer lengths. The three different studies were reported by Hanson and Kaar (1959); Kaar, LaFraugh, and Mass (1963), and Kaar and Magura (1965). The work done by Hanson and Kaar (1959) does not report any significant transfer length data. The purpose of that research was to investigate the *flexural bond* in pretensioned beams with different diameter strands. Research done by Kaar and Magura (1965) investigated the flexural bond behavior of debonded strands; therefore, there is no data specifically relevant to the transfer lengths of fully bonded prestressing strands. The study by Kaar, LaFraugh, and Mass (1963) is the only work cited in Section 12.9.1.1 that investigated the transfer length in pretensioned members. As previously mentioned, an FHWA study resulted in a new expression for the transfer length and flexural bond length (Lane 1998). Both of these studies will be discussed in this section.

2.6.2.1 Kaar, LaFraugh, and Mass (1963)

The objective of this study was to investigate the effects that different levels of concrete strength have on transfer lengths. Another variable that was investigated was time after prestress transfer. The study consisted of rectangular, concentrically prestressed members with two, three, four, five, or six strand configurations. Strand sizes of 1/4 in., 3/8 in., 1/2 in., and 6/10 in. were used. All strands except for the 6/10-in. strand were clean and free of rust; the 6/10-in. strand had very little surface rust. The members were all made from the same mixture, with concrete strengths at prestress transfer ranging from 1,660 psi to 5,000 psi. The transfer of the prestressing strand did not occur until the specified strength levels were met. Just prior to the strands being flame cut, a Whittemore strain gage was used to take reference readings on each member. Strain readings were taken again immediately after transfer, and then at ages up to one year after transfer.

The results of this study showed that the increase in concrete strength had little influence on the transfer length of the prestressing strand sizes up to ½ in. The 0.6 in. strand did show a slight reduction of transfer length in the cut, or live, end of the strand; this may have had to do with the surface rust on the strand. On average, the transfer lengths were found to be 30% greater on the live ends than the dead ends (end of the beam opposite the cut end) for the 6/10 in. strand. For the strand sizes up to ½ in., there was a 20% increase in the transfer length comparing the live ends to the dead ends. For the members prestressed with 6/10 in. strand with concrete strengths of 3,000 psi and less, end slip occurred. Sudden transfer of prestress, resulting from flame cutting, can cause the strand to "slip" some distance in a member before any concrete bonds with the strand. This is known as "free end slip" and can be detected by readings of zero strain along a portion of the specimen. As for the change in transfer length with time, a small average increase of 6% was detected for all sizes of strand. The maximum increase in transfer length over one year was 19%. It was concluded that the percentage increase in transfer length was independent of the concrete strength at time of transfer, f'_{ci}.

2.6.2.2 Lane (1998)

This researcher investigated the development length of sixteen AASHTO Type II prestressed concrete members using uncoated, fully bonded strands. Three different strands patterns were studied using Grade 270, low-relaxation strand. The strand had some surface rust, but no pitting. Two concrete mixtures, one low-strength and one high-strength, were used for the girders. The low-strength mixture had a concrete strength at release, f'_{ci}, of 4,600 psi and a 28-day moist-cured concrete strength, f'_c, of 7,200 psi. The high-strength mix had an f'_{ci} of 7,900 psi and an f'_c of 10,800 psi. Surface-mounted Whittemore gage points were used to measure the strain just after prestress transfer, and at 7, 14, and 28 days after prestress transfer. Strand draw-in was also measured at each of these reading times. Prestress transfer was accomplished by flame cutting the strand.

The transfer lengths from these beams increased an average of 30% from the time of transfer to 28 days after transfer. It was noticed that most of the growth occurred in this time period, but the transfer lengths did grow an additional 7% by the time the beams were tested for development length at an age of approximately 6 months. The only values of transfer length published in this report were the 28-day measurements. These transfer length values were greater than predicted by the AASHTO Standard Specifications equation in Article 9.28.1 (functionally equivalent to Equation 2-1 above). As a result, Lane and a group of researchers developed a more conservative expression for transfer (and development) length.

To develop this new equation, the data for transfer lengths from 19 different studies were collected. All of these studies used fully bonded, uncoated, Grade 250 or Grade 270 low-relaxation strand. These studies incorporated strand sizes of 3/8 in., 0.5 in., 0.5 in. "special", and 0.6 in. used in full-scale beams or rectangular cross-section specimens. All of the transfer lengths reported from these studies were determined using the 95% Average Maximum Strain Method (discussed later in Section 4.3.3). Equation 2-5 was the transfer length expression that resulted from this study. Since there were very few data points representing members with concrete strengths over 10,000 psi, the f'_c for this equation is limited to values no larger than 10 ksi.

2.6.3 Evolution of the Transfer Length Equation

The transfer length expression that appears in Section 12.9 of the ACI 318-05 and Section 9.28 of the AASHTO Standard Specifications (Equation 2-1) resulted from the research done by Kaar et al. (1963). Tabatabai and Dixon (1993) reported the history by which the transfer length expression that first appeared in the 1963 ACI Building Code and was later adopted in the 1973 AASHTO Standard Specifications evolved from this research.

By using unpublished results from the bond study reported by Hanson and Kaar (1959) and transfer length tests performed for the American Association of Railroads, Dr. Alan H. Mattock derived the equation for transfer length that made its way into the 1963 ACI Code. Using the reported average bond stress of 400 psi in the Hanson and Kaar (1959) studies and the data from Kaar, LaFraugh, and Mass (1963), and by employing equilibrium equations, Dr. Mattock offered this derivation to determine the transfer length:

$$U_t \Sigma o l_t = A_{ps} f_{pe}$$ ***Equation 2-6***

where:

U_t	=	Average bond stress = 0.4 ksi
Σo	=	Circumference of prestressing strand = $4/3\pi d_b$ (in.)
l_t	=	Transfer length (in.)
A_{ps}	=	Area of prestressing strand = $0.725\ \pi d_b^2/4$ (in^2)

d_b = Nominal strand diameter (in.)

f_{pe} = Effective prestress (ksi)

By substituting the above values into Equation 2-6 and simplifying, the result is:

$$l_t/d_b = (1/2.94)\, f_{pe} \qquad \textbf{\textit{Equation 2-7}}$$

Therefore, the transfer length was estimated as:

$$l_t \approx (1/3)\, f_{pe}\, d_b \qquad \textbf{\textit{Equation 2-8}}$$

For a stress value in the strand of 150 ksi (as used by Hanson and Kaar [1959]), Equation 2-8 simplifies to $l_t = 50d_b$. This simplified formula for transfer length is still suggested in the shear provisions of ACI 318-05 and the AASHTO Standard Specifications. What these provisions fail to mention is that currently-employed stress levels of prestressing strand under service conditions are usually five to fifteen percent higher than 150 ksi. Another shortfall of Equation 2-8 is that its derivation was based on certain factors used for the circumference and area of the prestressing strand as compared to diameter of the strand. Today these factors may be different, but not by a large margin. It is critical to understand that Equation 2.8 was developed from the *average* transfer lengths by Kaar et al. (1963), not from a conservative upper-bound estimate. Barnes et al. (1999) stated that not only was the expression developed from average transfer length values, but the stress in the strand immediately after transfer (f_{pt}) was used to produce the 400-psi average bond stress that Mattock used in his derivation. However, the effective prestress value after all losses (f_{pe}) is used in the derived expression. Because the value of f_{pe} decreases over time, the transfer length calculated with this expression also decreases with time. But the research by Kaar et al. (1963) show that transfer lengths usually *increase* slightly over time. Further investigation by

Barnes et al. (1999) showed that Equation 2-8 actually underestimates the real long-term transfer lengths of the test specimens from which it was derived. Assuming a long-term reduction of twenty percent taken from f_{pt} values to calculate corresponding f_{pe} values, transfer lengths predicted from the expression $l_t \approx 1/3\, f_{pe}\, d_b$ underestimate 90% of the measured transfer lengths from the results of Kaar et al. (1963). Barnes et al. (1999) also found that transfer lengths predicted by $l_t = 50d_b$ underestimate 80% of the measured transfer lengths from Kaar et al. (1963). This is a very important finding since current code expressions are based on the results from this research. However, these facts are not recognized in the ACI 318-05 or the AASHTO Standard Specifications.

2.7 TRANSFER BOND THEORY

As previously stated, the transfer length is the distance from the end of a member over which the effective prestress, f_{pe}, is fully developed in the prestressing tendon by bond. This is also the distance it takes to build up the full effective precompression in the concrete. When detensioning of the pretensioned tendons occurs, the tendons shorten and slip relative to the surrounding concrete along a finite length (Barnes et al. 1999). The stresses build up linearly from the free end, where there is zero stress, to a distance where the stress in the strand reaches a relatively constant value, f_{pe}, over the entire length between transfer lengths. There are several mechanisms and factors that contribute to the prestress transfer bond; they will be discussed in this section.

2.7.1 Mechanisms

Bond of pretensioned strand can be thought of as being attributable to three components: adhesion, friction, and mechanical interlock (Hanson and Kaar 1959). Upon detensioning of the prestressing strand, the sudden force causes slip of the steel relative to the concrete. Because this slip of the strand causes concrete to break away, adhesion plays little role in prestress transfer bond.

The principle factor causing stress transfer by bond is considered to be friction (Hanson and Kaar 1959). When a tendon is stressed, its diameter decreases; this reduction in diameter occurs due to the Poisson Effect. The member is then cast and the concrete sets around this stressed tendon. Upon transfer, the strand contracts longitudinally and tries to regain its original diameter, but the concrete resists the expansion of the strand. As a result, high radial pressures against the concrete develop, thus promoting frictional resistance between the two materials. At the free ends of the member, the prestressing steel attempts to expand to its original (unstressed) diameter. This behavior is known as the "Hoyer Effect" after the German engineer that first identified it in pretensioned construction.

Mechanical interlock contributes to transfer bond, and is dependent on the shape of the strand. Prestressing strand used in today's construction is made up of seven individual wires wound into a helical shape. Mortar from the concrete can fill the grooves around the periphery of the helix, thus providing an interlocking of concrete and strand. Since the wires that form the strand are wound in a spiral fashion, the strand will try to unwind as it slips into the member upon transfer. If this unwinding is not resisted, mechanical interlock cannot play a significant role in the transfer bond. However, researchers have theorized that the friction due to the Hoyer Effect helps to prevent this unwinding, generating a complex interaction between the two mechanisms (Russell and Burns 1996; Barnes et al. 1999).

2.7.2 Concrete Strength

There have been several research studies conducted to determine the influence of concrete strength on transfer lengths. It would be expected that with an increase in concrete strength, there would be a decrease in transfer length due to higher levels of friction and mechanical interlock resisted by the concrete.

Jack Janney (1954) studied bond in the transfer region of smooth, individual wires using different levels of concrete strength. He states that the transfer length is made up of an elastic zone and an inelastic zone. Due to high stresses resulting from the expansion of the steel, the concrete responds inelastically throughout most of the transfer length. In this zone, high radial pressure and the resulting hoop tension stresses from the expansion of the strand cause micro-cracking in the surrounding concrete, resulting in a softened response (Barnes et al. 1999). Concrete tensile strength and stiffness (the latter usually quantified by the modulus of elasticity) were found to be important factors affecting the bond strength in this section of the transfer length.

In a small portion of the transfer length, just before the axial strain in the concrete equals the axial strain in the strand, concrete is considered to behave elastically because the radial pressures between the strand and the concrete are not as high (Janney 1954). Thus, the length of this zone, and the bond strength within it, are functions of the stiffness and tensile strength of the concrete (Barnes et al. 1999).

The modulus of elasticity and tensile strength of the concrete are both assumed to be proportional to the square root of the concrete compressive strength according to ACI 318-05 Sections 8.5.1 and 9.5.2.3. Since bond stress has been hypothesized to be affected by both the elastic modulus and tensile strength of the concrete, it is reasonable to assume that transfer lengths are inversely proportional to $\sqrt{f_c^{'}}$ or $\sqrt{f_{ci}^{'}}$.

Several different studies have found that transfer length is related to concrete compressive strength. Research by Zia and Mostafa (1978) and Lane (1998) both found transfer length results to be inversely proportional to the concrete compressive strength. As previously mentioned, the relationship proposed by Lane (1998) is an alternative specified in the AASHTO LRFD Specifications.

Using the idea that the transfer length should be inversely proportional to $\sqrt{f_c^{'}}$, research by Mitchell et al. (1993) and Barnes et al. (1999) found that this type of relationship more accurately resembled measured transfer lengths within a single study than relationships with $f_c^{'}$ (without the square root), especially for high-strength concretes. Barnes et al. (1999) found that as concrete strengths increased significantly, transfer lengths calculated from relationships where l_t is inversely proportional to $f_c^{'}$, such as those proposed by Lane (1998) and Zia and Mostafa (1978), became inadequate. Transfer lengths predicted by these relationships were found to be shorter than those measured in high-strength specimens. By taking the $\sqrt{f_c^{'}}$ (or $\sqrt{f_{ci}^{'}}$), the predicted transfer lengths stayed more in line with those measured.

2.7.3 Effects Over Time

The stress in a prestressed tendon decreases over time. This decrease in stress is due to concrete creep, drying shrinkage, and relaxation of the tendon. At first thought, one might think that because of these losses and an increase in concrete strength over time, the transfer lengths would shorten. In reality, the transfer lengths of pretensioned elements have been shown to actually increase with time. As discussed in the previous section, the behavior of concrete in a majority of the transfer length is inelastic due to the softening of concrete around the tendons. The softening and tensile cracks surrounding the tendons contribute to the increase in transfer lengths over time. Once the concrete has been stressed above elastic levels, the concrete is permanently damaged and does not elastically respond to the stress changes in the strand over time.

Many different studies have proven the trend of transfer lengths increasing over time. As previously stated, Kaar, LaFraugh, and Mass (1963) reported an average increase of 6 percent in transfer lengths over one year. Lane (1998) reported an average increase of 30 percent in transfer lengths over 28 days, and an additional increase of 7 percent in approximately one-half a year. Barnes, Burns, and Kreger (1999) reported average increases of 10 to 20 percent over the first few weeks after casting, but no significant pattern of growth after that time period.

2.7.4 Other Influences on Transfer Length

The bonding of the concrete to the prestressing strand in the transfer zone is affected by many other factors. The strand characteristics, method of prestress transfer, pretensioned member size, and quality of concrete placement affect the bonding action in the transfer zone. Seven-wire, helical strand produces more bond by mechanical resistance than individual smooth wires (Hanson and Kaar 1959). Since there is more surface area and the shape of the seven-wire strand allows concrete to set around the spaces between the wires, bond due to mechanical interlock can play a larger role compared to that for individual wires. The surface condition of the strand has also been found to affect the bond between the two materials. Some research has shown that strands with surface rust produced shorter transfer lengths than those with clean strand (Hanson and Kaar 1959; Rose and Russell 1997). While this finding is mentioned in Section R12.9 of ACI 318R-05, the dependability of this prediction is not reliable. Barnes et al. (1999) showed that transfer lengths were shorter for rusted strands than clean strands in low-strength members; however, this was not always the case in members of higher compressive strengths. Several of the rusted strand transfer lengths were actually longer than those of clean strands in comparable specimens with high compressive strengths.

The method of prestress transfer can affect the length of the transfer zone. Two types of release have been investigated in the past: gradual release and sudden release. Transferring the prestress to the concrete by slowly detensioning the strand is referred to as gradual release. The sudden release method is often used in practice because it is easier to achieve than gradual release. Sudden release is achieved by flame-cutting the strand, imparting energy to the concrete much faster than gradual release. This sudden, violent energy release affects the bond and often results in end slip and increased micro-cracking around the tendon. Transfer lengths have been shown to increase as a result of the loss of bond at the live ends when the strands have been flame-cut (Kaar, LaFraugh, and Mass 1963). While differences in transfer lengths might not be very prevalent when comparing live to dead ends in larger members, members with smaller cross sections have been shown to behave differently.

Russell and Burns (1996) noted the effect size of a pretensioned member has on transfer length. They indicated that live end transfer lengths in members with smaller cross sections were much longer than those for full-scale members of the same concrete compressive strength. In their study, the larger members were flame-cut at full tension. For the smaller specimens, two different methods were used. One release method was achieved by gradually detensioning the strands to 70 percent of their full pretension, and then cutting. The other method was by cutting the strands at 100 percent of their full pretension. The smaller members that were cut at 100 percent produced much longer transfer lengths than the full-scale members. However, the transfer lengths from smaller members that experience partial gradual release resembled those measured for the larger members that experienced sudden release. Russell and Burns (1996) concluded that the longer transfer lengths from the smaller members that were cut at 100 percent tension resulted from damage caused by the sudden force. Because of larger mass, large cross sections possess a greater ability to absorb and distribute the energy at release than small cross sections have. They also pointed out that larger cross sections contain a greater numbers of strands that are flame-cut one at a time (Russell and Burns 1996). This is important since the original transfer length equations were based largely on smaller pretensioned members.

Another consideration that affects the bond in the transfer zone is the quality of concrete placement during the production of pretensioned elements. With the use of conventional-slump concrete, careful attention to the vibration of the concrete must be used to ensure that proper consolidation around the tendons is achieved. Concrete that is not fully consolidated around the strand can result in a reduction of mechanical interlock and friction and therefore a loss of bond capacity (Khayat, Petrov, Attiogbe, and See 2003). Since many prestressed girders that are produced today contain many strands and tightly spaced shear reinforcement, especially in the anchorage zone, it is often a difficult task to properly consolidate the concrete around such tight spacings; this is one of the reasons why the use of SCC can be of great importance to the prestressing industry.

2.8 BOND OF SCC TO REINFORCEMENT

The development of SCC in the precast industry is very important since it can reduce manufacturing time, decrease costs, and increase the quality of the final products. Because of the competitive nature of this industry, the use of SCC has steadily increased resulting in more investigations on how this concrete compares to conventional-slump, vibrated concrete. One of the issues to be investigated is the bond characteristics between SCC and steel reinforcement. The bonding action between regular deformed reinforcing bars and SCC as well as prestressing strands and SCC has been studied.

The bonding strength of regular deformed reinforcing bars used in full-scale reinforced concrete members was investigated by Chan, Chen, and Liu (2003). By comparing the bonding strengths between the reinforcement of beams cast with conventional-slump concrete and those cast with SCC, they found that beams cast with SCC produced higher bond strengths. They concluded that the lower bond observed in conventional-slump concrete was due to segregation in the form of bleeding (Chan et al. 2003). The use of SCC greatly reduces the amount of segregation because of its homogeneity, allowing greater bond strengths.

Research has been done to investigate the bond strengths of prestressing steel and SCC as well. In a study by Khayat, Petrov, Attiogbe, and See (2003), the uniformity of bond strength between concrete and horizontally positioned prestressing tendons along experimental wall elements was investigated. Mixtures of SCC were compared to mixtures of flowable, conventional-slump concrete. They found that the top-bar effect for the SCC elements and the conventional-slump concrete elements were very similar; the strand bond was not compromised in stable SCC (Khayat, Petrov, Attiogbe, and See 2003). The top-bar effect ratio, which is the ratio of bond strength of the bottom strand to that of the top strand, characterizes the homogeneity of a mixture. The closer the value of this ratio is to 1, the more uniform the bond strength is along the wall height (Khayat, Petrov, Attiogbe, and See 2003). The values ranged from 1.02 to 1.61 at 28 days for all the mixes. This is an important factor for larger beams that have prestressed strands running along the bottom and the top.

According to tests performed by Jaramillo et al. (2003), the bond strengths between prestressing steel and SCC were not significantly different from those between prestressing steel and equivalent traditional concrete. As a result, the transfer lengths were very similar for the two different concretes.

The transfer lengths of full-scale AASHTO Type II bridge girders cast with SCC were investigated by Labonte (2004). Strains were measured using surface-mounted strain gages along the estimated transfer length. The 95-percent Average Maximum Strain method was used to determine the transfer lengths. There was no difference evident in the transfer lengths when comparing the girders cast with SCC to the girders cast with conventional-slump concrete. Since surface strains were not measured along the entire transfer length, precise comparison among the girders is difficult. As with most test data for transfer length, the transfer lengths on the flame-cut ends were longer than those measured on the dead ends. The measured values for draw-in were similar between the two different girders. It is important to note that only two girders were used in comparing transfer lengths, one cast with SCC and one cast with conventional-slump concrete.

Naito et al. (2005) compared the performance of High Early Strength Concrete (HESC) to SCC in 45-in.-deep PCI Standard bulb-tee girders. One of the comparisons made was the difference in transfer lengths between a girder cast with HESC and one cast with SCC. Both mixes used ASTM C989 Grade 120 GGBF Slag as a mineral admixture. The strand used was 0.5 in. "special", Grade 270, low-relaxation prestressing strand. Concrete strains were measured from strain gauges mounted on strands at 5, 25, 76, and 152 in. from the end of the beam. Assuming linear strain distribution along the transfer zone, this study found the HESC and SCC to have comparable transfer properties. An approximate transfer length for both mixes was 25 in. This value was conservative according to the AASHTO transfer length estimate. Precise comparison of these transfer lengths is difficult since strains along the transfer zone were measured by only two strain gauges within the apparent transfer length.

CHAPTER 3

DESIGN AND FABRICATION OF EXPERIMENTAL SPECIMENS

3.1 INTRODUCTION

In this study, a total of thirty-six concentrically prestressed specimens were tested for transfer length and the associated strand draw-in. The design, details, fabrication, and instrumentation for the test specimens are discussed in this chapter.

3.2 SPECIMEN IDENTIFICATION

A detailed identification system was employed to uniquely describe each end of the thirty-six specimens tested. This identification system is summarized in Figure 3-1.

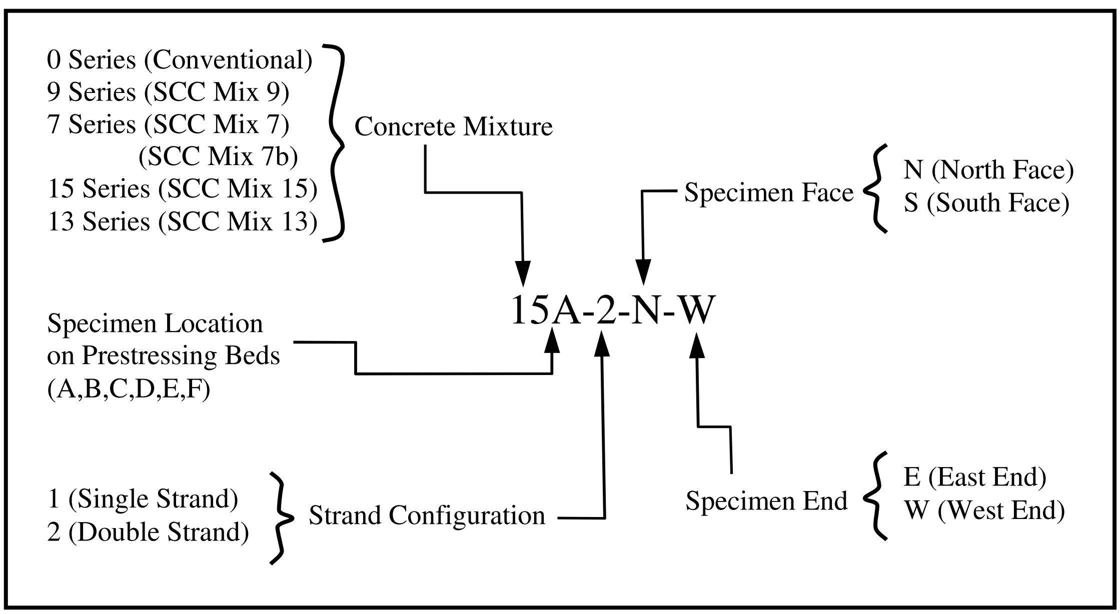

Figure 3-1: Specimen Identification System

The thirty-six concentrically prestressed specimens were cast in sets of six; each consisted of three single-strand specimens and three double-strand specimens. Each set of specimens was cast with a different concrete mixture: one conventional mixture and four different SCC mixtures. As a result of air content exceeding the targeted range, SCC Mix 7 was cast twice; the mixture that had acceptable air content is identified as SCC Mix 7b. The first letter in the identification system specifies the location at which the specimens were cast on the prestressing beds. The letters A, B, and C represent single-strand specimens. The letters D, E, and F represent double-strand specimens. Figure 3-2 shows a set of six specimens on the prestressing beds.

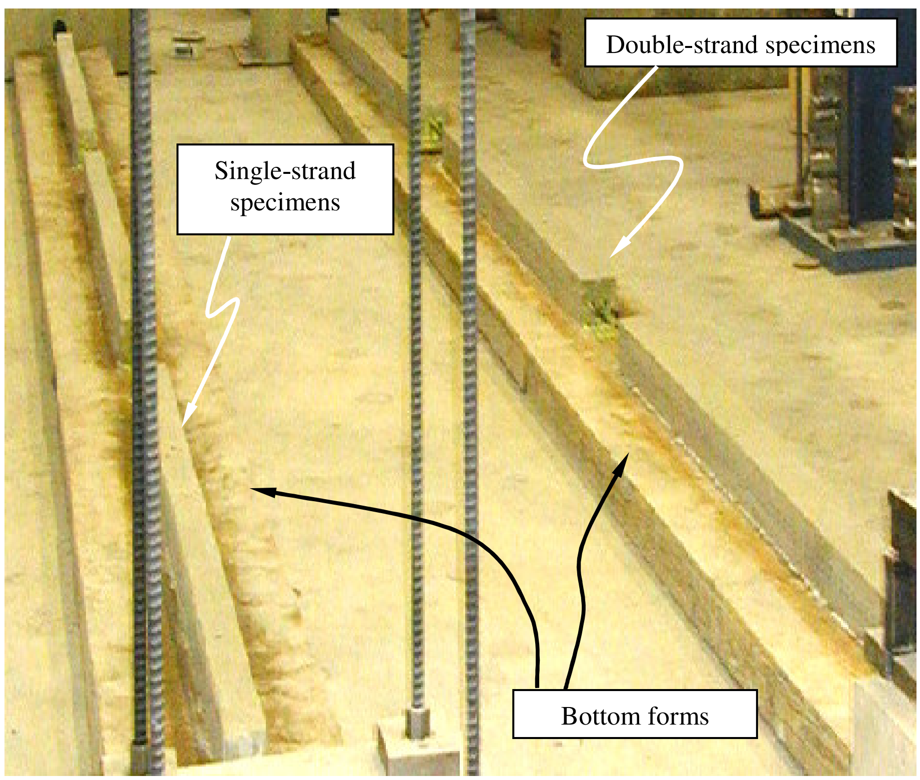

Figure 3-2: A Set of Prestressed Specimens

The locations for the single-strand specimens are illustrated in Figure 3-3, and the locations for the double-strand specimens are shown in Figure 3-4. The proceeding number (1 or 2) represents a single- or double-strand configuration. The next letter used in the identification system represents the specific side face (north or south) of a specimen. The last letter is the specimen end identifier; each end of the specimens was labeled as an east or west end. Thus, surface strains were measured in four general locations on each specimen—the north and south faces of the east end as well as the north and south faces of the west end. Since there was a single transfer length for each east and west end, a total of 72 transfer lengths were measured.

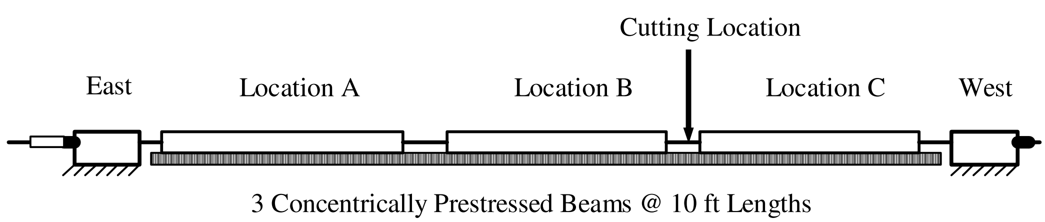

Figure 3-3: Casting Locations for Single-Strand Specimens

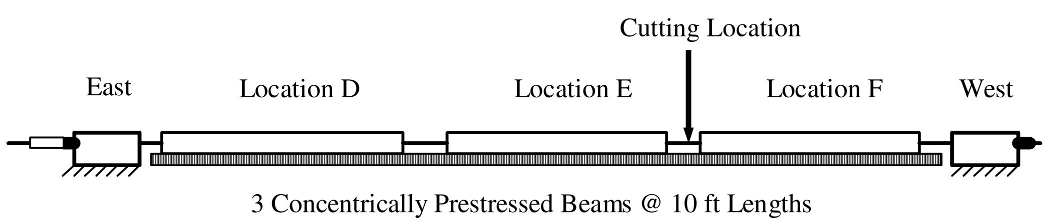

Figure 3-4: Casting Locations for Double-Strand Specimens

3.3 SPECIMEN DESIGN

Six prestressed specimens were cast for each mixture for determining transfer length. In order to estimate drying shrinkage that occurred in these specimens, four additional nonprestressed specimens were cast for each mix. The design of all of the specimens is discussed in this section.

3.3.1 CONCENTRICALLY PRESTRESSED SPECIMENS

The specimens in this study were concentrically prestressed specimens similar to those used in prior research on which the ACI Code transfer length equation was based (Kaar et al. 1963). Pretensioning of the specimens was achieved through the use of 1/2 in. oversized, ASTM A416, Grade 270, low-relaxation, seven-wire prestressing strand. The purpose for testing small concentrically prestressed specimens was to compare transfer lengths in SCC mixtures to transfer lengths in a comparable conventionally consolidated mixture. It is anticipated that transfer length data from these specimens will contribute to future research investigating the use of SCC mixtures for full-scale bridge girders. The specimens with the single-strand configuration had a 4 in. by 4 in. cross section, with the strand at the center of the cross section. The double-strand specimens were 6-in. wide by 4-in. deep, with the strands spaced horizontally two inches on center at the midheight of the specimen. These two cross sections are illustrated in Figure 3-5.

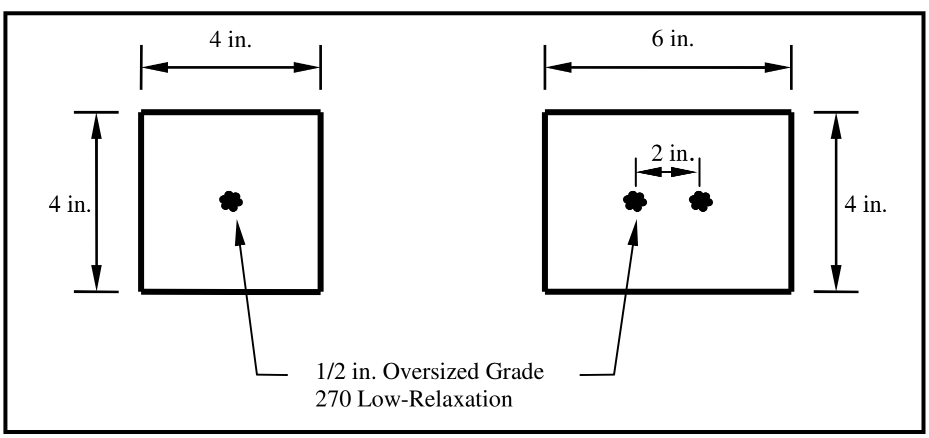

Figure 3-5: Single and Double-Strand Cross Sections

These dimensions were chosen to investigate the worst-case spacing of tendons allowed. The minimum center-to-center spacing of tendons larger than 1/2 in. nominal diameter is 2 in. according to Section 7.6.7.1 of ACI 318-05, Section 9.26.2 of AASHTO Standard Specifications, and Section 5.10.3 of AASHTO LRFD. All six of the specimens were ten feet in length to ensure that a strain plateau would occur on each side of midspan. To minimize bending effects, the prestressing tendons were placed at the midheight of the members.

To differentiate the individual strands in the double-strand specimens, each was identified as either the north or south strand, depending on the closest specimen face. To stay consistent with standard practice, all strands were tensioned to a target value of 75% of the specified tensile strength, f_{pu}. As a result, the target jacking stress, f_{pj}, was 202.5 ksi. When tensioning, strands were overstressed slightly to overcome anchorage displacements that occurred. The actual values of the prestress immediately prior to transfer, f_{pbt}, ranged from 195 to 205 ksi.

3.3.2 DRYING SHRINKAGE SPECIMENS

To determine the drying shrinkage deformations experienced by the prestressed specimens, four non-prestressed specimens were cast for each mixture. One specimen with a 4 in. x 4 in. cross section and another with a 4 in. x 6 in. cross section were cast with same strand pattern as the prestressed specimens. However, the strands were not prestressed. One other specimen for each cross section was cast that did not include any reinforcement. All of the drying shrinkage specimens were four feet in length.

3.4 MATERIAL PROPERTIES

All of the materials that were used in the fabrication of the test specimens are discussed in this section, including descriptions of each concrete mixture employed in the study.

3.4.1 CONCRETE

Five concrete mixtures were used in this study: one conventional concrete mixture and four unique SCC mixtures. Table 3-1 summarizes the required specifications for the concrete mixtures, which were developed in a meeting at the Alabama Department of Transportation. This meeting was made up of representatives from ALDOT, FHWA, the admixture industry, the Alabama prestressed concrete industry, and the Auburn University Highway Research Center. A $f_{ci}^{'}$ value of approximately 6,500 psi is routinely used in the Alabama prestressed concrete bridge industry, but values as low as 5,000 psi are sometimes specified. For this reason, the SCC mixtures were designed to have a $f_{ci}^{'}$ range from 5,000 to 9,000 psi at an age of 18 to 21 hours. To target the minimum and maximum values of the compressive strength range, two moderate-strength ($f_{ci}^{'}$ = 5,000 psi) and two high-strength ($f_{ci}^{'}$ = 9,000 psi) SCC mixtures were evaluated. For comparison with a conventional-slump concrete, a control mixture with a $f_{ci}^{'}$ value of 5,500 psi was also evaluated.

Table 3-1: Specifications for Concrete Mixtures

	Specification
Moderate-Strength Concrete (Mixtures 0, 9, and 15)	$f'_{ci} \approx 5000$ psi
High-Strength Concrete (Mixtures 7 and 13)	$f'_{ci} \approx 9000$ psi
Air Content	4% ± 1%
Slump Flow	27 in. ± 3 in.

The different SCC mixtures that were used for the prestressed specimens were chosen from a series of twenty-one experimental mixtures designed and characterized by researchers at the Auburn University Highway Research Center. Table 3-2 illustrates the matrix of mixtures evaluated. Powder combinations, sand-to-aggregate ratios, and water-to-powder ratios were varied to develop the most reliable mixtures for meeting the specified requirements. Mixtures SCC-7, SCC-9, SCC-13, and SCC-15 were selected for evaluation in this study. As indicated in Figure 3-2, Class C fly ash and Grade 100 ground-granulated blast-furnace (GGBF) slag were mineral admixtures chosen for this transfer length study. Two of the mixtures, one low-strength and one high-strength, contained GGBF slag as a mineral admixture. The other pair of SCC mixtures (one low-strength and one high–strength) contained fly ash. Table 3-3 provides the mixture proportions used for each of the SCC mixtures and for the conventional-slump concrete mixture.

Table 3-2: Experimental Mixture Matrix

Powder Combination	Sand/Aggregate (by volume)	Water-to-powder ratio 0.28	0.32	0.36	0.40
Type III cement + 30% Class C fly ash	0.38	SCC-1	SCC-2	SCC-3	
	0.42	SCC-4	SCC-5	SCC-6	
	0.46	SCC-7	SCC-8	SCC-9	
Type III cement + *x%* Grade 120 GGBF Slag		*(30% Slag)*	*(40% Slag)*	*(50% Slag)*	
	0.42	SCC-10	SCC-11	SCC-12	
	0.46	SCC-13	SCC-14	SCC-15	
Type III cement + 22% Class C ash + 8% Silica Fume	0.42		SCC-16	SCC-17	SCC-18
	0.46		SCC-19	SCC-20	SCC-21

To achieve the necessary flowing ability while maintaining a good resistance to segregation in the SCC mixes, chemical admixtures such as polycarboxylate-based mid-range water reducing admixture (WRA), polycarboxylate-based high-range water reducing admixture (HRWR), and viscosity-modifying admixture (VMA) were used. A slump flow of 27 to 28 in. is desirable for prestressed girder concrete; therefore, the SCC mixtures for this study were developed for a slump flow of 27 in. ± 3 in. Air-entraining admixture was used in all of these mixes in an attempt to meet the total air target value of 4%.

Table 3-3: Mixture Proportions

Mixture Constituents	Mixture ID					
	Control Mix 0	SCC Mix 7	SCC Mix 7b	SCC Mix 9	SCC Mix 13	SCC Mix 15
Water (pcy)	270	260	260	270	260	270
Cement (pcy)	640	650	650	525	650	375
Fly Ash (pcy)	0	279	279	225	0	0
GGBF Slag (pcy)	0	0	0	0	279	375
Coarse agg. (pcy)	1964	1529	1535	1607	1544	1613
Fine agg. (pcy)	1114	1252	1257	1316	1265	1321
AEA (oz/cwt)	0.33	0.80	0.40	0.40	3.75	1.50
Mid-Range WRA (oz/cwt)	4.0	4.0	5.0	4.0	6.0	6.0
HRWR Admixture (oz/cwt)	5.0	6.0	7.0	6.0	7.0	5.5
VMA (oz/cwt)	0.0	2.0	2.0	2.0	2.0	2.0

Note: AEA = air-entraining admixture, WRA = water-reducing admixture, HRWR = high-range water-reducing admixture, VMA = viscosity-modifying admixture

3.4.1.1 Development of Small-Batch Strength-Maturity Relationships

To get an accurate estimate of the time at which the specimens would reach the concrete strength required for prestress transfer, small batches of each mixture were tested to develop a strength-maturity relationship. Several weeks prior to the casting of prestressed specimens with a certain mixture, a small batch of the same mixture was mixed by researchers in the Auburn University Concrete Research Laboratory. A total of 45 cylinders were cast from each 5.0 ft^3 small batch mix. Table 3-4 summarizes the sizes, curing conditions, quantities, and testing schedules for all of the cylinders. The temperature profiles for the air-cured cylinders and match-cured cylinders were recorded using temperature probes in one cylinder of each type. Eight of the cylinders were match-cured to a typical prestressed girder curing temperature profile used in the prestressed precast industry.

Table 3-4: Summary of Small-Batch Strength-Maturity Cylinders

Cylinder Identification	Type of Curing	Cylinder Size	Quantity	Cylinder Test Ages (Average of Three Cylinders at Each Time)
Air-Cured	Air	4 x 8 in.	31	0.5, 1, 1.5, 2, 3, 4, 6, 7, 14, and 28 days
Match-Cured	Match-Cured to Elevated Temperature History	4 x 8 in.	8	1.5 and 28 days
ASTM C192	In accordance with ASTM C 192	6 x 12 in.	6	7 and 28 days

After the concrete strengths were determined for each of the air-cured cylinders at their specified break times, the temperature history for the air-cured cylinders was downloaded and the resulting strength-maturity relationship was determined. This process, known as the Maturity Method, is used to estimate the concrete strengths in elements with different temperature histories (ASTM C 1074 2004). This relationship is based on the fact that the strength in curing concrete increases with increasing temperatures. Concrete cured at lower temperatures will experience slower strength gains. The strength-maturity relationship was calculated using the Equivalent Age Method (ASTM C 1074 2004). Equation 3-1 is known as the Arrhenius equation and is used for calculating the equivalent age of the concrete from the downloaded temperature histories (Malhorta and Carino 1991).

$$t_e = \sum_0^t e^{\frac{-E}{8.3144}\left[\frac{1}{273+T_c} - \frac{1}{273+T_r}\right]} \cdot \Delta t \qquad \textbf{\textit{Equation 3-1}}$$

where

t_e = equivalent age (hours)

E = activation energy (J/mol)

T_c = average concrete temperature during the specified time interval (°C)

Δt = specified time interval (hours)

T_r = reference curing temperature (°C)

After determining the equivalent age, the exponential function expressed in Equation 3-2 can be used to determine the concrete strength at that equivalent age (Malhorta and Carino 1991).

$$S(t_e) = S_u \cdot \exp\left(- \left[\frac{\tau_s}{t_e} \right]^{\beta_s} \right) \qquad \textbf{\textit{Equation 3-2}}$$

where

$S(t_e)$ = strength at equivalent age, t_e, (psi)

t_e = equivalent age maturity at reference temperature (hrs)

τ_s = time constant for strength prediction (hrs)

β_s = shape constant for strength

S_u = ultimate strength (psi)

The best-fit strength-maturity relationship was determined from the exponential relationship by performing a multivariable, least-squares regression analysis using the results of the strength tests of the air-cured cylinders. After assuming an activation energy of 45,000 J/mol and determining S_u, τ_s, and β_s, estimates of concrete strength for the actual specimens were available. To check the accuracy of the calculated strength-maturity relationship, the equivalent ages and corresponding strengths of the match-cured cylinders were plotted along the best-fit curve. Determining the equivalent age of the match-cured cylinders was achieved using the temperature history of these cylinders. The compressive strengths of the match-cured cylinders at 18 hours fell close to the strength-maturity curve. If they had not, a modification of the strength-maturity relationship using a different value of activation energy would have been required.

Because of the complexities associated with scheduling laborers and concrete materials delivery, it was necessary to have an accurate estimation of the time needed for the prestressed specimens to reach the specified concrete strength for prestress transfer. Determination of the strength-maturity relationship for each mixture allowed for ease in planning the casting and prestressing operations. Although the pretensioned specimens were cast in a laboratory, the fine and coarse aggregates were stored outside; as a result, the effects of outside temperature on the strength-maturity relationship had to be considered. For the sets of specimens cast in February and March, colder temperature profiles were used for determining when the required release strength would be met. Warmer temperature profiles were used for the spring months. Without these strength-maturity relationships, planning for the required strengths would have been much more difficult.

3.4.1.2 Large Concrete Batch for Prestressed Specimens

The amount of concrete needed to cast all prestressed specimens, shrinkage specimens, shrinkage bars, and cylinders for each mixture was 1.5 cubic yards. A concrete truck from a local supplier, Twin City Concrete, was used to mix the required amount of concrete. Before the truck left the plant, the coarse aggregate, fine aggregate, 80% of the water, and the AEA were batched out and loaded into the truck's mixer. The remaining cementitious material, water, and chemical admixtures were added to the mixer after arrival at the Auburn University Structural Engineering Laboratory. The addition of cementitious material into the truck mixer is shown in Figure 3-6.

Figure 3-6: Adding Remaining Materials to the Mixer

Before the mixture was accepted and cast in the forms, the slump flow test was performed. For all of the SCC mixtures, the inverted slump flow procedure was used; this is demonstrated in Figure 3-7. Following acceptable slump flow test results, values for the J-Ring test, L-Box test, VSI, T-50, air content, and unit weight were determined from the fresh concrete. A summary of all of the fresh property test results is presented in Table 3-5.

Figure 3-7: Performing the Inverted Slump Flow Test with SCC

Table 3-5: Summary of Fresh Property Tests

FRESH PROPERTIES	MIXTURES					
	Mix 0	Mix 7	Mix 7b	Mix 9	Mix 15	Mix 13
Slump / Slump Flow (in.):	8.25	30.5	26	28.5	28.25	31.25
VSI:	—	2.5	1	2.5	2.5	2
T-50:	—	2.47	3.34	1.57	2.35	2.93
J-Ring (Difference/Rating):	—	0.5 / 0	0.75 / 0	1.25 / 1	2.25 / 2	2.2 / 2
L-Box (H_2/H_1):	—	1	0.5	0.96	0.92	0.33
Air (%):	4.9	9	2.4	4.5	3.3	1.8
Unit Weight (lb/ft^3):	147.2	143.5	153.2	147.9	147.6	153.8

Table 3-6: Summary of Hardened Property Tests

TEST	AGES FROM THE ADDITION OF WATER TO CEMENT											
	1d	Transfer	2d	3d	4d	7d	28d	56d	91d	16w	32w	62w
1) ASTM C 192 Cured Specimens												
4x8 in. f'_c & E_c						3	3		3			
6x12 in. f'_c & E_c						3	3		3			
2) Match-Cured Specimens												
4x8 in. f'_c & E_c		2(+1?)	2(+1?)				2					
3) Air-Cured Specimens												
4x8 in. f'_c & E_c	3	3		3		3	3		3			
4x8 in. Splitting Tensile Test	3	3		3		3	3		3			
4) Drying Shrinkage Prisms*												
Air-Cured	3@ stripping	3	3	3	3		3	3		3	3	3
7days in lime bath	3@ stripping	3	3	3	3		3	3		3	3	3
28days in lime bath	3@ stripping	3	3	3	3		3	3		3	3	3
5) Nonprestressed Shrinkage Specimens	x	x	x	x			x	x		x	x	x

Note: * ages are after the specimen is exposed to drying
d = days, w = weeks

Determination the strength-maturity relationship from the small batches helped to estimate the time required for the prestressed specimens to reach their specified strengths. Because of differences in batch size and the mixing procedure, a new strength-maturity relationship was determined from the compressive strength results for each large batch.

Table 3-6 presents a summary of the number and times of tests performed on hardened properties for all mixtures. Thermocouples recorded the temperature of air-cured cylinders, which were stripped from molds at the time of specimen form removal and for which the compressive strengths at 1, 3, 7, 28, and 91 days were determined. The compressive strength at the time of prestress transfer was also determined. All compressive strengths were measured according to ASTM C 39. Using the temperature profile and corresponding concrete strengths, the strength-maturity relationship was determined by the Equivalent Age Method. The procedure for calculating the strength-maturity of the large batch was the same as for the small batch. Figures 3-8 and 3-9 show the resulting strength-maturity relationship curves for one each of the low-strength and high-strength mixtures. The compressive strengths at prestress transfer were calculated using the recorded temperature profiles and the appropriate strength-maturity relationships for the two different sized specimens. Due to the greater volume of concrete, more heat was generated by the double-strand specimen. As a result, these specimens gained strength faster than the smaller specimens and the air-cured cylinders. The strength-maturity relationship was used to determine the compressive strength values for each set of specimens at prestress transfer. To check the accuracy of the relationship, the compressive strength of the cylinders match-cured to the temperature history of the 4 in. x 4 in. specimens was plotted on the strength vs. equivalent age graph. If this point

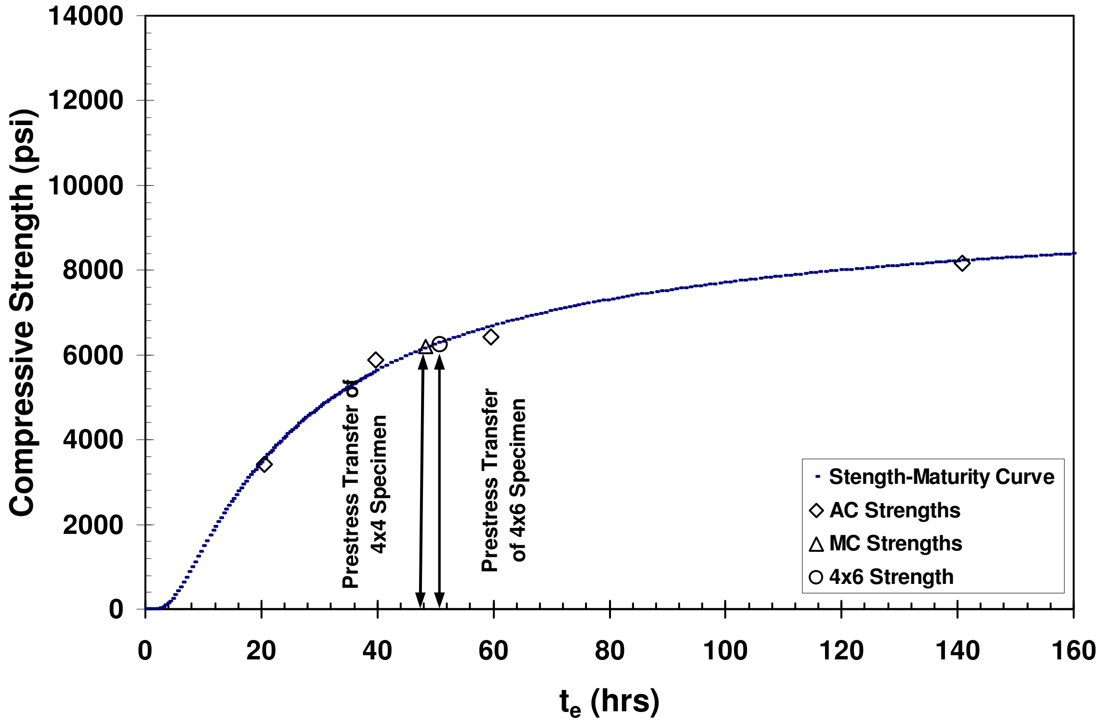

Figure 3-8: Strength-Maturity Relationship Curve for SCC Mixture 9

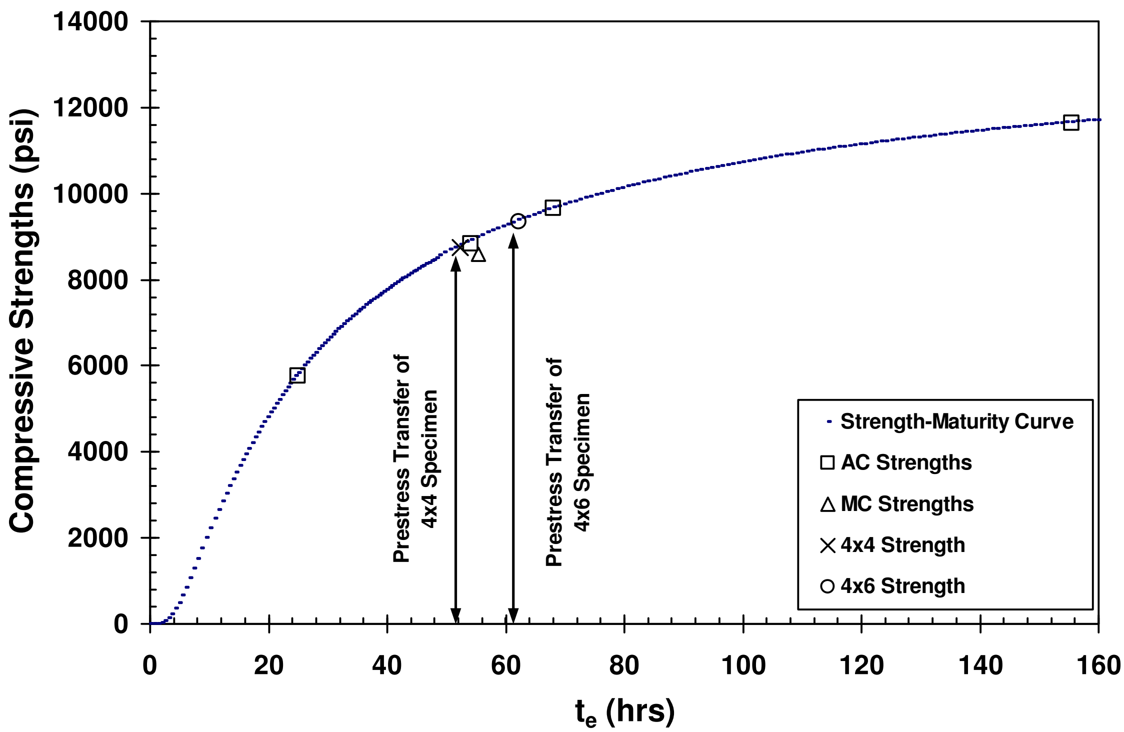

Figure 3-9: Strength-Maturity Relationship Curve for SCC Mixture 7b

fell along the strength-maturity curve, then the relationship was deemed acceptable and the calculated strengths for the specimens were used. If the strength of the match-cured cylinders did not coincide with the calculated value for their equivalent age, then the match-cured compressive strength value at time of prestress transfer was adopted as the 4 in. x 4 in. specimen compressive strength at prestress transfer. In this case, the 4 in. x 6 in. specimen compressive strength at prestress transfer calculated from the strength-maturity relationship was then adjusted by the difference between the actual and calculated match-cured strengths.

Match-curing of cylinders to the 4 in. x 4 in. specimens was achieved using a Sure-Cure mold system. This system monitored the curing temperature of the specimen and applied the same temperatures to the cylinders in the molds. Compressive strengths from the 4 in. x 8 in. match-cured cylinders were determined at one day, time of prestress transfer, and twenty-eight days. The match-cured cylinders cast in Sure-Cure molds are shown in Figure 3-10. Note that the Sure-Cure specimens were covered with damp burlap and plastic sheeting to provide a moist curing environment.

Figure 3-10: Match-Cured Cylinders in the Sure-Cure Molds

Along with the air-cured and match-cured 4 in. x 8 in. cylinders used to determine the strength-maturity relationship, 4 in. x 8 in. and 6 in. x 12 in. cylinders were cast in accordance with ASTM C 192. These cylinders were air-cured until twenty-four hours, at which time they were stripped from the molds and placed in the moist-cure room. The average cylinder strengths for both sizes of ASTM C 192 cylinders were determined at 7, 28, and 91 days.

Because the stiffness and the tensile strength of the concrete are of importance to evaluate the transfer length, measurements of the modulus of elasticity and and splitting tensile strength were performed on cylinders. Modulus of elasticity values were measured according to ASTM C 469 on each set of cylinders at specified break times. Air-cured cylinders were tested for splitting tensile strengths in accordance with ASTM C 496 at 1, 3, 7, 28, 91 days, and at the time of prestress transfer. Due to the limited number of match-cured specimens, splitting tensile strengths were not measured for these specimens.

The hardened concrete properties for each mixture at prestress transfer and at an age of 28 days are presented in Table 3-7. The compressive strength at transfer ($f_{ci}^{'}$), elastic modulus at transfer (E_{ci}), splitting tensile strength at transfer (f_{cti}), the 28-day compressive strength ($f_{c}^{'}$), the 28-day elastic modulus (E_c), and the 28-day splitting tensile strength (f_{ct}) are terms presented in Table 3-7 that have yet to be defined. It is important to note that the reported 28-day strengths were measured from 6 x 12 in. cylinders in accordance with ASTM C 192. Values for all of the hardened concrete properties are presented in Appendix B.

Table 3-7: Summary of Initial and 28-Day Hardened Properties

Strength	Mix 0		SCC Mix No. 7		SCC Mix No. 7b		SCC Mix No. 9		SCC Mix No. 13		SCC Mix No. 15	
	4x4	**4x6**	**4x4**	**4x6**	**4x4**	**4x6**	**4x4**	**4x6**	**4x4**	**4x6**	**4x4**	**4x6**
f'_{ci} (psi)	5060	5110	7460	7485	8750	9350	6190	6250	8760	9560	5020	5430
E_{ci} (ksi)	5150	5200	5150	5150	5400	5600	4800	4800	5950	6200	4850	5050
f_{cti} (psi)	455		630		610		540		695		550	
f'_{c} (psi)	7460		10060		12940		9390		13220		9010	
E_{c} (ksi)	6000		7650		7150		6400		7450		6450	
f_{ct} (psi)	620		695		835		715		905		765	

As already mentioned, the double-strand specimens developed a faster gain in strength as compared to the smaller specimens. The strength-maturity relationship was relied upon to calculate the $f_{ci}^{'}$ for both specimen sizes based on the measured temperature histories of the actual transfer length specimens. As with adjustments in compressive strengths, adjustments to the elastic modulus (E_c) for these specimens were required. According to AASHTO LRFD (*2004*) Section 5.4.2.4 and Section 8.5.1 of ACI (2005) Building Code, E_c can be calculated from Equation 3-3:

$$E_c = 33\, w_c^{1.5} \sqrt{f_c^{'}} \qquad \textbf{\textit{Equation 3-3}}$$

A modified method was used to determine the elastic modulus at prestress transfer, E_{ci}, for SCC specimens. Since E_c grows at a rate proportional to $\sqrt{f_c^{'}}$, this proportionality was determined using known E_c values from the match-cured cylinders at prestress transfer for each mixture. This expression is modeled in Equation 3-4:

$$E_{ci,MC} = \alpha \sqrt{f_{ci,MC}^{'}} \qquad \textbf{\textit{Equation 3-4}}$$

where $E_{ci,MC}$ and $f_{ci,MC}^{'}$ are known values for each set of match-cured cylinders. Once α was determined, this value can was used to calculate E_c corresponding to any compressive strength value for the same mixture. Thus, E_{ci} can be determined by Equation 3-5:

$$E_{ci} = \alpha \sqrt{f_c^{'}} \qquad \textbf{\textit{Equation 3-5}}$$

Values of $f_{ci}^{'}$ used for the different specimens were those determined by the strength-maturity relationship. When $f_{ci}^{'}$ for the single-strand specimens were taken as the match cured f'_{ci}, then E_{ci} for these specimens was taken as the same as the E_{ci} obtained from tests of the match-cured specimens. The double-strand specimen E_{ci} was determined from Equation 3-5 with the adjusted f'_{ci}. Because of the limited number of match-cured cylinders, the splitting tensile strengths were only measured on air-cured cylinders. Therefore, these strengths at prestress transfer are presumably not as accurate as the compressive strengths.

To determine the effects of drying shrinkage on the transfer lengths, nine drying shrinkage prisms were cast in accordance with ASTM C157. There were three sets of three bars each. One set was kept in a lime-saturated water bath for seven days. One set was kept in the lime-saturated water bath for twenty-eight days. The third set of three was cured exactly as the prestressed specimens were. The shrinkage bars and their testing schedules will be discussed further in Section 3.5.2. Casting of all of the required cylinders and shrinkage bars is shown in Figure 3-11.

Figure 3-11: Casting of Cylinders and Drying Shrinkage Prisms

3.4.2 Prestressing steel

The prestressing steel used in this study was 1/2 in. oversized, ASTM A416, Grade 270, low-relaxation, seven wire prestressing strand. It is important to note that this size strand was chosen with future research in mind. The data collected from this study will help to decide which SCC mixtures to use in full-scale bridge girders, which will be cast on the AASHTO Type I beds at Sherman Prestress in Pelham, Alabama. Since 0.6-in. strands cannot be used on these beds, 1/2 in. oversized prestressing strands were chosen to evaluate the largest diameter strands possible. The strand was manufactured at the Houston plant of American Spring Wire Corporation and shipped to Sherman Prestress. Before the strand was transported to the Structural Engineering Laboratory at Auburn University, it was exposed to outside weather for a couple of days. As a result, the surface of the strand was very slightly weathered, but no pitting was present. From a test sheet prepared by American Spring Wire Corporation for this particular strand, values for the cross-sectional area of 0.164 in^2 and elastic modulus of 28,890 ksi were given. The average outside diameter of the strand measured by the researchers was 0.515 in. This value is slightly larger than a 1/2 in. diameter strand, and is consistent with the cross-sectional area of 0.164 in^2 supplied by the manufacturer.

3.5 FABRICATION OF SPECIMENS

In this study, six concentrically prestressed specimens containing single and double strand patterns were constructed. Four additional nonprestressed specimens were fabricated to determine the effects of drying shrinkage. This section discusses the fabrication of the different types of specimens.

3.5.1 CONCENTRICALLY PRESTRESSED SPECIMENS

Prior to casting of the specimens, the strands were tensioned to the specified jacking stress, f_{pj}. This was accomplished by checking the hydraulic pressure from the jack and monitoring calibrated load transducers placed between the chuck and the jacking plate at the end of each strand. On the morning of casting, all strands were wiped down with clean rags to eliminate slight rust or contaminants. Release Agent 880 VOC from Cresset Chemical Company was sprayed carefully on the bottom and side forms and spread uniformly with a flexible brush, as depicted in Figure 3-12. To ensure that there was no contamination, each strand was temporarily wrapped in plastic during the application of the release agent to the forms. After the plastic was removed and the side and end forms were carefully placed and secured on the beds, as demonstrated in Figure 3-13, all seams were caulked to keep the paste from exiting the forms. Due to the flowing nature of SCC, making sure all seams were sealed was extremely important. While carefully monitored, minimal leakage still occurred on several specimens.

Figure 3-12: Applying Release Agent to Bottom Forms

Figure 3-13: Side and End Forms in Position

Only the set of specimens cast with conventional concrete, which had a slump of 8.5 in., required internal vibration. Five-gallon buckets were used in casting the specimens with SCC. Because of the flowability of SCC, the forms were very easy to fill. The flowing of SCC in the forms is shown in Figure 3-14. Wooden floats were used to strike off and finish the specimens, which is demonstrated in Figure 3-15. After initial set of the concrete, the specimens were covered with wet, AASHTO M182 Class 3 burlap and polyethylene plastic. To minimize moisture loss, the burlap was never allowed to dry. Rewetting of the burlap occurred each day after casting until the concrete reached its required strength for prestress transfer. Figure 3-16 shows the specimens being covered with burlap and plastic.

Figure 3-14: Casting of Prestressed Specimens with SCC

Figure 3-15: Finishing Prestressed Specimens with a Wooden Float

Figure 3-16: Covering Prestressed Specimens with Burlap and Plastic

3.5.2 SHRINKAGE SPECIMENS

To determine the effects of drying shrinkage for each concrete mix, four nonprestressed shrinkage specimens were cast along with the prestressed specimens. Two of the specimens were unreinforced, and two of the specimens had a single strand and double strand configuration. There was no pretension applied to the shrinkage specimens with strands. Each pair of shrinkage specimens had the same cross sections as the prestressed specimens (4 in. x 4 in. and a 4 in. x 6 in. cross-section). The same procedure for casting the prestressed specimens was applied to the shrinkage specimens. Curing of the shrinkage specimens was also the same; wet burlap and plastic covered these specimens until the forms were stripped at the same time as the prestressed specimens. Figure 3-17 shows the mechanical vibration of shrinkage specimens cast with conventional-slump concrete.

Figure 3-17: Vibrating Shrinkage Specimens Cast with Conventional-Slump Concrete

3.6 INSTRUMENTATION

After casting all of the prestressed specimens for a mixture, preparations were made before prestress transfer to allow for transfer length testing. This section details the procedures used before and after the prestress transfer.

3.6.1 Transfer length

On the morning of the day when the concentrically prestressed specimens reached the strength required for prestress transfer, all of the forms were removed. Form removal on the shrinkage specimens, shrinkage prisms, and air cured cylinders also occurred at this time. Prior to flame-cutting the strand, proper instrumentation for the transfer length testing was applied in the following manner.

A chalk-line was placed along the midheight of the strand for each prestressed specimen. Starting at the end of each specimen, distances of 25 mm, 75 mm, 125 mm, and 175 mm were measured and marked. Using a quick-setting epoxy, locating discs for a demountable mechanical (DEMEC) strain gauge were attached to the surface at these measured locations, as demonstrated in Figure 3-18. After the discs were attached to all faces of each specimen, four more locating discs were applied to the first specimen in the cycle. This was done using a 200-mm setting bar relative to the first four discs. In each cycle, four more points were applied with epoxy. This process was repeated until the targets that started at each end met in the middle. Upon completion of the lines of DEMEC targets, they were labeled with a marker with consecutive odd numbers starting with 1. The target at the center of the specimen had a value of 61.

After all targets were set, readings were taken using a DEMEC strain gauge for determining the unstrained gauge lengths for future strain measurements. These were taken on overlapping 200-mm gauge lengths. The reading for each length was taken twice, if the relative location readings were within 0.003 mm of each other, then the reader proceeded to the next interval. If these readings did not meet this requirement, the disc was removed and a replacement was set. These measurements are shown in Figure 3-19 and the procedure is discussed in more detail in Section 4.2.1.

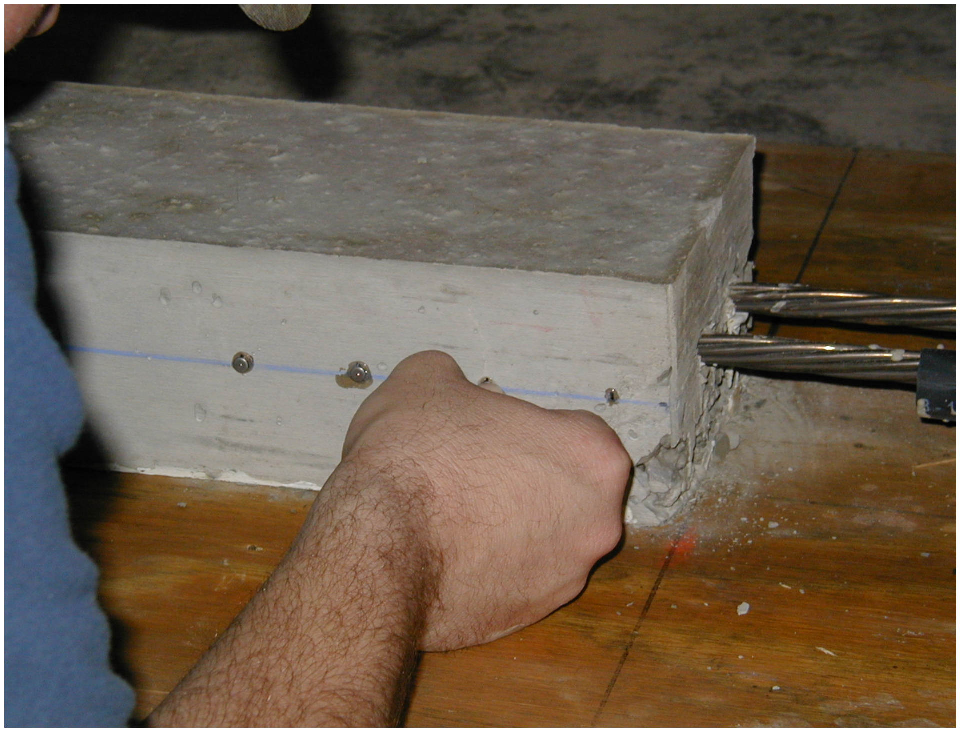

Figure 3-18: Applying First Four DEMEC Locating Discs to Specimen Ends

Figure 3-19: Performing DEMEC Gauge Measurements

3.6.2 Nonprestressed Shrinkage Specimens

In order to take shrinkage readings on the four nonprestressed shrinkage specimens, a line of DEMEC locating discs was placed on each north and south face. Unlike the prestressed specimens, an initial disc was attached 10 mm from the end on each face. The rest of the discs were applied using the 200-mm setting bar. Initial readings were taken at the same time as the readings for the prestressed specimens prior to prestress transfer.

3.6.3 Draw-in

Installation of the instrumentation for the strand draw-in measurements had to be applied prior to transfer also. This involved installing heat-shrink tubing around the strands at a distance of approximately one inch from the ends of specimens. This process is more thoroughly discussed in Section 5.3.

3.7 APPLICATION OF PRESTRESS FORCE

After all the initial measurements were completed and the target concrete strength was obtained, prestress in the strands could be transferred to the concrete specimens. To stay consistent with common practice in the precast, prestress industry, all strands in this study were transferred by sudden release. This method of sudden release was accomplished by flame-cutting all strands at one location for each bed. In compliance with the guidelines set by ALDOT (AHD 367-89), the strands were gradually heated by a low-oxygen flame played along the strand for a minimum of five inches. They were heated in such a manner that failure in the first wire of each strand occurred after the torch had been applied for a minimum of five seconds. The location of the specimens has already been shown in Figures 3-3 and 3-4. The strands were cut in the gaps between the B and C single-strand specimens and the E and F double-strand specimens. Thus, the four specimen ends adjacent to the cut were designated the “live” ends, all other ends were designated “dead” ends.

Caution had to be used when cutting the strands in this manner. With the first set of specimens, the individual wires “unwrapped” upon strand cutting. To keep the strands from unwrapping, two hose clamps were fastened to each strand on either side of the cutting location. This greatly cut down on the deformations caused by this behavior; as a result, loss of concrete on these ends was minimized with later mixes. Due to the violent amount of force created upon flame-cutting and the small self-weight of the specimens, steps had to be taken to keep the specimens from sliding and causing damage. Blocks made out of 2 x 4 wood studs were cut and placed in all spaces along the bed that were not in the way of strand cutting. Numerous cardboard pieces were placed in the ½-in. gap between the wood blocks and the specimen ends. The corrugated cardboard acted as a sacrificial shock-absorber and kept the specimens relatively free from damage. The use of the cardboard was only employed for the SCC mixtures; heavy objects were placed atop the specimens of the first mixture. Since the specimens were not free to move, the released energy was applied directly to a small section at the ends of the live end of the specimens prior to dissipation. This led to concrete bond loss around the cut strand in a couple of locations. Bond loss ranged from 0.6 to 2.25 in. among all of the specimens. Lost lengths of bonding are graphically indicated in Appendix D. Figure 3-20 shows the setup using wood and cardboard to reduce the amount of horizontal shift experienced when flame-cutting strands.

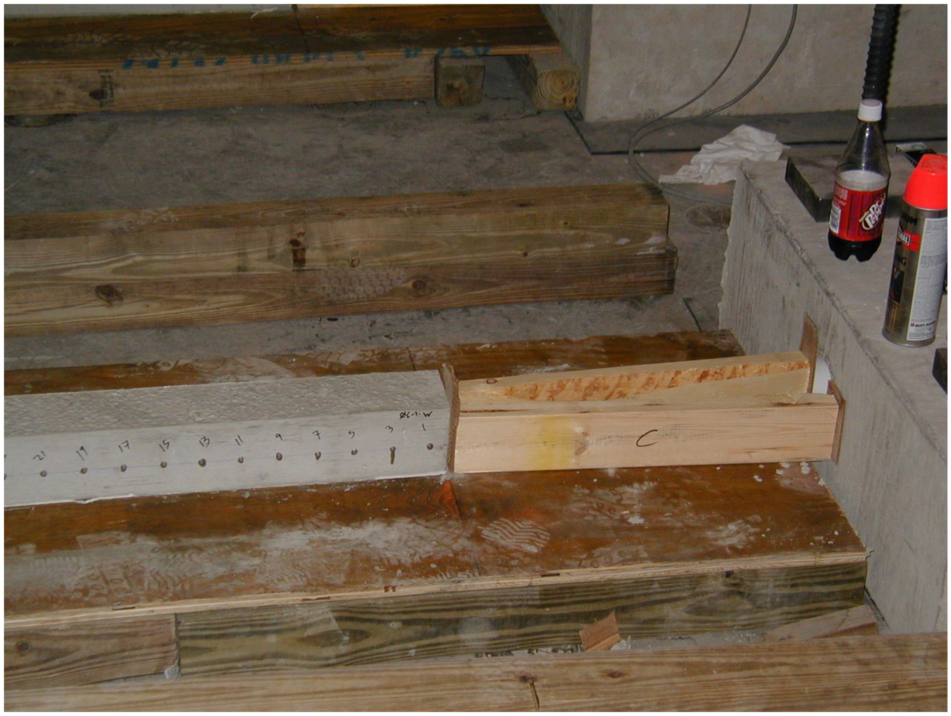

Figure 3-20: Using Wood Blocks and Cardboard to Minimize Sliding while Dissipating Energy at Prestress Transfer

3.7.1 STEPS AFTER PRESTRESS TRANSFER

Once the strands were cut, transfer length readings were taken on the specimens using the DEMEC strain gauge. This is explained in more detail in Section 4.2.2. To allow for more uniform drying shrinkage, the specimens were elevated off the beds so that all sides were exposed to air. This was done prior to the seven-day strain measurements. Two pieces of polyethylene plastic were placed in between the supporting blocks and the concrete specimens; therefore, only negligible restraint effects due to friction were experienced. The specimens were stacked a couple of days after prestress transfer to clear the beds so that another set of specimens could be cast. The same order from top to bottom was used with every set of specimens. Plastic was again placed between the concrete and wood blocks on both sides. Figure 3-21 shows how the specimens were stacked.

Figure 3-21: Stacked Prestressed Specimens

CHAPTER 4

TRANSFER LENGTH TESTING

4.1 INTRODUCTION

Transfer length testing was performed on all thirty-six concentrically prestressed specimens in the research study. With transfer zones located at the ends of each specimen, this resulted in a total of seventy-two transfer zones for testing. The transfer lengths were determined for all seventy-two ends. To the author's knowledge, this represents a larger number of results for transfer lengths in concentrically prestressed specimens cast with SCC than reported previously.

The transfer lengths were determined immediately after prestress transfer and at three additional time intervals after transfer for all specimens. The last measurements (henceforth referred to as "long-term testing") occurred at ages ranging from twenty-eight to forty-six days after prestress transfer. This chapter describes the method for determining the transfer length for each specimen end, the results obtained from the test program, and conclusions drawn from these results. The results from this study are compared to transfer length expressions developed from previous research.

4.2 TEST PROCEDURE

While there are many different methods for determining transfer lengths from concrete compressive strains, the most established method used is the 95% Average Maximum Strain (AMS) Method. This method was used for computing transfer lengths in the FHWA study upon which Equation 5.11.4.2-2 of the AASHTO LRFD is based (Lane 1998). Transfer lengths in this study were obtained using the 95% AMS Method. Concrete surface compressive strains were measured with a demountable mechanical (DEMEC) strain gauge with a 7.87-in. (200-mm) gauge length.

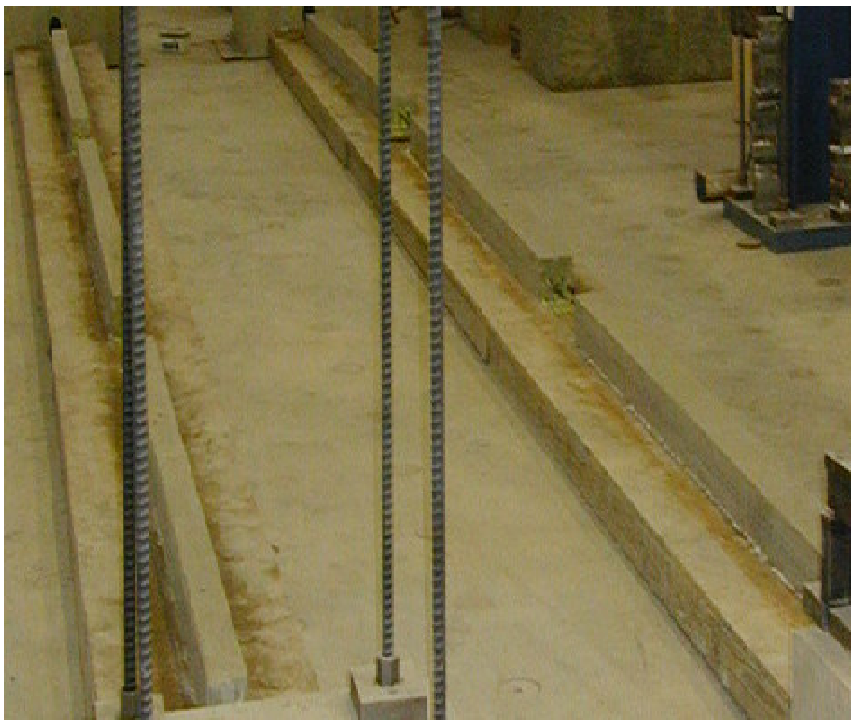

Figure 4-1: Concentrically Prestressed Specimens after Form Removal

4.2.1 Specimen Preparation

Specimen preparation began with the stripping of the side and end forms for each specimen. This took place approximately six hours before the specimens were expected to reach the compressive strength required for transfer of prestress. Figure 4-1 shows a set of the specimens after side and end form removal. As previously discussed in Section 3.6.1, a line of DEMEC locating discs were bonded to each side face after side and end form removal. These discs were placed at the same depth as the centroid of the strands for the entire length of the specimens. After all lines of locating discs had been attached to the specimens, initial strain readings were taken with the DEMEC gauge and recorded. As previously discussed in Section 3.6.1, overlapping readings were taken along the entire length of each specimen face.

4.2.2 Concrete Surface Strain Measurements

As described in Section 3.6.3, DEMEC measurements were performed again immediately following the transfer of prestress. The same procedure that was used to take initial strain measurements prior to transfer was used for the strain measurements after transfer. Prestress was first transferred in the single-strand specimens (A, B, and C). All DEMEC measurements were completed for the single-strand specimens prior to transfer of prestress in the double-strand specimens (D, E, and F). This procedure minimized the elapsed time between prestress transfer and completion of transfer length measurements for all specimens. Because of the different temperature histories and prestress transfer ages for the two lines of specimens, the maturity method was employed (as described in Chapter 3) to accurately estimate concrete strength and stiffness values for each line at the transfer age.

Concrete surface compressive strains were measured at four ages:

1. Immediately after transfer,
2. Two to four days after transfer,

3. Seven days after transfer, and
4. Twenty-eight to forty-six days after transfer.

The resulting concrete compressive strain profiles were used to determine the transfer lengths for each time of strain data collection.

4.3 DETERMINATION OF TRANSFER LENGTHS

The method for determining the transfer length for each specimen end by analyzing the concrete compressive strain profiles is described in this section.

4.3.1 ESTABLISHING THE SURFACE COMPRESSIVE STRAIN PROFILES

In order to determine the transfer length of a specimen end, the compressive strain profile for that end was constructed based on the DEMEC measurements. A typical line of DEMEC discs along a specimen face is illustrated in Figure 4-2.

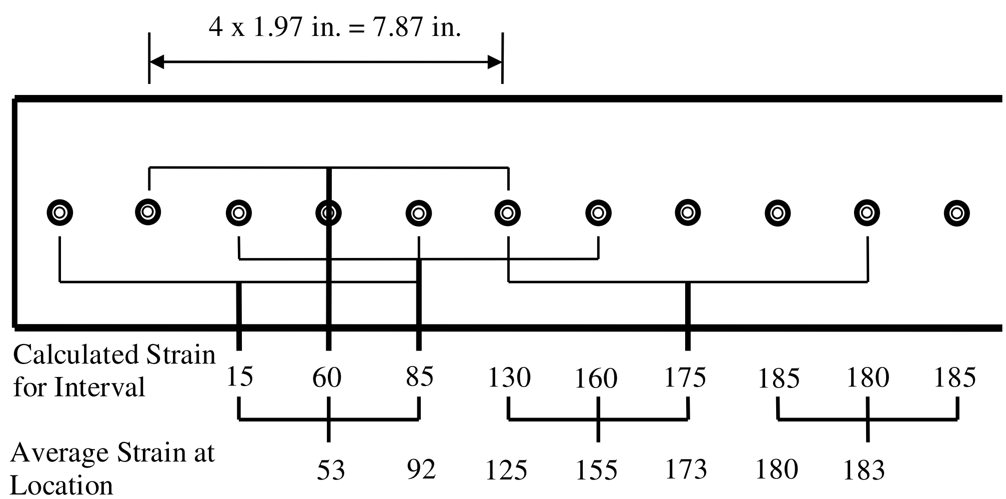

Figure 4-2: Determining Surface Compressive Strain Values

To calculate the strain for each 7.87-in. interval, the difference between the reading at the time in question and the initial reading prior to prestress transfer was multiplied by the

DEMEC gauge factor. Since the DEMEC gauge length is 7.87 in., placing the DEMEC discs in 1.97-in. intervals resulted in each DEMEC disc point falling within three overlapping gauge lengths. The strains from three overlapping lengths at a location were averaged to give the strain value for that location. By averaging the strain values, a smoother strain profile was achieved. Use of the 95% AMS technique compensates for the rounding of the strain profile at the end of the transfer length that results from this smoothing.

To determine the strain value at a specific location along a specimen axis, corresponding strain values on both (north and south) specimen faces were averaged. A single strain profile for each specimen end resulted from plotting the resulting average values along the length of the specimen. From this strain profile, a single transfer length was obtained for each specimen end at each measurement age.

The strain profiles for eccentrically prestressed beams should be corrected due to the self-weight of the beam, especially if the bonding stresses due to the self-weight are large (Barnes et al. 1999). Since the specimens tested in this study were concentrically prestressed, the self-weight was uniformly supported along the member, which resulted in no significant bending stresses. Therefore, no self-weight corrections were made to the measured strains for specimens in this study.

4.3.2 Determination of Average Maximum Strain (AMS)

After the concrete surface strain profiles were determined for each specimen end, the next step towards obtaining transfer lengths was to determine the average maximum strain (AMS) at the time of reading. Figure 4-3 shows the average maximum strain values of a typical transfer zone for two strain measurement events. Assuming that plane sections remain approximately plane for these small, uniformly stressed specimens, the transfer length ends where the surface strains reach a plateau value. In other words, shear lag is assumed to have minimal effect. To determine the AMS for each end, the strain profiles were visually inspected to find DEMEC locations that fell along this plateau. Since strain readings were taken along the total length of the specimen, all of the identified plateau locations from both specimen ends were averaged to determine a single AMS value for both ends of each specimen.

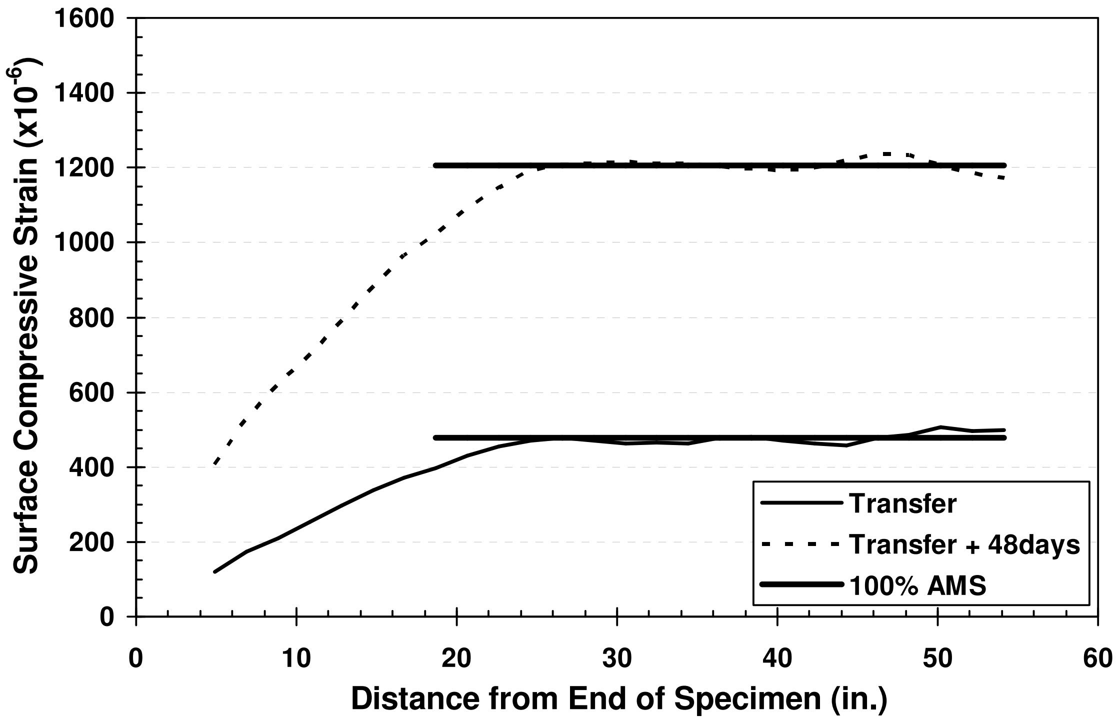

Figure 4-3: Location of Average Maximum Strain Values for Specimen 0A-1-E

4.3.3 Determination of 95% AMS Value

By using the 95% AMS Method, the apparent transfer length is bounded by the intersection of the compressive strain profile and the horizontal line representing 95 percent of the average maximum strain (Barnes et al. 1999). Due to effects on the specimens that occur over time, the 95% AMS Method was carefully applied to ensure accurate transfer length evaluation. This section describes how the 95% AMS Method was applied to determine the transfer lengths for initial and long-term strain profiles.

4.3.3.1 Initial Transfer Lengths

Determining the transfer length from the strain profile immediately after prestress transfer, i.e. initial transfer length, is a relatively straightforward process using the 95% AMS Method. To obtain the 95% AMS value, all that is required is to multiply the average maximum strain value by 0.95. Figure 4-4 illustrates the location at which the 95% AMS value crosses the initial strain plateau; the apparent transfer length is 21.9 in. for this specimen end. The drop from the initial AMS to the 95% AMS value is shown when comparing Figures 4-3 and 4-4.

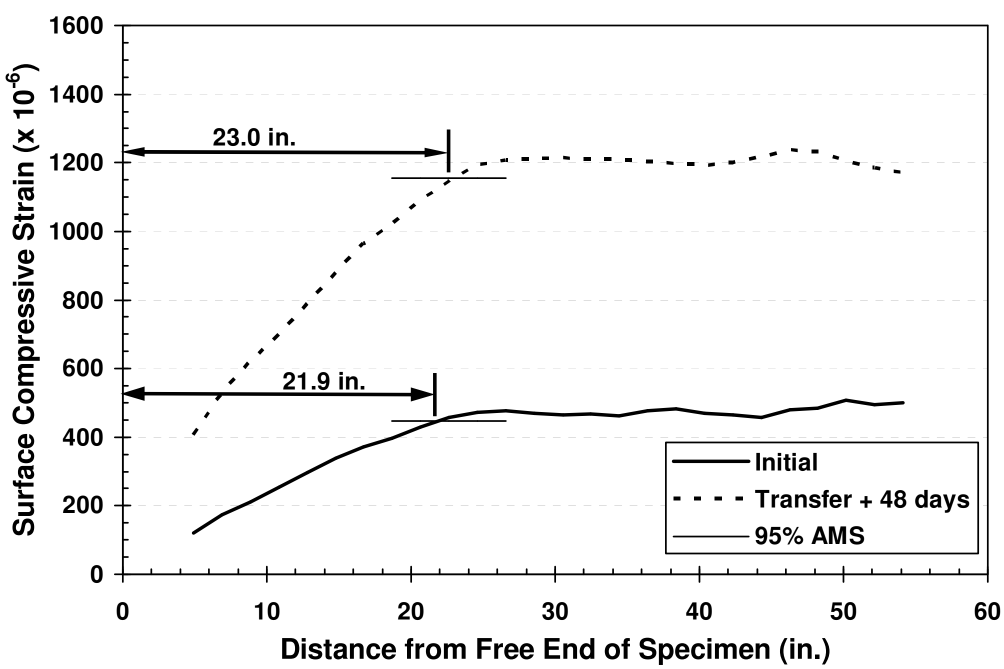

Figure 4-4: Determination of Transfer Lengths by Applying the 95% AMS Method (Specimen End 0A-1-E)

The use of the 95% AMS value has two benefits:

1. It greatly simplifies the identification of the transfer length through the use of a readily identifiable intersection point
2. It compensates for the slight lengthening of the apparent transfer length that results from the smoothing of the strain profile.

During the transfer of prestress, concrete spalled from ends of a few of the specimens. When this occurred transfer lengths were measured from the end of the concrete that remained surrounding the strand. The offset used for these specimens is indicated on the strain profile graphs in Appendix D.

4.3.3.2 Long-Term Transfer Lengths

Accurately calculating the long-term transfer lengths by applying the 95% AMS Method is not as straightforward as it is for initial transfer lengths. As illustrated in Figure 4-4, the long-term strains are approximately three times as large as the initial strains. This increase in strain is attributable to time-dependent deformations of the specimen. If the long-term AMS value is simply multiplied by 0.95 to obtain the long-term 95% AMS value, the strain reduction employed increases with the time-dependent deformations. If the 95% AMS method is not adjusted to account for time-dependent effects, the computed transfer lengths can appear to decrease with time, even when the actual transfer lengths does not.

Creep and shrinkage of the concrete specimens have the largest effect on the transfer length with increasing time. Since creep is dependent on the applied load and shrinkage is independent of the applied load, they affect the strain profile differently (Barnes et al. 1999). Creep deformations amplify the strain values, causing the slope of the non-plateau portion of the strain profile to increase as the plateau value increases. Since both (increasing and constant) portions of the strain profile increase together, multiplying the AMS value by 0.95 gives an accurate estimate of the transfer length if time-dependent deformations are solely due to creep. On the other hand, shrinkage effects cause an upward translation of the *entire* strain profile. This means that the plateau portion of the strain profile increases while the slope of the non-plateau portion remains the same; as a result, the *apparent* transfer length obtained by taking 95% of the AMS value would artificially shorten over time. The only accurate way to determine long-term transfer lengths for comparison with initial values is to determine the individual contributions of creep and shrinkage to the time-dependent strains, and apply the 95% AMS method appropriately.

Accurately determining concrete strains due to creep and shrinkage for all of the mixtures solely by computational methods would have been unreliable—especially because relatively little is known about the creep and shrinkage of SCC. Therefore, an easier and more accurate process for determining these strain losses was utilized in this study. The AMS values that are determined from the long-term DEMEC readings already include strain due to creep and shrinkage. By measuring the deformation of the nonprestressed shrinkage companion specimens, the strain due to shrinkage of the concrete was determined for each age of reading. Since the total time-dependent strain and the portion of those losses attributable to shrinkage were known, the losses due to creep were calculated for each long-term strain reading. After determination of these strains, a more appropriate 95% AMS values for each long-term reading was obtained by the following procedure.

As discussed above, the 5 percent reduction is only appropriate for the elastic and creep strains. Therefore, the 95% AMS value at a long-term date, LT1, was determined by:

$$\varepsilon_{c,95\%\ LT1} = \varepsilon_{c,100\%\ LT1} - 0.05(\varepsilon_{c,i} + \varepsilon_{c,cr\ LT1}) \qquad \textbf{\textit{Equation 4-1}}$$

where:

$\varepsilon_{c,95\%\ LT1}$	=	95% AMS value for long-term 1 strain reading
$\varepsilon_{c,100\%\ LT1}$	=	AMS value for long-term 1 strain reading
$\varepsilon_{c,i}$	=	AMS value for initial strain reading
$\varepsilon_{c,cr\ LT1}$	=	Strain due to creep for long-term 1 strain

Because the AMS value of LT1 is equal to the initial AMS plus the strains due to creep and shrinkage of LT1, Equation 4-1 can be simplified to yield:

$$\varepsilon_{c,95\%\ LT1} = \varepsilon_{c,100\%\ LT1} - 0.05(\varepsilon_{c,100\%\ LT1} - \varepsilon_{c,sh\ LT1}) \qquad \textbf{\textit{Equation 4-2}}$$

where:

$\varepsilon_{c,sh\ LT1}$	=	Strain due to shrinkage for long-term 1 strain

Further simplification results in Equation 4-3:

$$\varepsilon_{c,95\%\ LT1} = 0.95\varepsilon_{c,100\%\ LT1} + 0.05\varepsilon_{c,sh\ LT1} \qquad \textbf{\textit{Equation 4-3}}$$

Transfer lengths at all ages were determined by using the relationship in Equation 4-3.

4.4 RESULTS AND DISCUSSION

As mentioned previously, this study consisted of six different mixtures: a conventional mixture, two low-strength SCC mixtures, and three high-strength SCC mixtures. Originally there were only supposed to be two high-strength SCC mixtures, but due to the high air content realized the first time SCC Mix 7 was cast, this mixture was remixed and labeled SCC Mix 7b. All of the concrete strain profiles and apparent transfer lengths for each specimen end of the study are included in Appendix D. The initial and long-term transfer lengths for the conventional mix, low-strength SCC mixes, and high-strength SCC mixes are shown in Table 4-1, Table 4-2, and Table 4-3. This section covers the transfer length results, interpretation of the results, and comparisons to results from other studies and code expressions. "Live" refers to specimen ends directly adjacent to the location of strand cutting.

Table 4-1: Transfer Length Results for Conventional Mixture

Specimen ID	Method of Prestress Transfer	Initial Transfer Length (in.)	Long-Term	
			Age After Transfer (days)	Transfer Length (in.)
0A-1-E	Dead	21.9	48	23.0
0A-1-W	Dead	24.4	48	22.3
0B-1-E	Dead	22.1	48	22.2
0B-1-W	Live	32.1	48	33.1
0C-1-E	Live	28.7	48	29.7
0C-1W	Dead	23.1	48	22.3
0D-2-E	Dead	23.9	48	23.3
0D-2-W	Dead	20.8	48	22.4
0E-2-E	Dead	22.4	48	24.8
0E-2-W	Live	29.1	48	31.0
0F-2-E	Live	31.9	48	32.9
0F-2-W	Dead	26.8	48	26.8

Table 4-2: Transfer Length Results for Low-Strength SCC Mixes

Specimen ID	Method of Prestress Transfer	Initial Transfer Length (in.)	Long-Term	
			Age After Transfer (days)	Transfer Length (in.)
9A-1-E	Dead	22.6	41	26.9
9A-1-W	Dead	20.0	41	22.2
9B-1-E	Dead	23.9	41	23.5
9B-1-W	Live	31.4	41	32.8
9C-1-E	Live	28.2	41	29.8
9C-1W	Dead	25.4	41	27.9
9D-2-E	Dead	22.9	41	25.6
9D-2-W	Dead	25.9	41	27.3
9E-2-E	Dead	19.6	41	20.9
9E-2-W	Live	37.1	41	36.4
9F-2-E	Live	35.9	41	34.6
9F-2-W	Dead	22.2	41	22.5
15A-1-E	Dead	29.9	28	27.6
15A-1-W	Dead	29.8	28	35.1
15B-1-E	Dead	27.4	28	29.9
15B-1-W	Live	31.3	28	33.2
15C-1-E	Live	32.3	28	32.7
15C-1-W	Dead	20.1	28	20.4
15D-2-E	Dead	32.4	28	33.1
15D-2-W	Dead	35.4	28	33.8
15E-2-E	Dead	24.4	28	25.7
15E-2-W	Live	43.2	28	40.1
15F-2-E	Live	56.9	28	55.5
15F-2-W	Dead	30.4	28	31.9

Table 4-3: Transfer Length Results for High-Strength SCC Mixes

Specimen ID	Method of Prestress Transfer	Initial Transfer Length (in.)	Long-Term	
			Age After Transfer (days)	Transfer Length (in.)
7A-1-E	Dead	19.6	41	25.0
7A-1-W	Dead	16.6	41	20.9
7B-1-E	Dead	18.1	41	24.6
7B-1-W	Live	27.9	41	29.4
7C-1-E	Live	29.2	41	27.3
7C-1-W	Dead	19.6	41	17.9
7D-2-E	Dead	17.7	41	20.4
7D-2-W	Dead	16.0	41	29.4
7E-2-E	Dead	18.9	41	21.8
7E-2-W	Live	29.9	41	28.8
7F-2-E	Live	32.5	41	30.5
7F-2-W	Dead	20.6	41	24.9
7bA-1-E	Dead	15.4	28	19.5
7bA-1-W	Dead	16.7	28	18.5
7bB-1-E	Dead	16.0	28	17.4
7bB-1-W	Live	24.4	28	23.7
7bC-1-E	Live	27.3	28	25.0
7bC-1-W	Dead	16.8	28	17.7
7bD-2-E	Dead	15.3	28	18.4
7bD-2-W	Dead	17.6	28	19.7
7bE-2-E	Dead	18.3	28	20.0
7bE-2-W	Live	25.3	28	25.8
7bF-2-E	Live	33.0	28	34.4
7bF-2-W	Dead	15.8	28	19.1
13A-1-E	Dead	19.2	28	19.5
13A-1-W	Dead	15.1	28	16.1
13B-1-E	Dead	17.7	28	19.2
13B-1-W	Live	24.6	28	26.5
13C-1-E	Live	27.1	28	28.4
13C-1-W	Dead	14.2	28	17.0
13D-2-E	Dead	16.9	28	17.1
13D-2-W	Dead	21.0	28	23.2
13E-2-E	Dead	17.5	28	16.7
13E-2-W	Live	34.0	28	31.5
13F-2-E	Live	38.7	28	32.1
13F-2-W	Dead	15.3	28	18.2

4.4.1 Models for Expressing Transfer Length

From the different design codes and many past studies, several expressions are available for predicting true transfer lengths in pretensioned beams. Many of the expressions share similar forms with respect to relevant variables. Variables present in the different models include level of prestress, concrete strength, element size, tendon size, and method of prestress transfer, among others. Several models were investigated to determine which one best fits the results from this study. Once the best model was selected, it was ready for used in comparing transfer length behavior of specimens characterized by different values of the specified variables.

The models investigated to see which correlated best to the transfer lengths in this study were:

$$l_t = \alpha f_{pe} d_b \qquad \textbf{\textit{Equation 4-4}}$$

$$l_t = \alpha \frac{f_{pt}}{f'_{ci}} d_b + \beta \qquad \textbf{\textit{Equation 4-5}}$$

$$l_t = \alpha \frac{f_{pj}}{f'_c} d_b + \beta \qquad \textbf{\textit{Equation 4-6}}$$

$$l_t = \alpha \frac{f_{pt}}{\sqrt{f'_{ci}}} d_b \qquad \textbf{\textit{Equation 4-7}}$$

where:

α = Constant of proportionality, and

β = Constant (in.).

The model shown in Equation 4-4 represents the expression found in Section 12.9 of ACI 318-05. This expression was the first ACI 318 transfer length equation and is still in use today. The transfer length expression developed by Lane (1998) that is in the AASHTO LRFD Specifications as an alternative has the form of Equation 4-6. Zia and Mostafa (1978) previously developed an equation based on the model shown in Equation 4-5. The model of Equation 4-7 was first proposed by Mitchell et al. (1993) and further validated over a wide range of concrete strengths by Barnes et al. (2003). Concrete strengths and the different values of steel stress needed for each of these models are presented in Table 4-4. Linear regression analysis was used by plotting the measured transfer lengths for all of the specimens versus the combination of parameters in each model, and then determining the regression constants (α and β) that best fit the plotted data. Coefficient of determination values (R^2) were also determined for the best-fit line. Graphical representations, for each of the best-fit version of the four different models, are presented in Appendix F. The results obtained for each of the models are summarized in Table 4-5.

Table 4-4: Concrete Strengths and Tendon Stresses

Strength	Mix 0		SCC Mix No. 7		SCC Mix No. 7b		SCC Mix No. 9		SCC Mix No. 13		SCC Mix No. 15	
	4x4	4x6	4x4	4x6	4x4	4x6	4x4	4x6	4x4	4x6	4x4	4x6
f'_{ci} (psi)	5060	5110	7460	7485	8750	9350	6190	6250	8760	9560	5020	5430
E_{ci} (ksi)	5150	5200	5150	5150	5400	5600	4800	4800	5950	6200	4850	5050
f_{cti} (psi)	455		630		610		540		695		550	
f'_c (psi)	7460		10060		12940		9390		13220		9010	
E_c (ksi)	6000		7650		7150		6400		7450		6450	
f_{ct} (psi)	620		695		835		715		905		765	
f_{pj} *(ksi)*	243		243		243		243		243		243	
f_{pbt} *(ksi)*	198	198	199	201	204	202	199	195	201	201	205	200
f_{pt} *(ksi)*	184	180	184	178	186	187	184	178	189	188	191	184
$f_{pe,LT}$ *(ksi)*	162	154	170	169	180	176	164	156	179	178	178	171

Table 4-5: Correlation Values and Constants for Transfer Length Models

Model	Dead End			Live End		
	α	***β***	**R^2**	***α***	***β***	**R^2**
$l_t = \alpha f_{pe} d_b$	0.26	—	-0.22	0.36	—	-0.19
$l_t = \alpha \frac{f_{pt}}{f_{ci}^{'}} d_b + \beta$	0.94	9.52	0.34	0.83	19.91	0.13
$l_t = \alpha \frac{f_{pj}}{f_c^{'}} d_b + \beta$	1.29	9.63	0.30	1.05	20.98	0.12
$l_t = \alpha \frac{f_{pt}}{\sqrt{f_{ci}^{'}}} d_b$	0.63	—	0.41	0.86	—	0.16

A linear regression analysis of the dead-end transfer length results yielded a coefficient of determination, R^2, of 0.41 for this model. The R^2 value indicates how well the data correlates to the model used, with $R^2 = 1.0$ being the best possible value. It is apparent that the transfer lengths from this study correlated best with the model of Equation 4-7, $l_t = \alpha \frac{f_{pt}}{\sqrt{f_{ci}^{'}}} d_b$. The live-end transfer lengths exhibited much greater dispersion resulting in lower R^2 values; however, the best correlation still existed with Equation 4-7. A more detailed discussion of the findings relative to specific variables is presented in the following sections.

4.4.2 EFFECTS OF CONCRETE STRENGTH AND TENDON PRESTRESS

As previously discussed in Section 2.5.3, the first transfer length equation developed by Mattock that appeared in the 1963 ACI Building Code was based on strand diameter, tendon stress, and bond stress. This equation was in the form of:

$$l_t = \alpha \frac{f_{pe}}{U_t} d_b \qquad \textbf{\textit{Equation 4-8}}$$

The constant, α, and bond stress, U_t, were based on three different studies that used prestressing steel and concrete of lower strengths than used in today's prestressed construction practice. Prestressing steel used today experiences an effective prestress higher than 150 ksi, the value on which Mattock's equation was based. While the stress and size of the tendon are accounted for in Equation 4-8 with f_{pe} and d_b, the role that concrete strength and steel stress play in bond stress must be considered.

For the development of Equation 4-8, Mattock used an average transfer bond stress capacity. While there are many factors that influence bond stress, concrete strength is a factor that is most overlooked. As mentioned in Section 2.6.1, friction, promoted by the Hoyer Effect, is the principle factor influencing stress transfer by bond. Pressures applied to the concrete surrounding the expanding tendon are resisted by the tensile strength and stiffness of the concrete. Since these two properties are commonly related to the compressive strength of the concrete, it would be unreasonable to assume a constant value for bond stress capacity in determining transfer lengths for beams of widely varying strength levels.

The tensile strength and stiffness of normal-weight concrete are usually assumed to be proportional to the square root of the concrete compressive strength (ACI 318-05, 8.5.1, 9.5.2.3). For this reason, transfer bond capacity could also be assumed to be proportional to the square root of the concrete compressive strength. By substituting $\sqrt{f_c^{'}}$ for U_t in Equation 4-8, the resulting equation is:

$$l_t = \alpha \frac{f_{pe}}{\sqrt{f_c^{'}}} d_b \qquad \textbf{\textit{Equation 4-9}}$$

The expression in Equation 4-9 is very similar to the model found in Equation 4-7. The data from the present study, which correlated best with this model, support the hypothesis that transfer lengths, on average, are inversely proportional to the square root of the concrete compressive strength.

After selecting the appropriate model, different measures for tendon stress (f_{pt}, f_{pbt}, f_{pe}) and concrete strength (f'_c, f'_{ci}) were investigated to see which specific combination produced the best correlations with the data. Since growth in transfer lengths was observed over time, the relationships were compared to the long-term transfer lengths. The relationship of measured long-term transfer lengths and $\frac{f_{pt}}{\sqrt{f_{ci}^{'}}} d_b$ (model of Equation 4-7) yielded the best correlation values. Using this model, the measured long-term transfer lengths (in.) were plotted against corresponding values calculated from $\frac{f_{pt}}{\sqrt{f_{ci}^{'}}} d_b$, in units of ksi$^{0.5}$-in. From this plot, average, upper-bound, or lower-bound proportionality constants (α) could be determined. The slope of the line starting from the origin and passing through the average, upper-bound or lower-bound of the data was taken as the constant. This relationship is shown in Figure 4-5. If the model fit the data perfectly, the data would line up along the solid line. As found with other transfer length studies using demountable gauges (Barnes et al. 1999), there is significant dispersion among the data, especially at the live ends. An average value $\alpha_{dead\ end} = 0.63\ ksi^{-0.5}$ was determined from the best-fit line for the all the dead ends of the study.

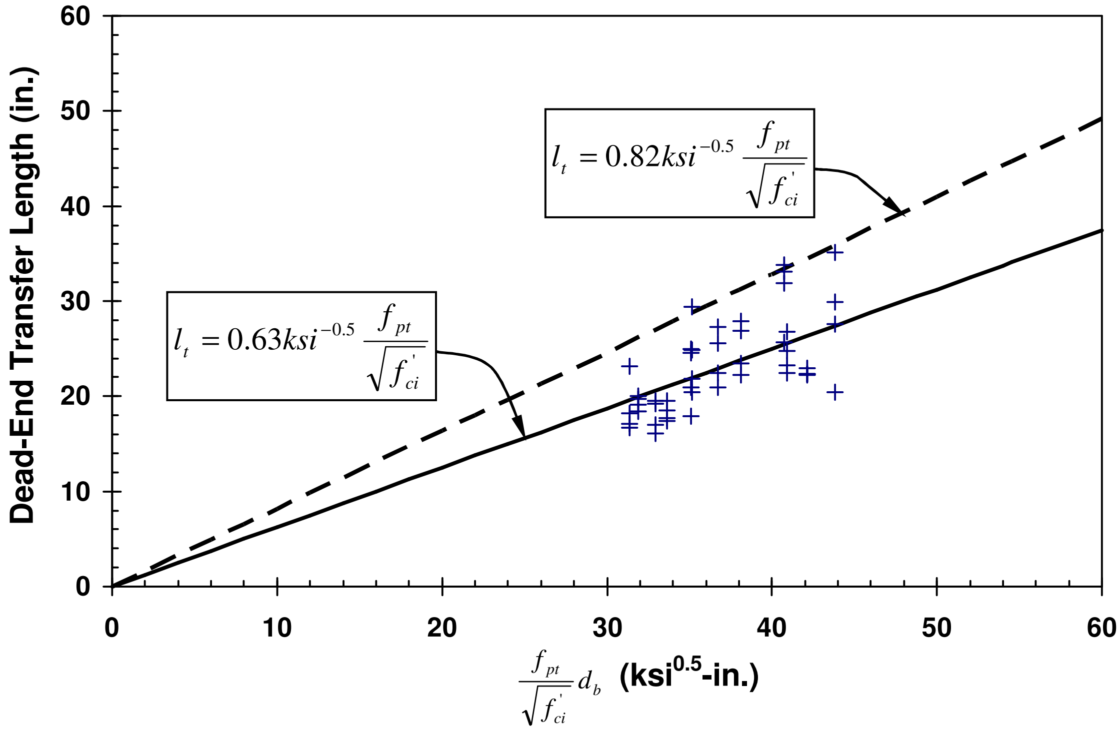

Figure 4-5: Dead-End Transfer Length as a Function of Tendon Prestress and Concrete Strength at Transfer

The average value $\alpha_{dead\ end} = 0.63\ ksi^{-0.5}$ for the dead-end transfer lengths is an approximate value from this study. Since it is important to be conservative in the calculation of transfer lengths, especially when calculating the shear capacity of a prestressed member, an upper-bound value exceeding 95% of all the dead-end transfer lengths was determined. Calculation of the 95% upper-bound was achieved by determining the number of dead-end transfer lengths representing 95% of the data. A line bounding this amount of data points was then drawn. The upper-bound value $\alpha_{dead\ end}$ = 0.82 ksi$^{-0.5}$ is illustrated in Figure 4-5.

While this upper bound works well for the dead-end transfer lengths, the live-end transfer lengths were longer and showed much greater dispersion. In Figure 4-6, the average value of $\alpha_{live\ end}$ = 0.86 ksi$^{-0.5}$ is illustrated for transfer lengths measured on the live ends. This represents an average increase of 38% relative to the corresponding dead-end value. The 95% upper bound value for the live ends was determined to be $\alpha_{live\ end}$ = 1.10 ksi$^{-0.5}$.

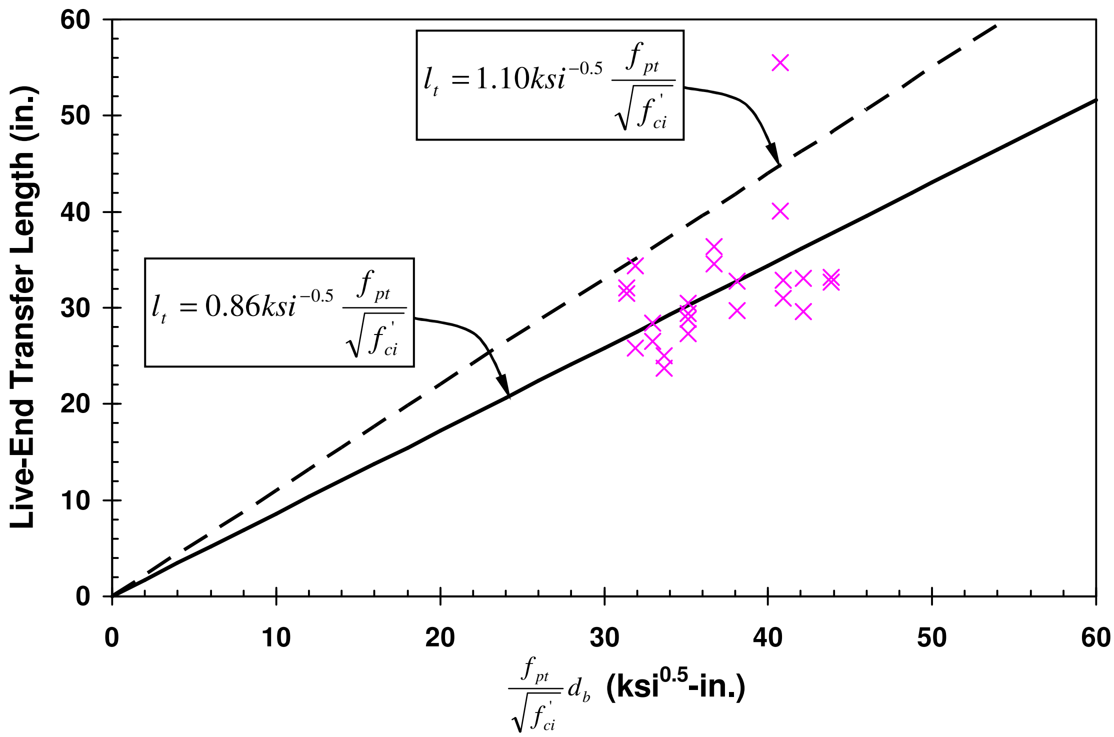

Figure 4-6: Live-End Transfer Length as a Function of Tendon Prestress and Concrete Strength at Transfer

This apparent increase in transfer lengths at the live ends is logical when considering the small specimens tested in this study; past research has shown there to be a significant increase in live-end transfer lengths relative to dead-end values for smaller prestressed specimens when prestress transfer was achieved by sudden release. Kaar et al. (1963) observed that the measured transfer lengths on the live ends exceeded transfer lengths on the dead ends by 20%. Zia and Mostafa (1978) reported a 15% increase in transfer lengths of live ends relative to dead ends. This result was also noted in transfer length tests performed by Russell and Burns (1997), where transfer lengths measured on the live ends were 34% greater on average than transfer lengths measured on the dead ends.

As already mentioned, several different parameters were substituted into this general relationship to see if any significant changes occurred. The square root of the 28-day concrete strength, $\sqrt{f_c'}$, was used instead of $\sqrt{f_{ci}'}$; no significant change in correlation was observed. Next, the effective strand stress after losses, f_{pe}, at the time of the long-term strain readings was substituted for the strand stress immediately after prestress transfer, f_{pt}. Use of f_{pe} with the square root of either the concrete strength at transfer or the 28-day concrete strength resulted in similar outcomes. The least-squares correlation values for both these relationships were slightly lower ($R^2 = 0.30$ for both) than determined for the first relationship, Equation 4-7 (f_{pt} with $\sqrt{f_{ci}'}$). Since the average bond stress is thought to be a function of the stiffness and tensile strength of the concrete, E_c, E_{ci}, f_{cti} and f_{ct} were each investigated in the denominator (replacing $\sqrt{f_{ci}'}$); however, very little correlation was evident when each was investigated independently.

The other models that were investigated (represented by Equations 4-4 through 4-6) showed very little correlation with the data. The model that yielded results furthest from the measured data was Equation 4-4, which appears in the ACI 318-05 Code. Concrete strength plays no role in this equation, while analysis of the data using Equation 4-7 indicates that concrete strength does play a significant role in the determination of transfer lengths. While the models of Equation 4-5 and Equation 4-6 contain $f_{ci}^{'}$ and $f_{c}^{'}$, they do not fit the data as well as the relationship employing the square root of these variables. According to Barnes et al. (2003), this is because tensile cracking in the surrounding concrete occurs well before the radial stresses approach the compressive strength of the concrete.

The values found for α in this study for live and dead ends correlate to the data from this experimental study only. Further research is needed to determine expressions for transfer lengths in full-scale members.

4.4.3 COMPARISON OF CONVENTIONAL AND SCC MIXTURES

To the author's knowledge, there has not been any previous study comparing transfer lengths in concentrically prestressed specimens cast with conventional concrete and those from specimens cast with SCC. Table 4-6 identifies the four different SCC mixtures that were compared to specimens cast with a conventional-slump concrete mixture typically used in prestressed concrete girder fabrication. Two of the four SCC mixtures contained Class C fly ash: one moderate $f_{ci}^{'}$ mixture and a high $f_{ci}^{'}$ mixture. The other two SCC mixtures contained Grade 100 Ground-Granulated Blast Furnace (GGBF) slag: one moderate $f_{ci}^{'}$ mixture and a high $f_{ci}^{'}$ mixture. The transfer lengths from these four mixtures were then compared to the transfer lengths from specimens cast with the conventional-slump mixture. Transfer lengths were measured for an additional high-strength Class C fly ash mix that had a 9% air content. Even though this high air content was not acceptable for use in ALDOT bridge girders, the transfer lengths from this set of data were consistent enough to include in comparisons.

Table 4-6: Summary of Mixtures Used in Test Specimens

Classification	Mixture ID	Mineral Admixture	4 in. x 4 in. f'_{ci} (psi)	4 in. x 6 in. f'_{ci} (psi)
Moderate *f'ci* SCC	SCC Mix 9	Class C Fly-Ash	6190	6250
	SCC Mix 15	GGBF Slag	5020	5430
High *f'ci* SCC	SCC Mix 7*	Class C Fly-Ash	7460	7490
	SCC Mix 7b	Class C Fly-Ash	8750	9350
	SCC Mix 13	GGBF Slag	8760	9560
Control	Control Mix 0	—	5060	5110

*Note: Air content for SCC Mix 7 exceeded the specified range

A least-squares regression analysis was performed to determine the value of α in the relationship $l_t = \alpha \frac{f_{pt}}{\sqrt{f'_{ci}}} d_b$ that best represented each group of data. In order to adequately compare all data from mixes with different strength levels, the transfer lengths were normalized with respect to $\frac{f_{pt}}{\sqrt{f'_{ci}}} d_b$. The data for each mixture were grouped into live ends and dead ends because of their significantly different transfer length values. Representative α values are reported in Table 4-7. The ratio, $\frac{\alpha}{\alpha_{conv.}}$, allows comparison of the normalized α values for SCC mixtures to α values of the control mixture. For fair comparisons, the dead-end SCC values are divided by dead-end conventional values; live-end SCC values are compared to live-end conventional values.

Table 4-7: Comparisons of Normalized α Values

Mixtures	Variable	Specimen End	
		Dead End	**Live End**
Conventional	α	0.56	0.76
	$\frac{\alpha}{\alpha_{conv.}}$	1.00	1.00
Class C Fly Ash	α	0.63	0.85
	$\frac{\alpha}{\alpha_{conv.}}$	1.13	1.12
GGBF Slag	α	0.65	0.94
	$\frac{\alpha}{\alpha_{conv.}}$	1.16	1.23
All SCC Mixes	α	0.64	0.89
	$\frac{\alpha}{\alpha_{conv.}}$	1.14	1.17
All Mixes	α	0.63	0.86
	$\frac{\alpha}{\alpha_{conv.}}$	1.11	1.13

The fly-ash dead-end transfer lengths were 13% longer than the conventional dead-end transfer lengths, and GGBF slag dead-end transfer lengths were 16% longer than the conventional values. Overall, the dead-end transfer lengths of specimens cast with the SCC were 14% longer on average than those cast with conventional concrete.

Percentage increases of normalized live-end transfer lengths of SCC specimens relative to corresponding values in conventional concrete specimens were comparable with the dead-end increases. Fly-ash specimens had the lowest increase of 12%. The greatest increase was found with the GGBF-slag specimens, which had transfer lengths 23% higher than transfer lengths in conventional specimens. A long transfer length measured on one of the live ends (15F-2-E) from the low-strength GGBF slag mixture led to this higher percentage. The average of the normalized live-end transfer lengths from all SCC mixes showed a 17% increase relative to the conventional concrete specimens.

Among the specimens cast with SCC, the two types of mineral admixtures produced very similar transfer lengths for both live and dead ends. Transfer lengths on the dead ends of GGBF-slag specimens were found to be only 3% longer than the specimens cast with fly ash. For the live ends, the transfer lengths of GGBF-slag specimens were 10% longer than the fly-ash specimens.

Dispersion among the different mixtures is easier to see on a plot of measured transfer lengths versus $\frac{f_{pt}}{\sqrt{f_{ci}^{'}}}d_b$ for both live and dead ends. In Figure 4-7, the measured dead-end transfer lengths are plotted versus $\frac{f_{pt}}{\sqrt{f_{ci}^{'}}}d_b$. The best-fit lines for the specimen groups demonstrate how these groups behave relative to each other. Tight grouping of the conventional-slump transfer lengths on the dead ends is shown. The data from the SCC mixtures of the same strength level do not exhibit such tight grouping. Transfer lengths from the low-strength slag mix ranged from 20.1 to 35.1 in. on the dead ends. As the concrete strength at transfer increases (moving left on the graph), the magnitude and dispersion of the transfer lengths decrease. This can be seen for both the fly ash and the GGBF slag mixtures in Figure 4-7. Overall, consistent behavior among the SCC specimens is evident, and this behavior appears to be significantly different than that of the conventional-slump concrete specimens.

The live-end results, plotted in Figure 4-8, are less consistent among the mixtures. There is no significant pattern among the data to conclude that the dispersion improves with changes in any certain parameter. This may be attributable to the limited number of live-end transfer lengths in the study.

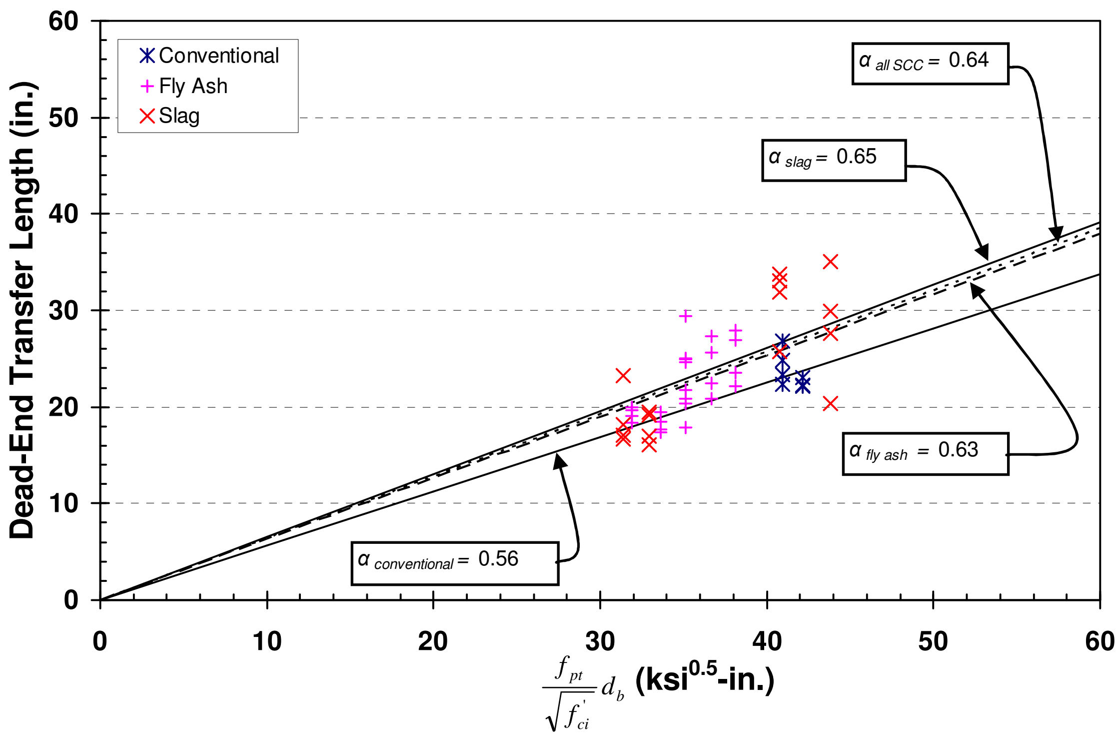

Figure 4-7: Comparisons of Dead-End Transfer Lengths for Different Mineral Admixtures

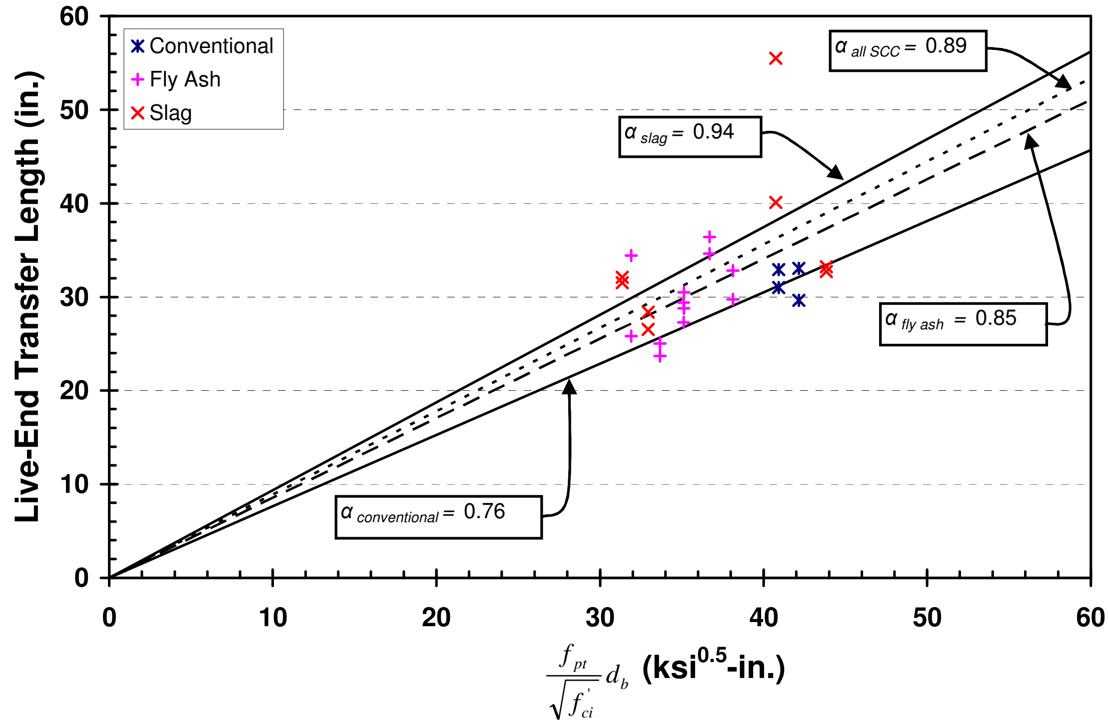

Figure 4-8: Comparisons of Live-End Transfer Lengths for Different Mineral Admixtures

4.4.4 Comparison of Dead and Live Ends

Transfer lengths from the live ends of the specimens were observed to be significantly longer than those on the dead end, as shown in Table 4-8.

Table 4-8: Comparison of Normalized Live to Dead-End α Values

	Specimen End		$\frac{\alpha_{LIVE}}{\alpha_{DEAD}}$
	α_{DEAD}	α_{LIVE}	
Conventional	0.563	0.762	1.35
Class C Fly Ash	0.633	0.851	1.34
GGBF Slag	0.653	0.937	1.43
All SCC Mixes	0.642	0.889	1.38
All Mixes	0.625	0.862	1.38

As seen in Table 4-8, the average increase in α values from dead to live ends was approximately 38%, which equals the average increase for all of the SCC specimens. Overall, the percent increase from dead to live ends for the mixture groups was consistent. One very long live-end transfer length in the low-strength GGBF slag specimens led to the slightly higher average increase (43%) for the GGBF slag results. From the data collected in this investigation, the increase from dead- to live-end transfer lengths remained consistent throughout all of the test specimens. Other researchers investigating concentrically prestressed specimens showed similar increases from dead ends to live ends (Kaar et al. 1963; Russell and Burns 1996).

4.4.5 Effects of Time

A very important feature that should not be overlooked when determining transfer lengths in pretensioned specimens is their change over time. Do the transfer lengths increase, decrease, or stay approximately unchanged over time? Since the present study investigated the transfer lengths on small concentrically prestressed specimens, growth over time should be compared to research that studied similar specimens. Kaar, LaFraugh, and Mass (1963) reported a 6% average increase in transfer lengths over a one-year period, with a maximum increase of 19%. They concluded that the increase in transfer lengths with time was independent of concrete strength at the time of transfer. Lane's work (1992) showed that there was no significant pattern of transfer length growth in a one-year period.

To get a good understanding of the growth, or lack thereof, in transfer lengths with time, transfer lengths were determined at the four ages mentioned previously:

1. Immediately after transfer, $l_{t,i}$

2. Two to four days after transfer, $l_{t,LT1}$

3. Seven days after transfer, $l_{t,LT2}$

4. At least twenty-eight days after transfer, $l_{t,LT3}$

Within each of the six mixtures, the changes in length were determined by comparing each long-term transfer length to the initial transfer length. Comparisons between the growth in transfer lengths on the live ends and dead ends were investigated. The values from these comparisons are presented in Table 4-9.

Table 4-9: Effect of Time on Transfer Length

	Beam End	**Days After Transfer**	$\frac{l_{t,LT1}}{l_{t,i}}$	**Days After Transfer**	$\frac{l_{t,LT3}}{l_{t,i}}$
Conventional	**Dead**	2	1.01	48	1.01
	Live		1.05		1.04
SCC Mix 9	**Dead**	4	1.08	41	1.08
	Live		1.04		1.01
SCC Mix 7	**Dead**	3	1.20	41	1.27
	Live		0.98		0.97
SCC Mix 7b	**Dead**	3	1.14	28	1.14
	Live		1.00		0.99
SCC Mix 15	**Dead**	3	1.05	28	1.04
	Live		1.02		0.99
SCC Mix 13	**Dead**	4	1.07	28	1.08
	Live		1.00		0.97
SCC Fly Ash	**Dead**	3 or 4	1.14	28 or 41	1.16
	Live		1.01		0.99
SCC Slag	**Dead**	3 or 4	1.06	28 or 41	1.06
	Live		1.01		0.98
All SCC	**Dead**	3 or 4	1.10	28 or 41	1.11
	Live		1.01		0.99

The only mixture that showed more percentage growth in the live ends than in the dead ends was the conventional mixture: there was only 1% growth in the dead ends compared to 4% in the live ends over 48 days. For all the other mixtures, there was more average growth in the dead ends than in the live ends. In fact, the live-end transfer lengths for the SCC mixtures appeared to remain the same or decrease slightly on average over time. The decrease in transfer length was only on the order of one to two percent, which could be attributable to uncertainties in creep and shrinkage deformations. The average increase of transfer lengths in all dead ends was 11%, with a maximum growth of 27% in SCC Mix 7. There was no significant variation in the time-dependent behavior of transfer lengths among the different SCC mixture types (strength level or type of mineral admixture).

Growth for a majority of the transfer lengths in the dead ends stabilized within the first couple of days. This can be seen by comparing the normalized $l_{t,LT1}$ and $l_{t,LT3}$ results reported in Table 4-9. The only mixture that did not stabilize within the first two to four days was SCC Mix 7. The unstable behavior was observed in four out of the six dead-end specimens in that group. Specimens for this mixture had to be recast because of the excessive air content. Other studies have indicated mixed results concerning the growth of transfer length over time. Lane (1998) reported an average increase of 30% in the first twenty-eight days, and only 7% thereafter. Barnes et al. (2003) stated that there was no significant growth after the first few weeks after casting.

4.4.6 Comparison of Single-strand Verses Double-strand

This study consisted of specimens with two different strand configurations: single-strand specimens and double-strand specimens. By normalizing the transfer lengths from these specimen types with Equation 4-7 ($l_t = \alpha \frac{f_{pt}}{\sqrt{f'_{ci}}} d_b$), comparisons were made. The average proportionality constants for the single- and double-strand specimens are presented in Figure 4-9. The α value for the average data of single-strand specimen transfer lengths was 0.62. The average data of double-strand specimen transfer lengths had a α value of 0.80. Thus, the average normalized transfer lengths for the double-strand specimens were 29% longer than the average transfer lengths for the single-strand specimens. The correlation value of the single-strand specimens was 0.30 and the double strands had a correlation value of 0.33.

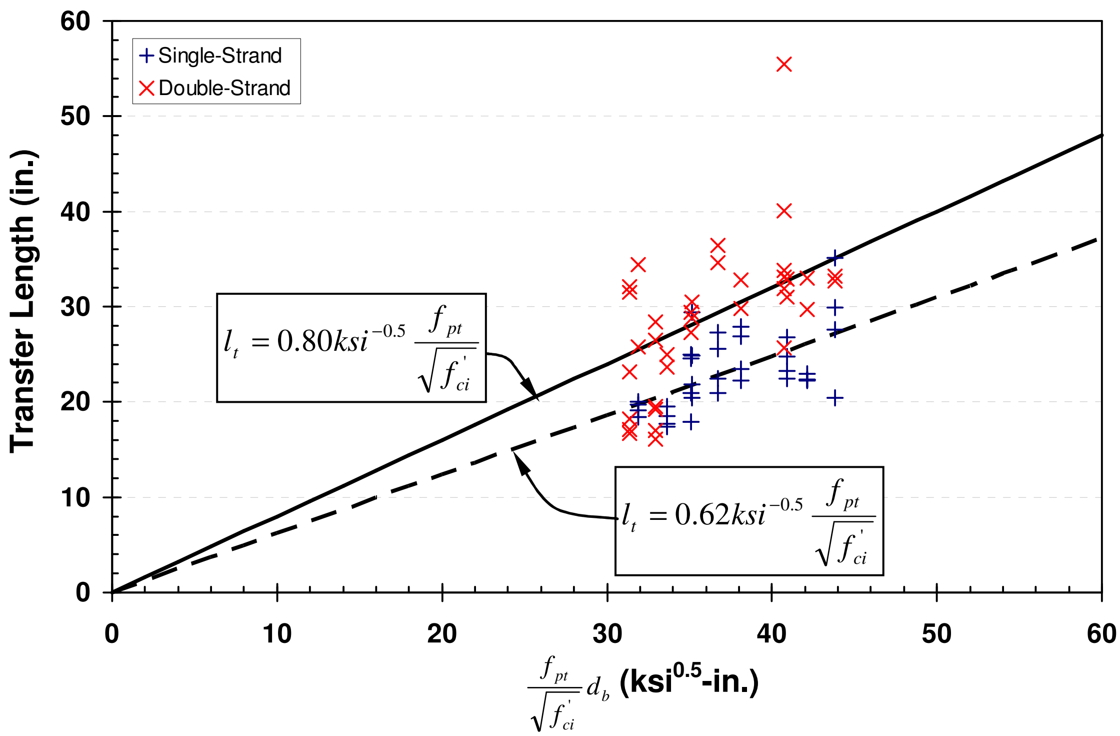

Figure 4-9: Comparisons of Transfer Lengths between Different Strand Configurations

As for the effects of time, there was no identifiable pattern to the difference in behavior when the transfer lengths in the single-strand specimens were compared to those in the double-strand specimens. In some cases the double-strand specimens experienced more growth than the single-strand specimens of the same mixture, and in other cases the opposite occurred.

4.5 COMPARISONS OF TEST DATA WITH RECOMMENDED EXPRESSIONS

From the first published code expression in 1963 (ACI318-1963) to the present, many different expressions for determining transfer lengths have been recommended. While some researchers recommended expressions based on data collected from specimens cast in a single study, other expressions have resulted from statistical analyses performed on a collection of data from many different transfer length studies. As discussed earlier, the expression that contained some form of concrete strength resulted in much better correlation to the data collected in this study. Comparisons of transfer length data from this study with recommended expressions that contain a concrete strength parameter and those that do not are discussed in this section.

By applying linear regression analysis to the test data from this research, the best-fit expression discussed in Section 4.4.2 was determined. The expression, $l_t = 0.82ksi^{-0.5} \frac{f_{pt}}{\sqrt{f_{ci}^{'}}} d_b$, was the upper bound for 95% of the dead-end transfer lengths. The upper bound of 95% of the live-end transfer lengths is given by the expression $l_t = 1.10ksi^{-0.5} \frac{f_{pt}}{\sqrt{f_{ci}^{'}}} d_b$. These expressions incorporate the value of strand prestress immediately after transfer, f_{pt}, and the concrete strength at transfer, $f_{ci}^{'}$. For comparisons to other expressions that will be discussed in this section, the predicted transfer lengths using the expression $l_t = 1.10 ksi^{-0.5} \frac{f_{pt}}{\sqrt{f'_{ci}}} d_b$ for the live-end data and

$l_t = 0.82 ksi^{-0.5} \frac{f_{pt}}{\sqrt{f'_{ci}}} d_b$ for the dead-end data were plotted in Figure 4-10 against the

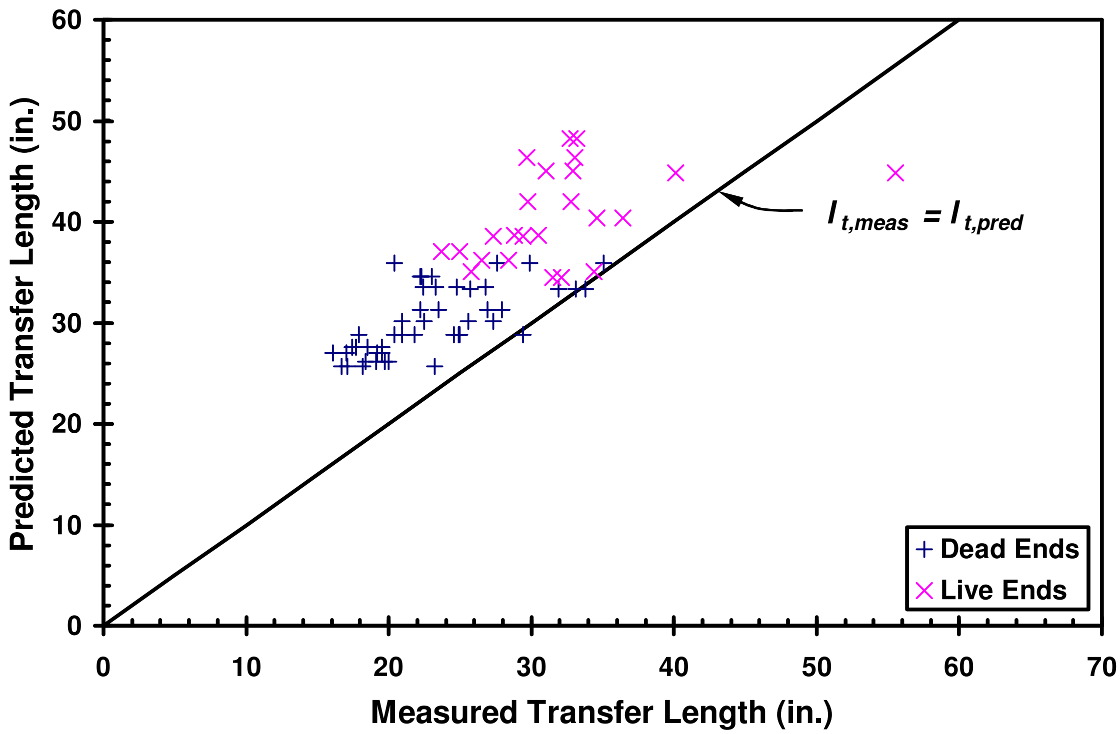

Figure 4-10: Comparison of Best-Fit Upper-Bound Relationships to Measured Transfer Lengths

measured transfer lengths from this study. A line running through the origin in this figure shows where the measured transfer length equals the predicted transfer length. For design purposes, this line should represent the upper bound of 95% of the measured transfer lengths. Since the measured transfer lengths are represented on the horizontal axis, any data points that fall below this line of equality are considered unconservative. All of the data ideally should fall closely along the predicted side of the line of equality.

In Figure 4-10, this is reasonably true for the data from this study. It is important to note that the 95% of the data compares very well to this expression because this relationship was based solely on transfer lengths from this study.

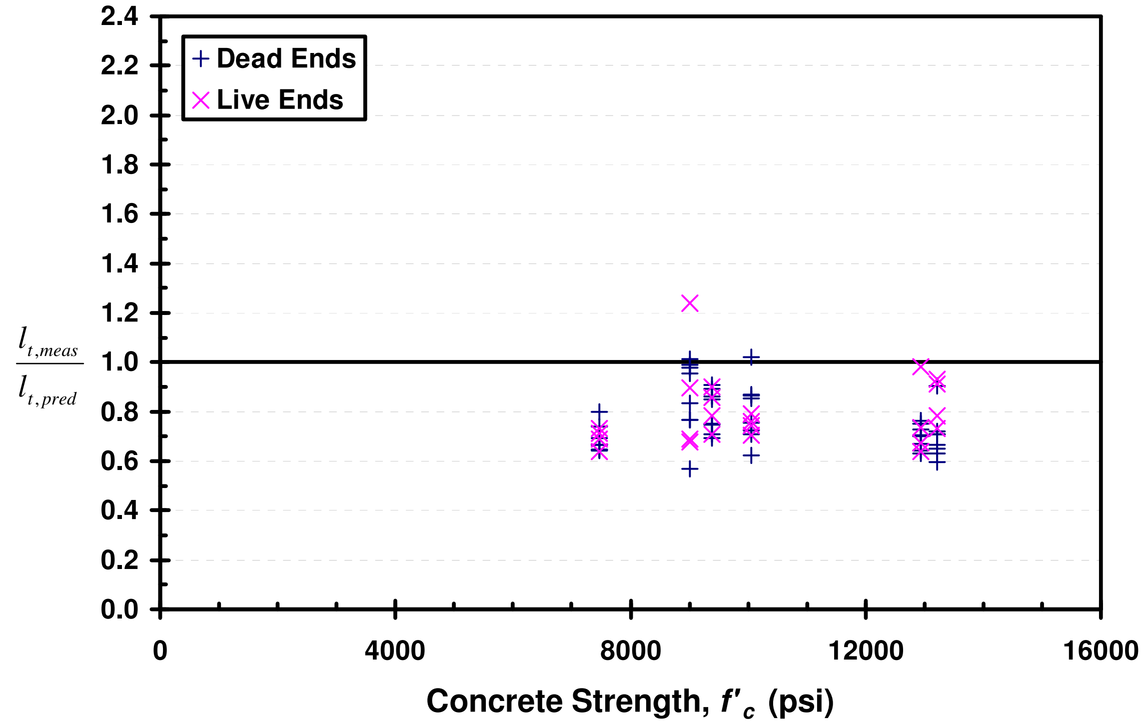

Figure 4-11: Comparisons to Best-Fit Upper-Bound Relationships to Concrete Strength

Figure 4-11 is a plot of the ratios of transfer length predicted from these two expressions to the measured transfer length versus the 28-day concrete strength, $f_c^{'}$. This figure and other similar figures that follow illustrate how conservative the expressions estimate the transfer length across a wide range of concrete strengths. Like before, 95% of the data should fall below the line of unity, which is now the horizontal line $\frac{l_{t,meas}}{l_{t,pred}}$ = 1.0. As shown in Figure 4-11, it is clear that as the concrete strengths increase, the data points remain evenly spread under the line of unity. This indicates that these two expressions correlate well to the data across the full range of concrete strengths.

4.5.1 RECOMMENDED EXPRESSIONS THAT NEGLECT CONCRETE STRENGTH

The transfer lengths predicted from the expression $l_t = \frac{f_{pe}}{3000} d_b$ located in Article 12.9.1 of ACI 318-05 are compared to the measured transfer lengths in Figure 4-12. This equation is unconservative for the some of the data collected in this investigation. As discussed in Section 2.5.1, this equation originated based on an average of transfer lengths from three different studies. In Figure 4-13, the lack of conservatism can be seen when comparing this equation over the range of concrete strengths from this study. The majority of the live-end values are above the unity line.

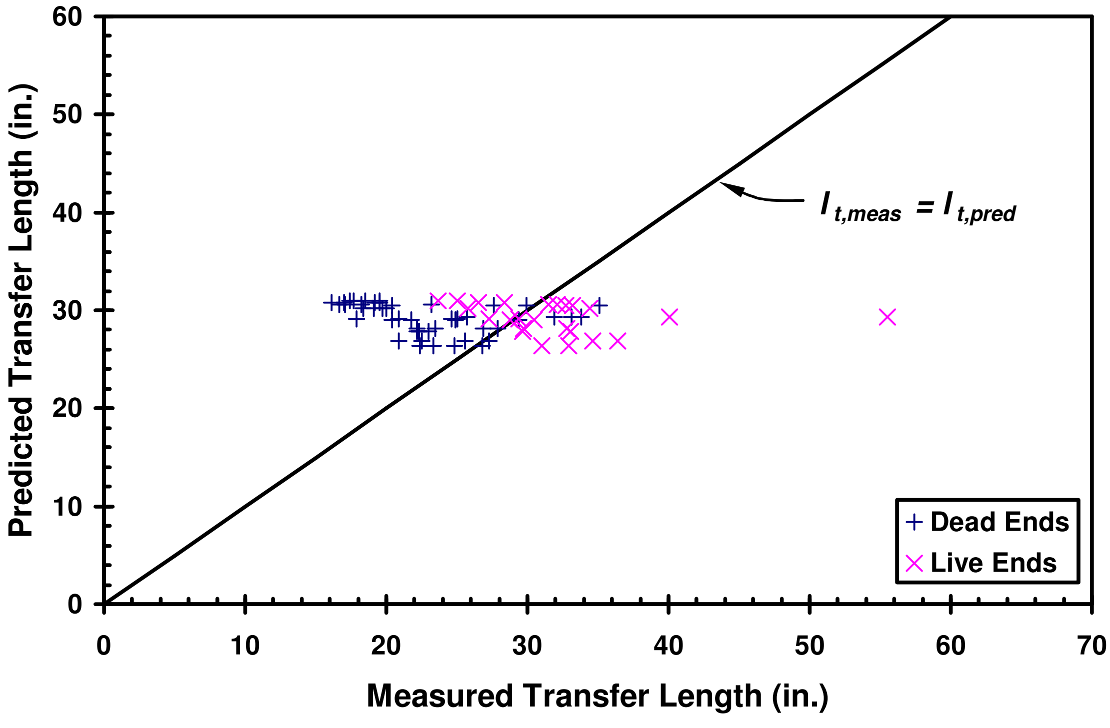

Figure 4-12: Comparison of ACI 318-R12.9 Values to Measured Transfer Lengths

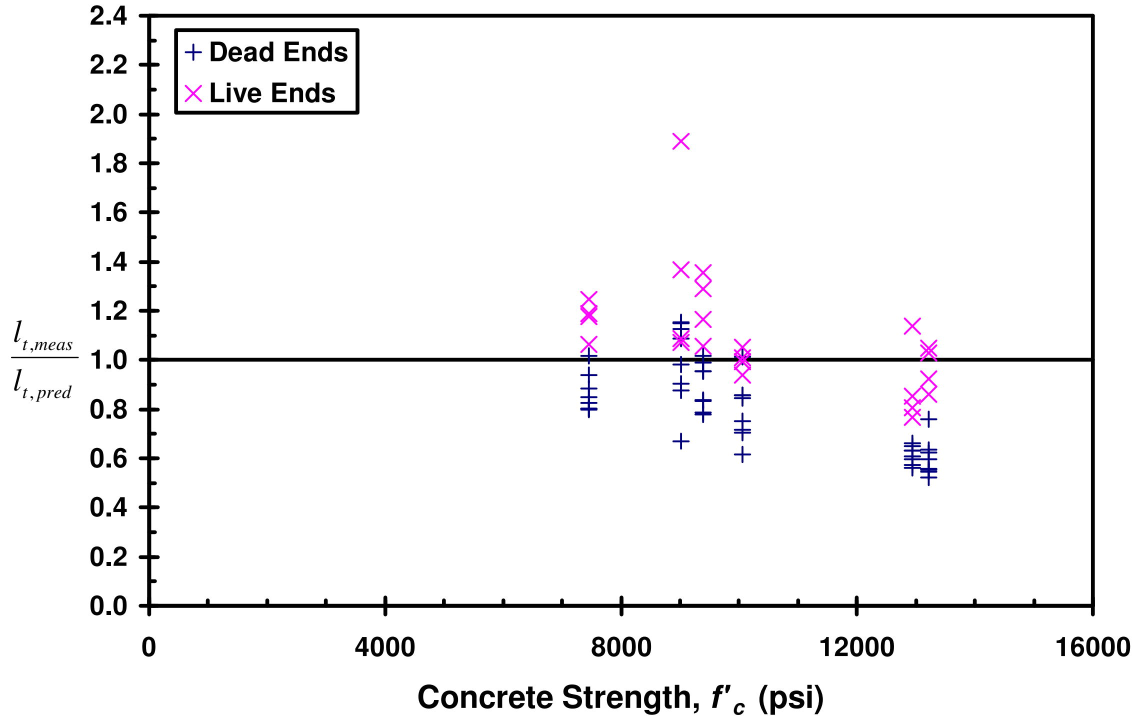

Figure 4-13: Comparison to ACI 318-R12.9 to Concrete Strength

The next group of recommended expressions that exclude the concrete strength are included in the shear provisions of ACI 318-05, AASHTO Standard, and AASHTO LRFD. Figures 4-14 and 4-15 compare the data from this study to the relationship for transfer length found in the ACI Building Code (ACI 318-05. 11.4.3, 11.4.4) and the AASHTO Standard Specifications (AASHTO 2002 9.20.2.4), $l_t = 50d_b$. In Figures 4-16 and 4-17, the data from this study are also compared to the expression for transfer length included in the AASHTO LRFD Specifications (AASHTO 2004 5.11.4.1), $l_t = 60d_b$. Neither expression is a satisfactory upper bound for the test data. This is especially true for the live-end transfer lengths. These expressions are unconservative for transfer lengths from the live ends of the test specimens. As for the dead-end transfer lengths, these expressions bound the majority of the data. The second equation, $l_t = 60d_b$, has a larger multiplier than the other; as a result, this equation was found to be more conservative. When comparing the ratio of these equations to the measured transfer lengths for the dead-end data over the range of concrete strength, a trend exists as the concrete strengths increase. For lower strength data, a majority of the transfer lengths appear above the upper-bound line. As the strengths increased, these equations appear to become more and more conservative. If a line were drawn connecting the average of the dead-end groups across the concrete strength range, a negative slope would result. A best-fit expression would result in an approximately horizontal line, slightly below the line of unity.

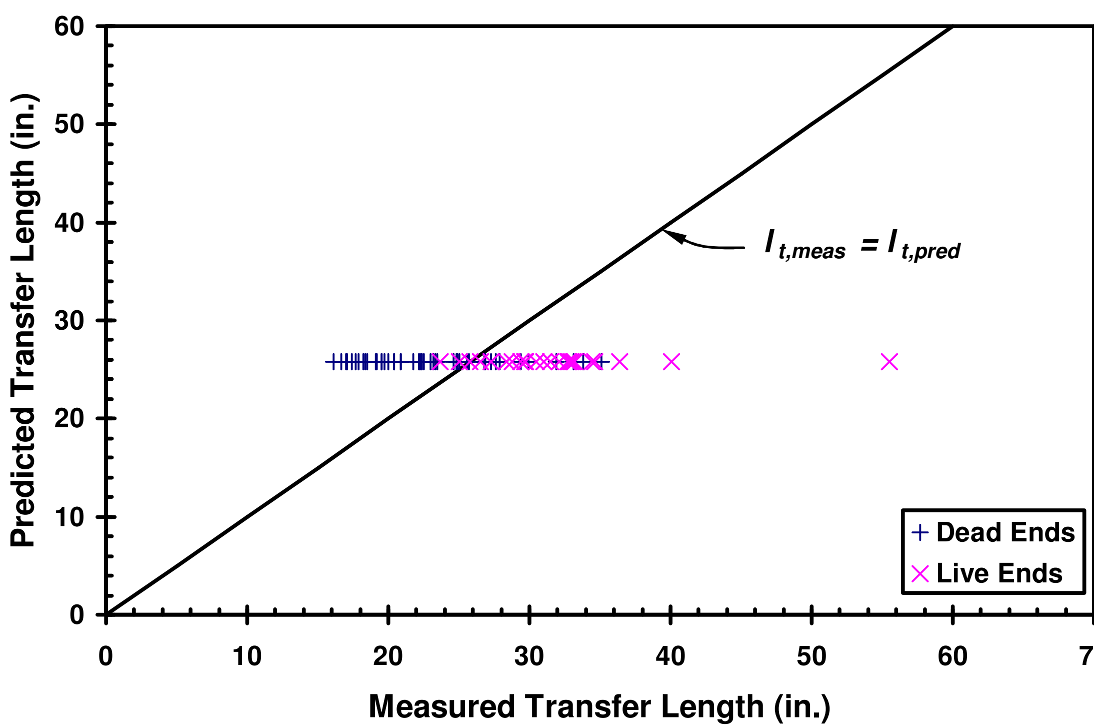

Figure 4-14: Comparison of Values from ACI 318 and AASHTO Standard Shear Provisions to Measured Transfer Lengths

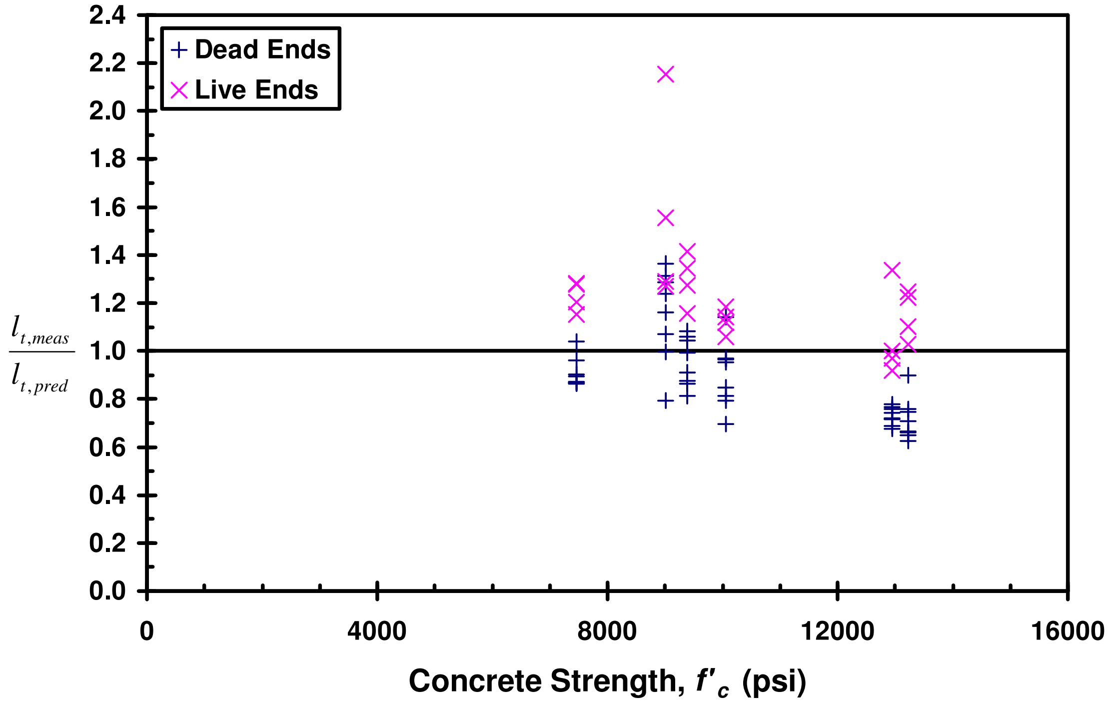

Figure 4-15: Comparison to Values from ACI 318 and AASHTO Standard Shear Provisions to Concrete Strength

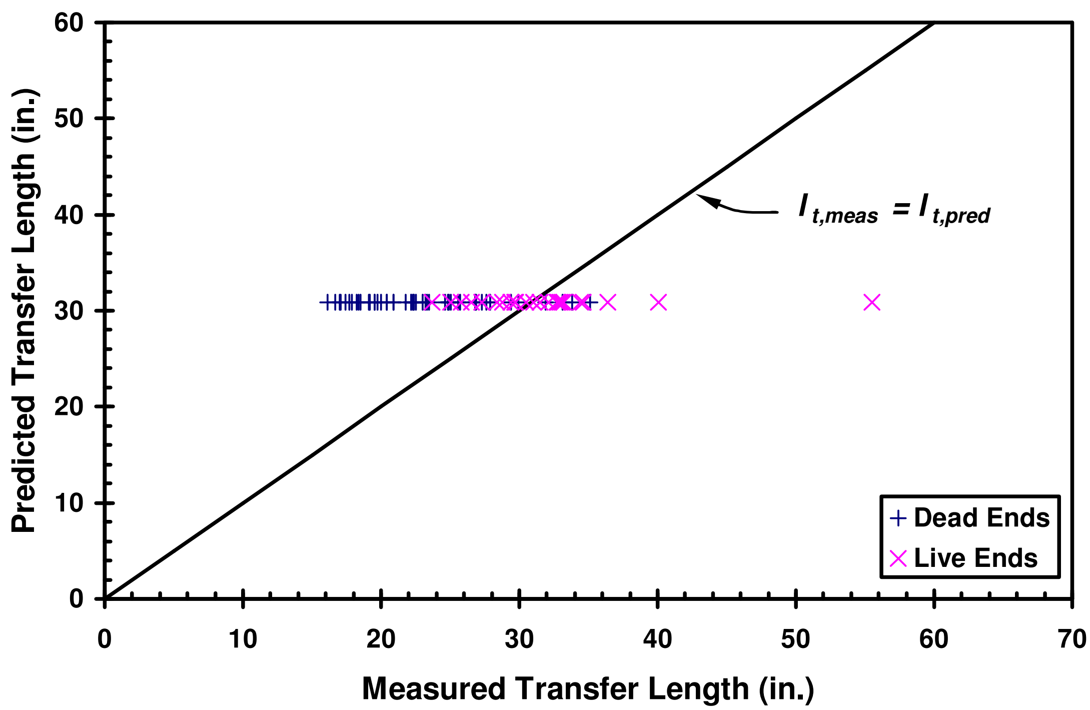

Figure 4-16: Comparison of Values from AASHTO LRFD to Measured Transfer Lengths

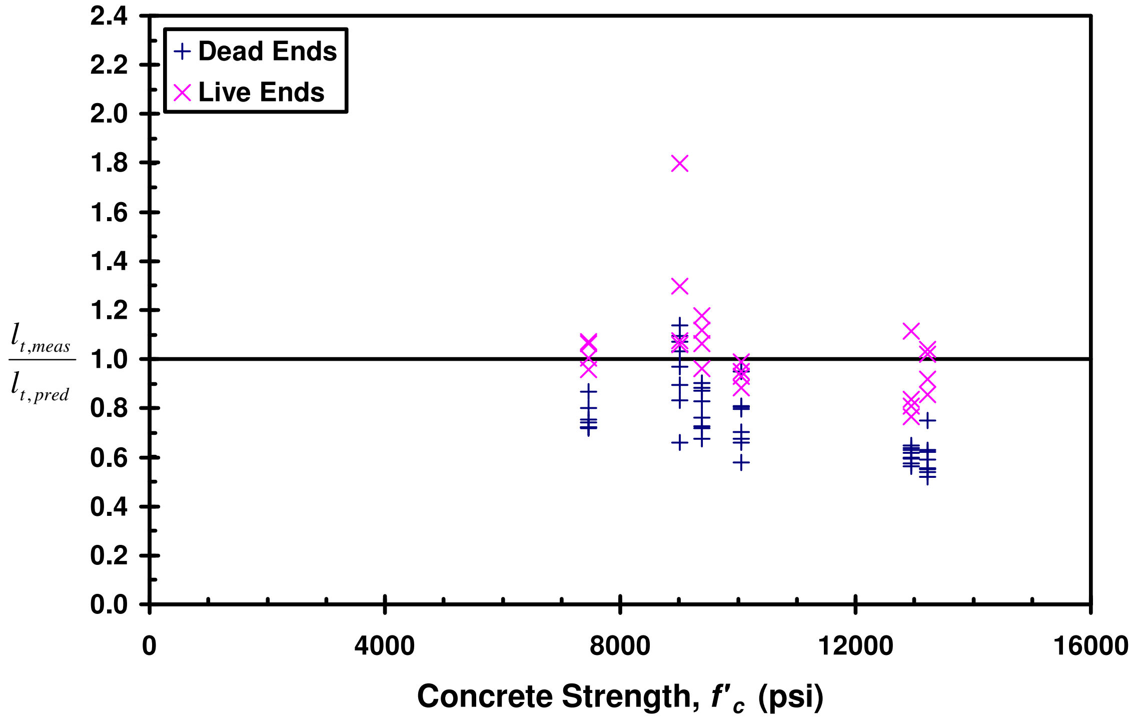

Figure 4-17: Comparison of Values from AASHTO LRFD to Concrete Strength

4.5.2 Expressions that contain Concrete Strength

Expressions that contain concrete strength in some form correlate with data from the present study much better than those that do not. Figure 4-18 and 4-19 compare the results from this study to the relationship developed by Zia and Mostafa (1978), $l_t = 1.5 \frac{f_{pt}}{f'_{ci}} d_b - 4.6$ in. This expression was developed by performing a statistical analysis with data from several published studies and determining the overall best-fit equation; this empirical equation was not based on any theory. Physically-based transfer lengths from specimens with 28-day concrete compressive strengths ranging from 2,000 to 8,000 psi were used to formulate the expression. Concrete strengths routinely exceed this range in modern prestressed bridge girders. Figures 4-18 and 4-19 illustrate how

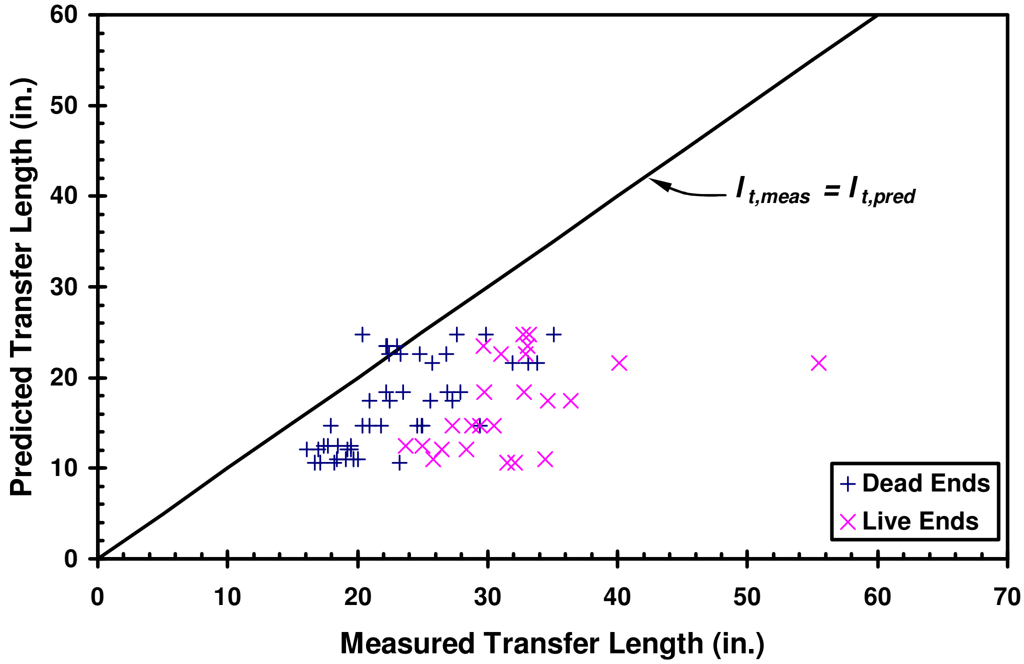

Figure 4-18: Comparison of Values from Zia and Mostafa (1978) Expression to Measured Transfer Lengths

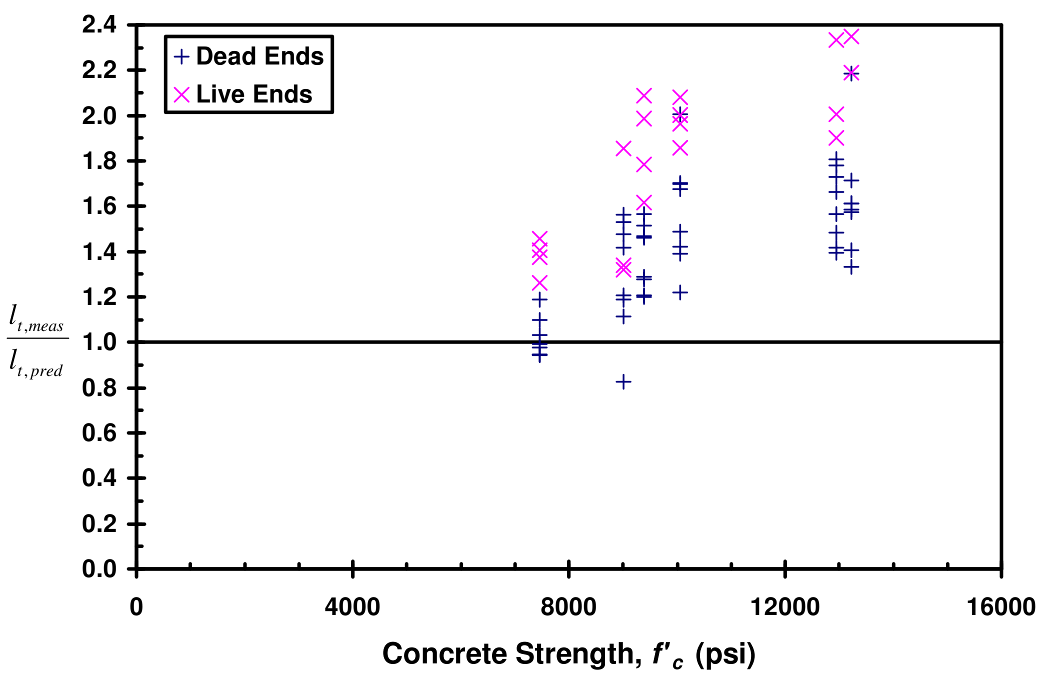

Figure 4-19: Comparison of Values from Zia and Mostafa (1978) Expression to Concrete Strength

ineffective this expression is for predicting the transfer lengths from this study. For all concrete strengths included, the transfer lengths predicted become increasingly unconservative. It is clear from the comparison that this expression cannot effectively represent data from the present study.

The next expression, $l_t = 4\frac{f_{pbt}}{f_c^{'}}d_b - 5in.$, is the transfer length portion of the development length equation developed by Lane (1998) and currently included in the AASHTO LRFD Specifications (AASHTO 2004, 5.11.4.2). This research and the background of this equation's developement were discussed at length in Section 2.5. Like the Zia and Mostafa expression, this relationship is based on statistical analysis alone and not on physical theory. This is the reason for the constant value of -5 in. included in the equation. Application of this equation with prestress values approaching zero and/or very high concrete strengths would produce a negative value for transfer length; clearly, there is no possible way this could physically happen. Data used in the equation's development was limited to 28-day concrete strengths less than 10 ksi. If the 28-day strength is higher than this, a value of $f_c^{'}$ = 10 ksi must be used in the expression.

Figure 4-20 compares the values from this expression to the measured transfer lengths. These predicted transfer lengths included the limitation of $f_c^{'}$ = 10 ksi. Unlike all the other expressions, both the dead-end and the live-end measurements were shorter than predicted, except for one that exceeded the upper bound. Figure 4-21 shows how this expression, calculated with the 10-ksi limitation, performs over the full concrete strength range. Over ninety-five percent of the data were below the upper bound, indicating this is a conservative expression when considering both the dead- and live-end transfer lengths. However, must of the data were well below the upper bound, which indicates that the expression may be overly conservative. This figure illustrates the trend of expression to get more conservative at higher levels of actual concrete strength when the value of $f_c^{'}$ used is limited to 10 ksi. The negative slope through the higher concrete strengths is apparent in this comparison. The expression appears to be least conservative for concrete strengths near 9 ksi. As the concrete strengths move away from this value (higher and lower) the conservatism increases.

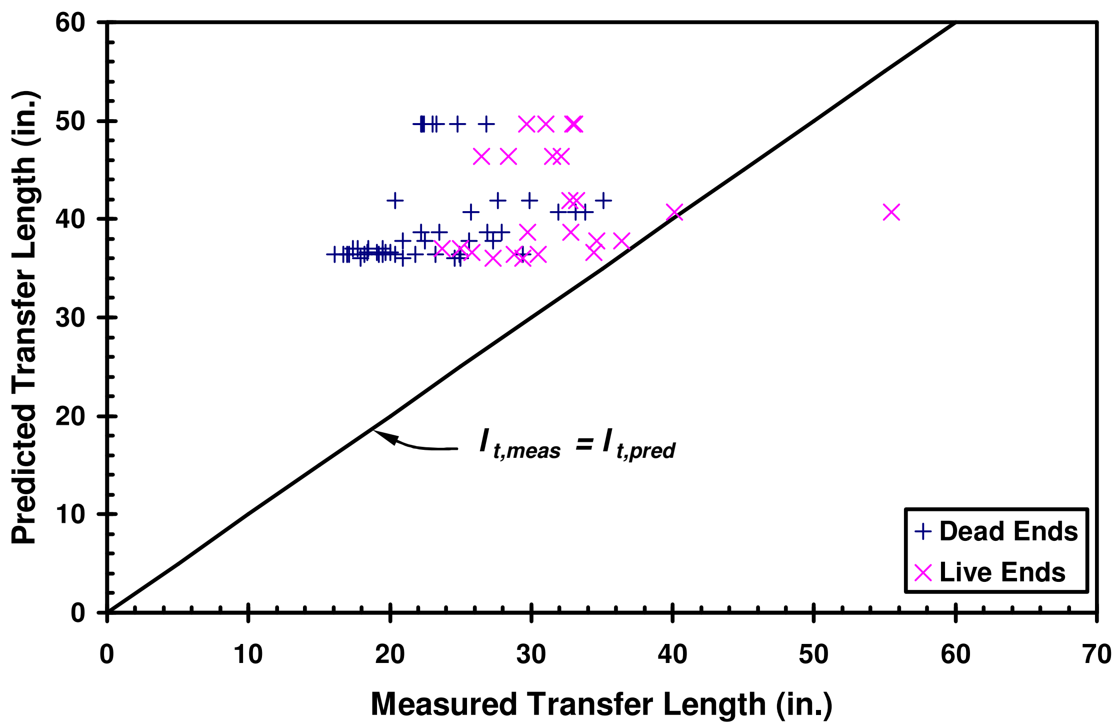

Figure 4-20: Comparison to Values from Lane (1998) Expression to Measured Transfer Lengths

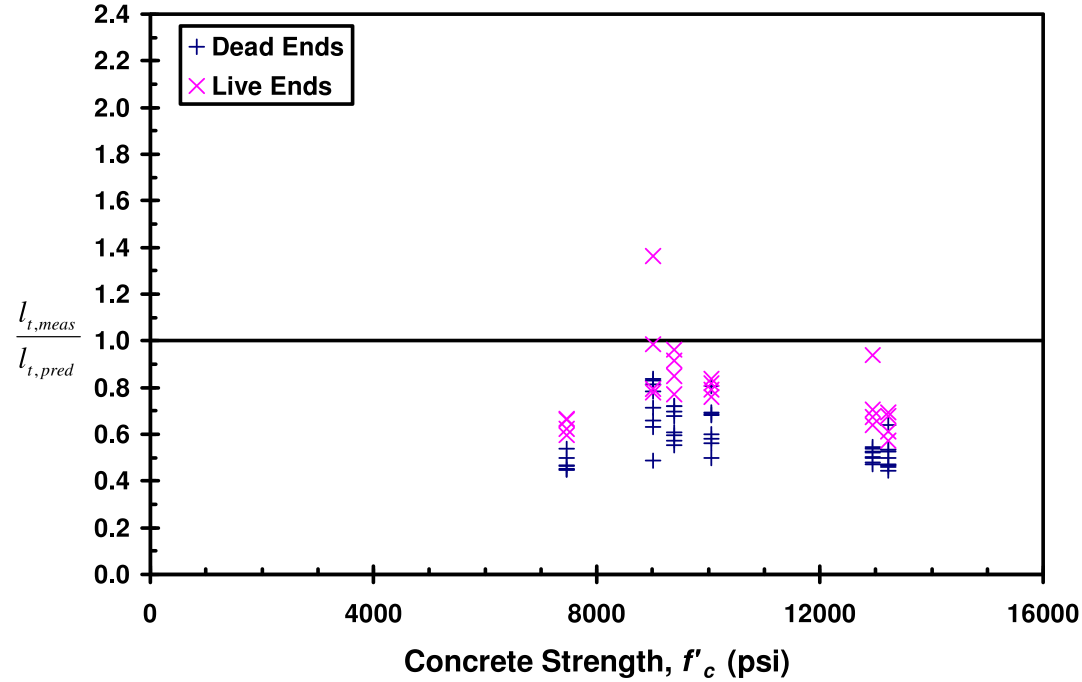

Figure 4-21: Comparison to Values from Lane Expression to Concrete Strengths

When 28-day concrete compressive strengths exceeding 10 ksi are used in the Lane expression, the transfer length predictions become less conservative. This observation is apparent in Figures 4-22 and 4-23. The $f_c^{'}$ limitation was neglected for the predicted values in these two figures, which resulted in live-end transfer lengths that exceeded their corresponding predictions. Since it has become common for pretensioned members to have 28-day concrete compressive strengths well over 10 ksi, this equation will not effectively bound transfer lengths across the full range of practical concrete strengths. Therefore, the 10-ksi limitation should not be lifted from the Lane expression.

While the expressions developed by Zia and Mostafa (1978) and Lane (1998) included concrete compressive strength, the model that best fit all of the data from this parameter

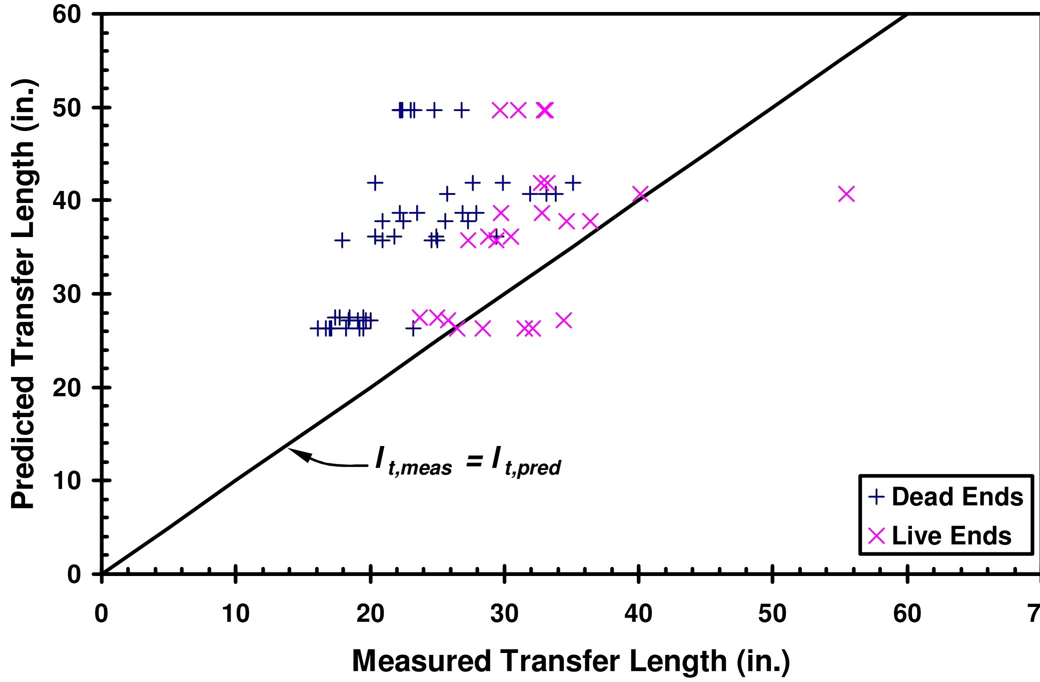

Figure 4-22: Comparison to Values from Lane Expression to Measured Transfer Lengths (Excluding the Limitation $f_c^{'} = 10$ ksi)

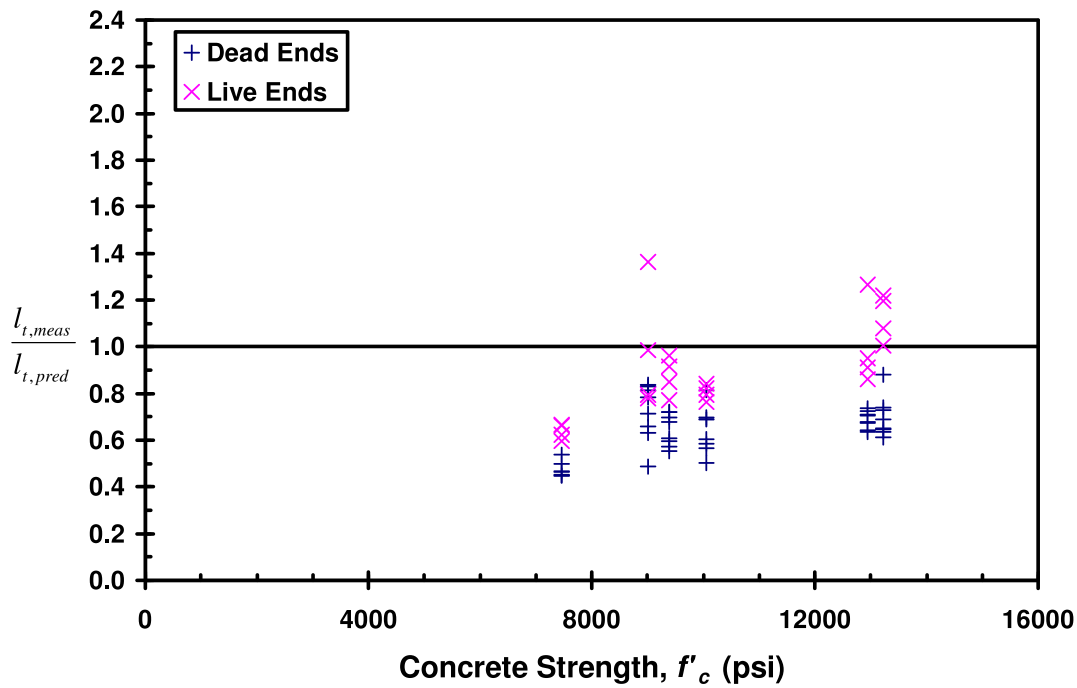

Figure 4-23: Comparison to Values from Lane Expression to Concrete Strengths (Excluding the Limitation $f_c^{'} = 10$ ksi)

is used in the expression recommended by Barnes et al. (2003), $l_t = 0.57\ \text{ksi}^{-0.5} \frac{f_{pt}}{\sqrt{f'_{ci}}} d_b$.

This expression was the result of an experimental study involving 0.6-in. strand in full-scale AASHTO Type II beams with 28-day concrete strengths ranging from 5700 to 14,700 psi. The equation in question was developed to be an upper bound for 95% of the data from that study. Possibly because of the smaller size of the specimens in the present study, that expression is not an accurate upper bound for the data collected. Although the expression results in unconservative predictions for most of the transfer lengths in this study, Figures 4-24 and 4-25 indicate that the prediction error remains relatively uniform over the full range of concrete strengths.

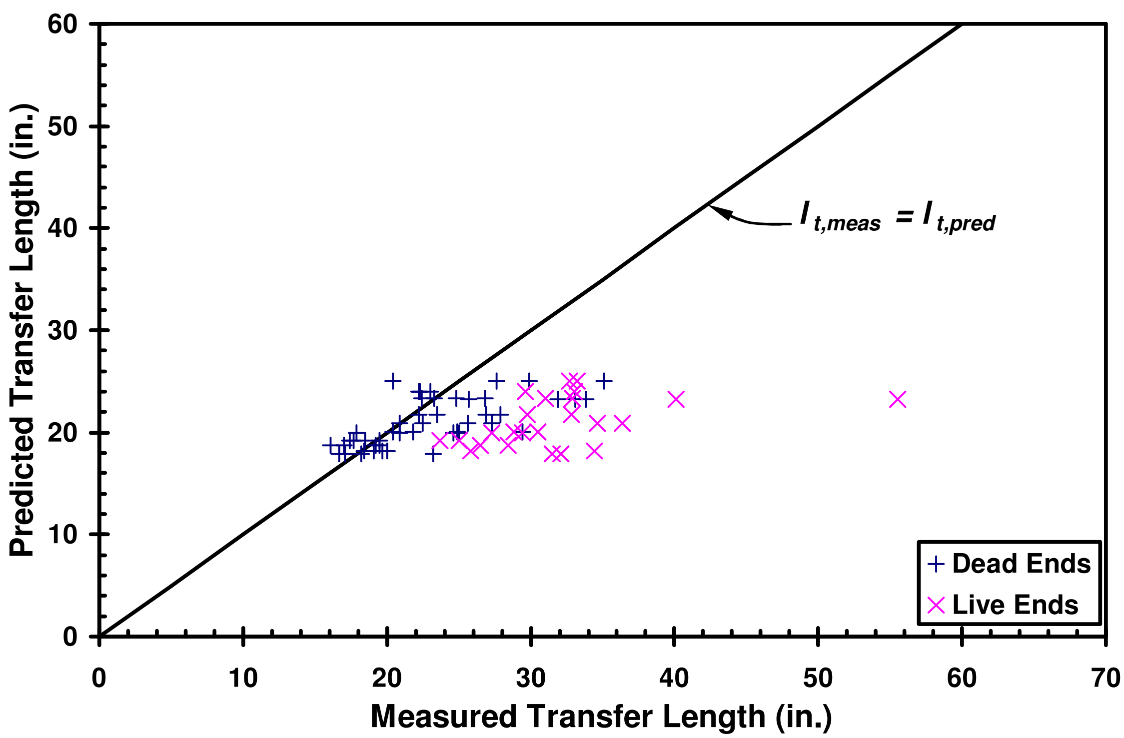

Figure 4-24: Comparison of Values from Barnes et al. Expression to Measured Transfer Lengths

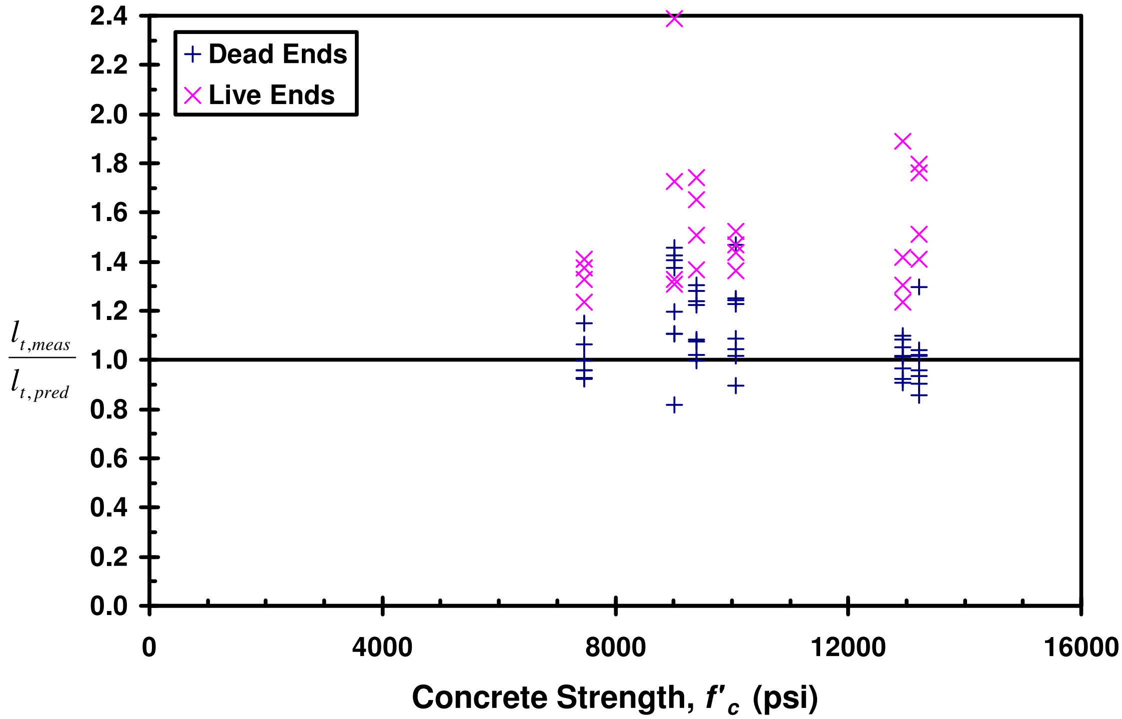

Figure 4-25: Comparison of Values from Barnes et al. Expression to Concrete Strengths

4.6 SUMMARY AND CONCLUSIONS

This study investigated the transfer lengths for five different concrete mixtures: one conventional mixture and four SCC mixtures. One of the high-strength mixtures, SCC Mix 7, was cast twice due to an unacceptable air content. Even though there was an excessive air content, the transfer lengths were still consistent with the other SCC mixes; therefore, the transfer length data from this mixture were still included in the comparisons. For each mixture, three single-strand specimens and three double-strand specimens, ten feet in length were cast, totaling thirty-six specimens for the entire test study. Since there were two live ends for each of the two strand patterns in a mixture, a total of forty-eight dead-end and twenty-four live-end transfer lengths were obtained.

From all the prediction models investigated, the model from the relationship recommended by Barnes et al. (2003), $l_t = \alpha \frac{f_{pt}}{\sqrt{f_{ci}^{'}}} d_b$, produced the best correlation with the data from this study. The dispersion of dead-end transfer length was much less than that from the live ends. After normalizing the results with respect to $\frac{f_{pt}}{\sqrt{f_{ci}^{'}}} d_b$, the specimens cast with SCC exhibited dead-end transfer lengths 14% longer than dead-end transfer lengths in conventional concrete. For the live ends, transfer lengths from the specimens cast with SCC were 17% longer than the average transfer lengths of specimens cast with conventional concrete.

Code expressions pertaining to transfer lengths were found to be unconservative when compared with data from this study, except in specimens with higher levels of concrete compressive strength. At the higher values of compressive strength, these expressions became increasingly conservative. These expressions were found in Sections 12.9 and 11.4 of ACI 318-05 (2005), Article 9.20.2.4 of AASHTO Standard (AASHTO 2002), and Article 5.11.4.1 of AASHTO LRFD (AASHTO 2004). The transfer length portion of the alternative development length expression in Article 5.11.4.2 of AASHTO LRFD (AASHTO 2004) was found to be conservative throughout all concrete compressive strength levels as long as the f'_c limitation was employed. Using the limitation of $f_c^{'}$ = 10 ksi given in this article, this equation became increasingly conservative in specimens of higher concrete compressive strengths. Without this limitation, many of the transfer lengths predicted by this expression for the high-strength specimens were unconservative. None of the code expressions accurately predicted the trend of the transfer lengths to decrease with increasing concrete compressive strength.

Transfer lengths of specimens cast with SCC mixtures containing two different mineral admixtures were consistent. There was an average increase of 43% from dead-end to live-end transfer lengths with SCC using Class C fly ash. For SCC that contained 100-grade GGBF slag as the mineral admixture, there was a 34% increase from dead-end to live-end transfer lengths. The average increases of 38% among the SCC mixtures resemble the average 35% increase from dead ends to live ends experienced with the specimens cast with conventional concrete. The average of the normalized, double-strand transfer lengths were 29% longer than the average, normalized, single-strand transfer lengths.

Only a small average growth with time (5% or less) was observed among the dead-end and live-end transfer lengths in the specimens cast with conventional concrete. An average 10% growth over time was experienced in the dead ends with specimens cast with SCC, with a maximum average growth of 27% in the dead ends cast with SCC Mix 7. No significant differences of growth existed between SCC mixtures with different types of mineral admixtures, or among the single- and double-strand specimens. For all mixtures, the growth of the transfer lengths stabilized within the first several days after prestress transfer.

For this test data, the best-fit, upper-bound expression that exceeded 95% of the dead-end transfer lengths for SCC specimens was $l_t = 0.82\ \text{ksi}^{-0.5} \dfrac{f_{pt}}{\sqrt{f'_{ci}}} d_b$. Increasing this expression by 35%, $l_t = 1.10\ \text{ksi}^{-0.5} \dfrac{f_{pt}}{\sqrt{f_{ci}^{'}}} d_b$, resulted in the best-fit, upper-bound expression for 95% of the live-end transfer lengths. These expressions provide the best correlation among the data from SCC specimens throughout the entire range of concrete strength. Because these expressions are based on test results from small specimens, only the model of these expressions is recommended for determining transfer lengths in full-scale pretensioned beams cast with SCC. Further testing is necessary to calibrate the model for full-size beams.

In most cases, an upper-bound estimate of transfer length is desirable; however, for comparison with allowable stress limits at transfer, it is usually conservative to use a lower-bound estimate.

CHAPTER 5

DRAW-IN TESTING

5.1 INTRODUCTION

When the prestress force is transferred in pretensioned beams, the inward movement of the free strand relative to the beam end is referred to as strand draw-in. The term "free end slip" is often used instead of draw-in; however, because the former term has multiple meanings for different types of bond behavior, the latter term is used in this thesis. Draw-in measurements were performed on all specimens in this study in conjunction with the transfer length measurements discussed in Chapter 4. Results of draw-in testing and comparisons of these results to the transfer length test results are presented in this chapter.

5.2 BACKGROUND

Transfer lengths of pretensioned strands can be determined from the measured strand draw-in by applying fundamental mechanics and strain compatibility. More simply, the transfer length of a pretensioned strand can be calculated based on the differences between concrete and steel strains throughout the transfer zone (Rose and Russell 1997). They report that the draw-in length, $l_{draw\text{-}in}$ in pretensioned elements can be determined by:

$$l_{draw\text{-}in} = \Delta_{ps} - \Delta_c \qquad \textbf{\textit{Equation 5-1}}$$

where:

Δ_{ps} = total elastic shortening of tendon along transfer length, and

Δ_c = total elastic shortening of concrete along transfer length.

Immediately following prestress transfer, the stress in the strand ranges from zero stress at the free end of the specimen to a value f_{pt} at the end of the transfer length. The elastic shortening of both the tendon and concrete may be calculated by integrating steel and concrete strain changes that result from the transfer of prestress over the transfer length (Barnes et al. 1999). As a result, further derivation of Equation 5-1 gives:

$$l_{draw-in} = \int_{l_t} \left(\Delta\varepsilon_p - \Delta\varepsilon_c \right) dx \qquad \textit{\textbf{Equation 5-2}}$$

where:

$\Delta\varepsilon_p$ = change in steel strain resulting from transfer of prestress, and

$\Delta\varepsilon_c$ = change in concrete compressive strain resulting from transfer of prestress.

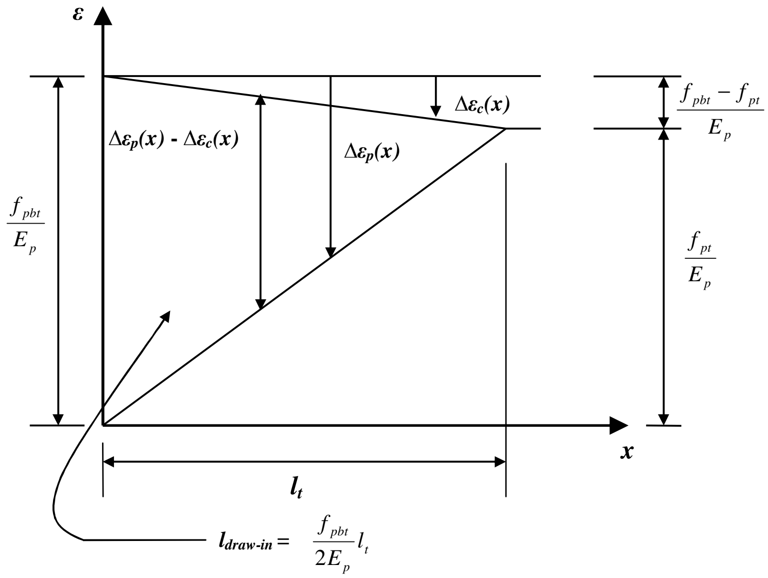

Figure 5-1: Relationship between Draw-In and Transfer Length (Anderson and Anderson 1976)

As illustrated in Figure 5-1, where $x = 0$ represents the free end of a strand, the change of strain in the tendon over the transfer length may be taken as $\frac{f_{pbt} - f_{pt}}{E_p}$. The concrete and steel strain changes are compatible at the end at the end of transfer length (Barnes et al. 1999). This compatibility results in Equation 5-3 at this location:

$$\Delta\varepsilon_c = \Delta\varepsilon_p = \frac{\Delta f_p}{E_p} = \frac{f_{pbt} - f_{pt}}{E_p} \qquad \textbf{\textit{Equation 5-3}}$$

where:

Δf_p = change in steel stress resulting from transfer of prestress,

E_p = modulus of elasticity of the prestressing steel, and

f_{pbt} = stress in the prestressing steel immediately prior to transfer.

Assuming the buildup of prestress force in the tendon varies linearly along the transfer length, Equation 5-2 simplifies to:

Equation 5-4

$$l_{draw-in} = \frac{f_{pbt}}{2E_p} l_t$$

which is graphically represented by the triangular area indicated in Figure 5-1. By rearranging Equation 5-4, the transfer length can be calculated from the measured draw-in. The resulting expression in Equation 5-5 is:

Equation 5-5

$$l_t = \frac{2E_p}{f_{pbt}} l_{draw-in}$$

Since it is proportional to the transfer length, the draw-in should indicate the quality of transfer bond development in a pretensioned member (Anderson and Anderson 1976). Rose and Russell (1997) found that measured transfer lengths in test specimens compared very well to transfer lengths predicted from measured draw-in values using the relationship expressed in Equation 5-5. Among several bond performance tests, prediction of transfer length by draw-in correlated best to the data. To better predict the transfer lengths from draw-in values, the authors recommended inclusion of a proportionality constant in the expression to result in a safe upper bound for the data. Results of research conducted by Barnes et al. (1999) indicated that, on average, the values predicted by Equation 5-5 slightly underestimated the transfer lengths. They recommend that this method should only be used for determining general trends in bond behavior, not for trying to predict transfer lengths in small sample sizes.

Equation 5-5 is based on the assumption that the steel stress gradient is linear throughout the transfer length, i.e. the transfer bond stresses are uniform throughout. If the bond stresses are largest at the end of the member and decrease along the transfer length, the steel stress profile will be nonlinear and concave-down. If this is the case, Equation 5-5 will underestimate the actual transfer length.

5.3 DRAW-IN TEST PROCEDURE

The identical procedure for measuring draw-in was used for every set of prestressed specimens in the study. Before initial stressing, six pieces of plastic heat-shrink tubing were slid onto each strand so that a piece of tubing was on each strand at each specimen end. The inside portion of the plastic heat-shrink tubing was coated with an adhesive. The pieces were cut to one-inch lengths to allow for good bonding action between the tubing and the strands. Before casting, the heat-shrink tubing was positioned outside of the end forms, as illustrated in Figure 5-2. After form removal, researchers marked a line one inch from the specimen end on each strand and heated the tubing so that the end of the tubing closest to the specimen abutted this mark. A heat gun was used to shrink the tubing. After the heat-shrink tubing was in place, researchers spray-painted both ends of the tubing to mark its position. Because of the sudden, violent force that results from flame cutting, there was a good possibility that the strand could slip through the tubing at transfer. By painting either end, this slippage would be noticed and measurements could be addressed accordingly. Figure 5-3 shows a specimen end after preparations for draw-in measurements were completed.

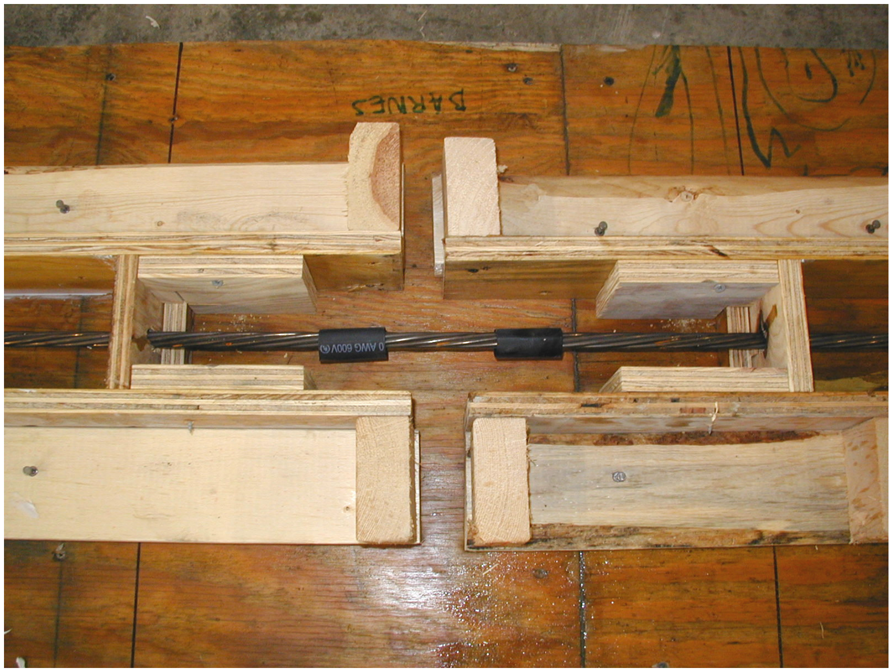

Figure 5-2: Heat Shrink Tubing in Place Prior to Casting of Specimens

Figure 5-3: Heat-shrink Tubing Bonded and Painted

Once the preparations were completed, the distance between the surface of the specimen end and the closest end of the heat-shrink tubing specimen was measured. To ensure more accurate data, this distance was measured in two different places: along the top and side of the strand. Calipers that can measure to the nearest 0.001 in. were used for determining these distances. Benchmark readings were taken and recorded prior to cutting the strands; the location on the concrete surface from which each distance was measured from was marked so that the post-transfer readings were taken from the same location. This procedure is shown in Figure 5-4.

Figure 5-4: Performing Draw-In Benchmark Readings

Draw-in measurements were taken immediately after transfer and at the same time as the later transfer length readings described in Section 5.2. In several instances, loss of concrete surrounding the strand occurred at prestress transfer. The accuracy of the draw-in values for these specimen ends was suspect, resulting in data that were not consistent with other values; however, these values were included in the analysis for comparison purposes. Another factor that led to inconsistent data was the unraveling of the strands on the cut ends. In Figure 5-5, concrete loss and strand unraveling at the cut end is shown. To help prevent the unraveling of the strands, two hose-clamps were fastened along the strand at each live end. While some of the strands in the later test specimens still unraveled, the degree of this unraveling was decreased significantly. To ensure the most accurate estimate of deformations possible for the draw-in testing program, one researcher performed all of these measurements.

Figure 5-5: Concrete loss and Strand Unraveling Due to Sudden Prestress Transfer

5.4 DETERMINATION OF DRAW-IN VALUE

The determination of the draw-in value for each specimen end in the study was a straightforward process. The draw-in was calculated by taking the difference of the measured distance at each time of reading from the benchmark distance measured prior to prestress transfer. The portion of the tendon between the end of the concrete and the reference point contracts freely as a result of the decrease in stress from f_{pbt} to zero stress. While this unrestrained contraction is reflected in the total distance change, it is not a part of the actual draw-in. This free contraction was calculated over the distance from the end of the specimen to the reference location on the tendon. The value of the free contraction was calculated as $\frac{f_{pbt}}{E_p}\Delta_o$, where Δ_o is the distance from the reference point to the end of the specimen prior to prestress transfer. This results in the following expression used to calculate the actual strand draw-in:

$$l_{draw-in} = \Delta_t - \Delta_o - \frac{f_{pbt}}{E_p}\Delta_o \qquad \textit{Equation 5-6}$$

where:

$l_{draw-in}$ = draw-in value at time t,

Δ_t = distance from the reference point to specimen end at time t,

Δ_o = distance from the reference point to specimen end prior to prestress transfer,

f_{pbt} = stress in tendon immediately prior to prestress transfer, and

E_p = modulus of elasticity of tendon.

5.5 DISCUSSION OF RESULTS

As reported in Section 5.3, draw-in measurements were taken in conjunction with the transfer length measurements during this study. For comparison purposes, only the initial and long-term draw-in values will be discussed in this section. Since there were three single-strand and three double-strand concentrically prestressed specimens for each mixture, draw-in values were investigated on seventy-two specimen ends. As with the determination of transfer lengths, the draw-in values from the specimens of SCC Mix 7 (mixture with unacceptable air content) were used in comparisons with the other mixes. The draw-in values from this set of specimens were consistent with the data from other sets. Figure 5-6 shows the initial and long-term draw-in values for SCC Mix 7b. Draw-in values for all of the mixtures are reported in Appendix D.

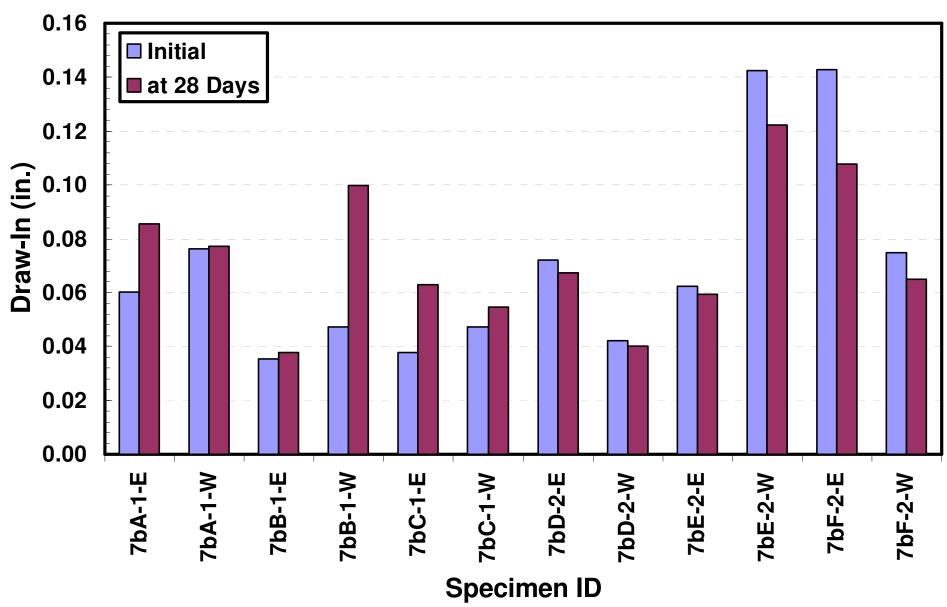

Figure 5-6: Strand Draw-In Results for SCC Mix 7b

Due to the violent force produced at prestress transfer from flame cutting, values of strand draw-in on live ends were much higher than those for dead ends. Increased values of draw-in for live ends can be seen in Figure 5-6 at locations 7bB-1-W, 7bE-2-W, and 7bF-2-E. 7bC-1-E was also a live end, but the draw-in was not as pronounced at this end. Increased damage to the concrete surrounding the tendon on the live ends may have led to this finding. While the draw-in on the live ends appeared to be longer, the certainty of this is questionable. Difficulties in obtaining accurate measurements on these ends were attributed to concrete loss, loosening of the heat-shrink tubing, and strand unwinding. The locations from which the benchmark readings were taken were dependent on the judgment of the researcher performing the readings; as a result, the draw-in values for live-end strands were inconsistent compared to other strands in the same mixture. Overall, the draw-in values obtained from strands on the dead ends were much more consistent, at both initial and long-term readings. The mean of the initial draw-in values was 0.068 in. and the mean of the long-term draw-in values was 0.072 in. on the dead ends. Reference points were rarely lost on these ends, which allowed for more accurate draw-in measurements.

Comparisons between measured transfer lengths and transfer lengths predicted by Equation 5-5 were made based on draw-in values. The modulus of elasticity of the strand given by the manufacturer was 28,890 ksi, and the average value for stress in the strand immediately prior to prestress transfer was 200 ksi. The only difficulty found for using Equation 5-5 was the selection of which value of draw-in to use for specimens with multiple strand configurations, as was the case in the double-strand specimens in this study. Therefore, two different approaches for predicting the transfer lengths from strand draw-in were investigated. In the first approach, Equation 5-5 was applied using the average measured draw-in for the two strands on each specimen end. For the second approach, the maximum draw-in from the two strands on each end was used in Equation 5-5. These two different approaches were investigated to see which produced the best correlation with the measured data. The following six figures compare the measured transfer lengths to the strand draw-in at initial and long-term measurement times.

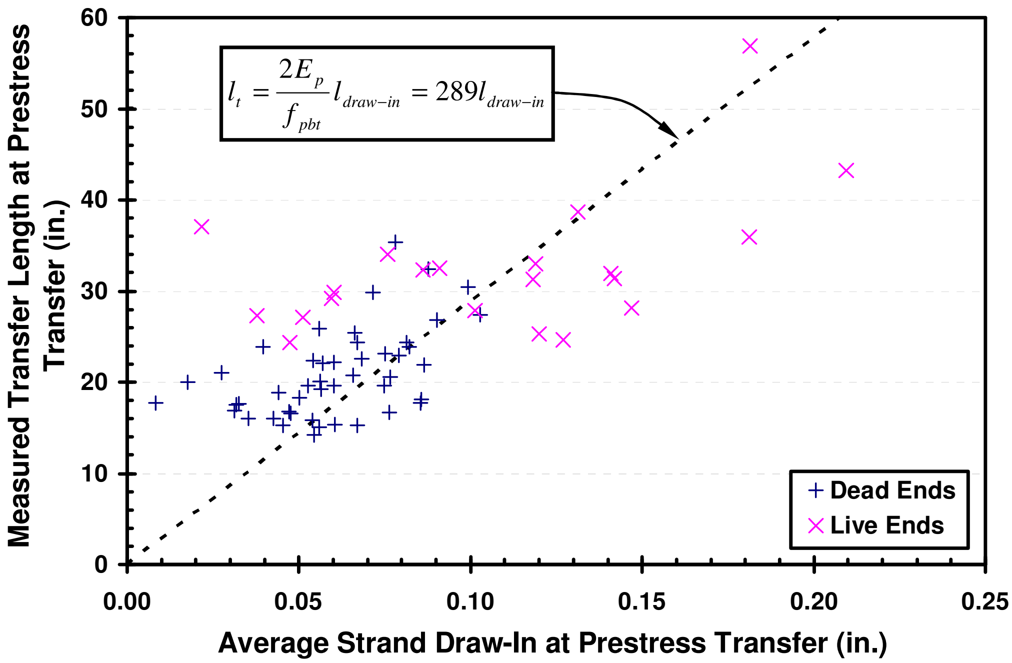

Figure 5-7: Measured Initial Transfer Length vs. Average Draw-In Value at Prestress Transfer

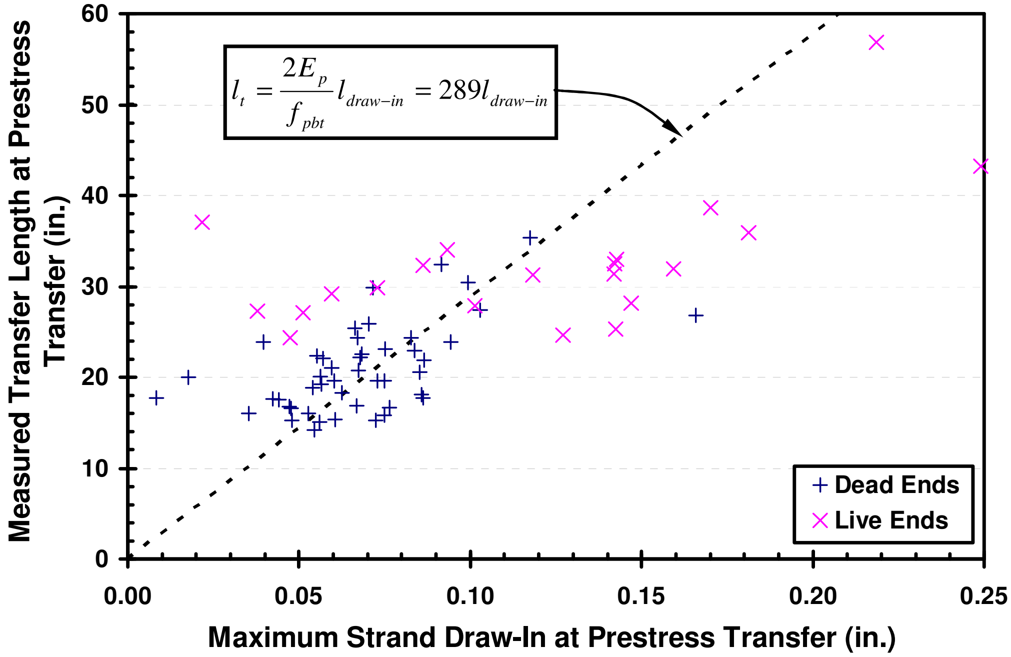

Figure 5-8: Measured Initial Transfer Length vs. Maximum Draw-In Value at Prestress Transfer

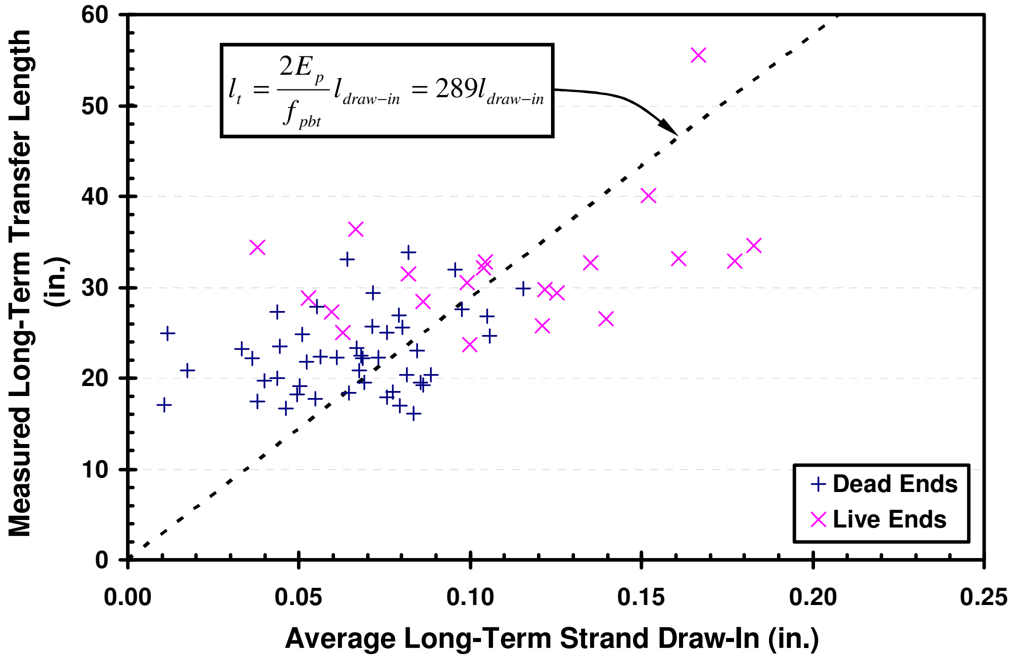

Figure 5-9: Measured Long-Term Transfer Length vs. Average Long-Term Draw-In Value

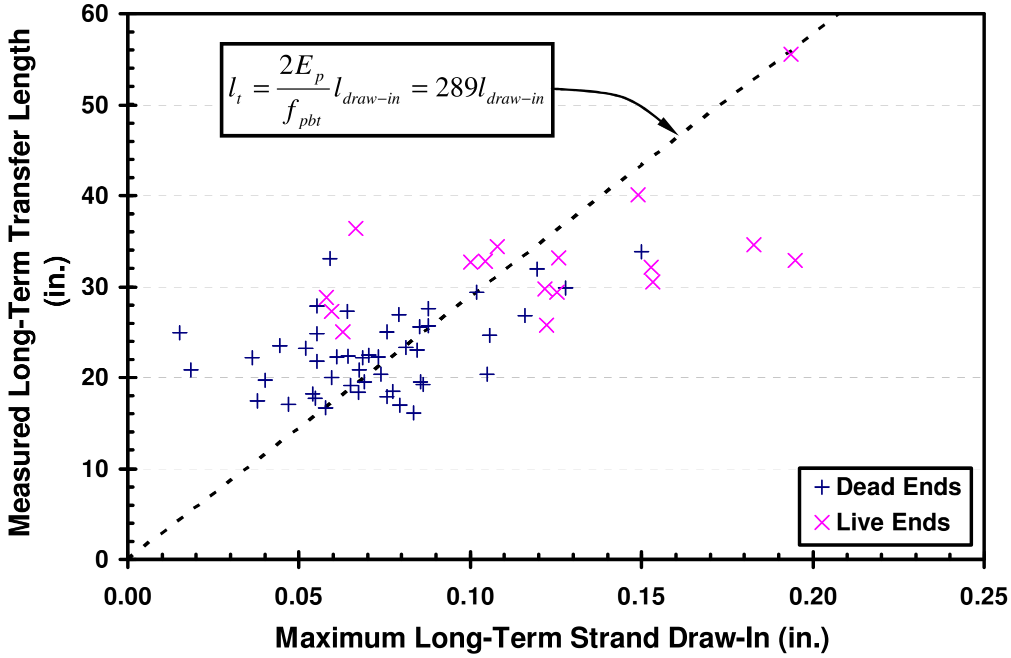

Figure 5-10: Measured Long-Term Transfer Length vs. Maximum Long-Term Draw-In Value

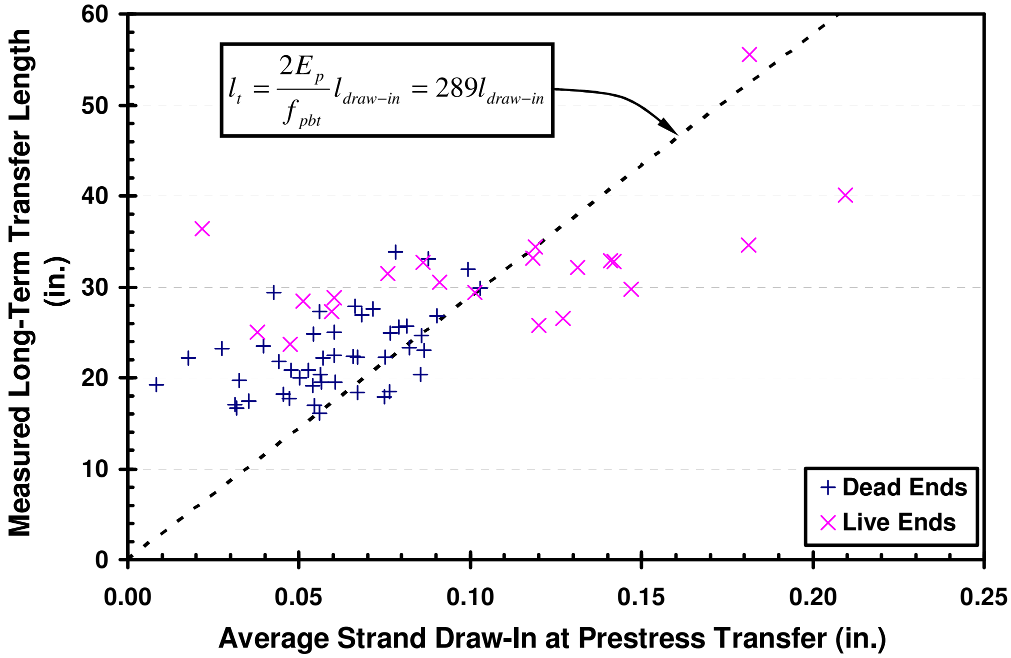

Figure 5-11: Measured Long-Term Transfer Length vs. Average Draw-In Value at Prestress Transfer

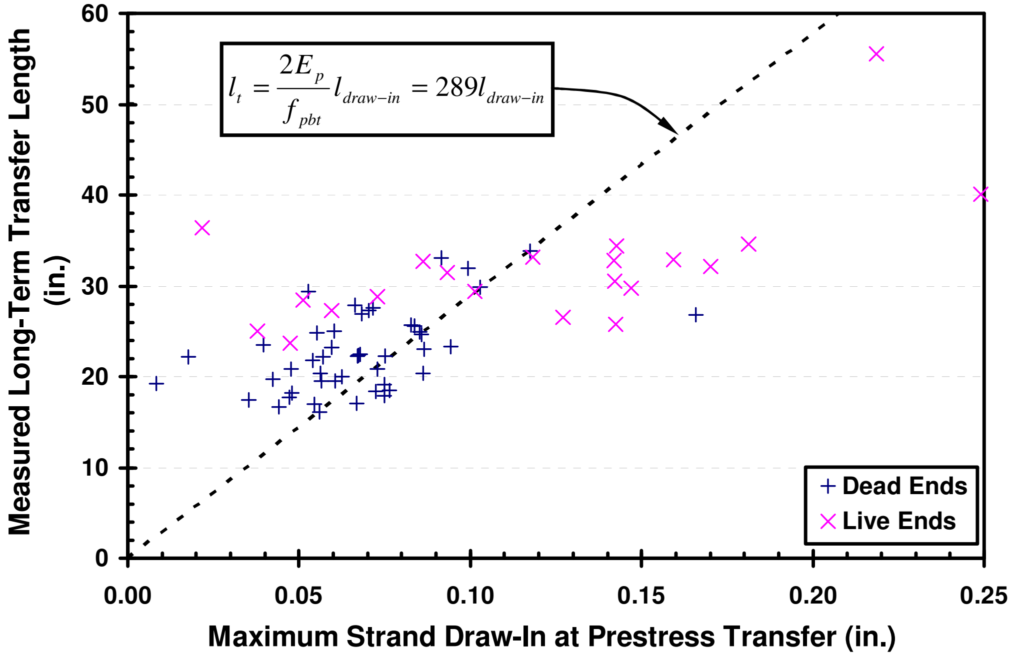

Figure 5-12: Measured Long-Term Transfer Length vs. Maximum Draw-In Value at Prestress Transfer

The dashed line intersecting the origin in each of the last six figures represents the calculated value using the expression in Equation 5-5. Although each set of specimens had slightly different stress values for f_{pbt}, these were minor differences and an average proportionality coefficient of 289 is shown. Table 5-1 summarizes the results from linear regression analyses of the six different comparisons.

Table 5-1: Results from Linear Regression Analyses for l_t vs. $l_{draw\text{-}in}$

Relationship	Dead End		Live End	
	Proportionality Coefficient	**Correlation Value, R^2**	**Proportionality Coefficient**	**Correlation Value, R^2**
$l_{t,initial}$ vs. Average $l_{draw\text{-}in,initial}$	322	-0.85	263	-1.81
$l_{t,intial}$ vs. Maximum $l_{draw\text{-}in,initial}$	285	-0.65	234	-1.74
$l_{t,long\text{-}term}$ vs. Average $l_{draw\text{-}in,long\text{-}term}$	316	-2.02	260	-1.61
$l_{t,long\text{-}term}$ vs. Maximum $l_{draw\text{-}in,long\text{-}term}$	289	-1.54	249	-1.03
$l_{t,long\text{-}term}$ vs. Average $l_{draw\text{-}in,initial}$	347	-1.13	258	-2.10
$l_{t,long\text{-}term}$ vs. Maximum $l_{draw\text{-}in,intitial}$	306	-1.40	230	-2.20

As can be seen in Figures 5-7 through 5-12 and Table 5-1, neither the average nor maximum produced significant correlation between draw-in values and transfer lengths. The best correlation occurred with dead-end values when comparing initial transfer length to maximum draw-in at prestress transfer in Figure 5-8. Comparing the measured initial transfer lengths to the maximum initial draw-in values resulted in a $R^2 = -0.65$ and a proportionality constant of 285. This constant is close to the theoretical proportionality constant of 289. Unlike past studies that have reported strong correlation between draw-in and transfer length (Rose and Russell 1997), individual transfer lengths do not appear to be reliably proportional to the representative strand draw-in values. Separate investigations involving comparisons between the transfer lengths and draw-in values for the double-strand specimens and single-strand specimens produced no significant improvement in correlation. The same can be said with investigations for the values among the individual mixtures.

The previous relationships were also investigated by isolating the conventional concrete and SCC specimens. Table 5-2 summarizes the results of linear regression analyses for relationships between measured transfer lengths and corresponding draw-in values for conventional concrete and SCC specimens. Once again, comparisons among dead-end initial transfer lengths to maximum initial draw-in at prestress transfer resulted with the best correlation. SCC specimens had a proportionality constant of 299 and an R^2 value of -0.19. The same comparison with conventional concrete produced a proportionality constant of 245 and an R^2 of -17.26. The correlations between transfer lengths and draw-in were greater for SCC as compared to conventional concrete, though the correlations were still poor. The poorer correlation evident from the conventional concrete data is likely due to all of these data being tightly grouped near one value of predicted transfer length (because the concrete strength was not varied for the conventional concrete).

Table 5-2: Results from Linear Regression Analyses for l_t vs. $l_{draw\text{-}in}$ of SCC and Conventional Concrete

Relationship	**Conventional Concrete**		**SCC**	
	Proportionality Coefficient	**Correlation Value, R^2**	**Proportionality Coefficient**	**Correlation Value, R^2**
$l_{t,intial}$ vs. Average $l_{draw\text{-}in,initial}$	314	-2.81	325	-0.57
$l_{t,intial}$ vs. Maximum $l_{draw\text{-}in,initial}$	245	-17.26	299	-0.19
$l_{t,long\text{-}term}$ vs. Average $l_{draw\text{-}in,long\text{-}term}$	317	-7.99	316	-1.91
$l_{t,long\text{-}term}$ vs. Maximum $l_{draw\text{-}in,long\text{-}term}$	297	-7.91	287	-1.41
$l_{t,long\text{-}term}$ vs. Average $l_{draw\text{-}in,initial}$	315	-5.00	357	-1.00
$l_{t,long\text{-}term}$ vs. Maximum $l_{draw\text{-}in,intitial}$	246	-24.60	328	-0.56

The proportionality of transfer length to draw-in has been studied in hopes of finding an expedient method for estimating transfer lengths. Figures 5-13 to 5-18 also illustrate how unreliable the relationship from Equation 5-5 was with data from this study. These figures compare measured transfer lengths, l_t, to predicted transfer lengths, $l_t^{'}$, based on measured draw-in values using Equation 5-5:

$$l_t^{'} = \frac{2E_p}{f_{pbt}} l_{draw-in}$$

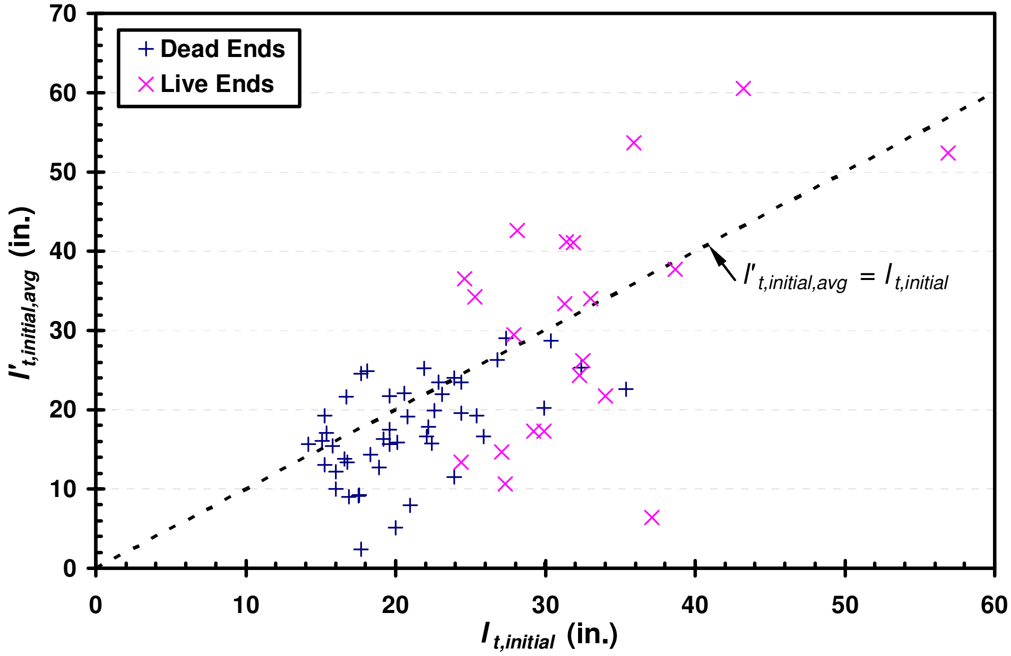

Figure 5-13: Predicted Initial Transfer Length Calculated From Average Draw-In vs. Measured Initial Transfer Length

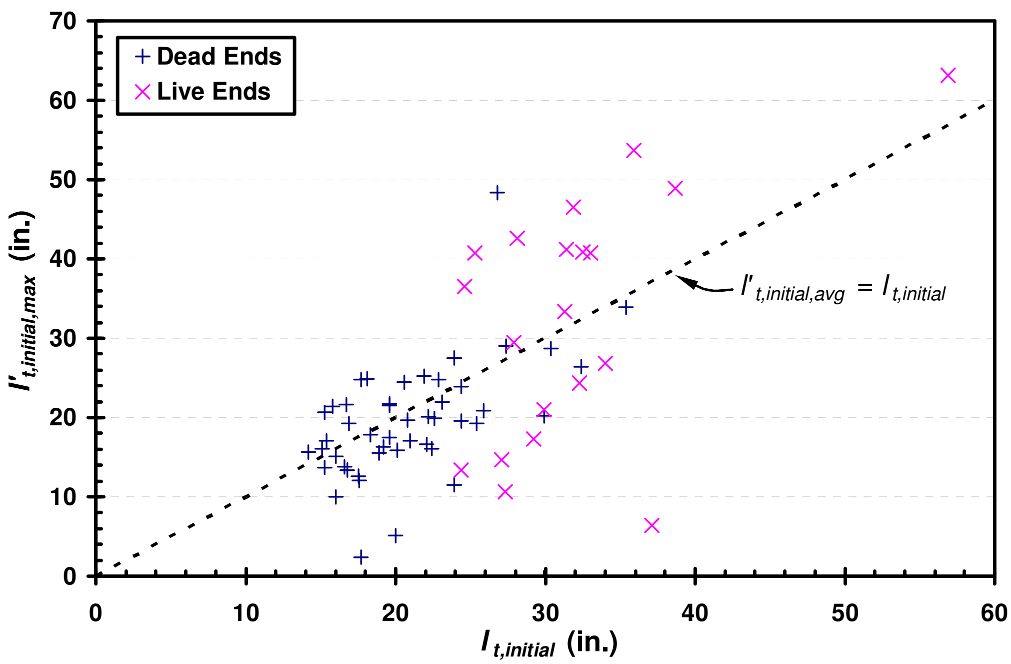

Figure 5-14: Predicted Initial Transfer Length Calculated From Maximum Draw-In vs. Measured Initial Transfer Length

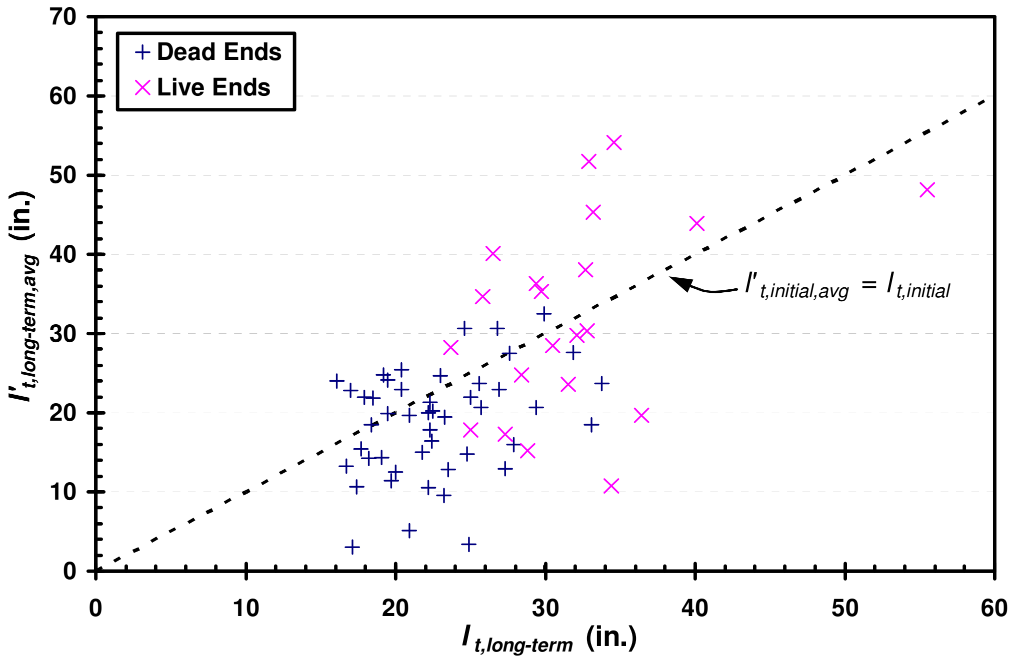

Figure 5-15: Predicted Long-Term Transfer Length Calculated From Average Draw-In vs. Measured Long-Term Transfer Length

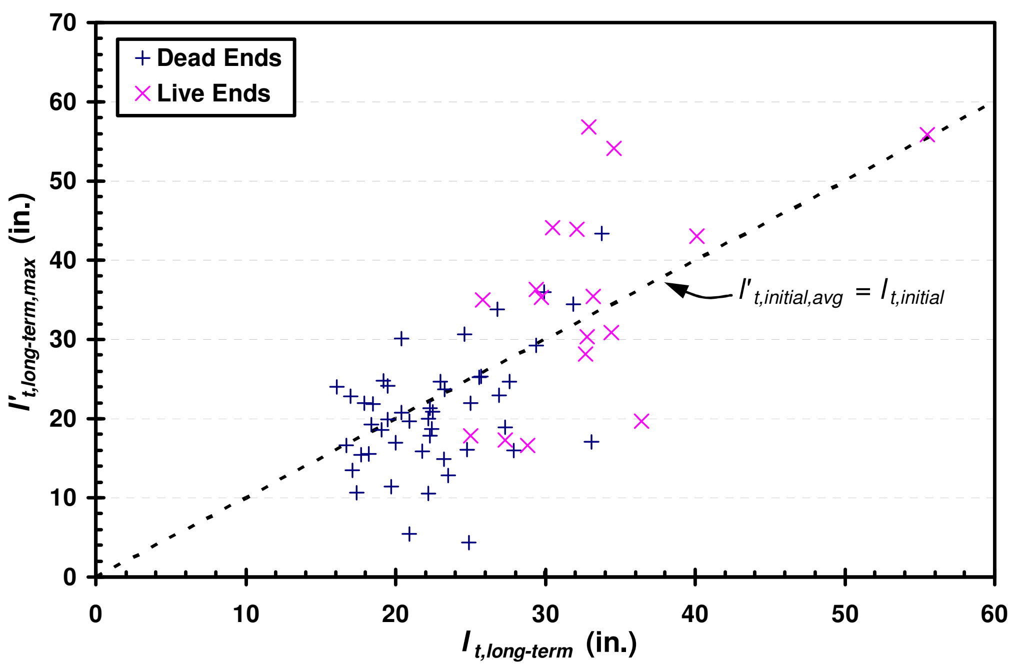

Figure 5-16: Predicted Long-Term Transfer Length Calculated From Maximum Draw-In vs. Measured Long-Term Transfer Length

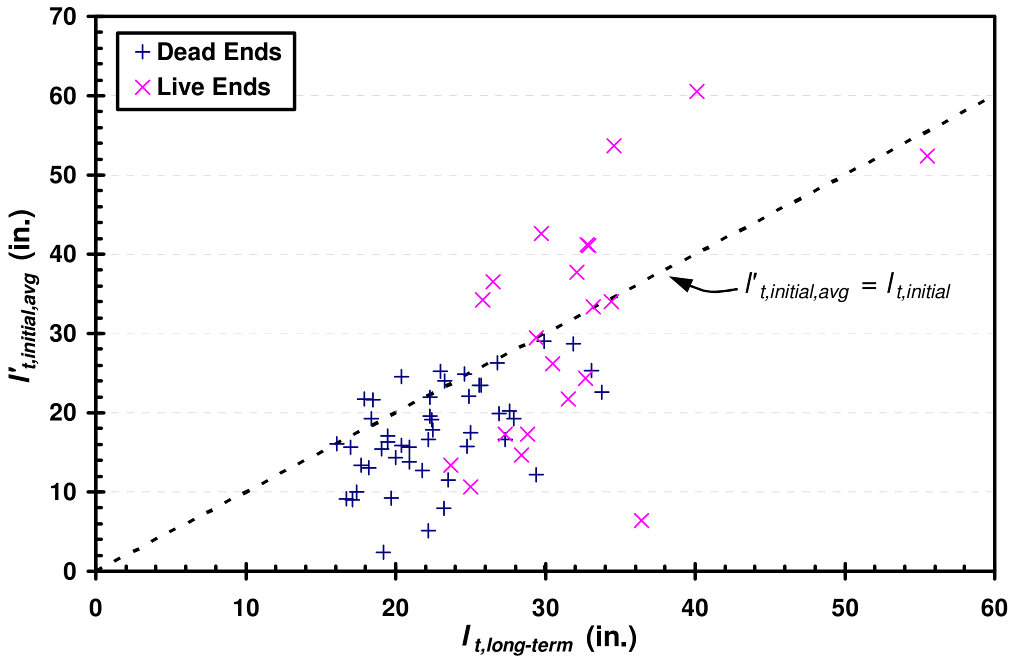

Figure 5-17: Predicted Initial Transfer Length Calculated From Average Draw-In vs. Measured Long-Term Transfer Length

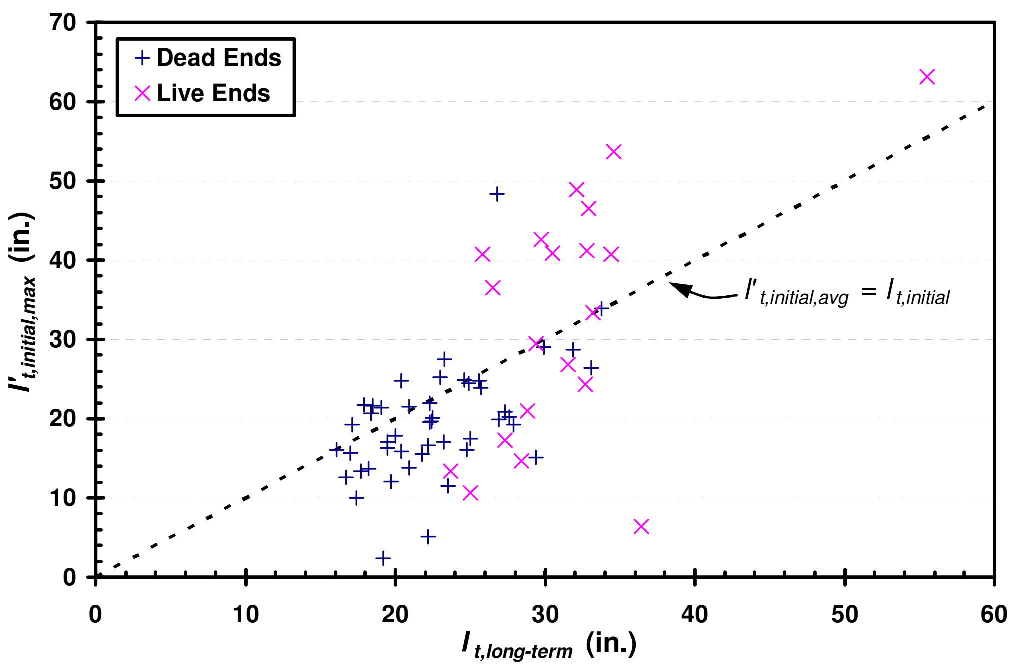

Figure 5-18: Predicted Initial Transfer Length Calculated From Maximum Draw-In vs. Measured Long-Term Transfer Length

The dashed line intersecting the origin in each of Figures 5-13 through 5-18 represents the line of equality between the predicted and measured transfer lengths. Data points falling below the line represent measured transfer lengths longer than predicted by Equation 5-5. For both approaches, the majority of measured transfer lengths for the dead and live ends were longer than predicted. Greater dispersion of the live-end data existed, as compared to the dead-end data. Much of this may be attributable to the difficulty in obtaining accurate measurements on these ends. The violent force created from sudden prestress transfer applied to such a small cross section could have affected the draw-in on the live ends too. This can be seen from a typical live-end strain profile presented in Figure 5-19. This strain profile illustrates that the gradient is certainly not linear, thus violating the assumption upon which Equation 5-5 is based. This behavior was also observed in the study by Kaar et al. (1963). They reported an increase of "free end slip" on the cut end of their test specimens.

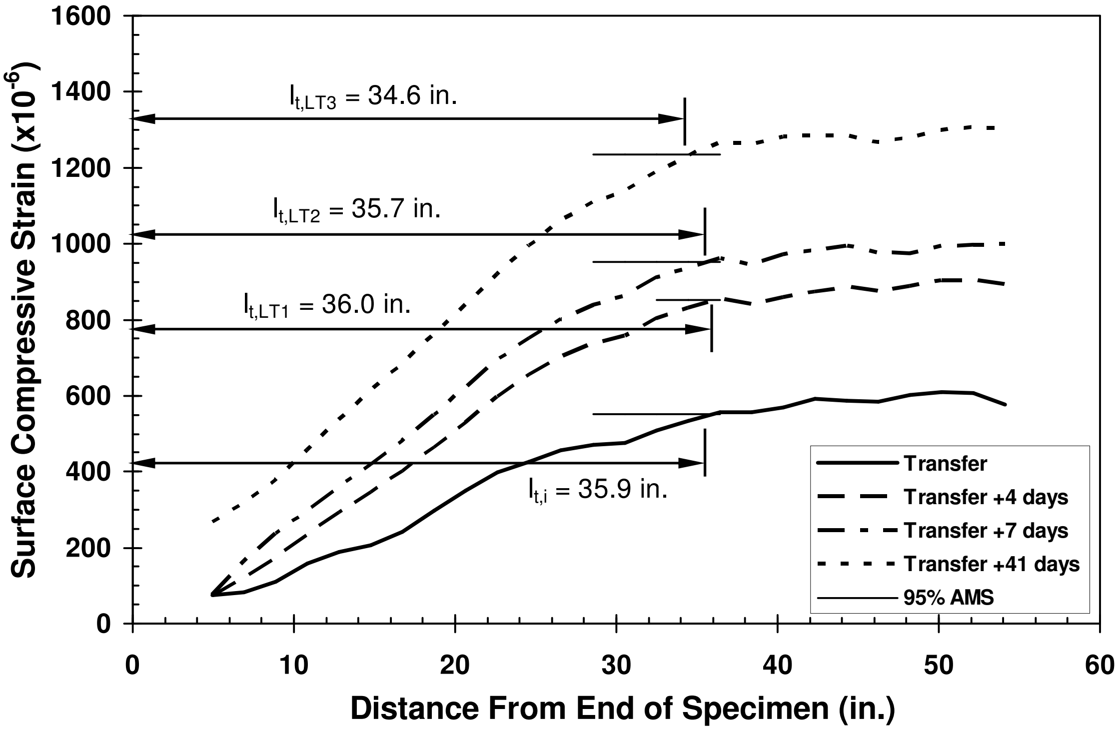

Figure 5-19: Typical Live-End Concrete Strain Profile (9F-2-E)

5.6 SUMMARY AND CONCLUSIONS

Measurements for strand draw-in were conducted with transfer length measurements to determine if proportionality existed between these two parameters on test specimens from this study. After the actual draw-in values were determined by subtracting out the free contraction of the strand, predicted transfer lengths, $l_t^{'}$, were calculated from the expression, $l_t^{'} = \frac{2E_p}{f_{pbt}} l_{draw-in}$.

Comparison of the predicted transfer lengths to the measured transfer lengths resulted in very poor correlation. For these predictions, two different methods were used to determine the draw-in for specimens with a two-strand configuration: in the first, the average value of draw-in between the two strands on each specimen end was used in Equation 5-5, and in the second , the maximum value of draw-in for the two strands on each specimen end was used. Overall, the best correlation was found between the initial maximum draw-in values and the measured initial transfer lengths. Although this combination exhibited the best correlation, it was still poor. Using this relationship, only 23% of the predicted transfer lengths were within 10% of the measured transfer lengths for the dead ends. Predicted transfer lengths were within 20% of the measured transfer lengths for 62% the dead ends. Predictions of live-end transfer lengths were even less reliable. Only 10% of predicted lengths fell within 10% of measured transfer lengths. Fourteen percent of the predicted lengths were within 20% of the measured transfer lengths. There was no difference among the various mixtures with respect to the relationship between draw-in and measured transfer lengths. No trend was evident that linked the initial and long-term draw-in values. For some strands the long-term draw-in was greater than the initial, while the opposite was true for others.

The dead end draw-in values were more consistent than the draw-in values from the live ends. The decrease in live end consistency was due to less accurate measurements and concrete loss from sudden release of the strand at prestress transfer. Since the draw-in values are approximately 0.1 in., the slight movement of the measurement reference points can introduce significant error.

From analysis of all of the draw-in data, it can be concluded that very little reliable proportionality existed between draw-in and transfer length for all test specimens in the study. The only value that can be obtained from the draw-in values is an approximate estimate of the average transfer length for a number of specimens, and a large quantity of draw-in values may be needed to do this reliably. While better correlation existed between predicted and measured transfer lengths in specimens cast with SCC, they still were not reliably proportional. As previously discussed, the small cross-sectional areas of specimens investigated in this study may have contributed to longer draw-in values. This could especially be the case on the live-end draw-in values. The data collected in this study revealed that individual specimen transfer lengths can not reliable be predicted from individual draw-in measurements for either SCC or conventional concrete specimens.

CHAPTER 6

SUMMARY AND CONCLUSIONS

6.1 SUMMARY

From benefits associated from the use of self-consolidating concrete in the precast, pretensioned industry, there is a great interest in evaluating the bond behavior between prestressing strands and SCC. Since use of SCC in prestressed elements can decrease the cost of production while increasing performance, this interest has heightened in recent years. At the present time, very little research has been conducted to investigate the use of SCC in prestressed concrete, especially comparing specimens cast from several different mixtures.

The objective of this study was to examine how transfer lengths in concentrically prestressed specimens cast with different SCC mixtures of different strength levels compared to transfer lengths in conventional-slump concrete. Pretensioning of the specimens was accomplished using 0.5-in. oversized strand. The proportionality between draw-in values and the corresponding transfer lengths was examined.

In this study, transfer lengths of thirty-six concentrically prestressed concrete specimens were measured. Initial and long-term transfer lengths measurements were performed on all specimens in the study. Corresponding draw-in measurements were performed at the same time intervals. The mixing, fabrication, and measurements were performed at the Structural Research Laboratory at the Auburn University Department of Civil Engineering.

One conventional mixture and four different SCC mixtures were tested. The SCC mixtures were made up of a high- and moderate-strength mixture for each type of mineral admixture, Class C Fly Ash or GGBF Slag. The high-strength mixtures had compressive strengths at prestress transfer ranging from 8,700 to 9,700 psi. The moderate-strength mixtures for SCC and the conventional concrete varied from 5,020 to 6,250 psi at transfer. Six specimens were cast for each mixture. Included in the set of six were three pretensioned with a single strand and three with two strands spaced at two inches on center. Due to unacceptable air content, the high strength fly-ash mixture was cast twice; transfer length data were taken for both batches.

Background research for the development of SCC and transfer length prediction equations were presented in Chapter 2. The sections that cover SCC discuss the history, properties, testing, and current uses for the flowable concrete. Current code provisions for transfer length calculations and the basis for these provisions were discussed in this chapter. The theory behind transfer length in prestressed concrete and use of SCC in prestressed concrete are also reported in Chapter 2.

Chapter 3 detailed the construction and material properties of the test specimens used in this study. Details of the small batches mixed to determine the strength-maturity relationships were also presented in this chapter. This chapter concluded with a description of the instrumentation employed for measuring strain.

The transfer length testing and analysis of results was covered solely in Chapter 4. The processes for taking strain readings and developing strain profiles for each specimen end was discussed. The 95% AMS method used for determining the transfer lengths and a summary of the relationship that best correlates to the data in this study are presented. The effects of concrete strength, time, and comparisons between specimens cast with conventional concrete and SCC were examined in this chapter. Comparisons among the different code expressions and others from previous research were made in this chapter. Based on the results from the transfer lengths in this study, a model relationship was recommended.

Chapter 5 examined the relationships between draw-in and corresponding transfer lengths from the specimens in the study. The test procedures and analysis of results were discussed. The possibility of predicting transfer lengths from draw-in values was examined in this chapter.

6.2 CONCLUSIONS

The conclusions presented in this section are based on the results of the data analyzed in this study. Many of the analysis techniques used were developed based on the background research and these were applied to the results.

6.2.1 TRANSFER LENGTH TESTING

- Transfer lengths were affected by increasing the concrete compressive strengths at prestress transfer. As a result, any expression used for determining the transfer lengths should take the level of concrete strength into consideration.
- Overall, transfer lengths were found to be inversely proportional to the square root of the concrete compressive strength at transfer, $\sqrt{f'_{ci}}$.

- Code expressions for calculating transfer lengths from ACI 318-05 (ACI 2005), AASHTO Standard (AASHTO 2002), and AASHTO LRFD (AASHTO 2004) did not consistently provide a 95% upper-bound of the measured transfer lengths from this study. While the code equations were unconservative for specimens with lower concrete compressive strength values, they were increasingly conservative for higher compressive strength levels. Poor correlation was observed when comparing measured transfer lengths to all existing code expressions.
- Dead-end transfer lengths in specimens cast with SCC were 14% longer on average than in specimens cast with conventional-slump concrete.
- The live end transfer lengths were much longer than the dead end transfer lengths. An average increase of 34% existed between dead end and live end transfer lengths among specimens cast with SCC containing Class C Fly-Ash as the mineral admixture. Specimens cast with SCC containing 100 grade GGBF Slag showed an increase of 43% from dead-end to live-end transfer lengths.
- Live-end transfer lengths in SCC specimens were 17% longer on average than in conventional-slump concrete specimens.
- Dead-end transfer lengths in SCC specimens using 100 grade GGBF slag were 3% longer than those using Class C fly ash, and. The slag live-end transfer lengths were 10% longer than those with fly ash. Therefore, transfer lengths among the SCC mixtures were very consistent with each other.
- The transfer lengths in the double-strand specimens were 29% longer than the transfer lengths in the single-strand specimens.

- No significant growth in transfer lengths over time existed in specimens cast with conventional concrete. A 10% growth existed in specimens cast with SCC, with a maximum growth of 27% in the dead ends of the high strength fly-ash mixture.
- For all mixtures, the growth of transfer lengths stabilized within the first couple of days after prestress transfer.
- Due to the effects of creep and shrinkage, further investigations with SCC in full-scale specimens is needed to determine how these properties will effect the transfer lengths in these members.
- The following expression is the best-fit model for determining the transfer lengths for SCC specimens from the results in this study. A constant, α, of 0.82 $ksi^{-0.5}$ provides a 95% upper-bound of the transfer lengths measured at the dead ends. Increasing this constant by 35% gives a 95% upper-bound of the transfer lengths measured at the live ends, which is equal to 1.10 $ksi^{-0.5}$.

$$l_t = \alpha \frac{f_{pt}}{\sqrt{f_{ci}^{'}}} d_b$$

where:

α = Constant of proportionality,

f_{pt} = Stress in tendon immediately after prestress transfer, ksi

$f_{ci}^{'}$ = Concrete compressive strength at prestress transfer, ksi,

and

d_b = Nominal diameter of the tendon

- In most cases, an upper-bound estimate of transfer length is desirable; however, for comparison with allowable stress limits at transfer, it is usually conservative to use a lower-bound estimate.

6.2.2 Draw-in Testing

- Comparing draw-in to the corresponding transfer lengths resulted in very poor correlation. The initial draw-in compared to the initial transfer lengths provided the best correlation.
- No significant pattern existed between the initial and long-term draw-in values. For some strands, the long-term value was greater, and for other strands, the opposite was true.
- Due to the violent energy at release, many readings on the live ends were found to be faulty from difficulties in reading deformed benchmarks. Therefore, draw-in values on the dead ends were much more consistent.
- Very little proportionality existed between the draw-in and corresponding transfer lengths. As a result, only an approximate estimation of the transfer length can be achieved from draw-in from this study.

6.2.3 Recommendations for Future Study

The data collected from this study was measured from a series of tests on small concentrically prestressed specimens. Further testing with full-scale SCC prestressed members is necessary to calibrate the model for transfer length predictions.

REFERENCES

AASHTO. 2004. *AASHTO LRFD Bridge Design Specifications: Customary U.S. Units*. 3rd ed. Washington D.C.: American Association of State Highway and Transportation Officials (AASHTO).

AASHTO. 2002. *Standard Specifications for Highway Bridges*. 16th ed. Washington D.C.: American Association of State Highway and Transportation Officials (AASHTO).

ACI 318. 2005. "Building Code Requirements for Structural Concrete." In *ACI Manual of Concrete Practice 2005*. Farmington Hills, Michigan: American Concrete Institute (ACI).

Anderson, A. R., and R. G. Anderson. 1976. An Assurance Criterion for Flexural Bond in Pretensioned Hollow Core Units. *ACI Journal. Proceedings* 73, no. 8: 457-464

ASTM C 39. 1998. "Standard Test Method for Compressive Strength of Cylindrical Concrete Specimens". *ASTM International*. West Conshohocken, Pennsylvania.

ASTM C 138. 1998. "Standard Test Method for Unit Weight, Yield, and Air Content." *ASTM International*. West Conshohocken, Pennsylvania.

ASTM C 192. 1998. "Standard Practice for Making and Curing Concrete Test Specimens in the Laboratory." *ASTM International*. West Conshohocken, Pennsylvania.

ASTM C 469. 1998. "Standard Test Method for Static Modulus of Elasticity and Poisson's Ratio Strength of Concrete in Compression." *ASTM International*. West Conshohocken, Pennsylvania.

ASTM C 989. 1998. "Specification for Ground Granulated Blast Furnace Slag for Use in Concrete and Mortars." *ASTM International*. West Conshohocken, Pennsylvania.

Barnes, R. W., N. H. Burns, and M. E. Kreger. 1999. "Development Length of 0.6-Inch Prestressing Strand in Standard I-Shaped Pretensioned Concrete Beams." In *Research Report No. 1388-1*. Austin: Center for Transportation Research, The University of Texas at Austin.

Barnes, R.W., J.W. Grove, and N.H. Burns. 2003. Experimental Assessment of Factors Affecting Transfer Length. *ACI Structural Journal* 100(6): 740–748.

Bartos, P. 1999. Measurement of Key Properties for Self-Compacting Concrete. *Concrete* 33, no. 4 (April): 9-14

Gibbs, J.C. and Zhu W. 1999. "Strength of Hardened Self-Compacting Concrete". In *Self-Compacting Concrete*: *Proceedings of the First International RILEM Symposium*, ed. A. Skarendahl and O. Petersson. Cachan Cedex, France: RILEM Publications, 199-209

Hanson, N.W. and P. H. Kaar. 1959. Flexural Bond Tests of Pretensioned Prestressed Beams. *ACI Journal. Proceedings* 55, no. 7: 783-802

Janney, J. R. 1954. Nature of Bond in Pre-Tensioned Prestressed Concrete. *ACI Journal. Proceedings* 50, no. 9: 717-736

Jarmillo, A., R. Victor, M. Vargas, and P. Barbosa. 2003. "Bond Characteristics of Prestressed Strands In Self-Compacting Concrete". In *Self-Compacting Concrete*:

Proceedings of the Third International RILEM Symposium, ed. O. Wallevik and I. Nielsson. Bagneux, France: RILEM Publications, 684-691

Kaar, P. H., R. W. LaFraugh, and M. A. Mass. 1963. Influence of Concrete Strength on Strand Transfer Length. *PCI Journal* 8, no. 5: 47-67

Kaar, P. H. and D. D. Magura. 1965. Effect of Strand Blanketing on Performance of Pretensioned Girders. *PCI Journal* 10, no. 6: 20-34

Khayat, K. H., N. Petrov, E. K. Attiogbe, and H. T. See. 2003. "Uniformity of Bond Strength of Prestressing Strands in Conventional Flowable and Self-Consolidating Concrete Mixtures". In *Self-Compacting Concrete*: *Proceedings of the Third International RILEM Symposium,* ed. O. Wallevik and I. Nielsson. Bagneux, France: RILEM Publications, 703-709

Lane, S. N. 1992. Transfer Lengths in Rectangular Prestressed Concrete Concentric Specimens. *Public Roads* 56, no. 2: 67-71

Lane, S. N. 1998. "A New Development Length Equation For Pretensioned Strands in Bridge Beams and Piles." In *Report No. FHWRA-RD-98-116*. McLean, Virginia: Federal Highway Administration

Labonte, T. 2004. Construction and Testing of Type II AASHTO Girders Using Self-Consolidating Concrete. M.S. Thesis., University of Florida.

Malhorta, V.M., and N.J. Carino. 1991. "CRC Handbook on Nondestructive Testing of Concrete." CRC Press, Florida: 101-145.

Mindess, S., J. F. Young, and D. Darwin. 2003. *Concrete*, 2nd edition. Upper Saddle River, New Jersey: Prentice Hall.

Mitchell, D., W. D. Cook, A. A. Kahn, and T. Tham. 1993. Influence of High-Strength Concrete on Transfer and Development Length of Pretensioning Strand. *PCI Journal* 38, no. 3: 52-66

Naito, C., G. Brunn, G. Parent, and T. Tate. 2005. "Comparative Performance of High Early Strength and Self-Consolidating Concrete for Use in Precast Bridge Beam Construction." In *PITA Project PIT-457-04*. Lehigh University

Neville, A. M. 1996. *Properties of Concrete*, 4th edition. New York, New York: John Wiley & Sons, Inc

Okamura, H. and M. Ouchi. 1999. "Self-Compacting Concrete. Development, Present Use and Future". In *Self-Compacting Concrete*: *Proceedings of the First International RILEM Symposium,* ed. A. Skarendahl and O. Petersson. Cachan Cedex, France: RILEM Publications, 3-14.

Perrson, B. 1999. "Creep, Shrinkage and Elastic Modulus of Self-Compacting Concrete". In *Self-Compacting Concrete*: *Proceedings of the First International RILEM Symposium*, ed. A. Skarendahl and O. Petersson. Cachan Cedex, France: RILEM Publications, 239-250

Petersson, O. 2000. "L-Shape Box Test". In *State-of-the-Art Report (23) of RILEM Technical Committee 174-SCC*, ed. A. Skarendahl and O. Petersson. Cachan Cedex, France: RILEM Publications, 126-128.

Precast/Prestressed Concrete Institute (PCI). 2003. *Interim Guidelines for the Use of Self-Consolidating Concrete in Precast/Prestressed Concrete Institute Member Plants*, 1st edition. Chicago Illinois: Precast/Prestressed Concrete Institute.

Ramsburg, P. 2003. The SCC Test: Inverted or Upright. *Concrete Producer* 21, no. 7: 34-38.

Rose, D. R. and B. W. Russell. 1997. Investigation of Standardized Tests to Measure the Bond Performance of Prestressing Strand. *PCI Journal* 42, no. 4: 56-80

Russell, B. W. and N. H. Burns. 1996. Measured Transfer Lengths of 0.5 and 0.6 in. Strands in Pretensioned Concrete. PCI Journal 41, no. 5: 44-65

Simmons, M. B. 1995. Transfer and Development in Pretensioned, Prestressed Concrete Girders Using ½ Inch Diameter Strands. Ph.D. diss., Auburn University.

Skarendahl, A. 2000. "Definitions". In *Self-Compacting Concrete. State-of-the-Art Report (23) of RILEM Technical Committee 174-SCC*, ed. A. Skarendahl and O. Petersson. Cachan Cedex, France: RILEM Publications, 3-5.

Skarendahl, A. 2003. "The Present – The Future". In *Self-Compacting Concrete*: *Proceedings of the Third International RILEM Symposium,* ed. O. Wallevik and I. Nielsson. Bagneux, France: RILEM Publications, 6-14

Takada, K. and S. Tangtermsirikul. 2000. "Testing of Fresh Concrete". In *Self-Compacting Concrete*. *State-of-the-Art Report (23) of RILEM Technical Committee 174-SCC*, ed. A. Skarendahl and O. Petersson. Cachan Cedex, France: RILEM Publications, 25-39.

Su, J. K., S. W. Cho, C. C. Yang, and R. Huang. 2002. Effect of Sand Ratio on the Elastic Modulus of Self-Compacting Concrete. *Journal of Marine Science and Technology* 10, no.1: 8-13.

Tabatabai, H. and T. J. Dickson. 1993. The History of Prestressing Strand Development Length Equation. *PCI Journal* 38, no. 6: 64-75

Tragargh, J. 1999. “Microstructural Features and Related Properties of Self-Compacting Concrete”. In *Self-Compacting Concrete*: *Proceedings of the First International RILEM Symposium*, ed. A. Skarendahl and O. Petersson. Cachan Cedex, France: RILEM Publications, 175-186.

Zia, P. and T. Mostafa. 1978. Development Length of Prestressing Strands. *PCI Journal* 22, no. 5: 54-65

APPENDICES

APPENDIX A

FRESH CONCRETE PROPERTIES

Table A-1: Results of Fresh Property Testing

FRESH PROPERTIES	MIXTURES											
	Mix 0		Mix 9		Mix 7		Mix 7b		Mix 15		Mix 13	
	Start*	End*	Start*	End*	Start*	End*	Start*	End*	Start*	End*	Start*	End*
Slump Flow (in.):	8.25**	4.5**	28.5	23.25	30.5	23.5	26	26.25	28.25	25.75	31.25	25.5
VSI:	—	—	2.5	0.5	2.5	0.5	1	1	2.5	1.5	2	1
T-50:	—	—	1.57	4.84	2.47	4.97	3.34	5.79	2.35	5.34	2.93	7.69
J-Ring (Value @ Slump Flow):	—		23 @ 24.25		27 @ 26.5		26.25 @ 26.25		28 @ 25.75		25.75 @ 27	
L-Box :	—		h_1=3, h_2=2.875		h_1= h_2		h_1=3.0, h_2=1.5		h_1=3, h_2=2.75		h_1=1.5, h_2=0.5	
Air (%):	4.9	4.5	4.5	4.9	9	4.9	2.4	2.1	3.3	2.8	1.8	1.2
Unit Weight (lb/ft^3):	147.2	149.8	147.9	148.4	143.5	143.5	153.2	154.6	147.6	147.8	153.8	154.0

*note: Fresh property tests taken at start and end of concrete placement
**note: Standard slump test performed on conventional concrete Mix 0

Table A-2: Summary of Values for Fresh Property Testing

FRESH PROPERTIES	MIXTURES					
	Mix 0	Mix 9	Mix 7	Mix 7b	Mix 15	Mix 13
Slump Flow (in.):	8.25	28.5	30.5	26	28.25	31.25
VSI:	—	2.5	2.5	1	2.5	2
T-50:	—	1.57	2.47	3.34	2.35	2.93
J-Ring (Difference/Rating):	—	1.25 / 1	0.5 / 0	0.75 / 0	2.25 / 2	2.2 / 2
L-Box (H_2/H_1):	—	0.96	1	0.5	0.92	0.33
Air (%):	4.9	4.5	9	2.4	3.3	1.8
Unit Weight (lb/ft^3):	147.2	147.9	143.5	153.2	147.6	153.8

APPENDIX B

HARDENED CONCRETE PROPERTIES

Table B-1: Summary of Results for Hardened Concrete Property Testing

		Mix 0		SCC Mix No. 9		SCC Mix No. 7		SCC Mix No. 7b		SCC Mix No. 15		SCC Mix No. 13	
		f'_c (psi)	E_c (ksi)	f'_c (psi)	E_c (ksi)	f'_c (psi)	E_c (ksi)	f'_c (psi)	E_c (ksi)	f'_c (psi)	E_c (ksi)	f'_c (psi)	E_c (ksi)
Air Cured	1	3480	4200	3420	3550	4480	4000	5760	4850	1880	2750	6540	5150
	Transfer	4570	4900	5880	5050	7860	5750	8840	5600	5280	4550	8640	5850
	3	5420	4900	6430	5100	7860	5750	9670	5900	4620	4250	9980	5900
	7	6270	4900	8170	4950	9230	5400	11650	6400	7650	5250	12390	6500
	28	6960	5400	9180	5350	10390	5900	12860	6400	8950	5350	14310	6650
	91	6240	4800	8880	5300	11100	6150	12120	7150	8220	5400	15210	7300
ASTM 4x8	7	6390	5550	8040	5800	9380	6150	11840	6700	7500	5700	12320	6500
	28	7980	6300	10290	6500	11620	7000	13590	7250	9320	5900	14550	7300
	91	8580	6250	11900	6750	12870	6550	15340	7600	9910	6500	15800	7650
ASTM 6x12	7	6440	6200	8040	5800	8550	6200	10310	7000	7010	5650	11390	7050
	28	7460	6000	10290	6500	10060	7650	12940	7150	9010	6450	13220	7450
	91	8260	6400	11900	6750	11400	7350	14030	7800	9860	6400	13910	7650
Match-Cured	1	4750	4900	—	—	—	—	—	—	4680	4450	—	—
	Transfer	5060	5150	6190	4800	7460	5150	8600	5400	5260	4850	8770	5950
	28	8720	6200	10860	6500	10770	6300	13360	7150	10090	6450	15450	7900
		f_{ct} (psi)		f_{ct} (psi)		f_{ct} (psi)		f_{ct} (psi)		f_{ct} (psi)		f_{ct} (psi)	
Splitting Tensile	1	435		430		500		580		240		615	
	Transfer	455		540		630		610		550		695	
	3	565		520		630		765		530		675	
	7	600		725		730		775		665		895	
	28	620		715		695		835		763		905	
	91	595		765		785		945		875		990	

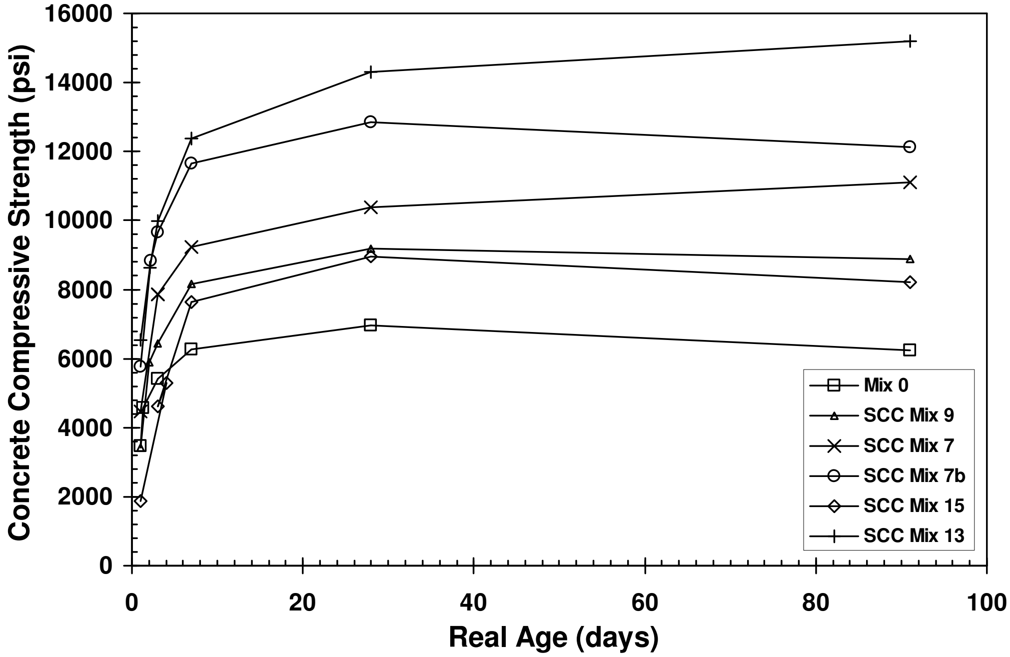

Figure B-1: Air-Cured 4 x 8 in. Cylinder Compressive Strength vs. Real Age

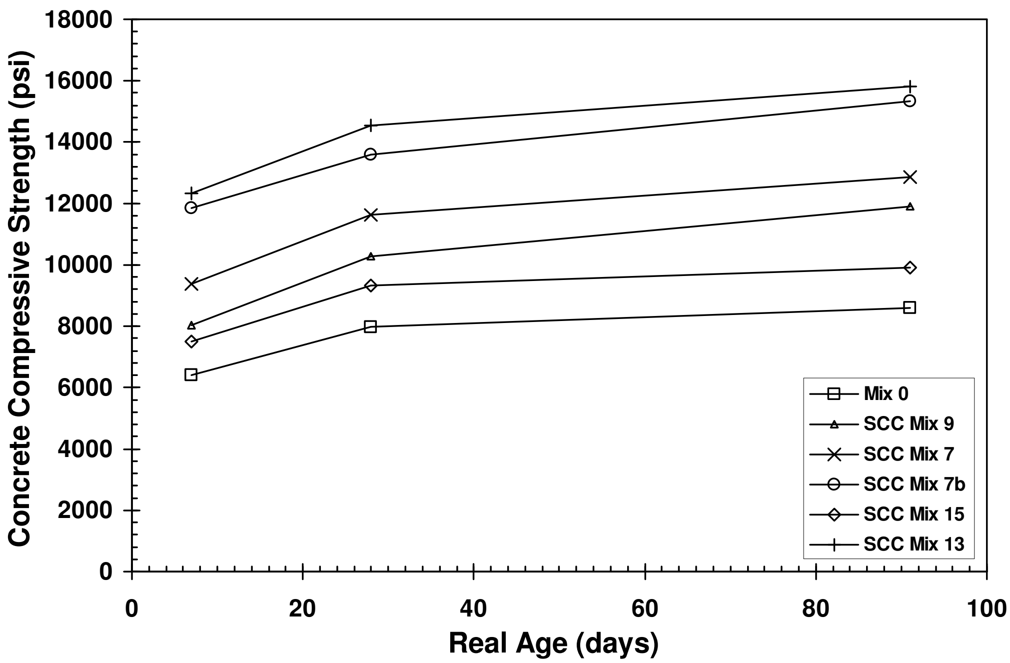

Figure B-2: ASTM C 192 4 x 8 in. Cylinder Compressive Strength vs. Real Age

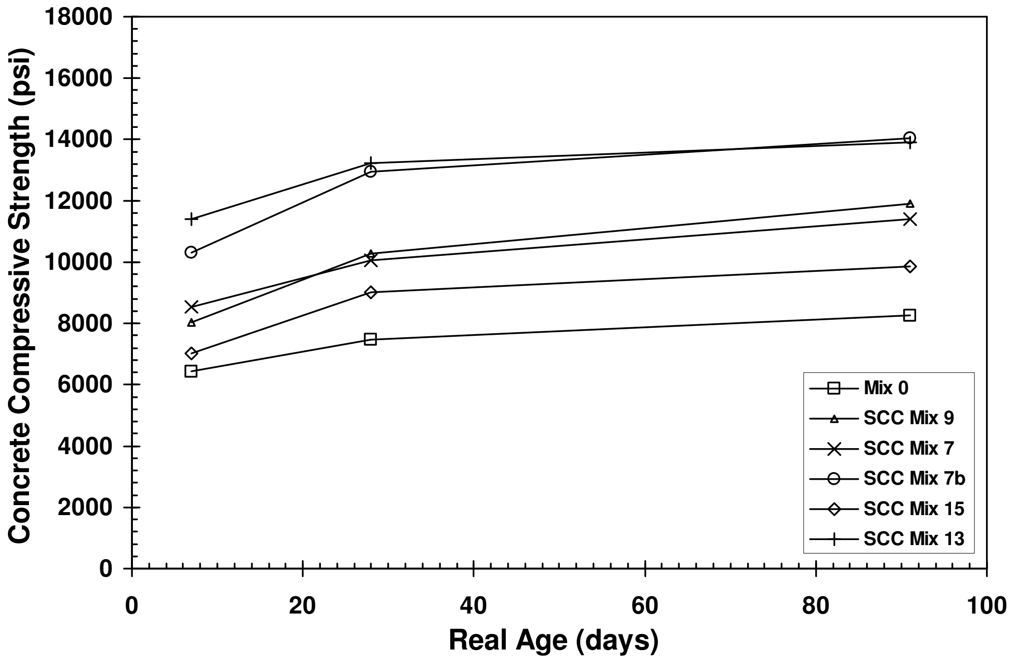

Figure B-3: ASTM C 192 6 x 12 in. Cylinder Compressive Strength vs. Real Age

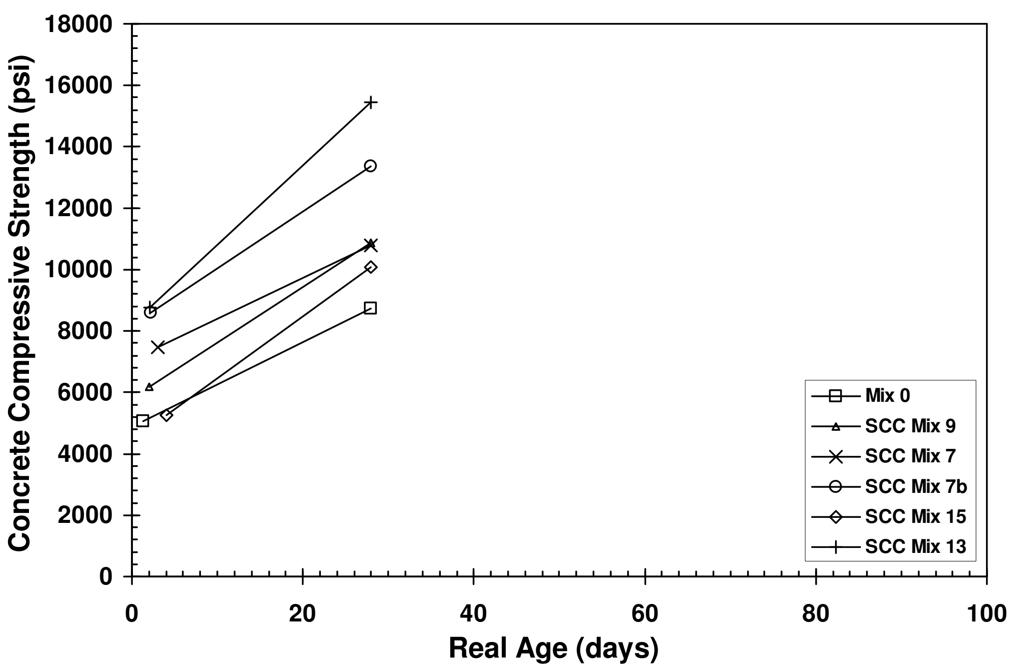

Figure B-4: Match-Cured 4 x 8 in. Cylinder Compressive Strength vs. Real Age

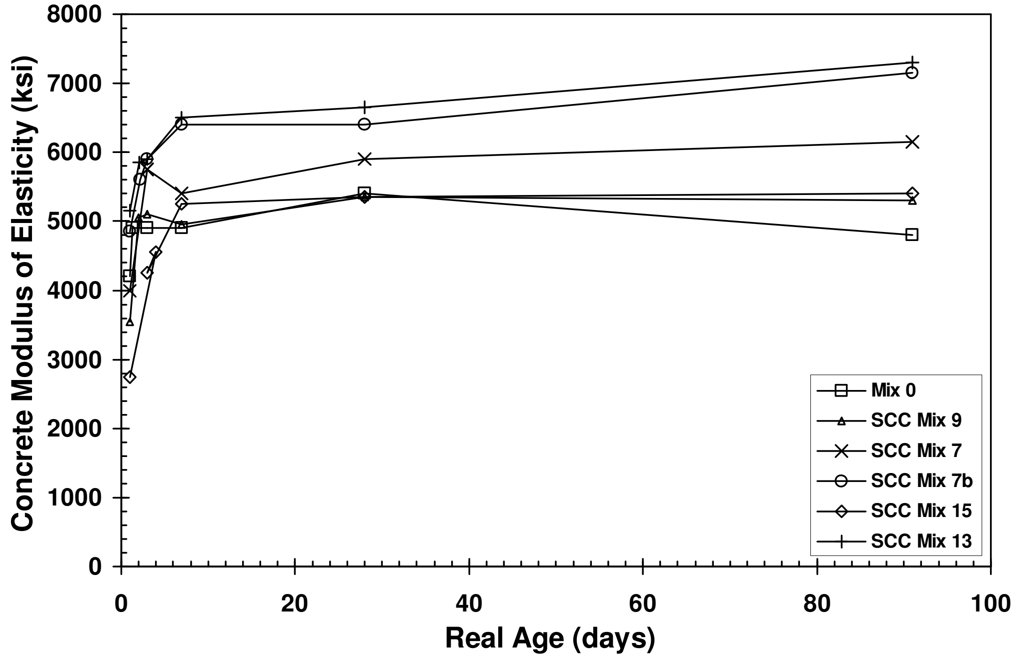

Figure B-5: Air-Cured 4 x 8 in. Cylinder Elastic Modulus vs. Real Age

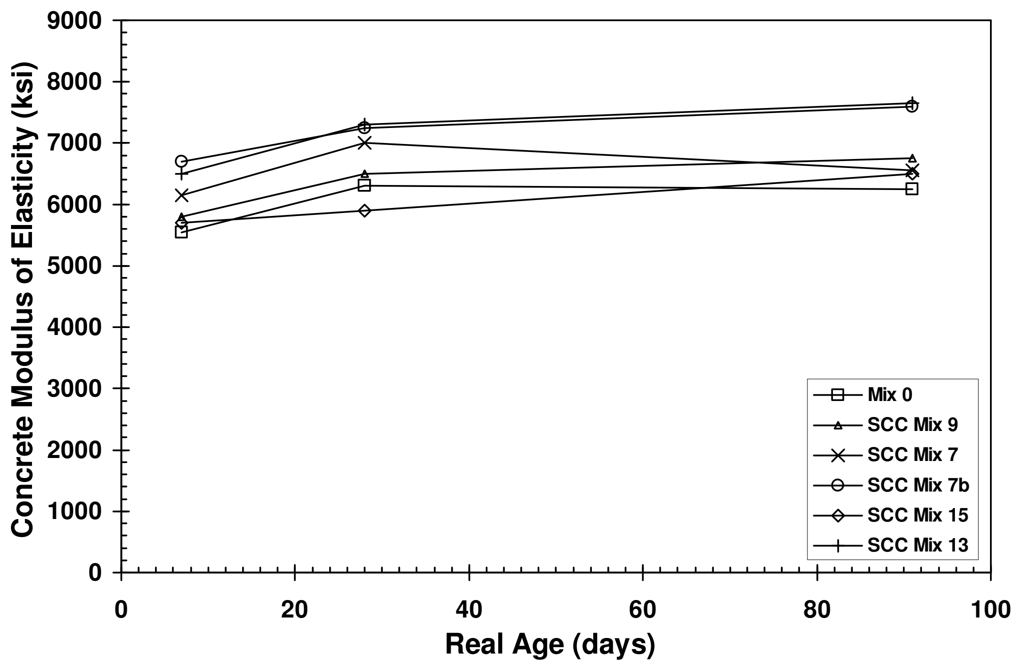

Figure B-6: ASTM C 192 4 x 8 in. Cylinder Elastic Modulus vs. Real Age

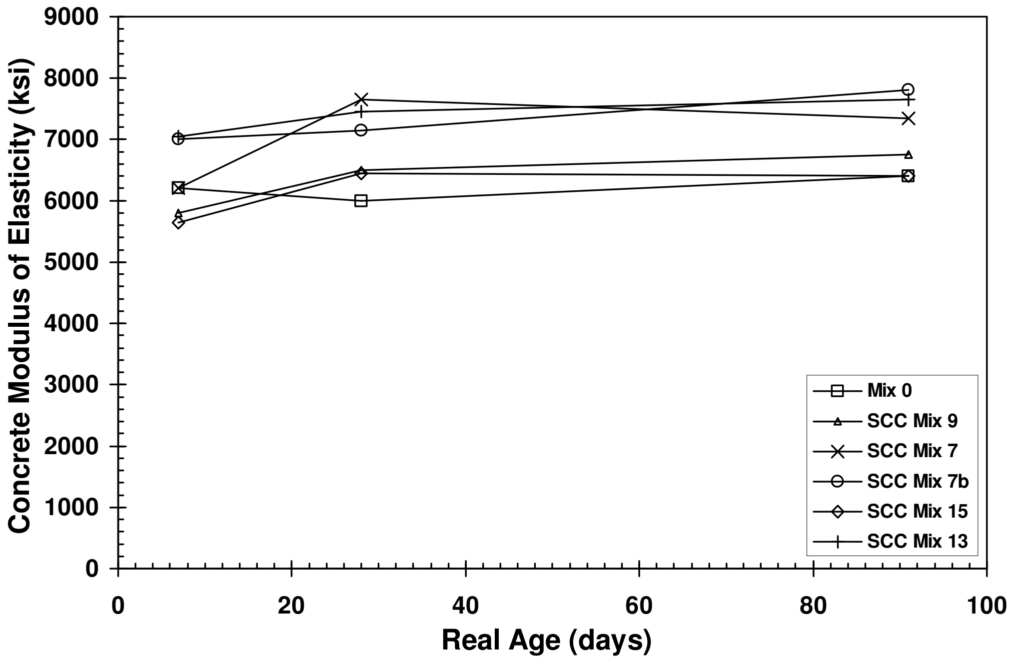

Figure B-7: ASTM C 192 6 x 12 in. Cylinder Elastic Modulus vs. Real Age

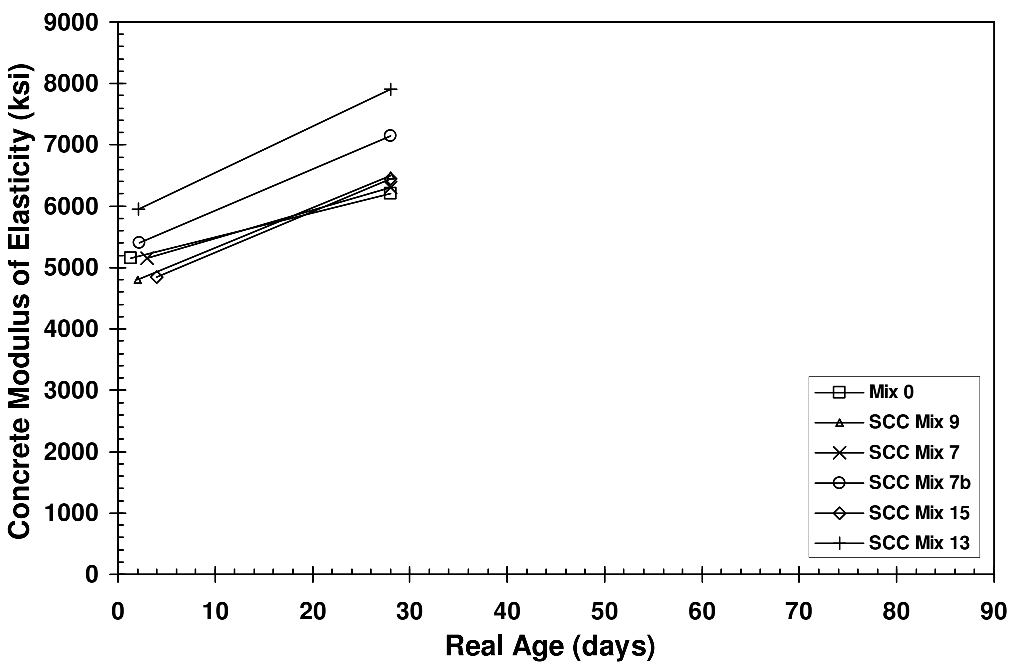

Figure B-8: Match-Cured 4 x 8 in. Cylinder Elastic Modulus vs. Real Age

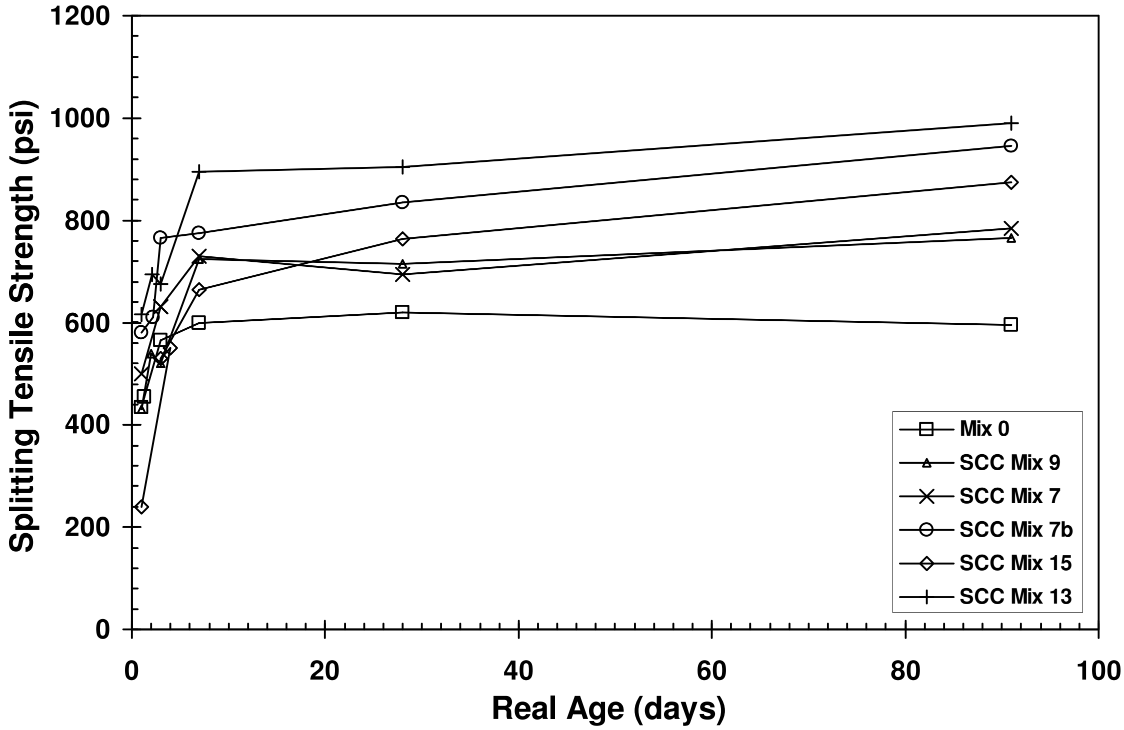

Figure B-9: Air-Cured Cylinder Splitting Tensile Strength vs. Real Age

APPENDIX C

STRENGTH-MATURITY RELATIONSHIP CURVES

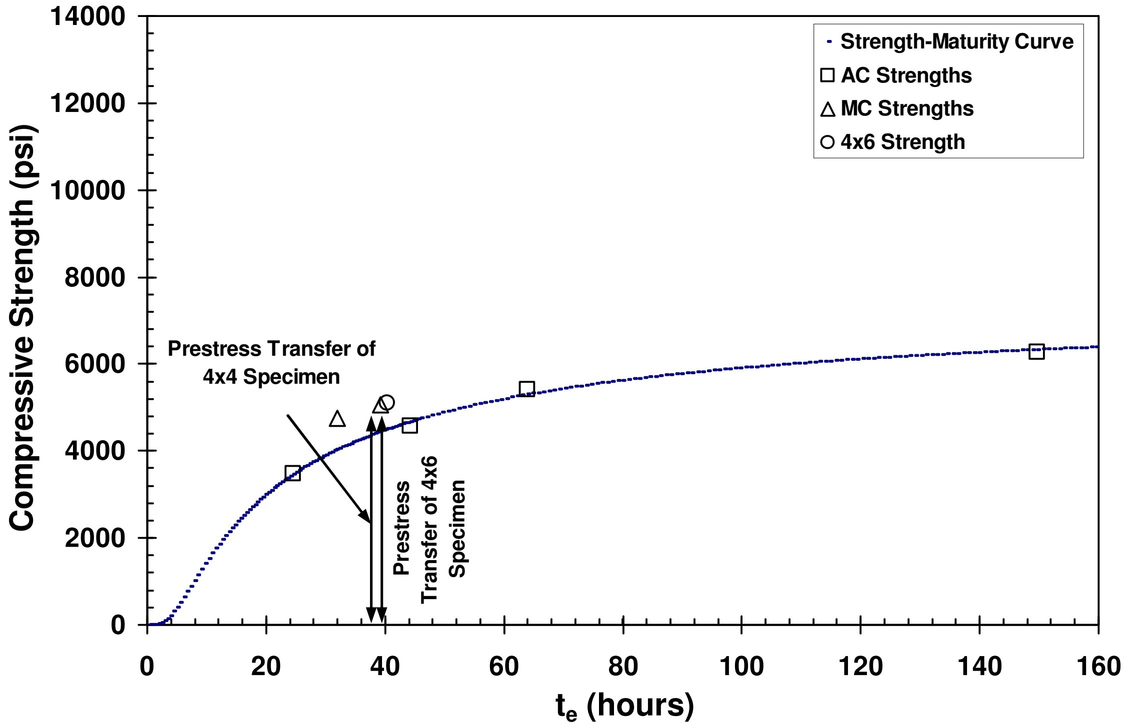

Figure C-1: Strength-Maturity Relationship Curve for Conventional Mix 0

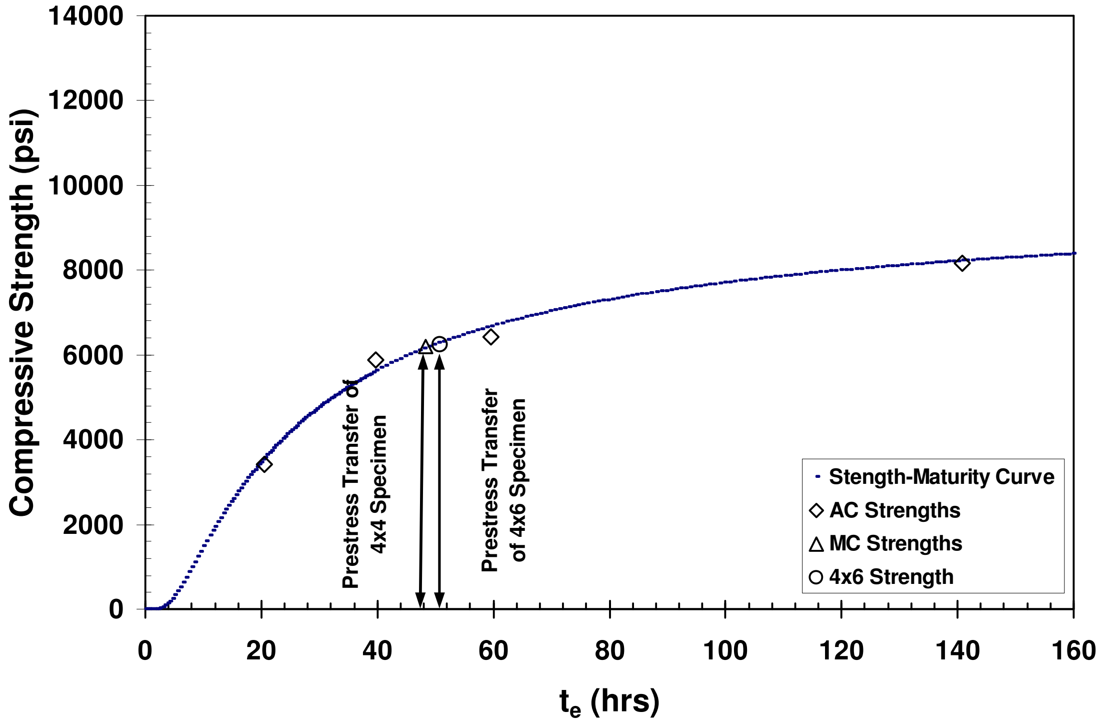

Figure C-2: Strength-Maturity Relationship Curve for SCC Mixture 9

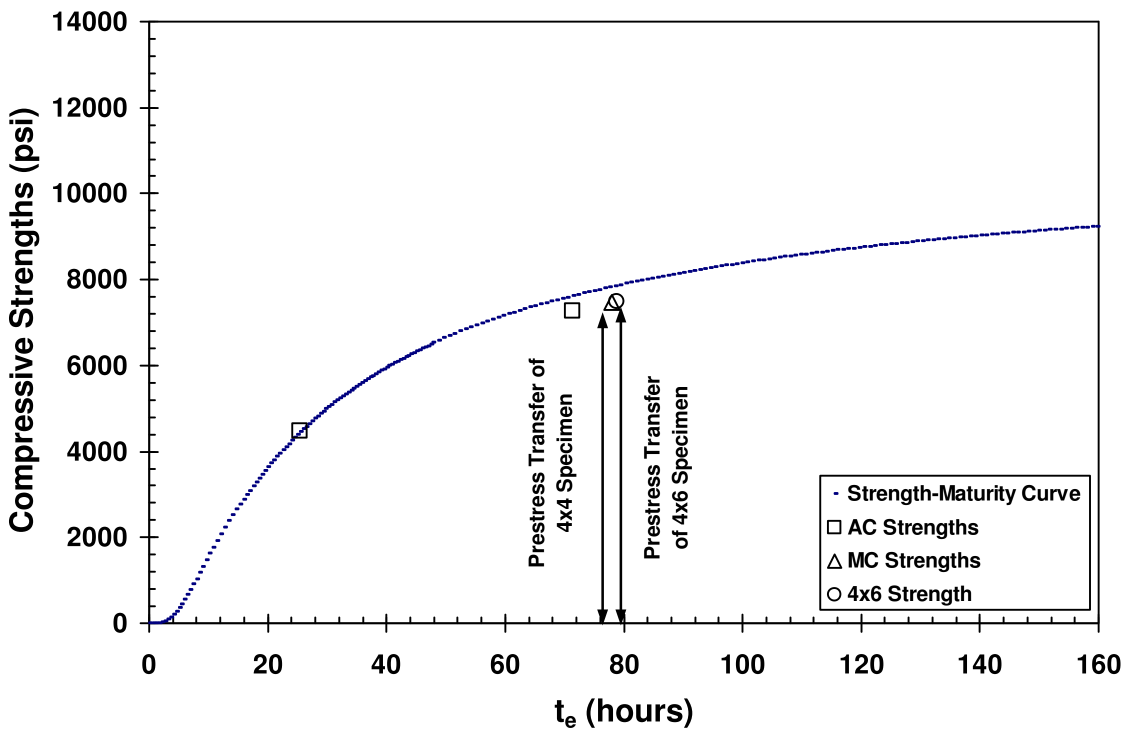

Figure C-3: Strength-Maturity Relationship Curve for SCC Mixture 7

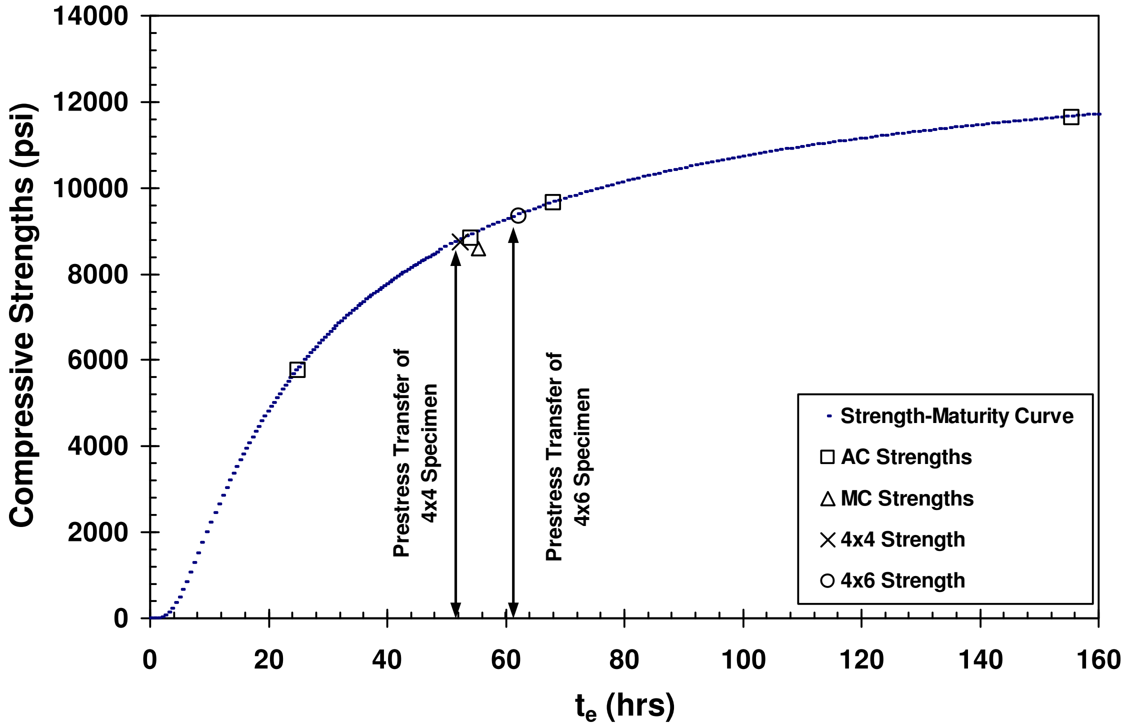

Figure C-4: Strength-Maturity Relationship Curve for SCC Mixture 7b

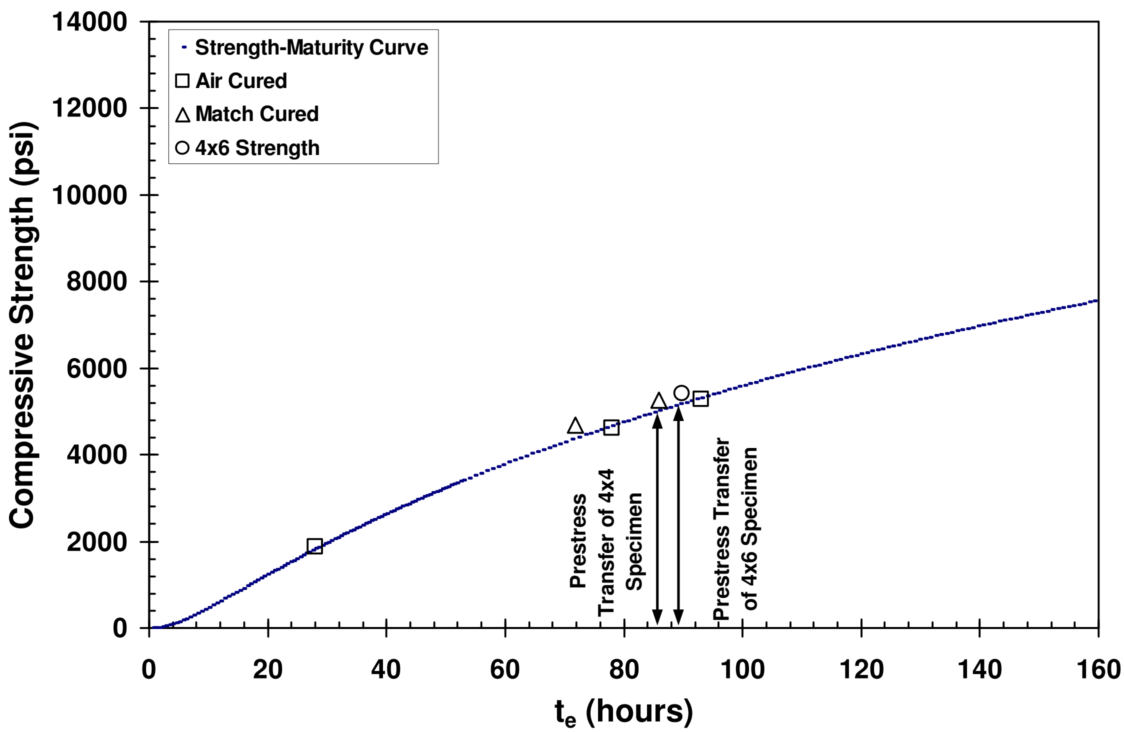

Figure C-5: Strength-Maturity Relationship Curve for SCC Mixture 15

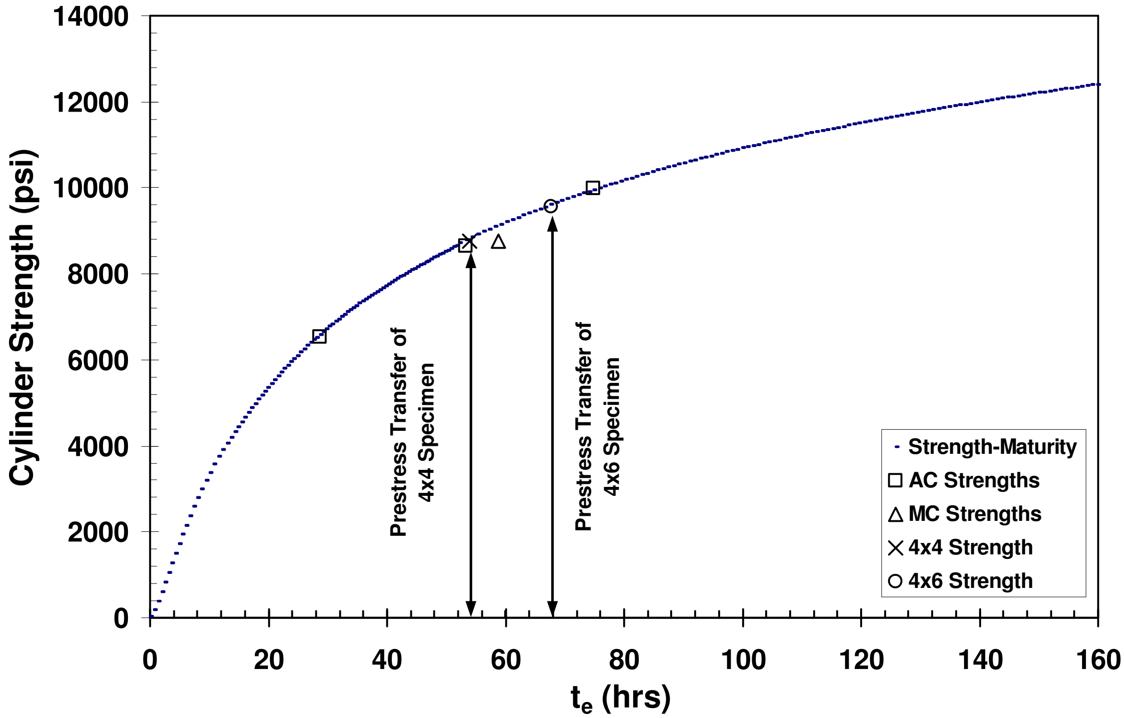

Figure C-6: Strength-Maturity Relationship Curve for SCC Mixture 13

APPENDIX D

CONCRETE STRAIN PROFILES

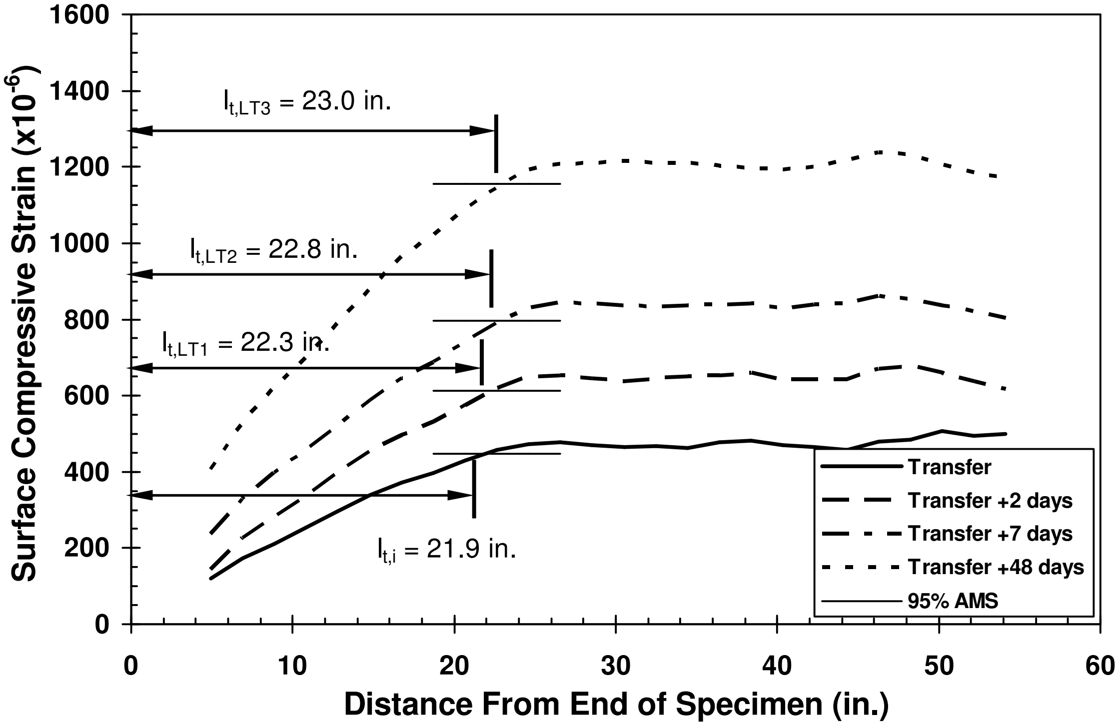

Figure D-1: Transfer Lengths at Various Ages for 0A-1-E

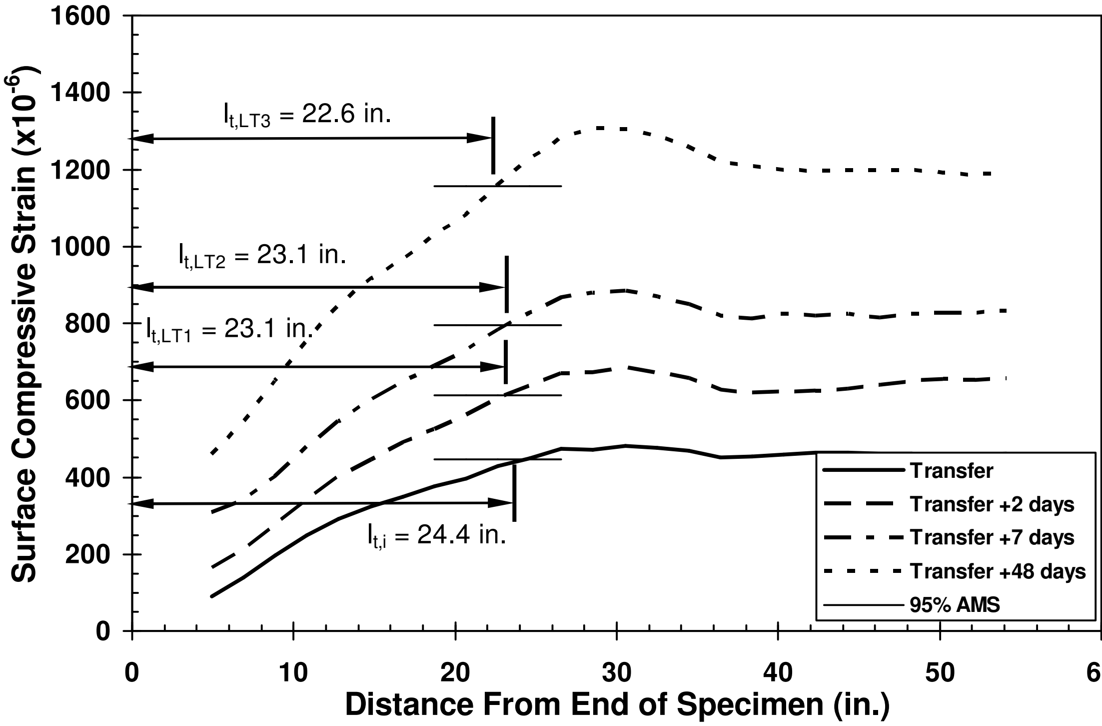

Figure D-2: Transfer Lengths at Various Ages for 0A-1-W

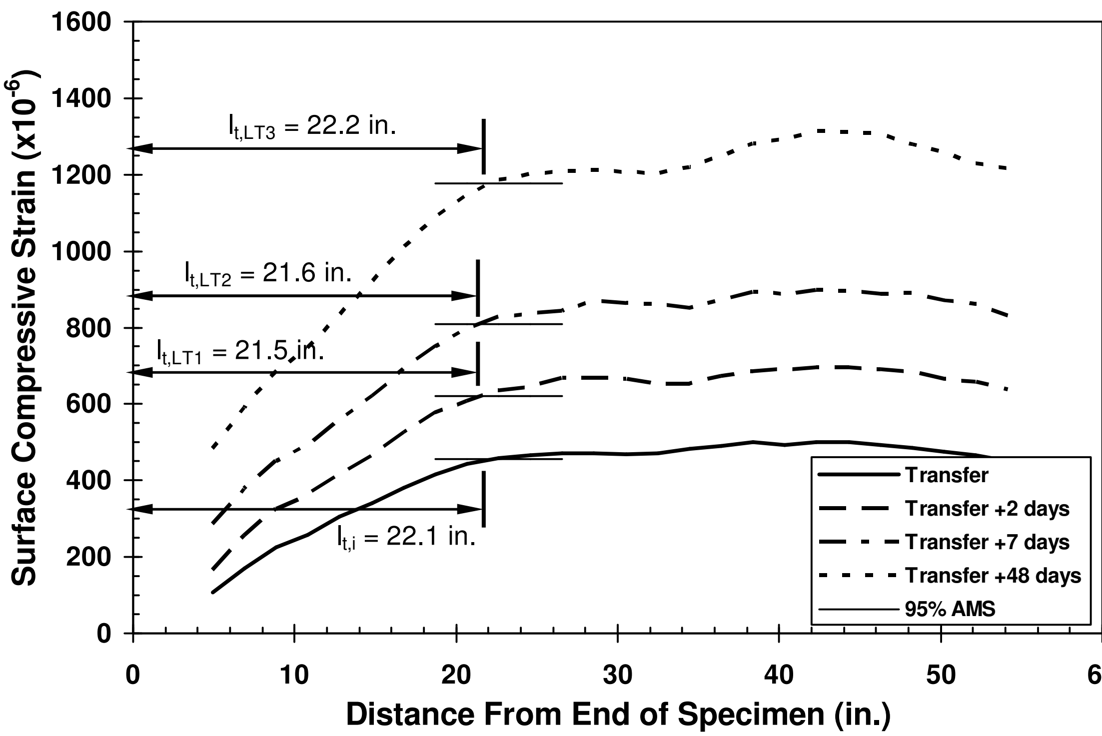

Figure D-3: Transfer Lengths at Various Ages for 0B-1-E

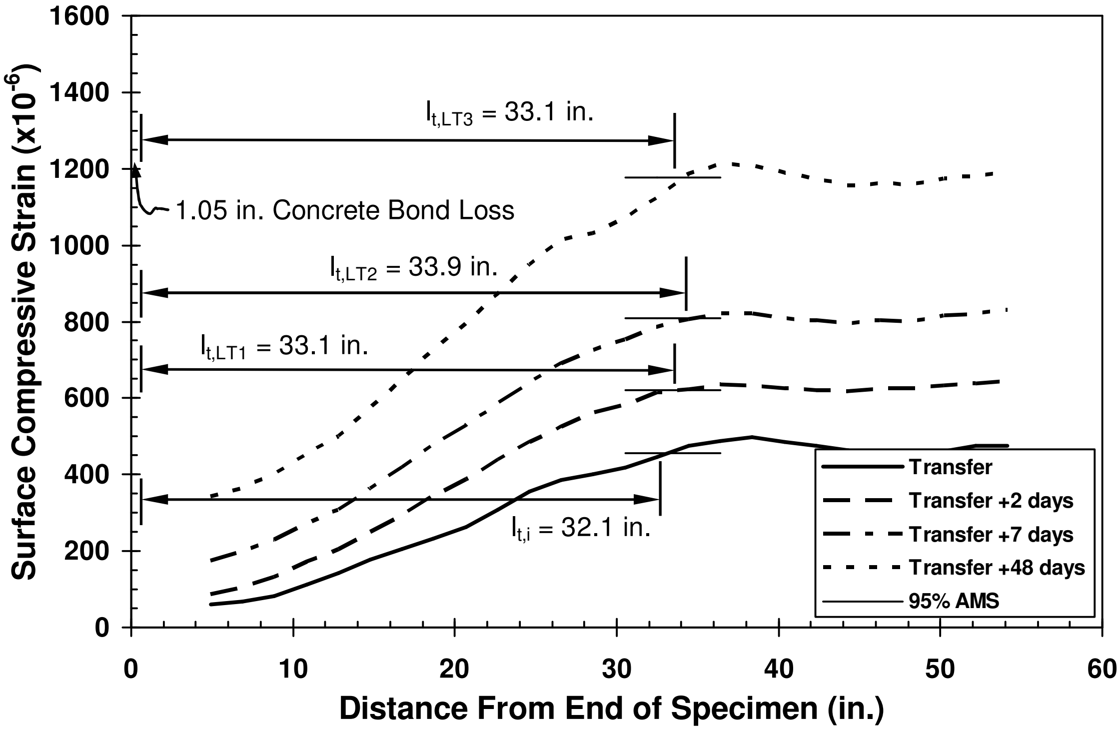

Figure D-4: Transfer Lengths at Various Ages for 0B-1-W

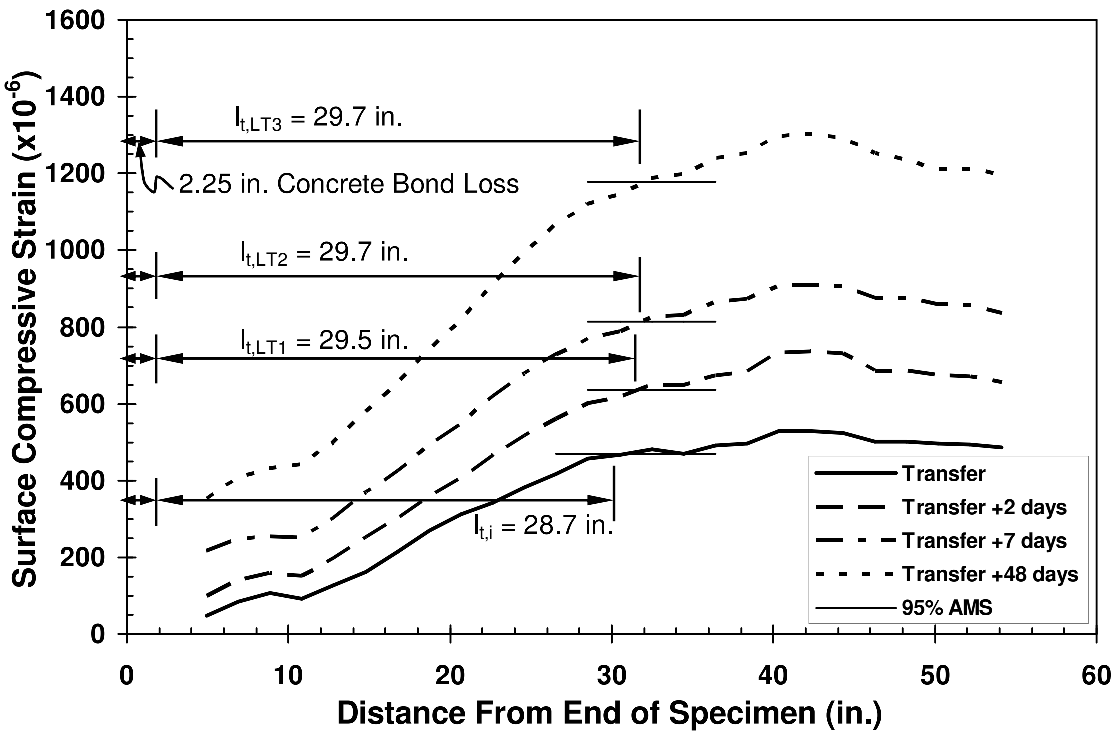

Figure D-5: Transfer Lengths at Various Ages for 0C-1-E

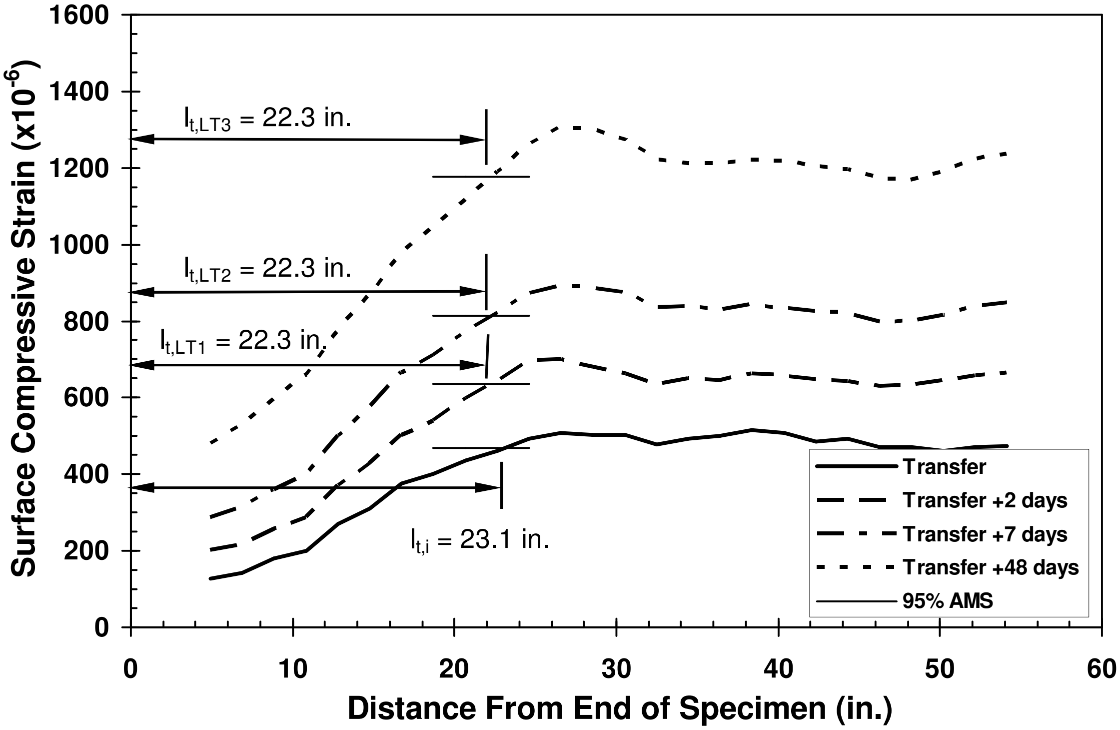

Figure D-6: Transfer Lengths at Various Ages for 0C-1-W

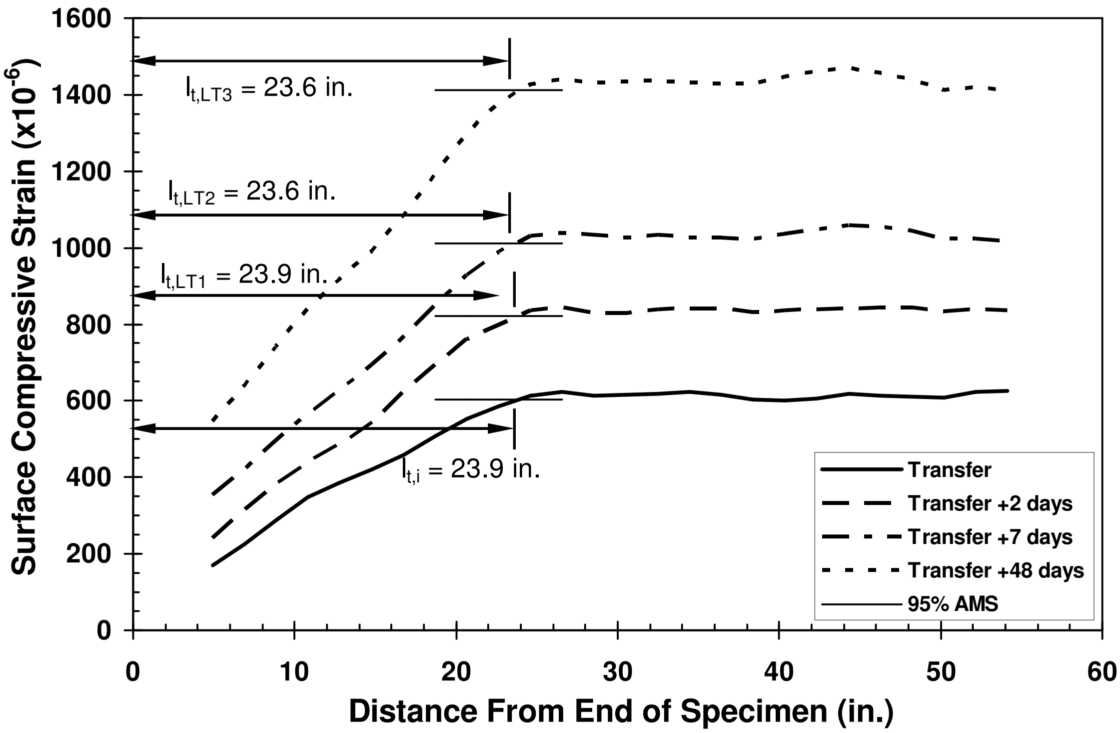

Figure D-7: Transfer Lengths at Various Ages for 0D-2-E

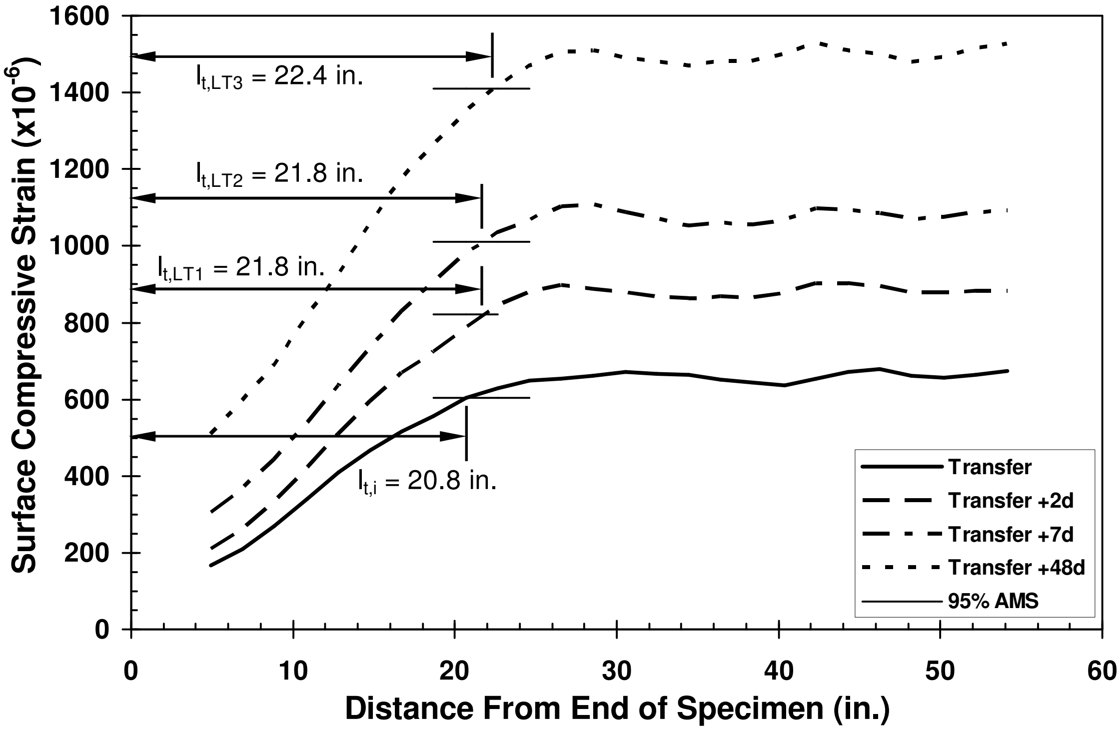

Figure D-8: Transfer Lengths at Various Ages for 0D-2-W

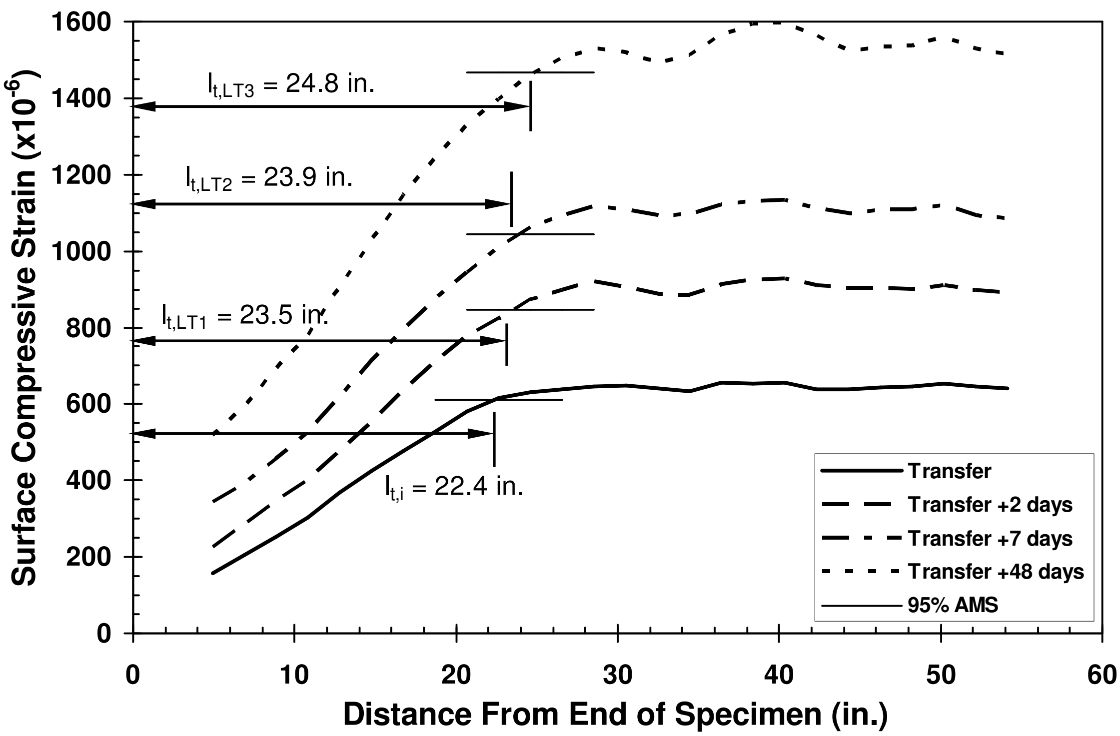

Figure D-9: Transfer Lengths at Various Ages for 0E-2-E

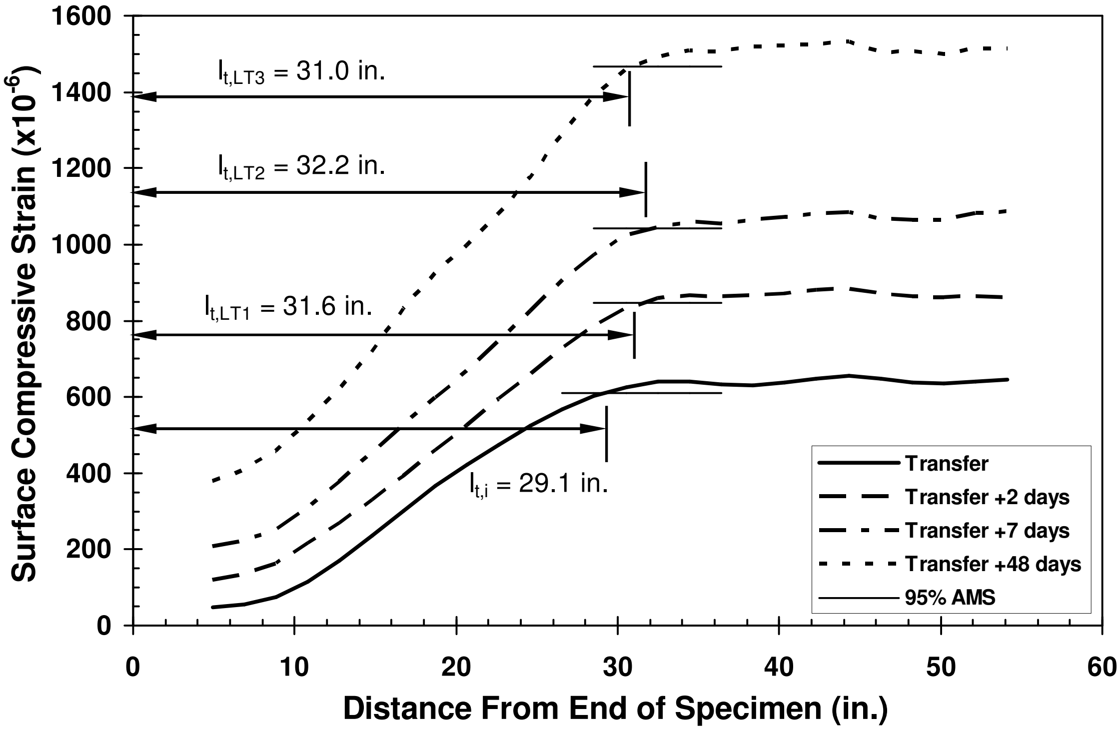

Figure D-10: Transfer Lengths at Various Ages for 0E-2-W

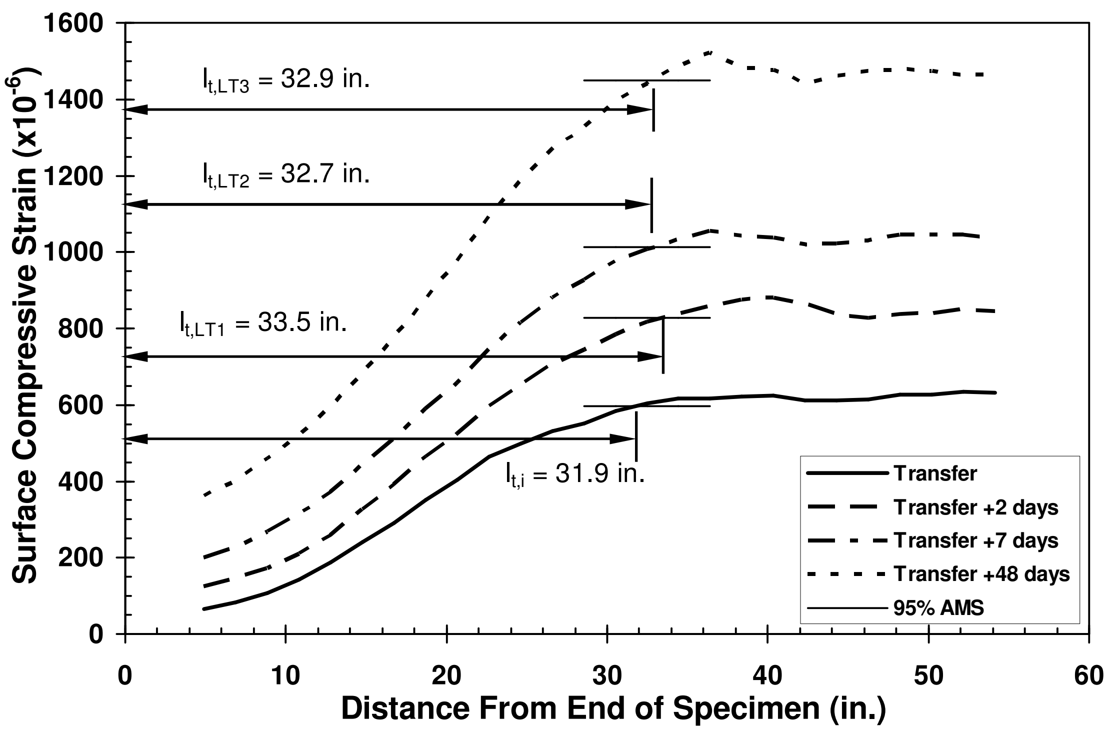

Figure D-11: Transfer Lengths at Various Ages for 0F-2-E

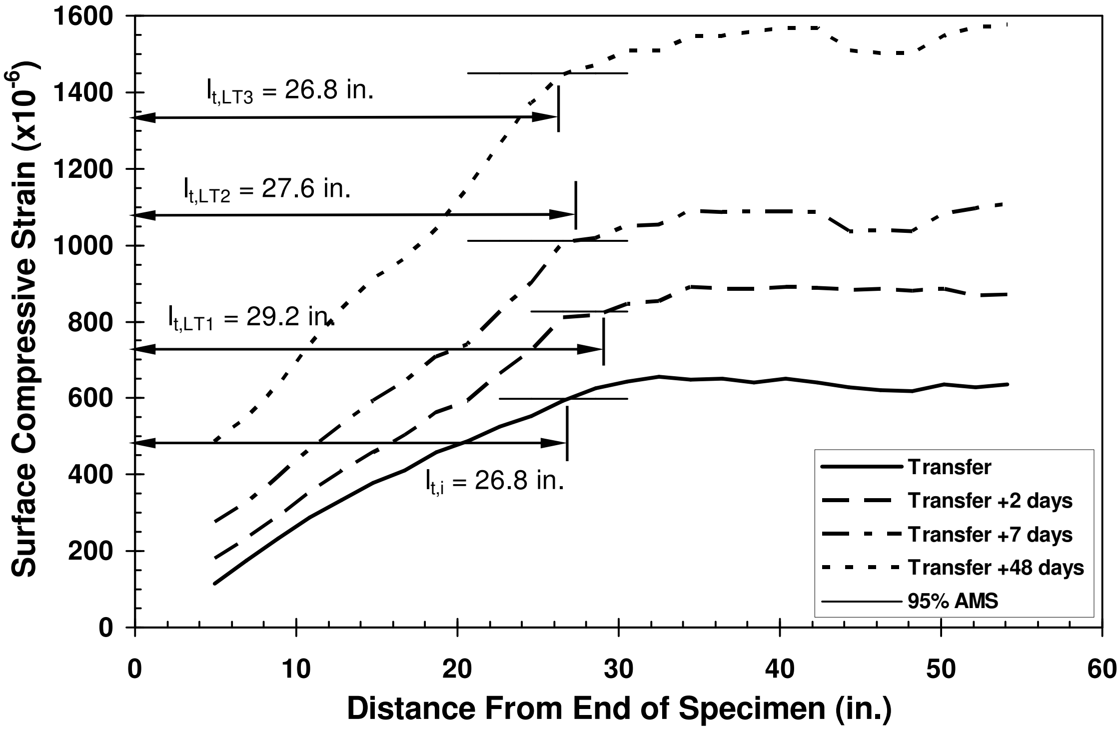

Figure D-12: Transfer Lengths at Various Ages for 0F-2-W

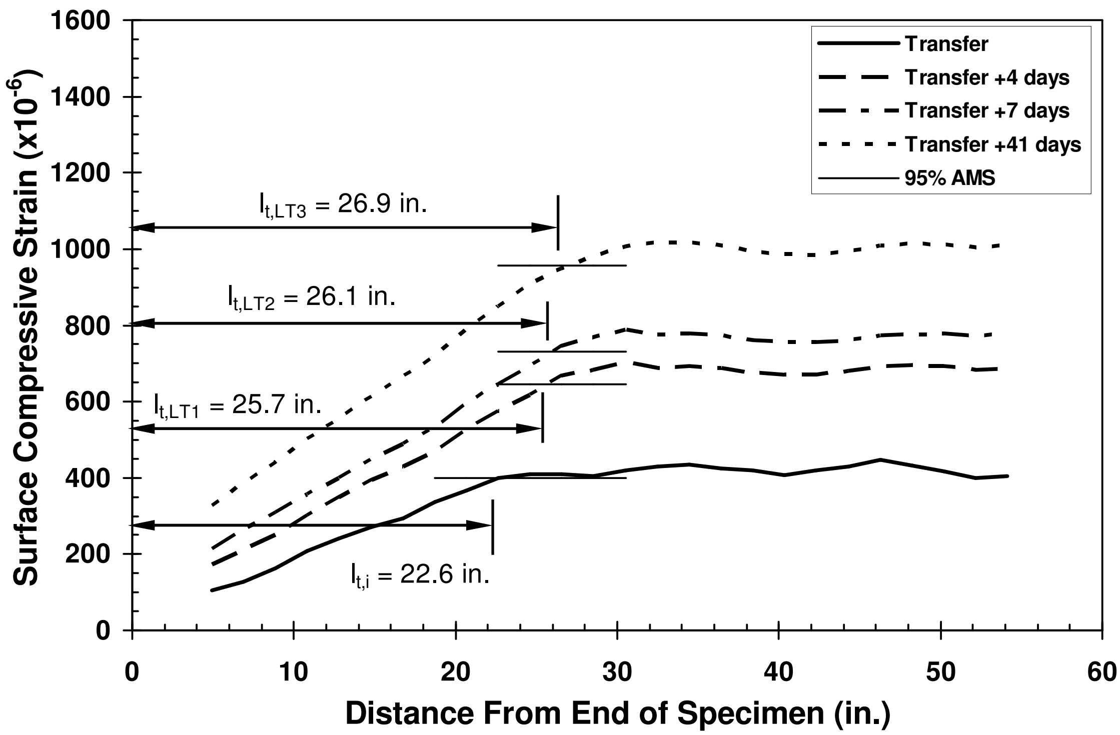

Figure D-13: Transfer Lengths at Various Ages for 9A-1-E

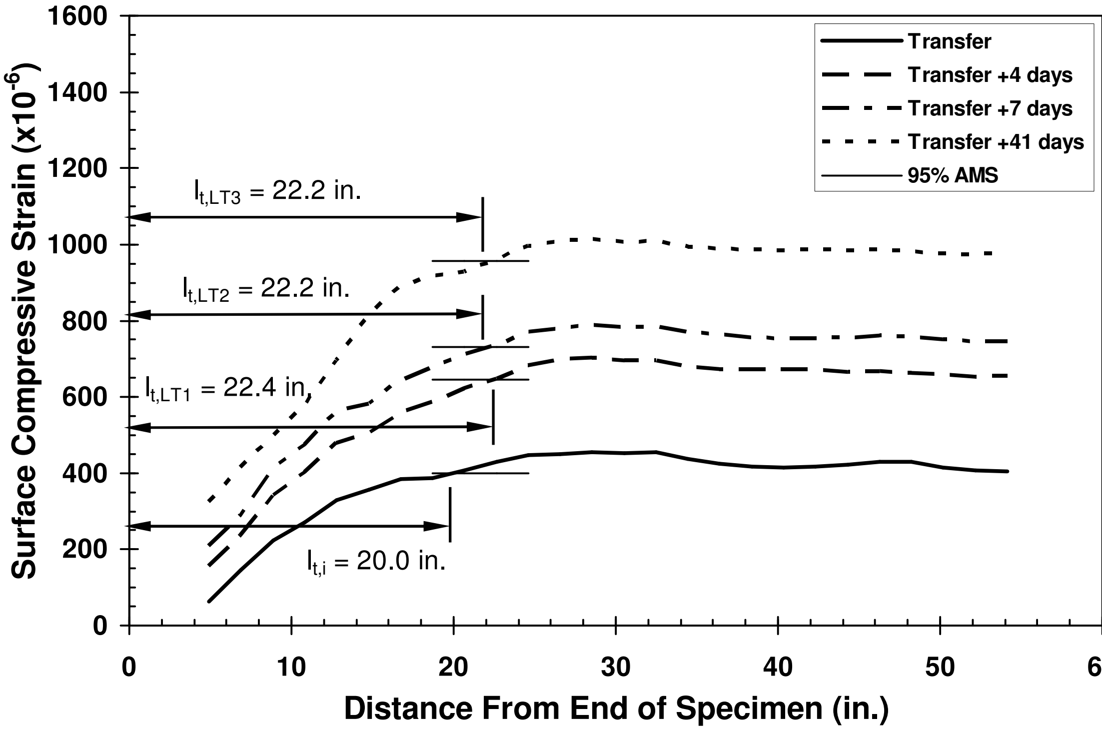

Figure D-14: Transfer Lengths at Various Ages for 9A-1-W

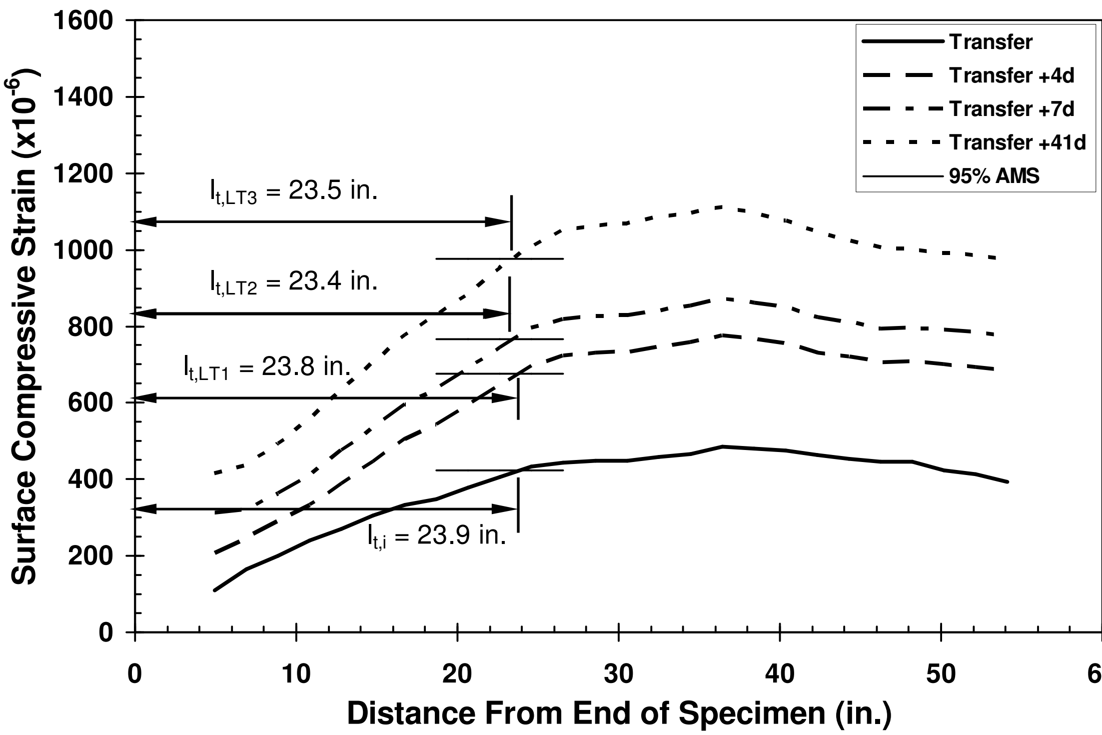

Figure D-15: Transfer Lengths at Various Ages for 9B-1-E

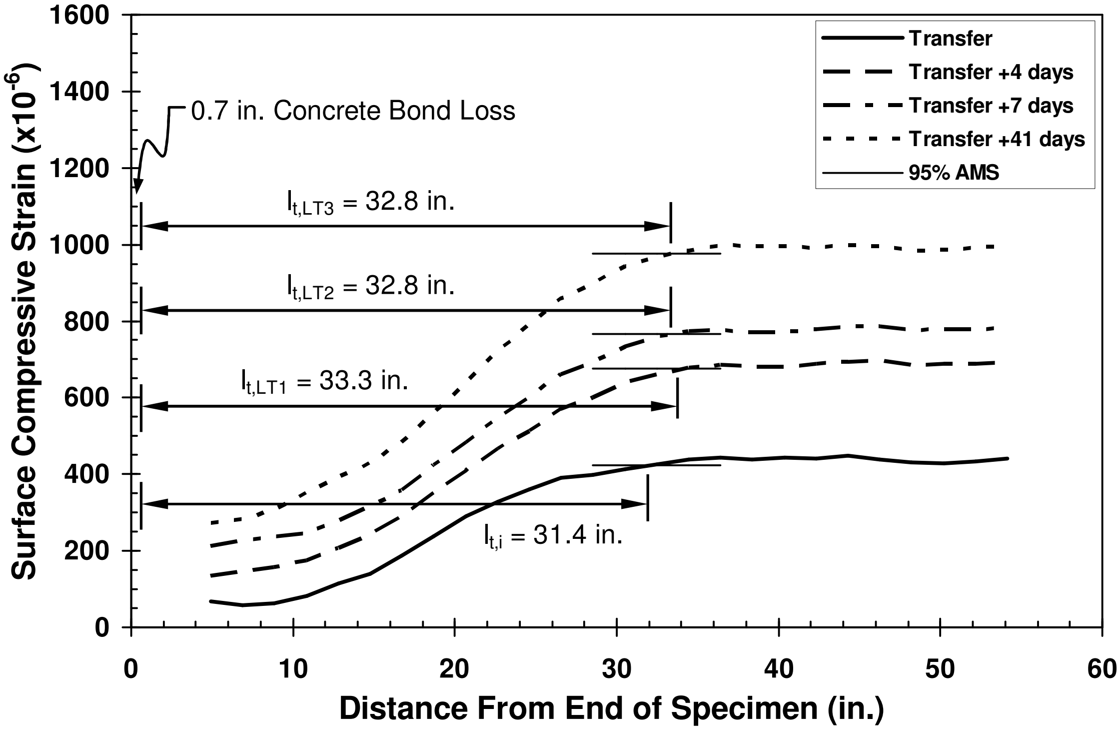

Figure D-16: Transfer Lengths at Various Ages for 9B-1-W

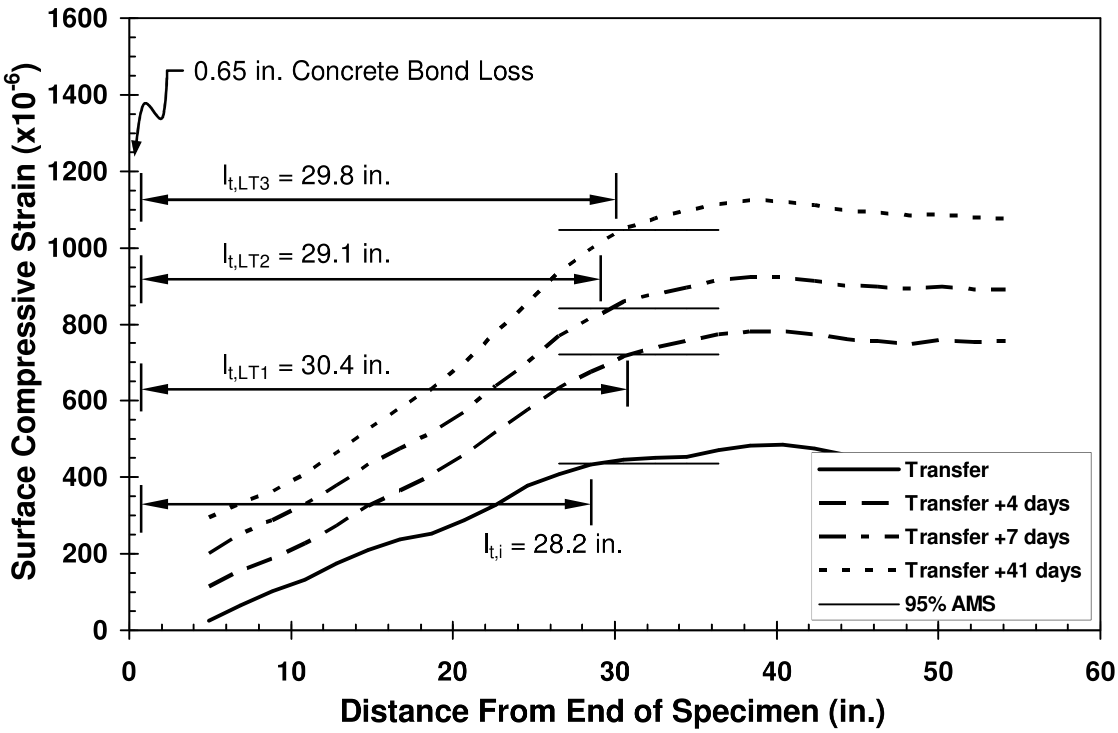

Figure D-17: Transfer Lengths at Various Ages for 9C-1-E

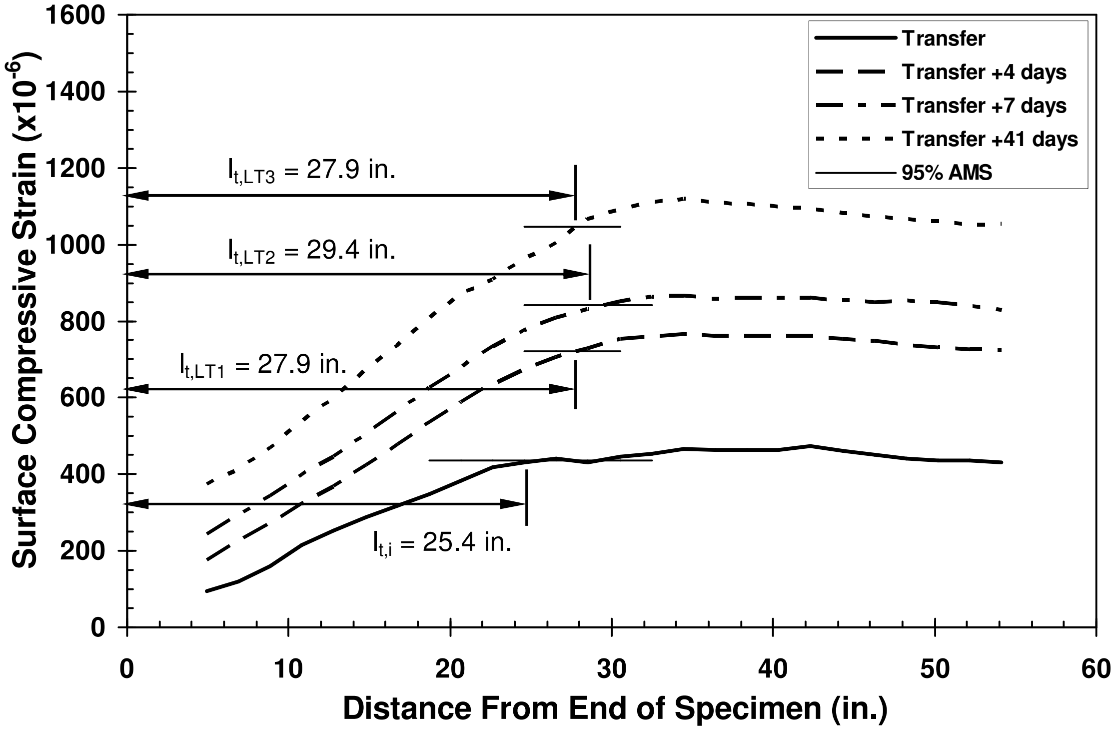

Figure D-18: Transfer Lengths at Various Ages for 9C-1-W

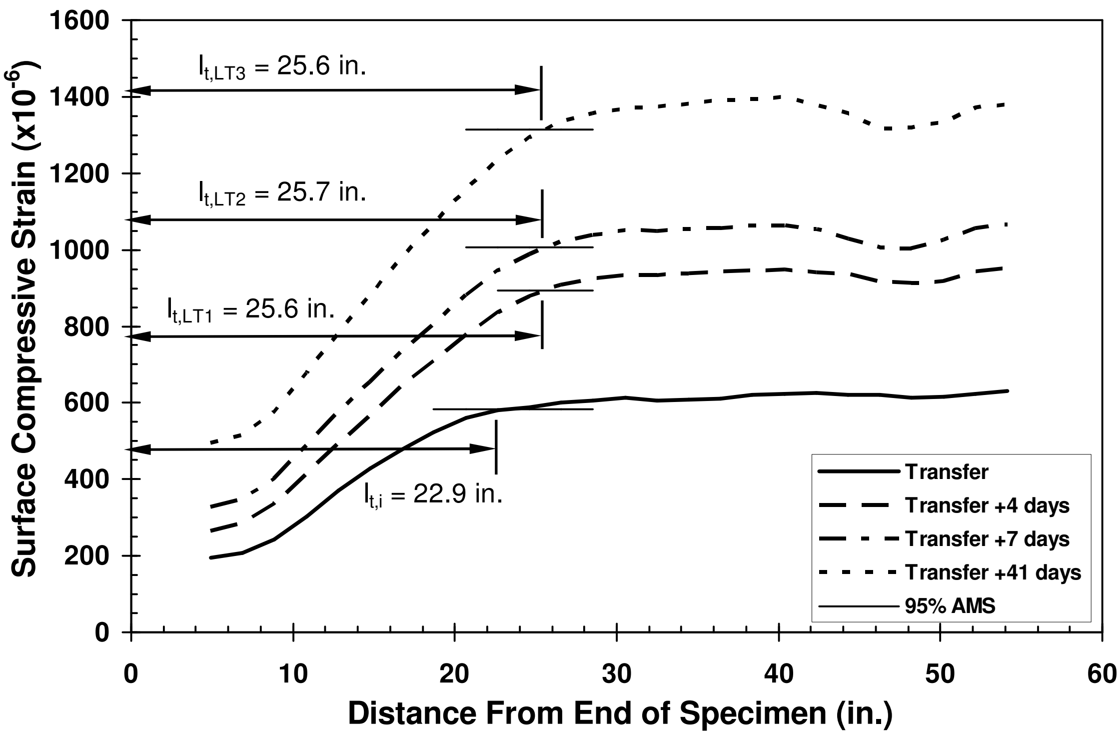

Figure D-19: Transfer Lengths at Various Ages for 9D-2-E

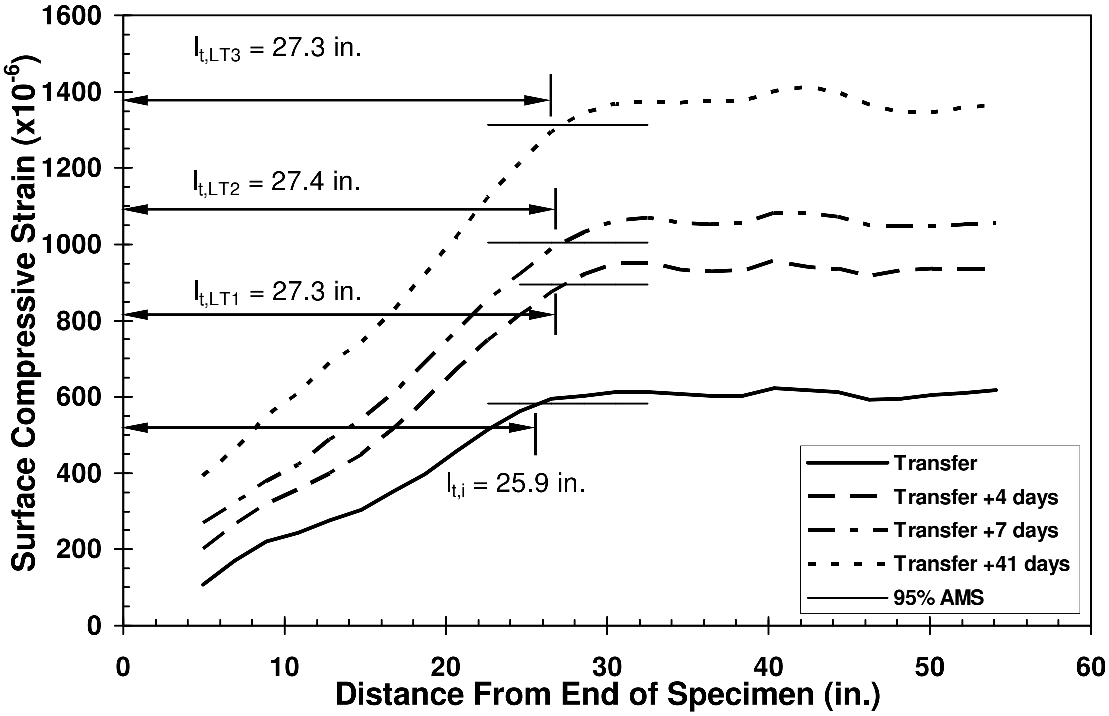

Figure D-20: Transfer Lengths at Various Ages for 9D-2-W

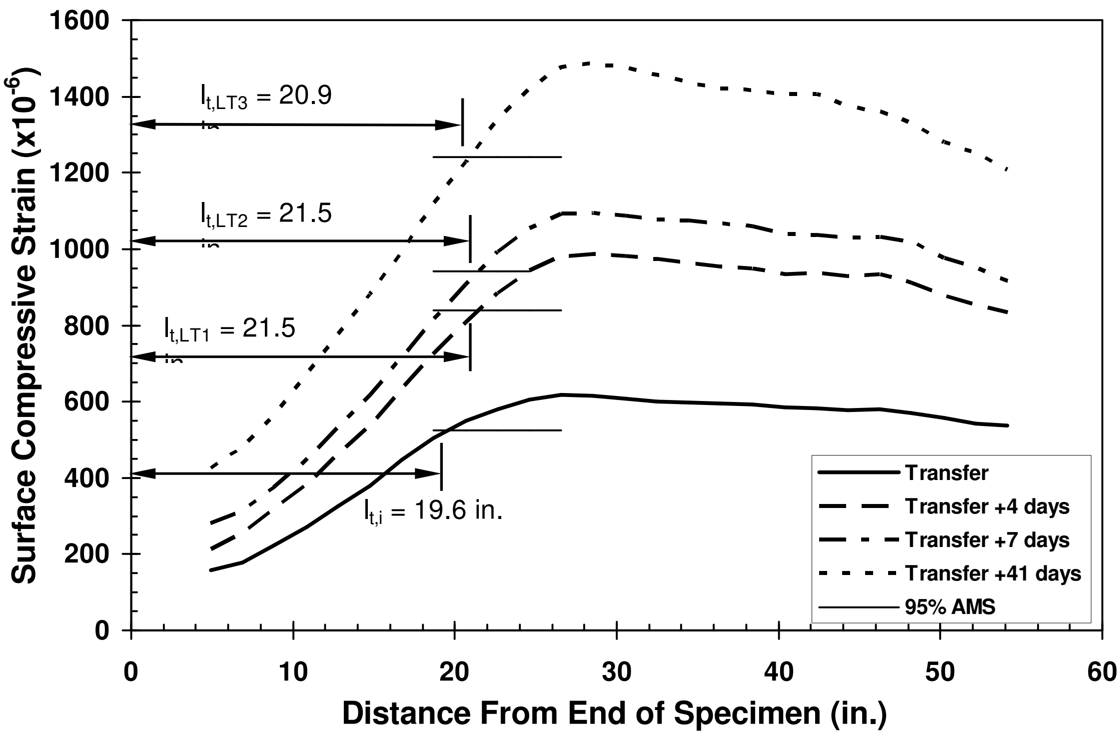

Figure D-21: Transfer Lengths at Various Ages for 9E-2-E

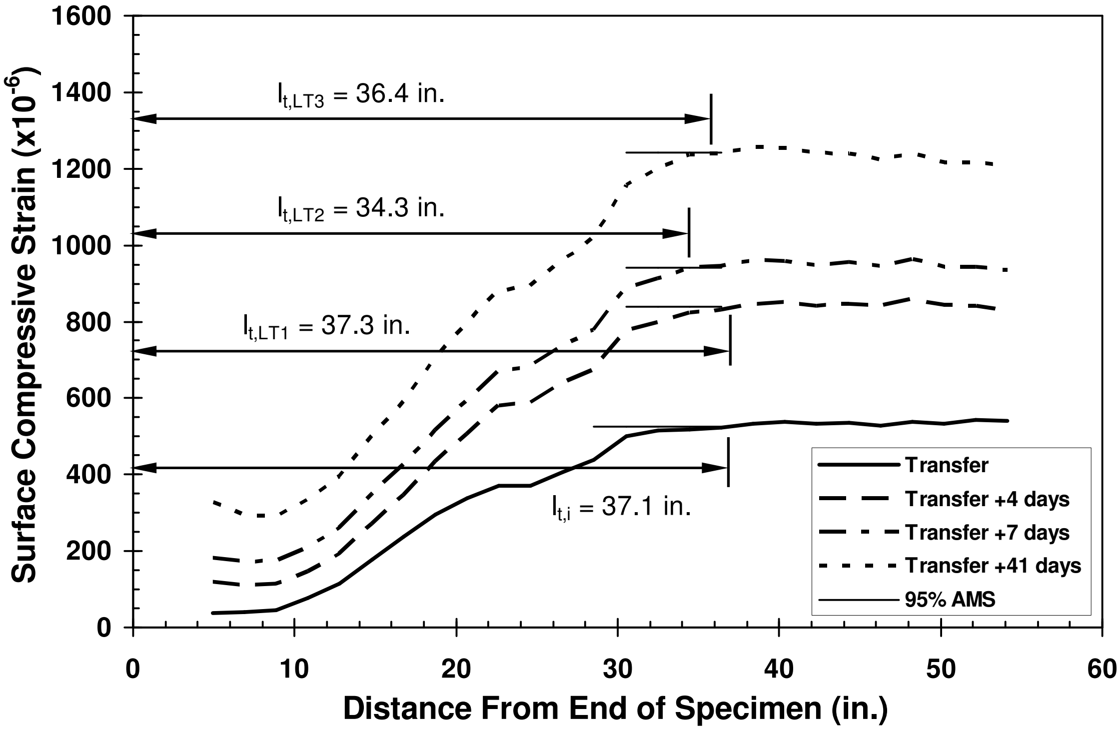

Figure D-22: Transfer Lengths at Various Ages for 9E-2-W

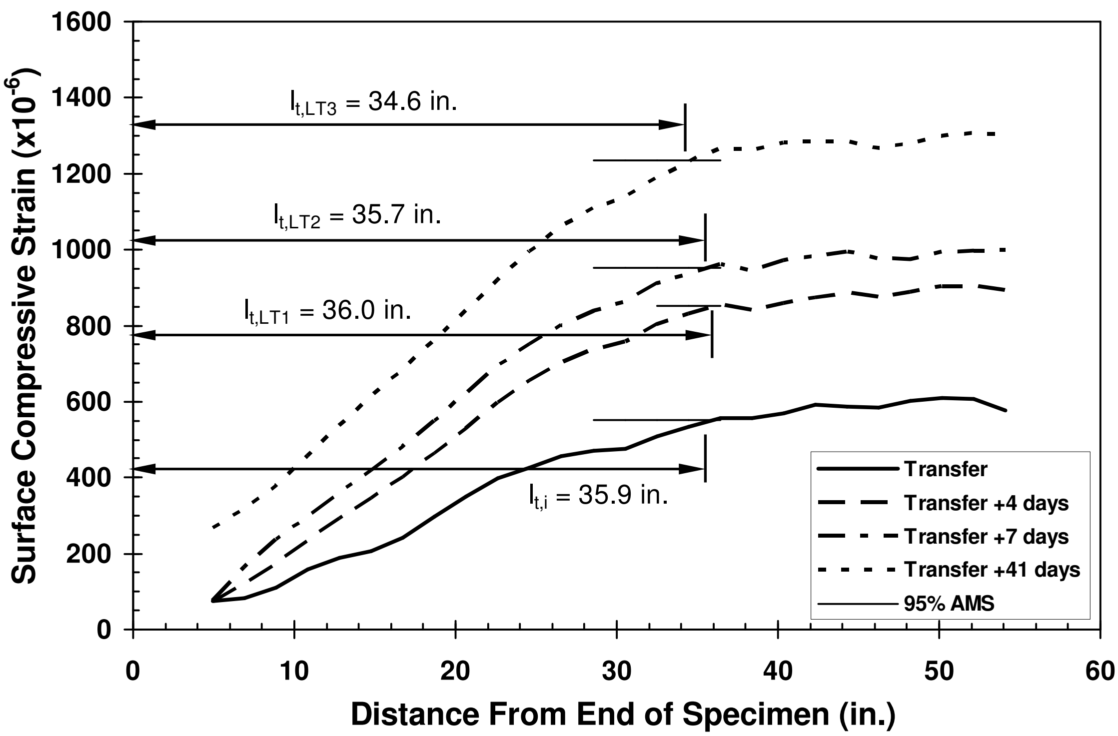

Figure D-23: Transfer Lengths at Various Ages for 9F-2-E

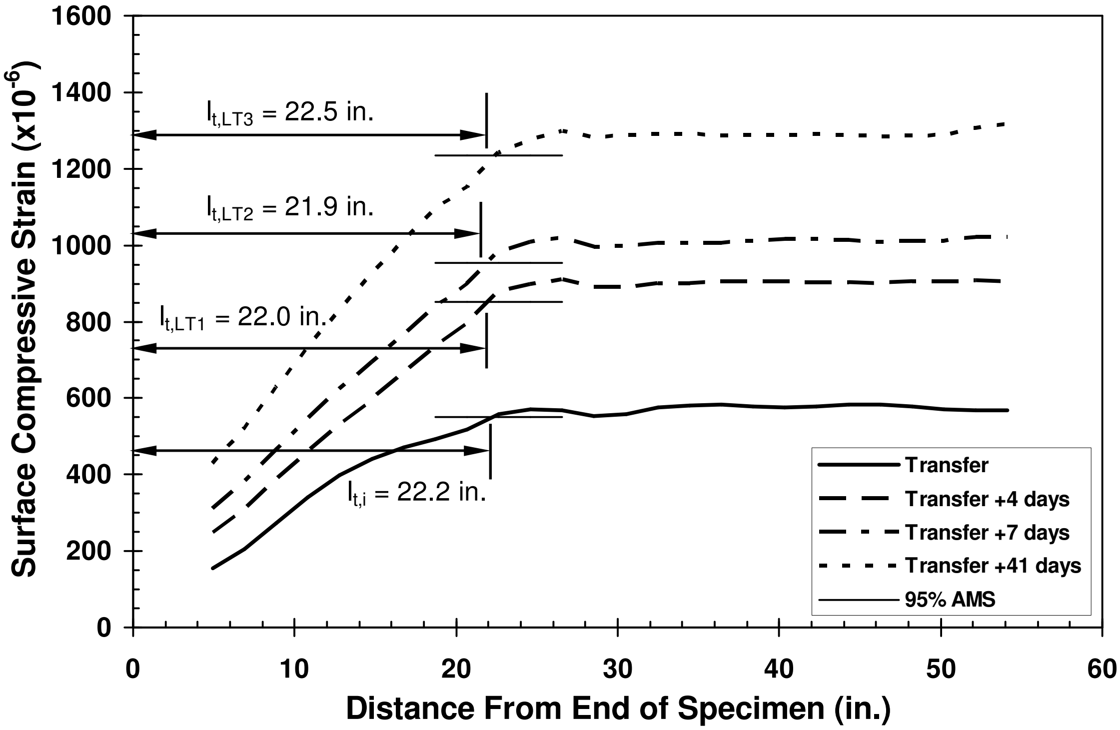

Figure D-24: Transfer Lengths at Various Ages for 9F-2-W

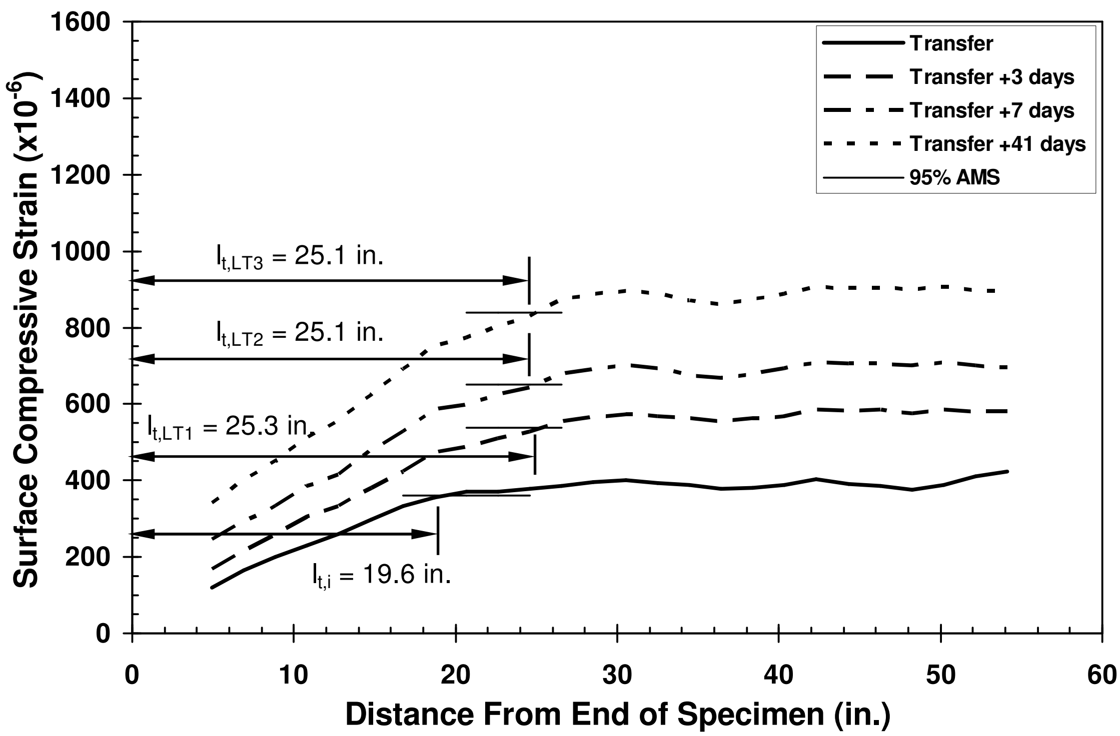

Figure D-25: Transfer Lengths at Various Ages for 7A-1-E

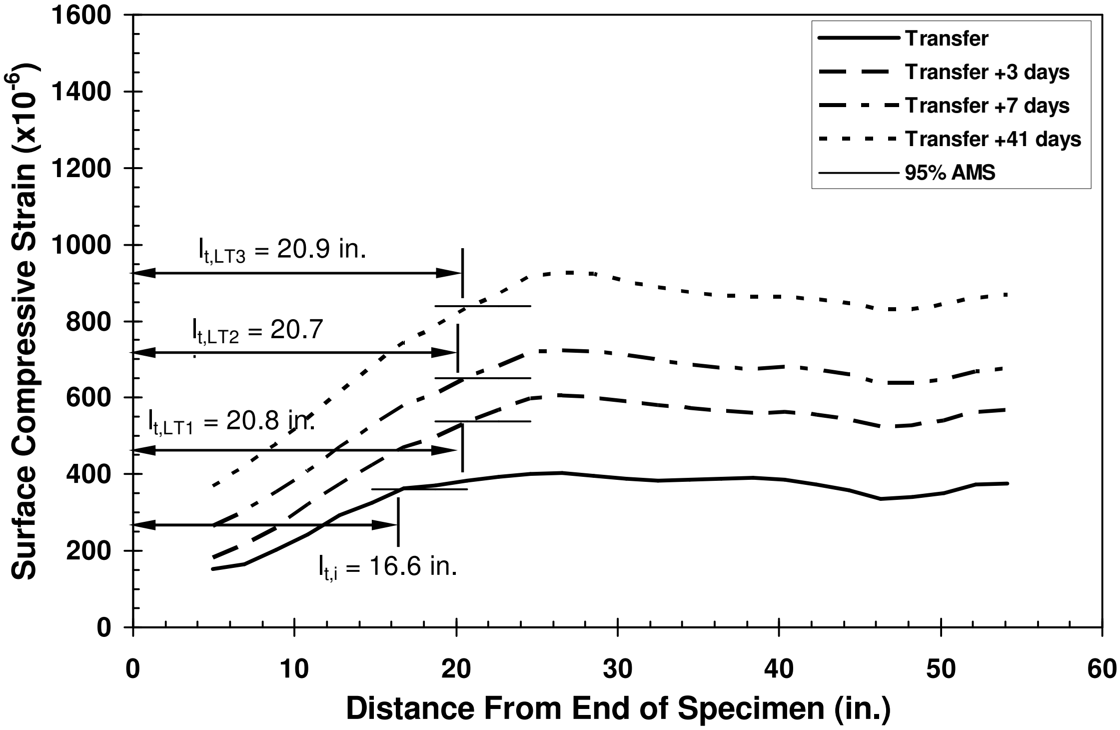

Figure D-26: Transfer Lengths at Various Ages for 7A-1-W

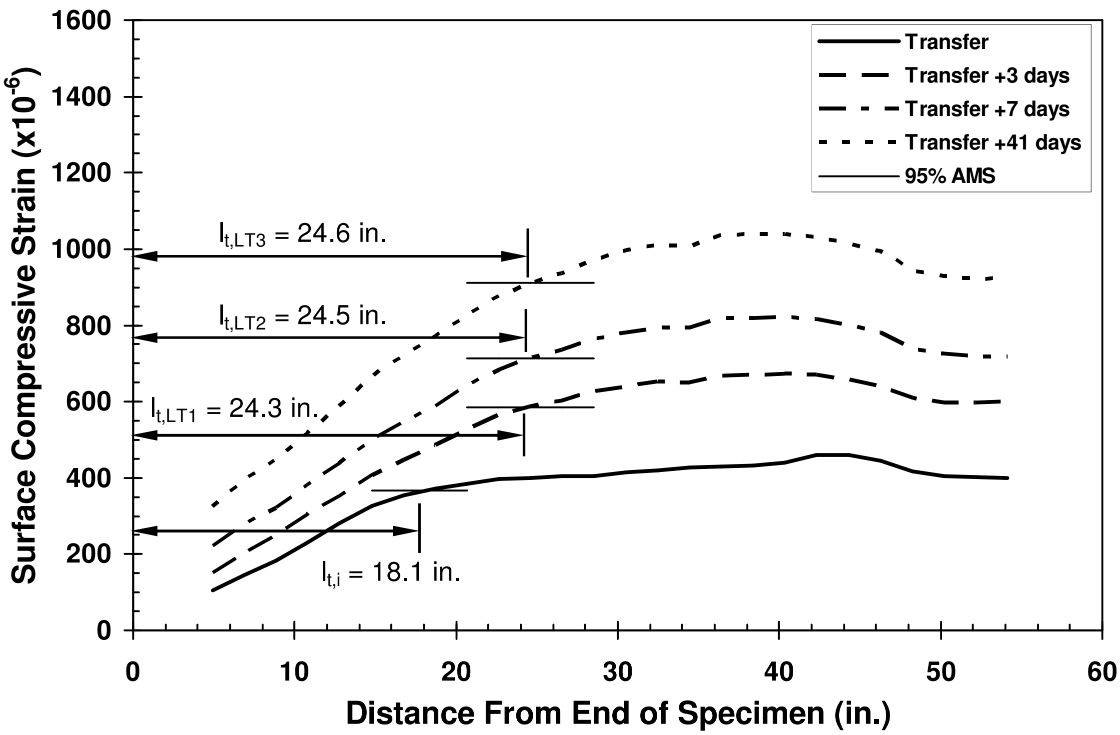

Figure D-27: Transfer Lengths at Various Ages for 7B-1-E

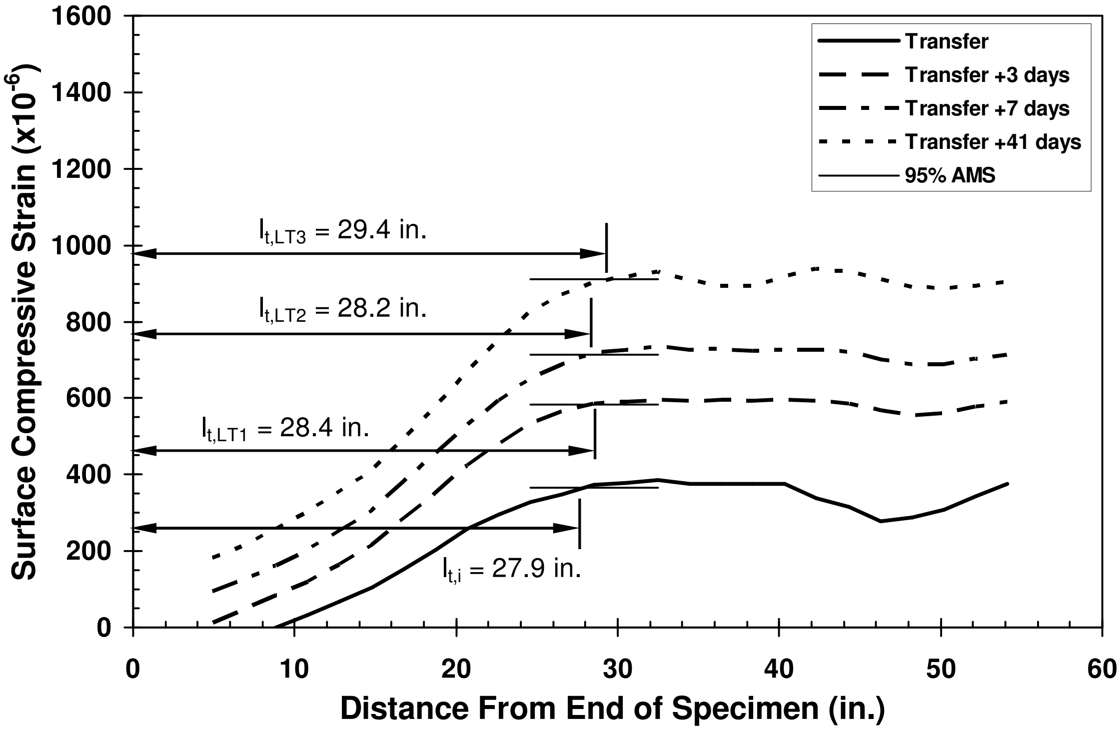

Figure D-28: Transfer Lengths at Various Ages for 7B-1-W

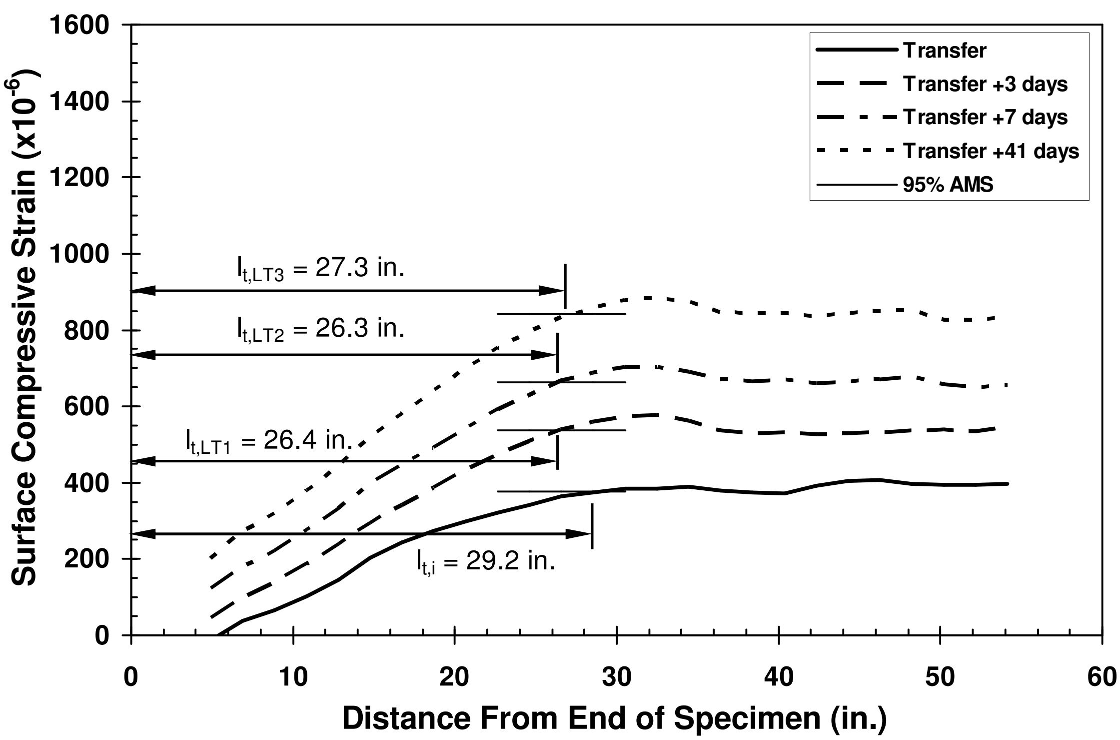

Figure D-29: Transfer Lengths at Various Ages for 7C-1-E

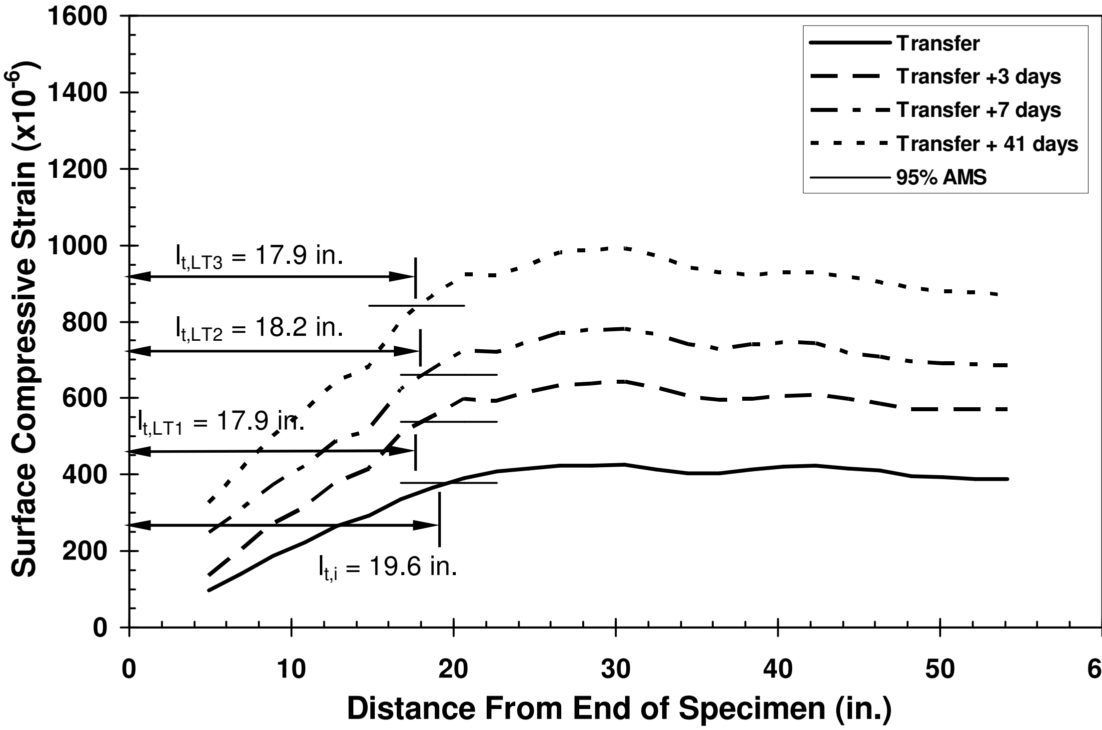

Figure D-30: Transfer Lengths at Various Ages for 7C-1-W

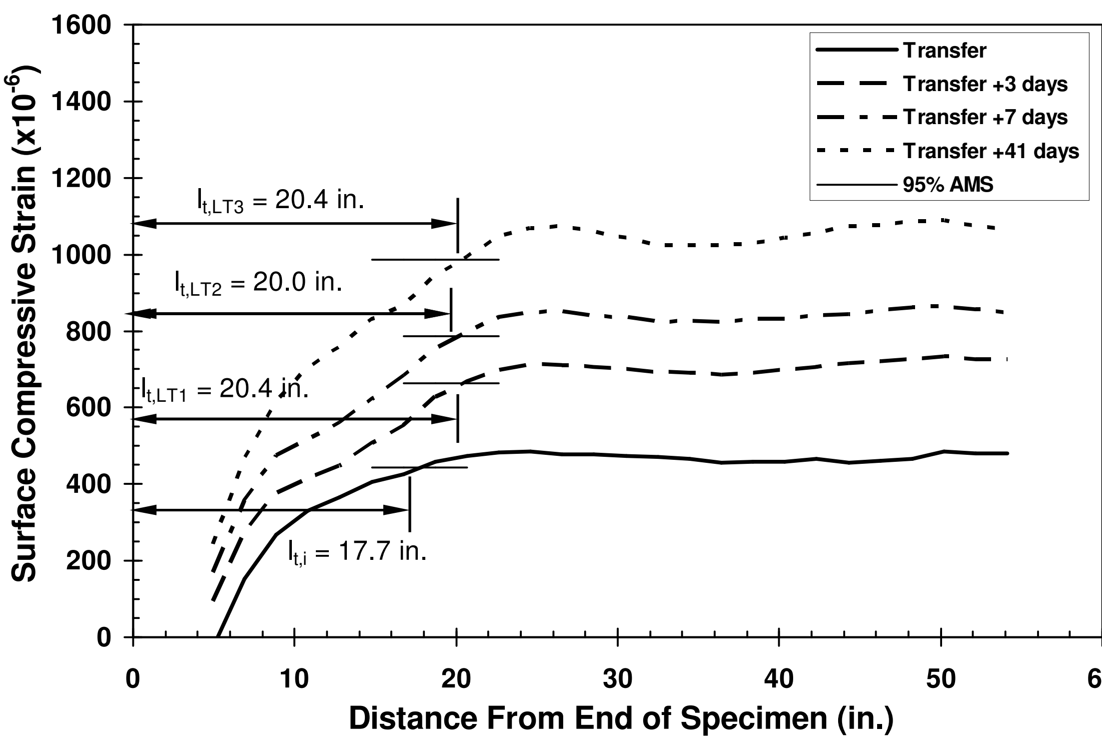

Figure D-31: Transfer Lengths at Various Ages for 7D-2-E

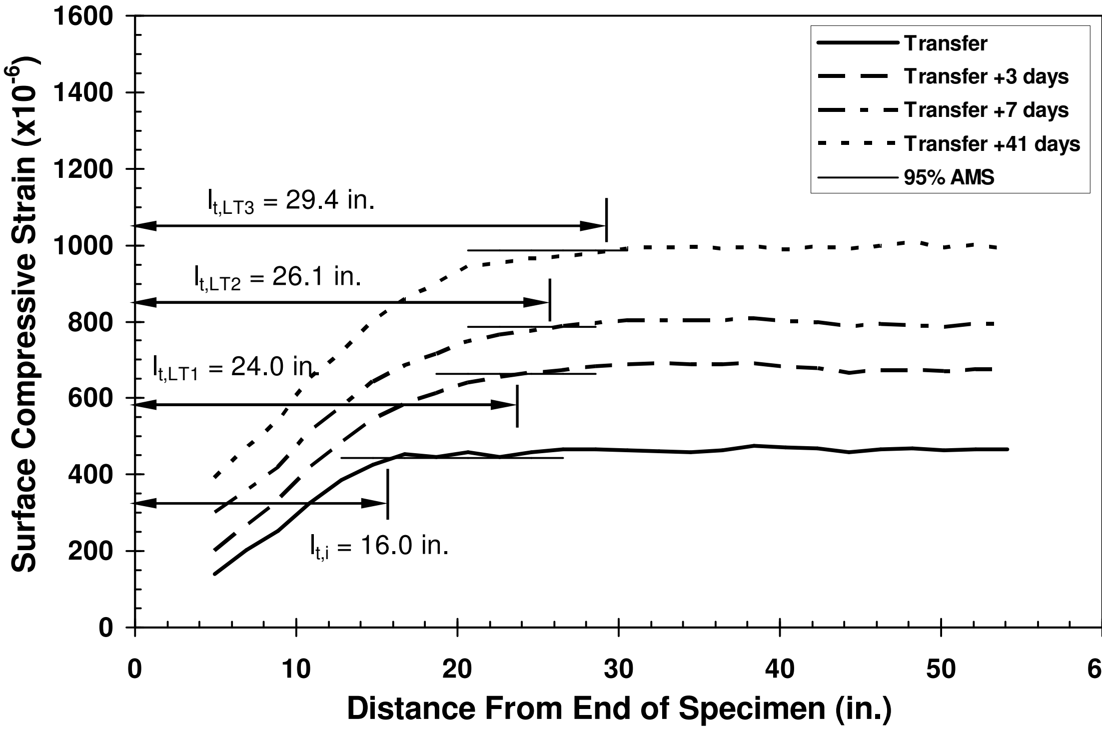

Figure D-32: Transfer Lengths at Various Ages for 7D-2-W

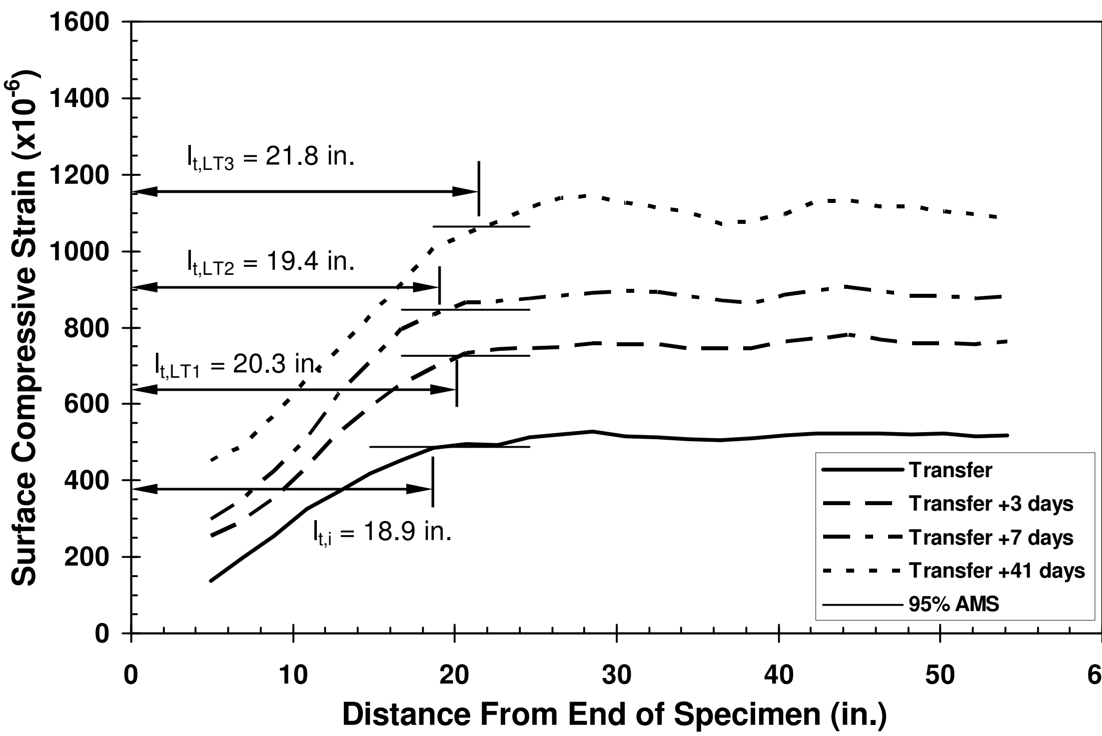

Figure D-33: Transfer Lengths at Various Ages for 7E-2-E

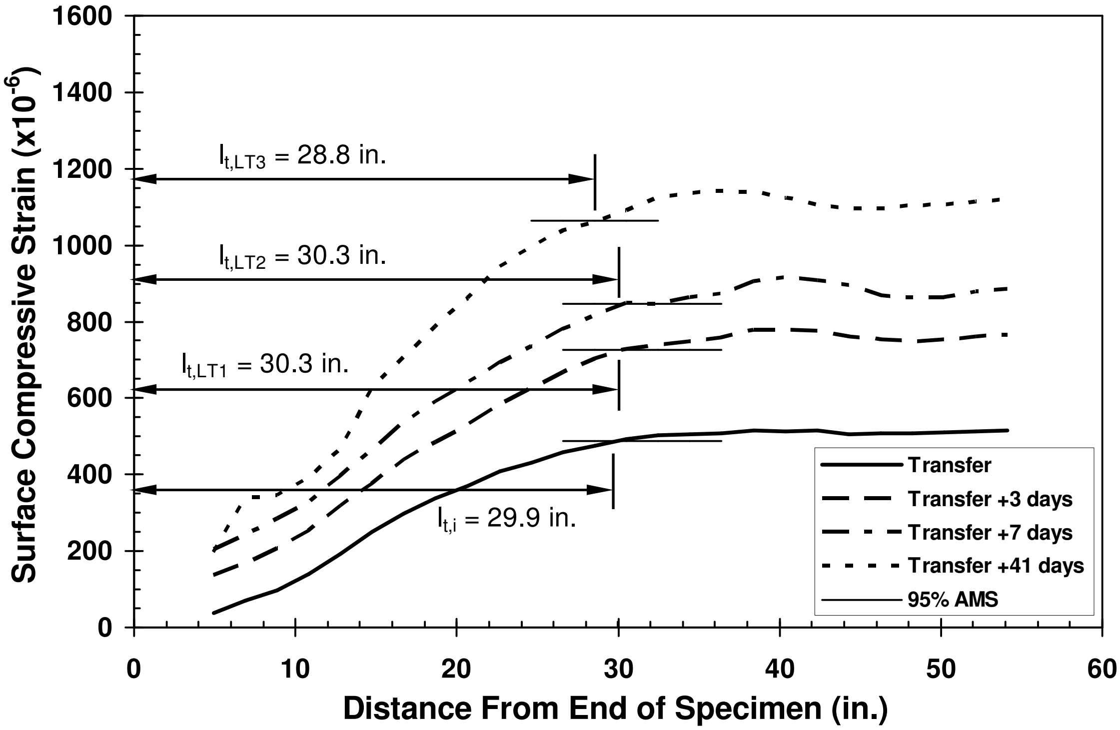

Figure D-34: Transfer Lengths at Various Ages for 7E-2-W

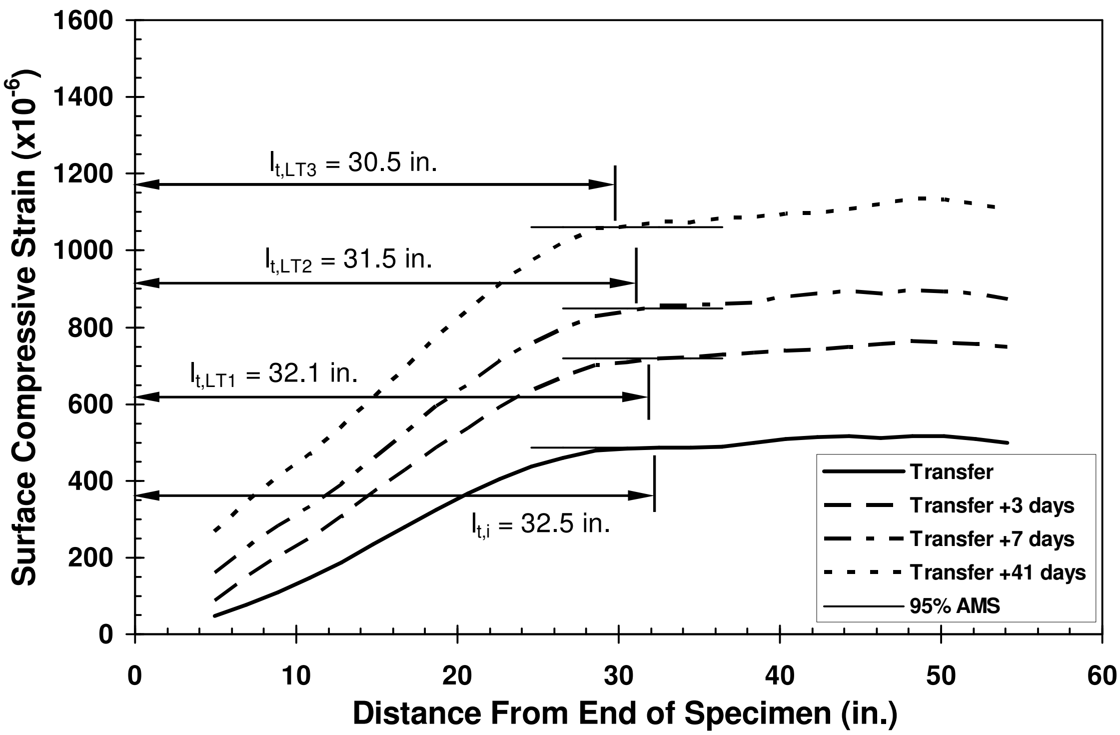

Figure D-35: Transfer Lengths at Various Ages for 7F-2-E

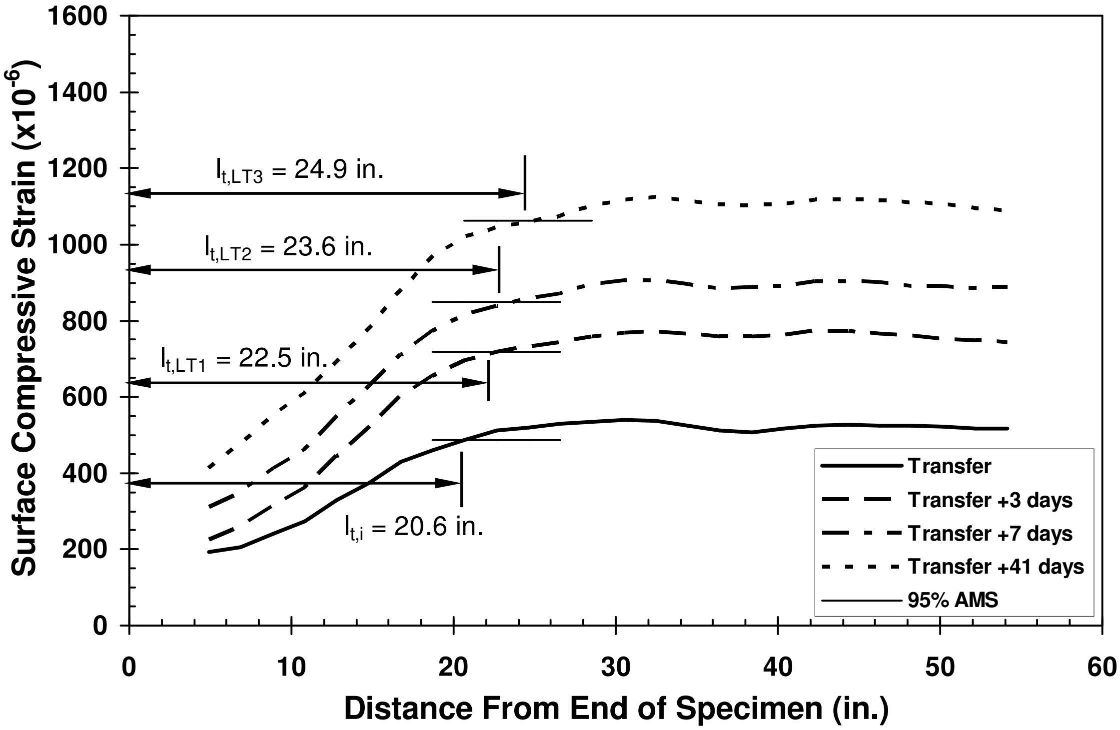

Figure D-36: Transfer Lengths at Various Ages for 7F-2-W

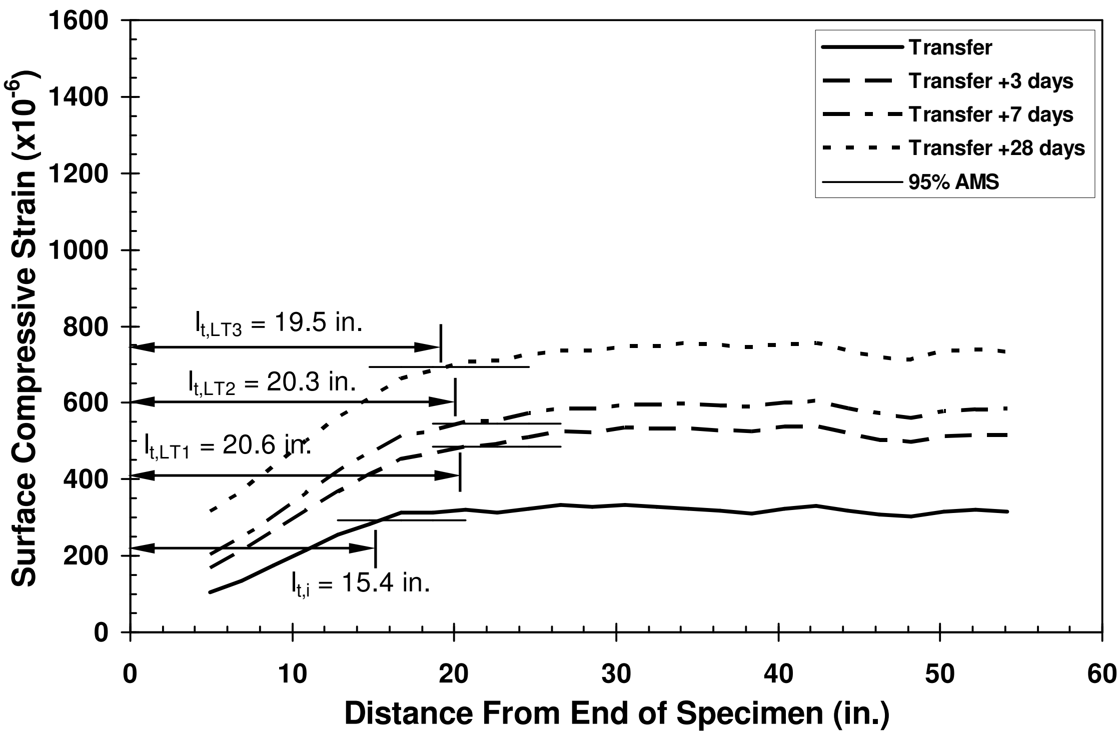

Figure D-37: Transfer Lengths at Various Ages for 7bA-1-E

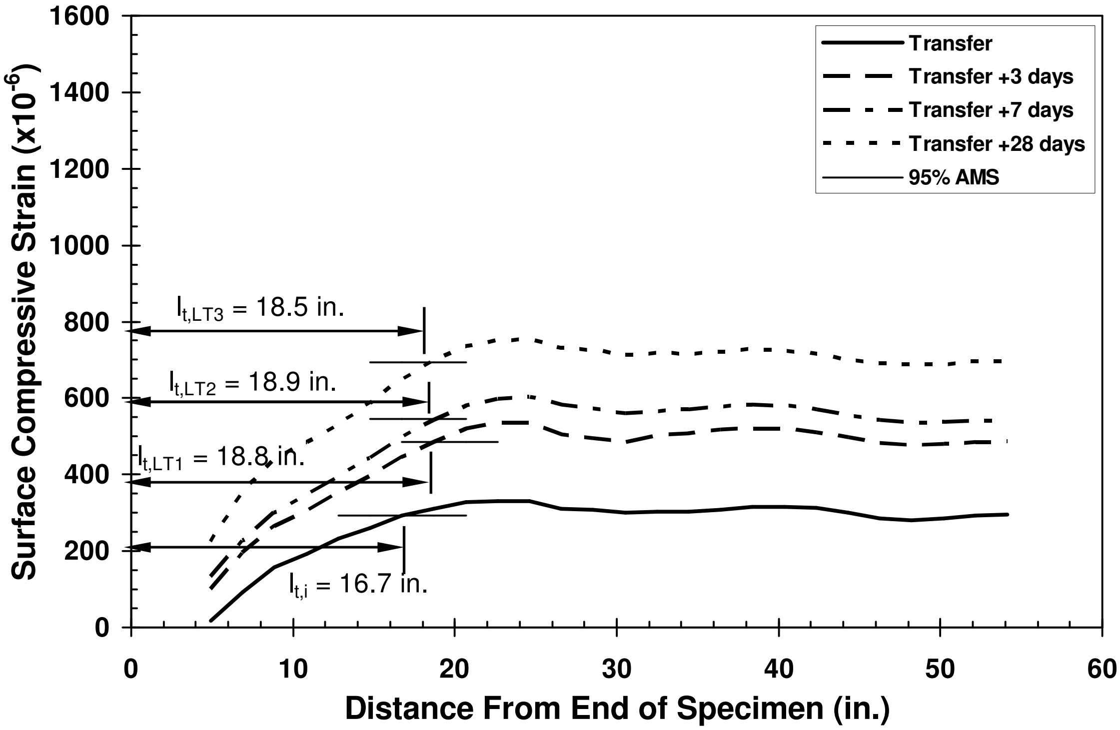

Figure D-38: Transfer Lengths at Various Ages for 7bA-1-W

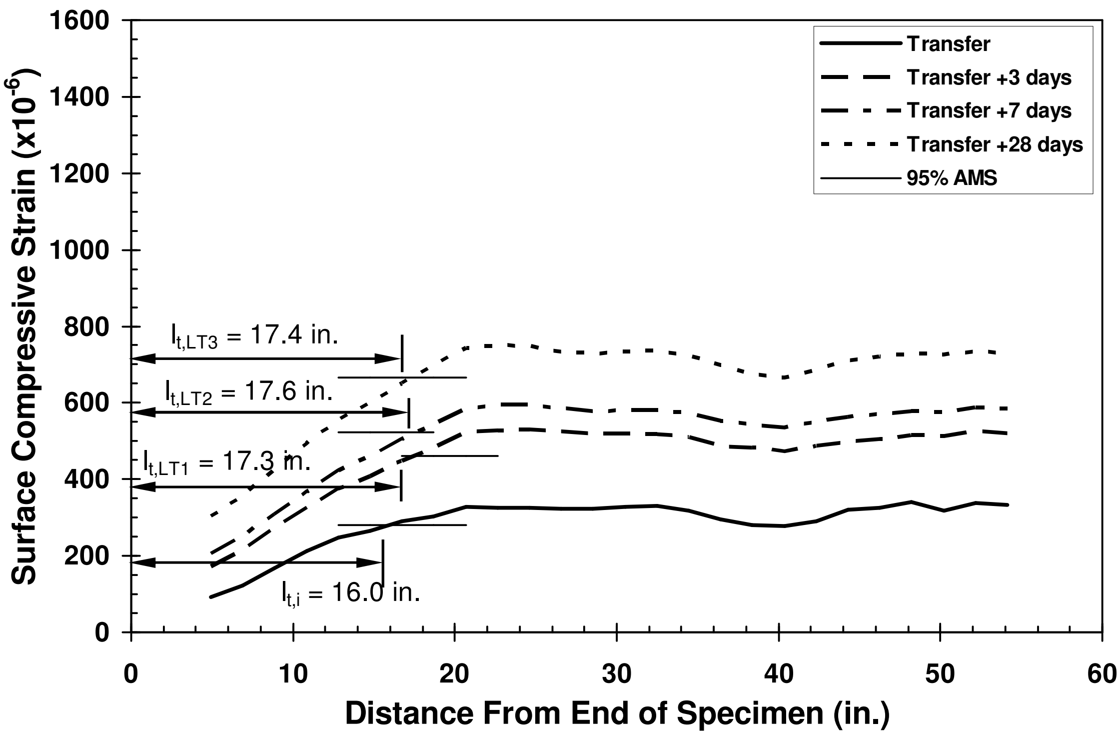

Figure D-39: Transfer Lengths at Various Ages for 7bB-1-E

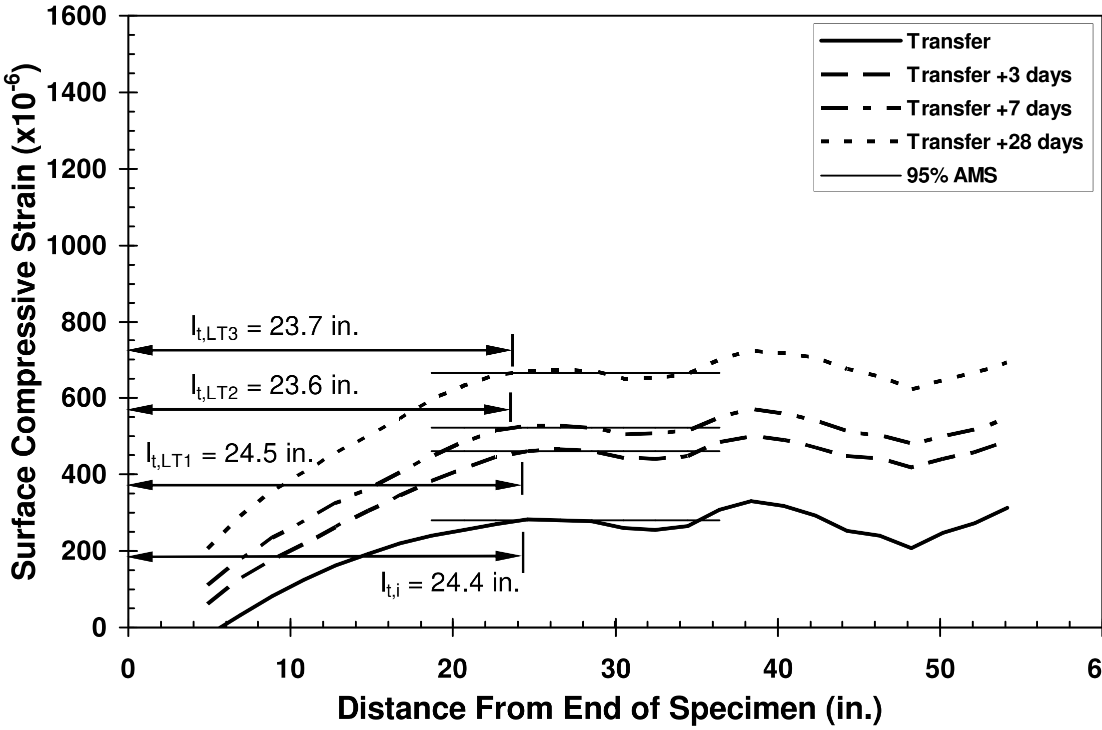

Figure D-40: Transfer Lengths at Various Ages for 7bB-1-W

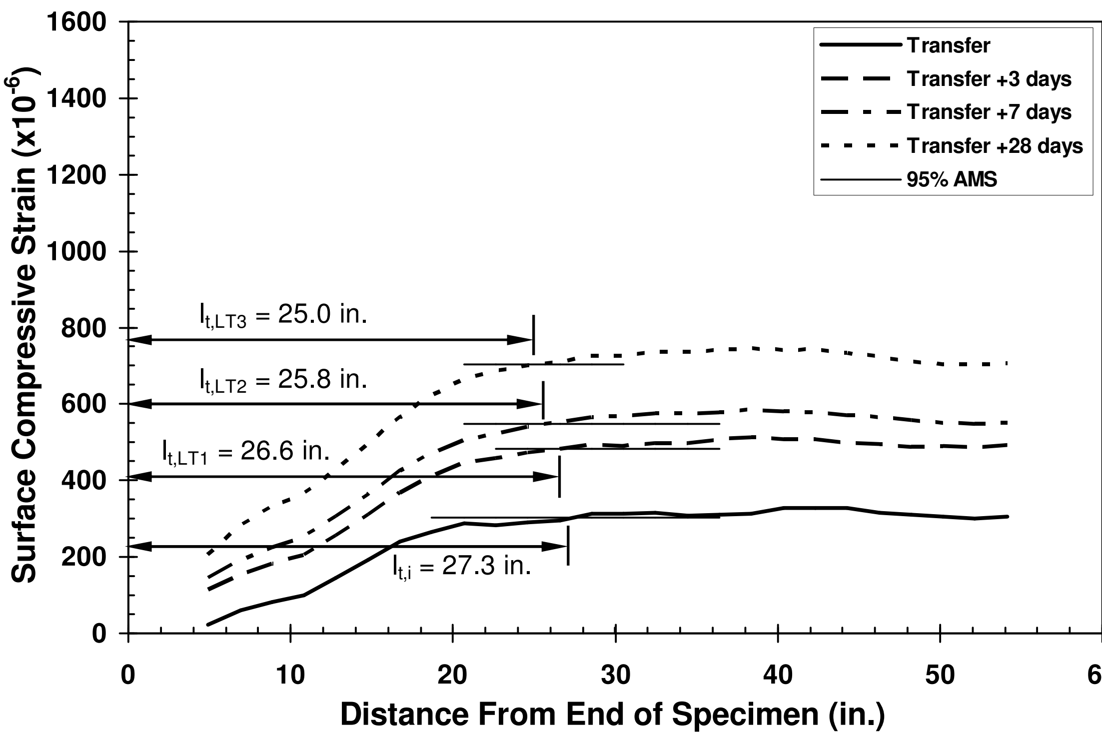

Figure D-41: Transfer Lengths at Various Ages for 7bC-1-E

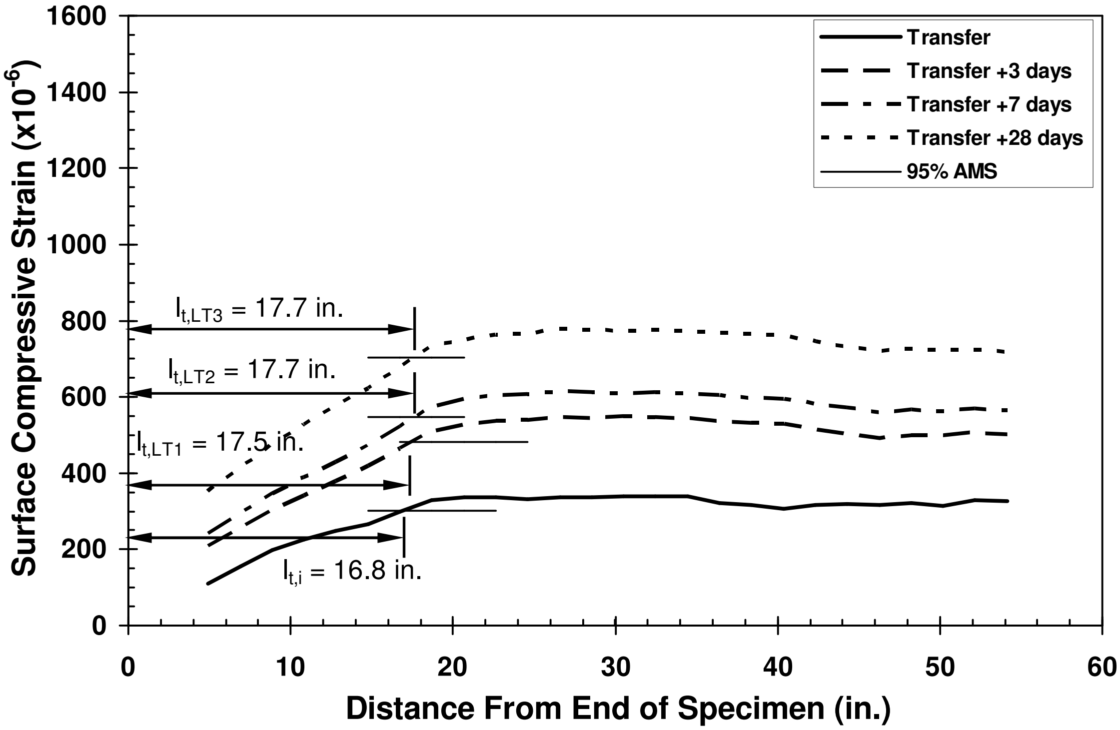

Figure D-42: Transfer Lengths at Various Ages for 7bC-1-W

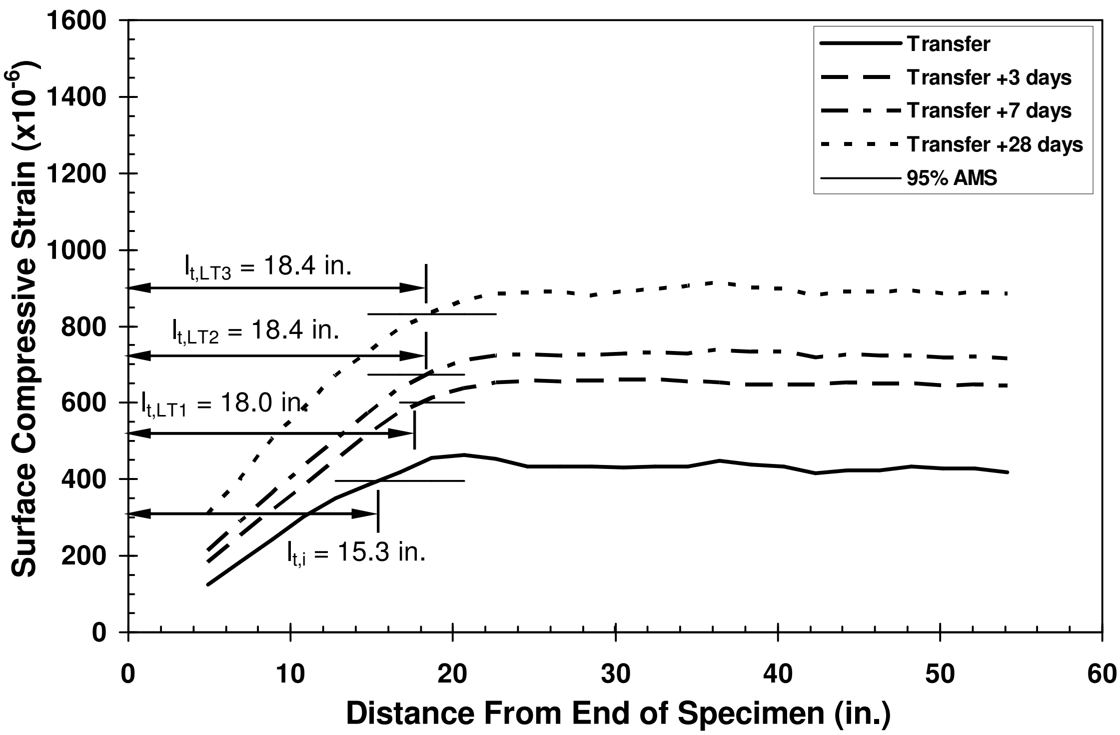

Figure D-43: Transfer Lengths at Various Ages for 7bD-2-E

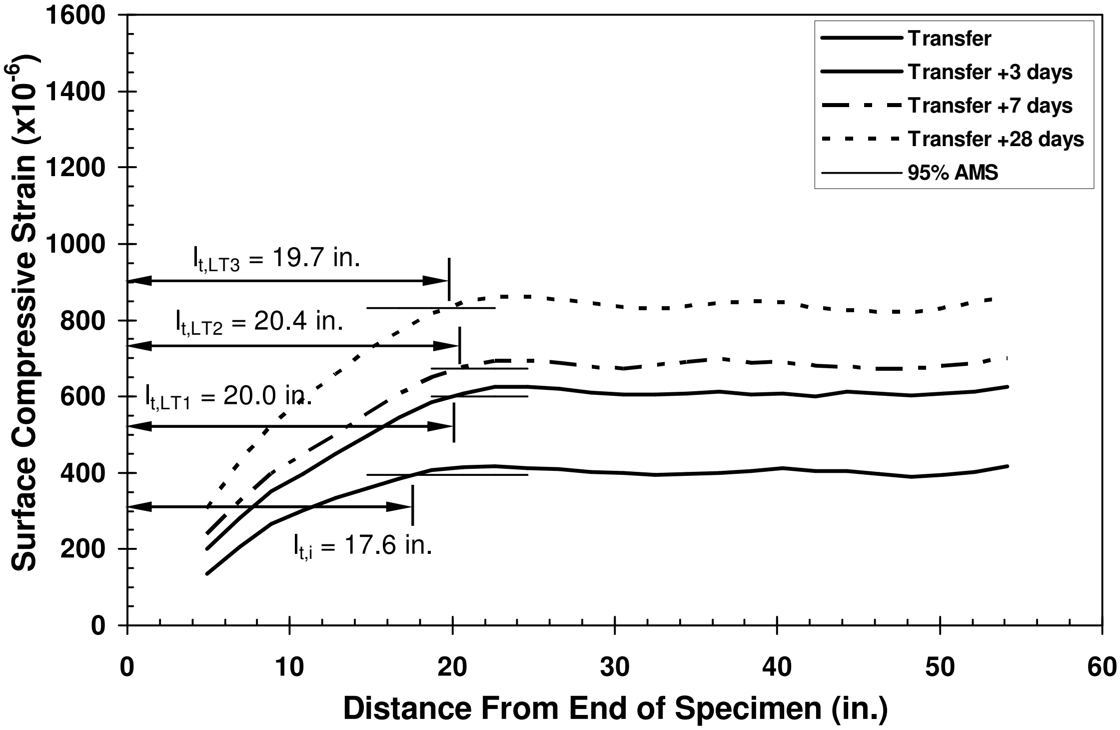

Figure D-44: Transfer Lengths at Various Ages for 7bD-2-W

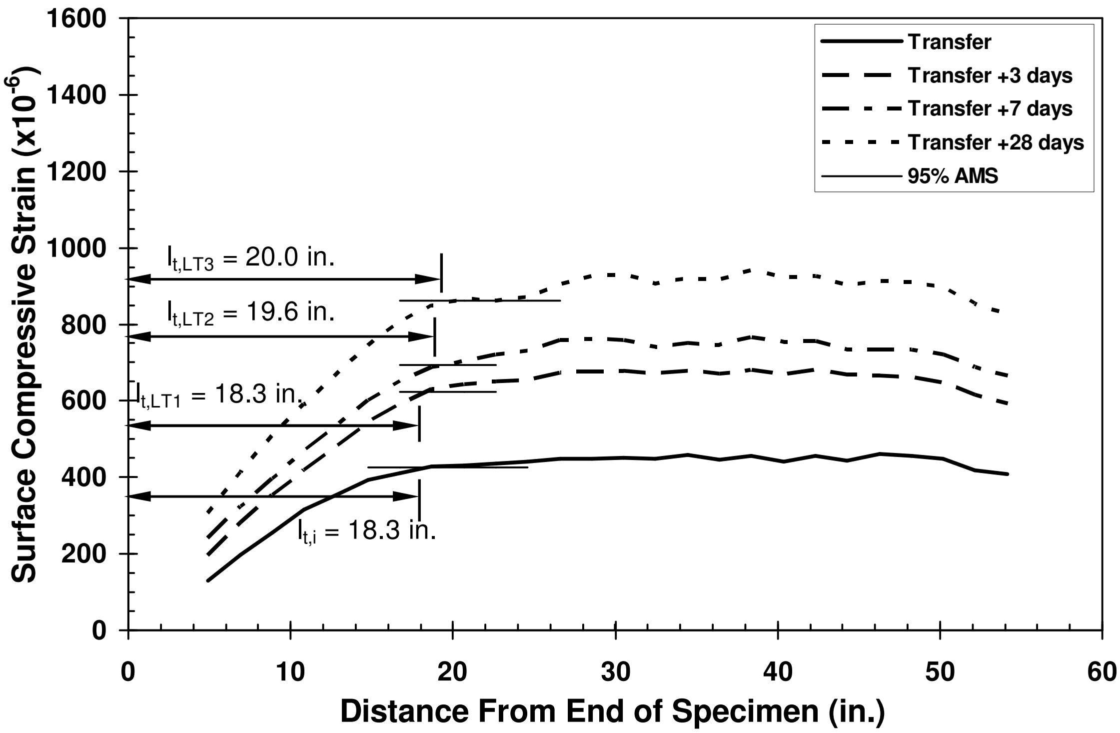

Figure D-45: Transfer Lengths at Various Ages for 7bE-2-E

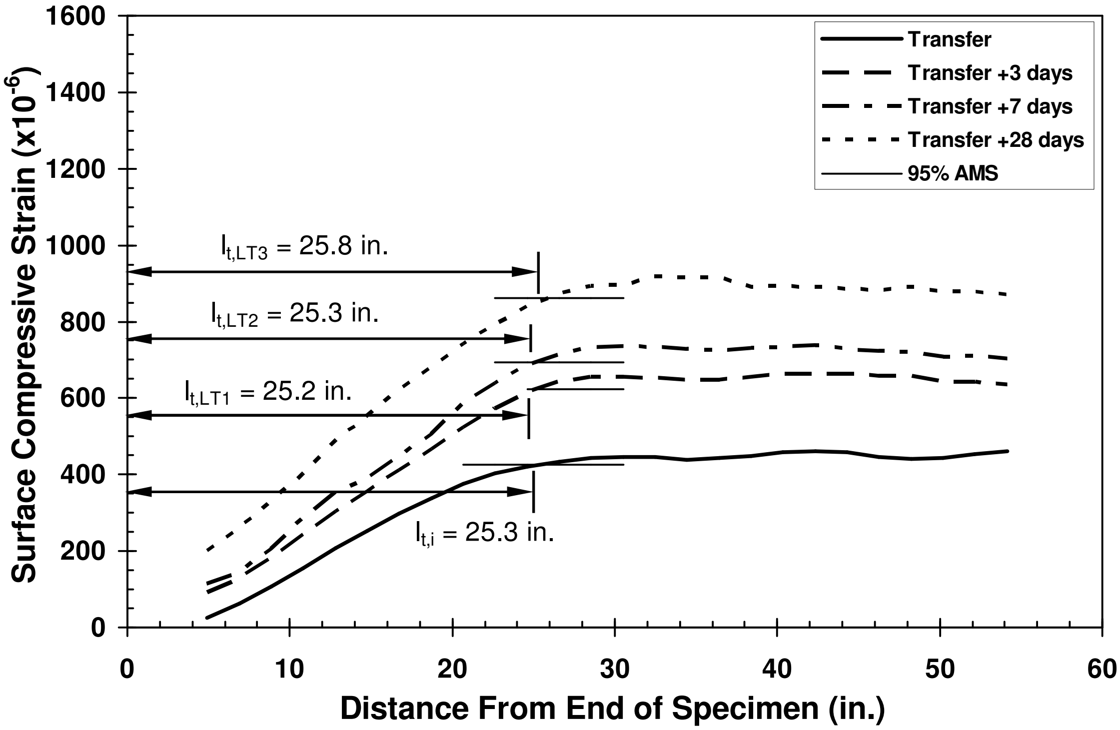

Figure D-46: Transfer Lengths at Various Ages for 7bE-2-W

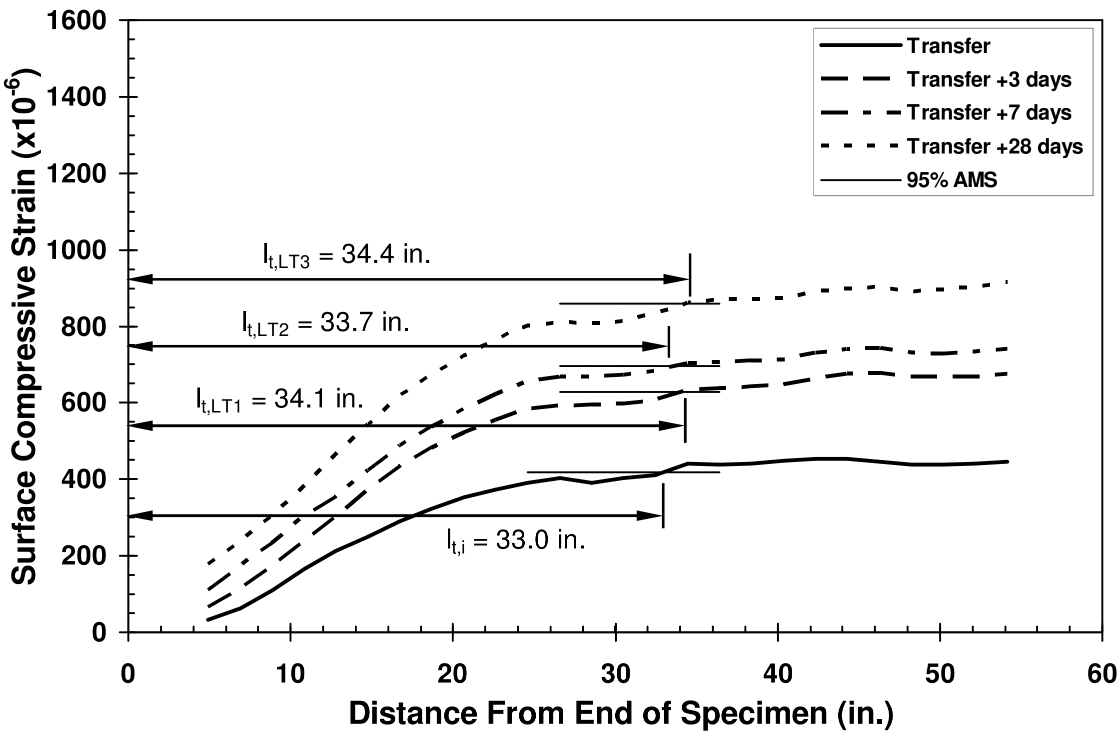

Figure D-47: Transfer Lengths at Various Ages for 7bF-2-E

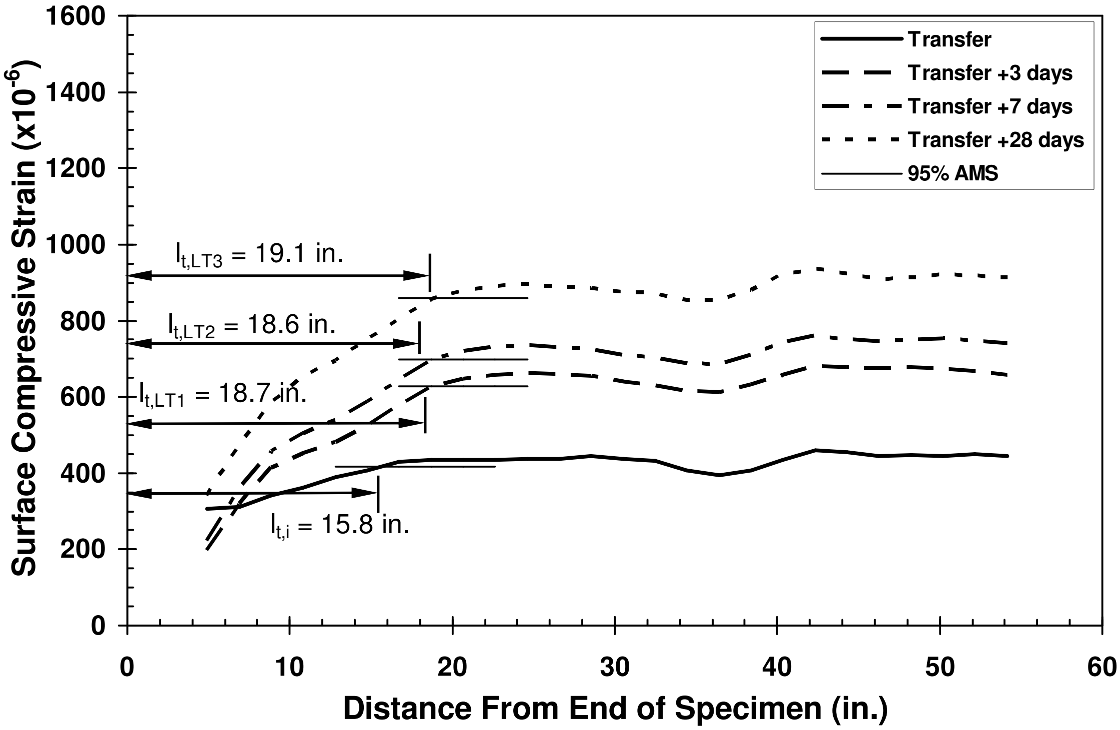

Figure D-48: Transfer Lengths at Various Ages for 7bF-2-W

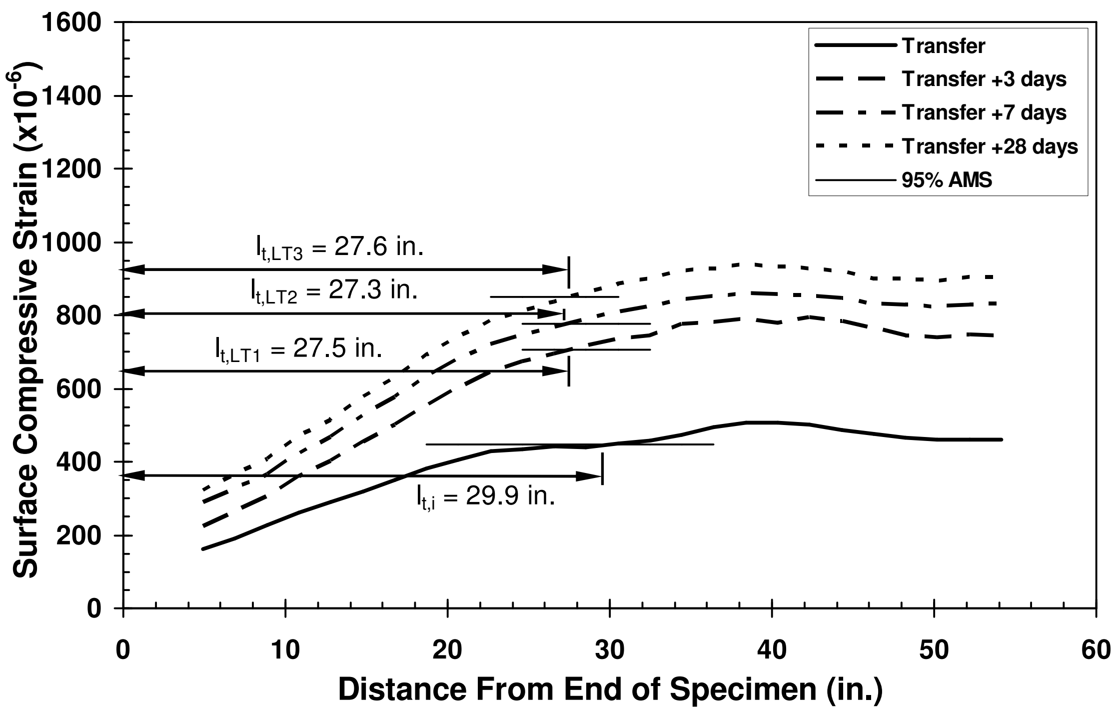

Figure D-49: Transfer Lengths at Various Ages for 15A-1-E

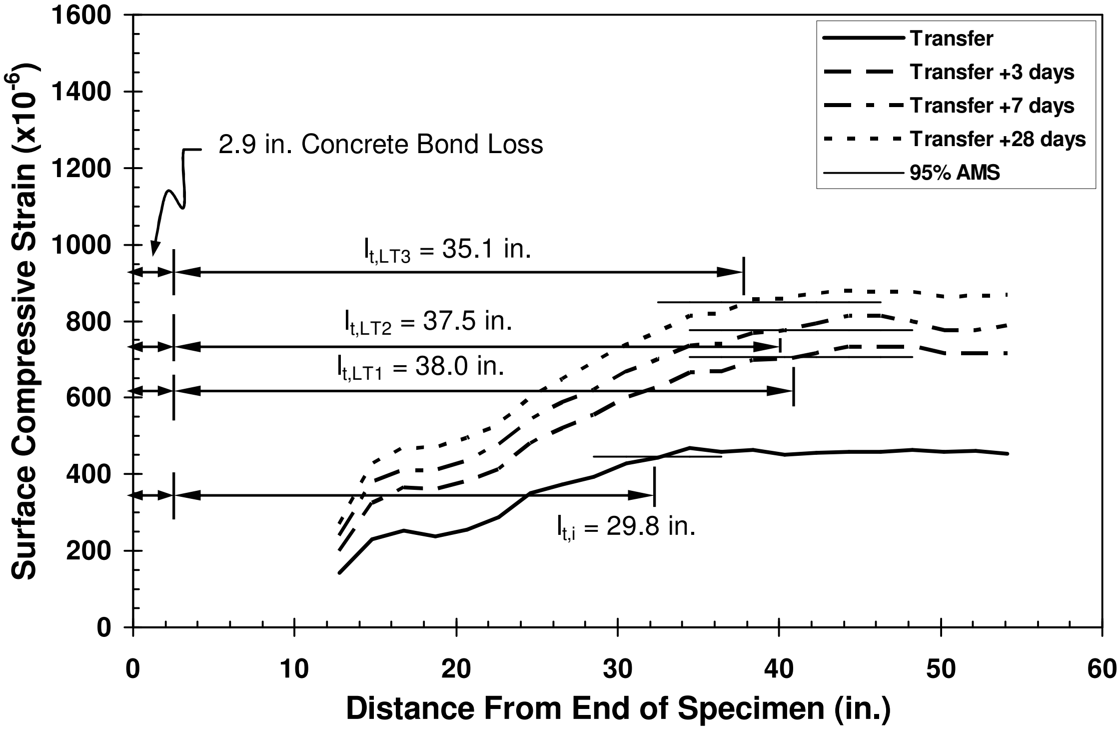

Figure D-50: Transfer Lengths at Various Ages for 15A-1-W

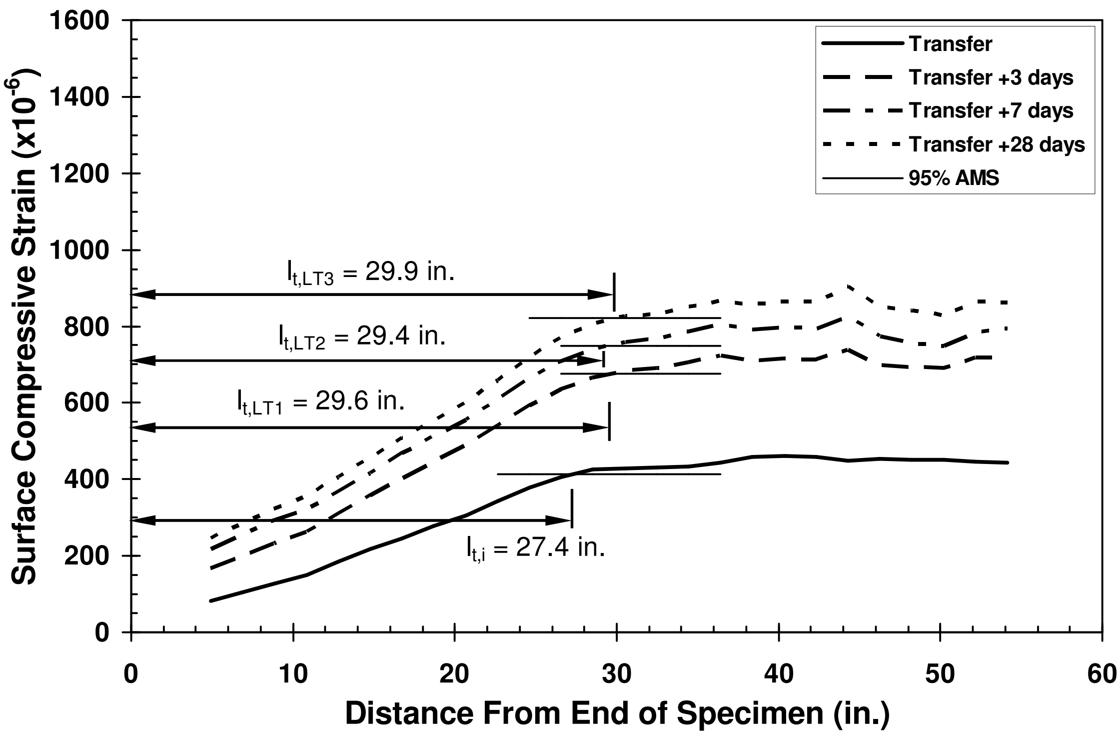

Figure D-51: Transfer Lengths at Various Ages for 15B-1-E

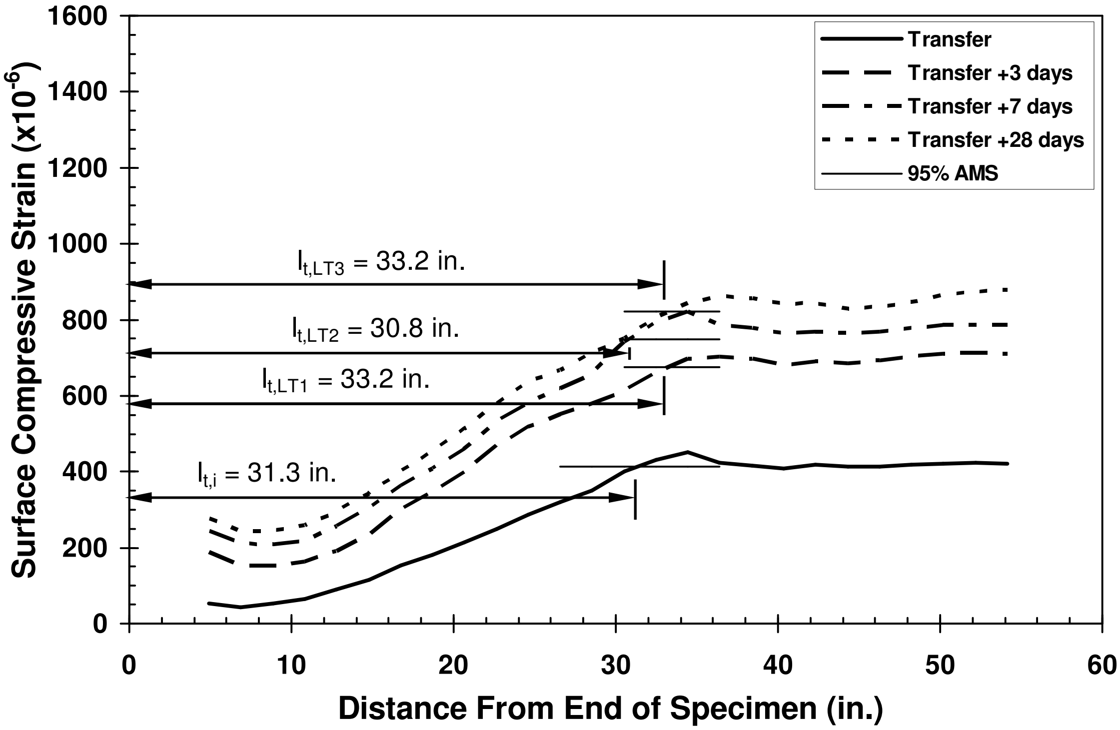

Figure D-52: Transfer Lengths at Various Ages for 15B-1-W

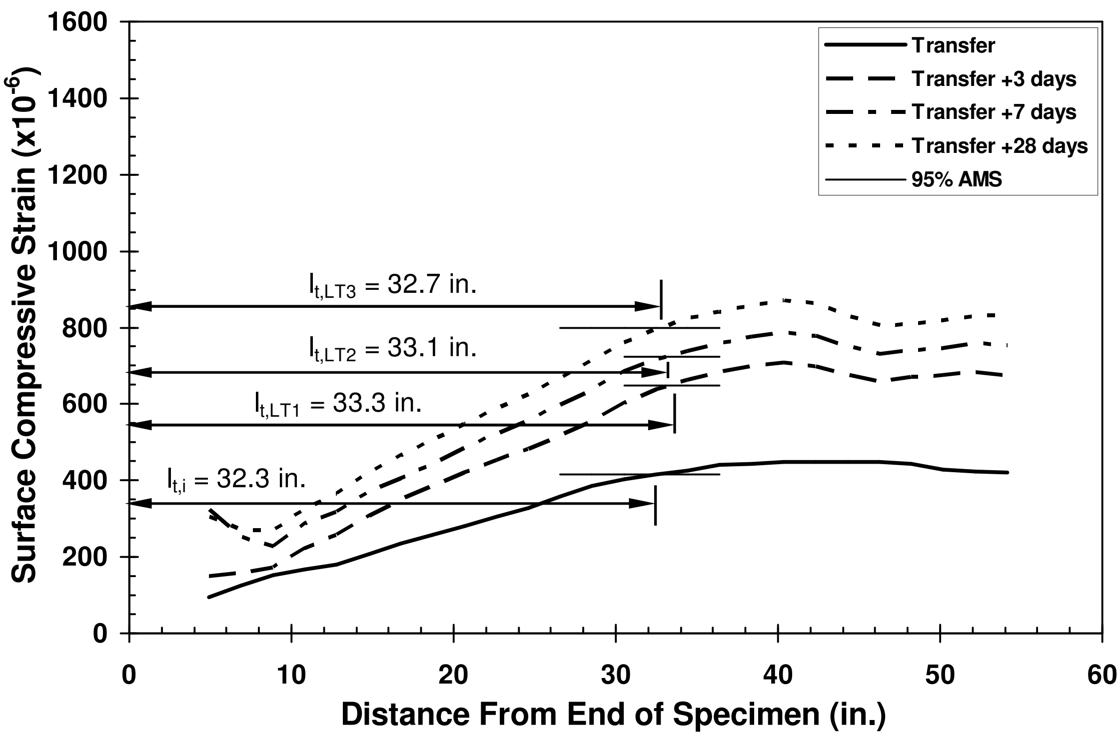

Figure D-53: Transfer Lengths at Various Ages for 15C-1-E

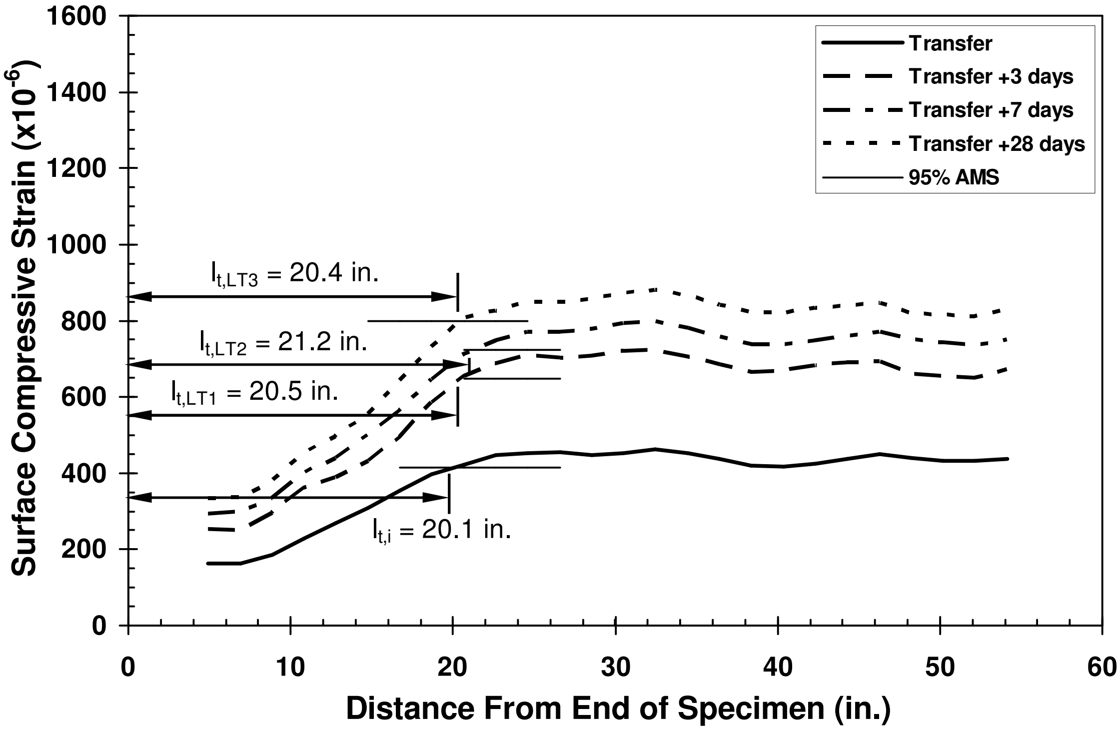

Figure D-54: Transfer Lengths at Various Ages for 15C-1-W

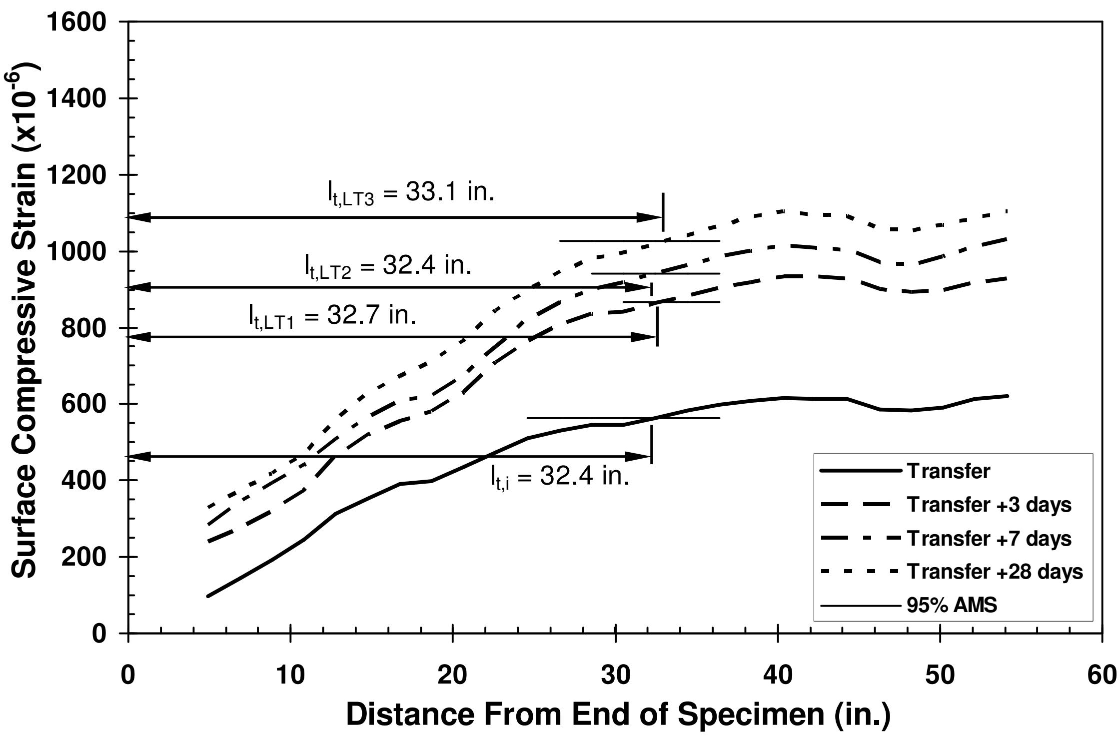

Figure D-55: Transfer Lengths at Various Ages for 15D-2-E

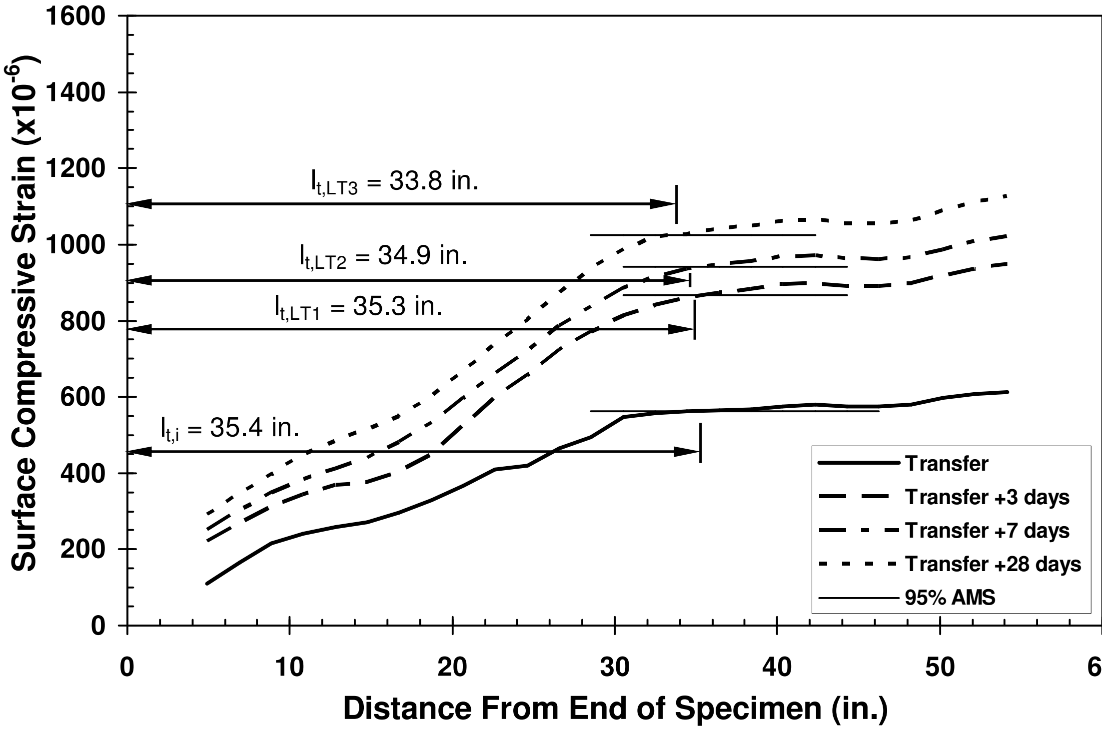

Figure D-56: Transfer Lengths at Various Ages for 15D-2-W

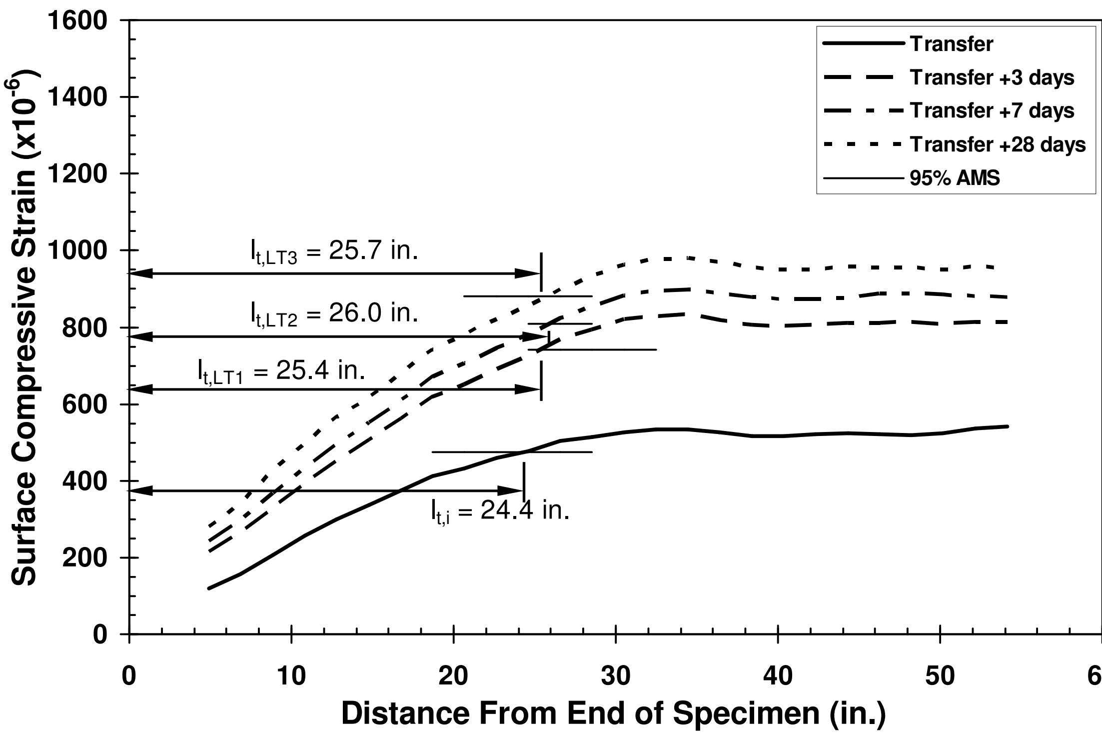

Figure D-57: Transfer Lengths at Various Ages for 15E-2-E

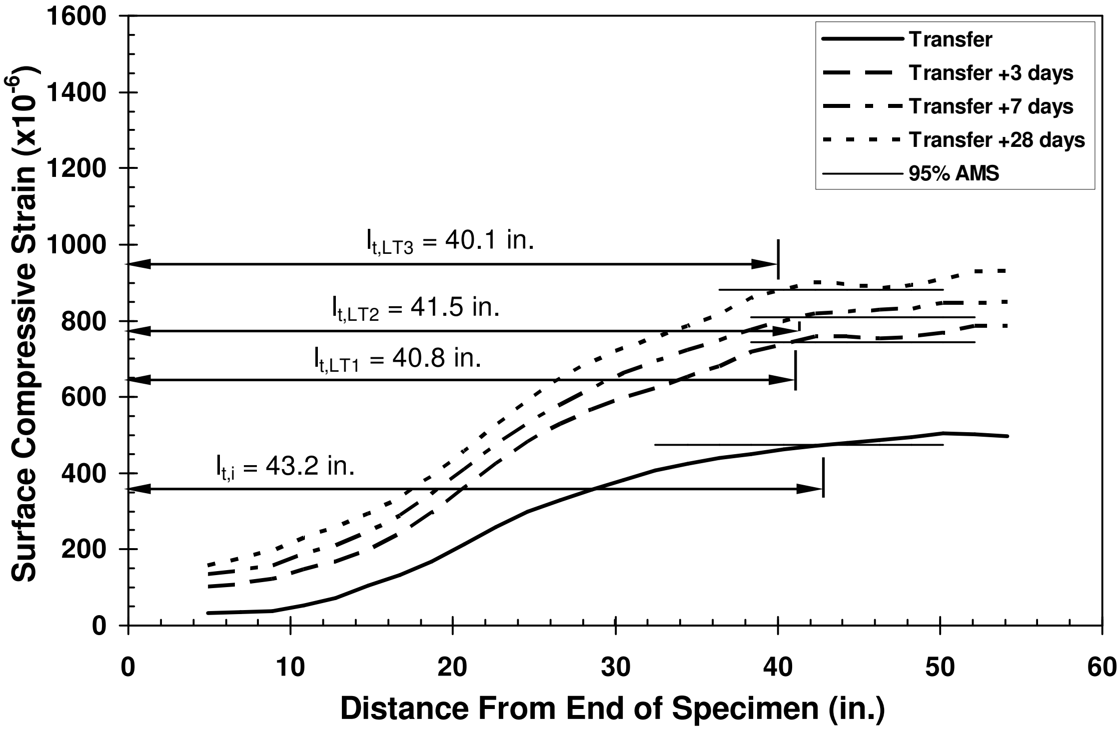

Figure D-58: Transfer Lengths at Various Ages for 15E-2-W

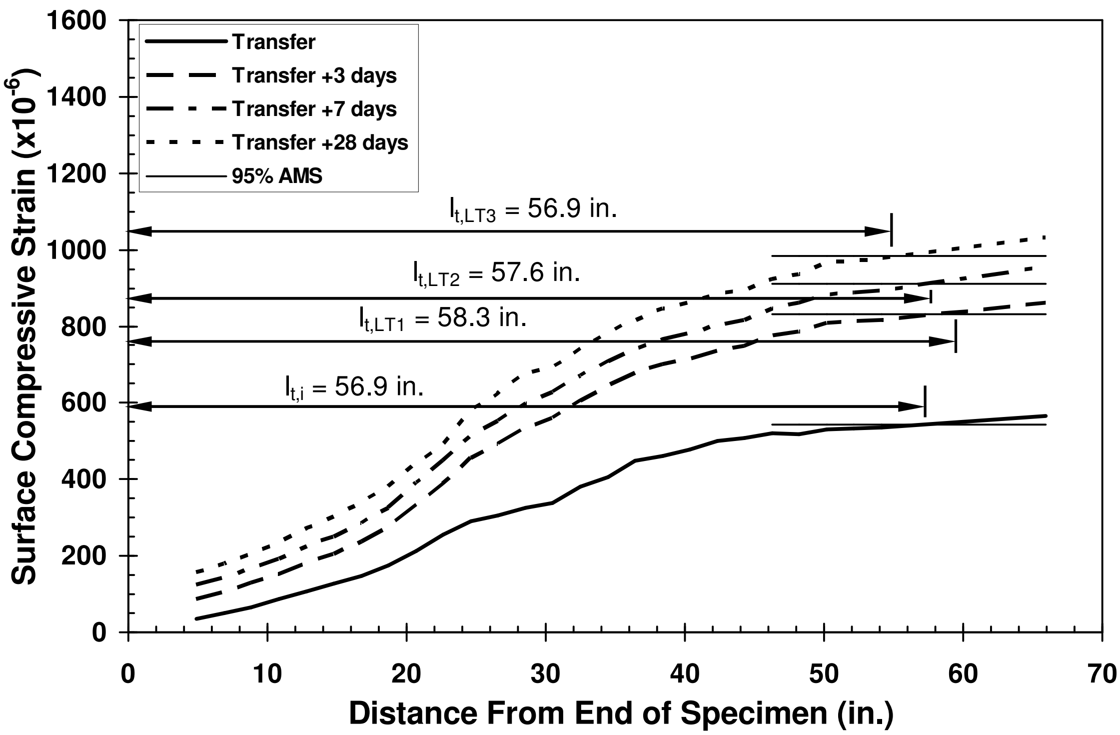

Figure D-59: Transfer Lengths at Various Ages for 15F-2-E

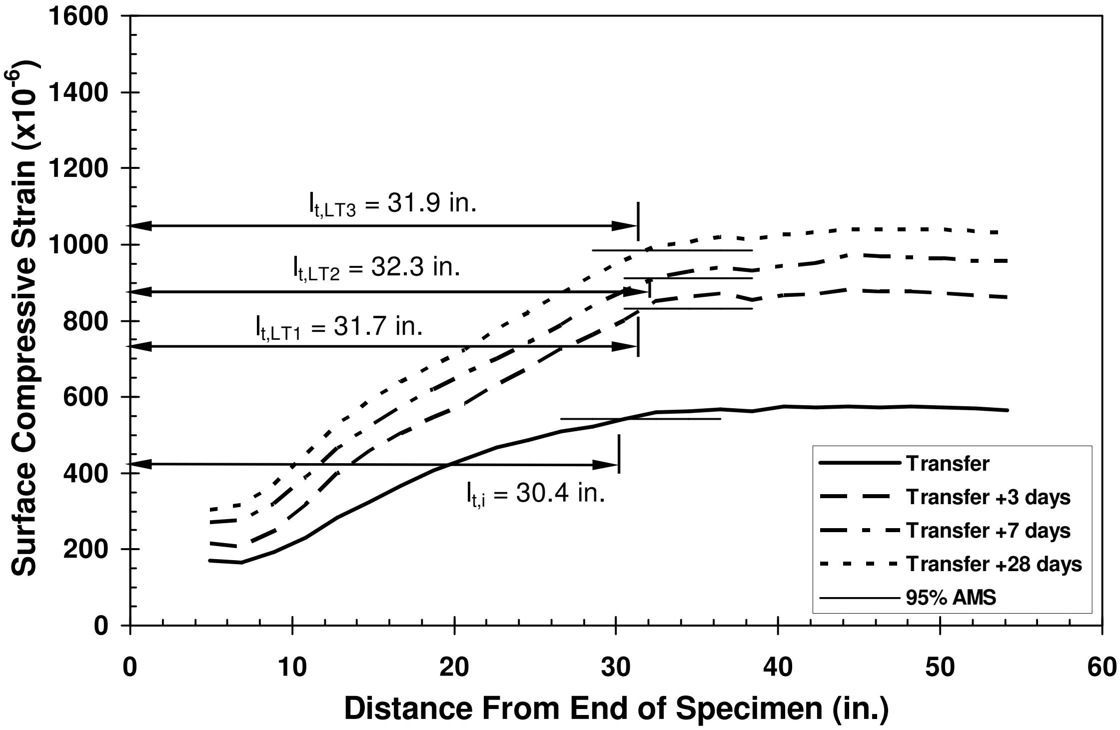

Figure D-60: Transfer Lengths at Various Ages for 15F-2-W

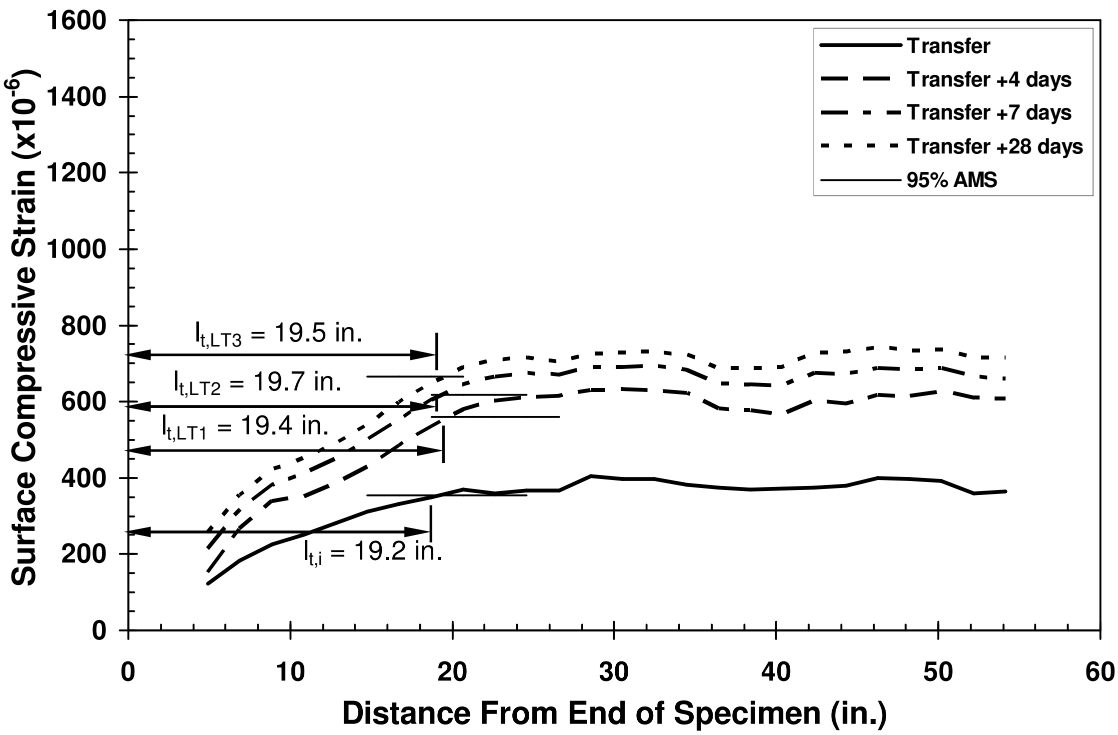

Figure D-61: Transfer Lengths at Various Ages for 13A-1-E

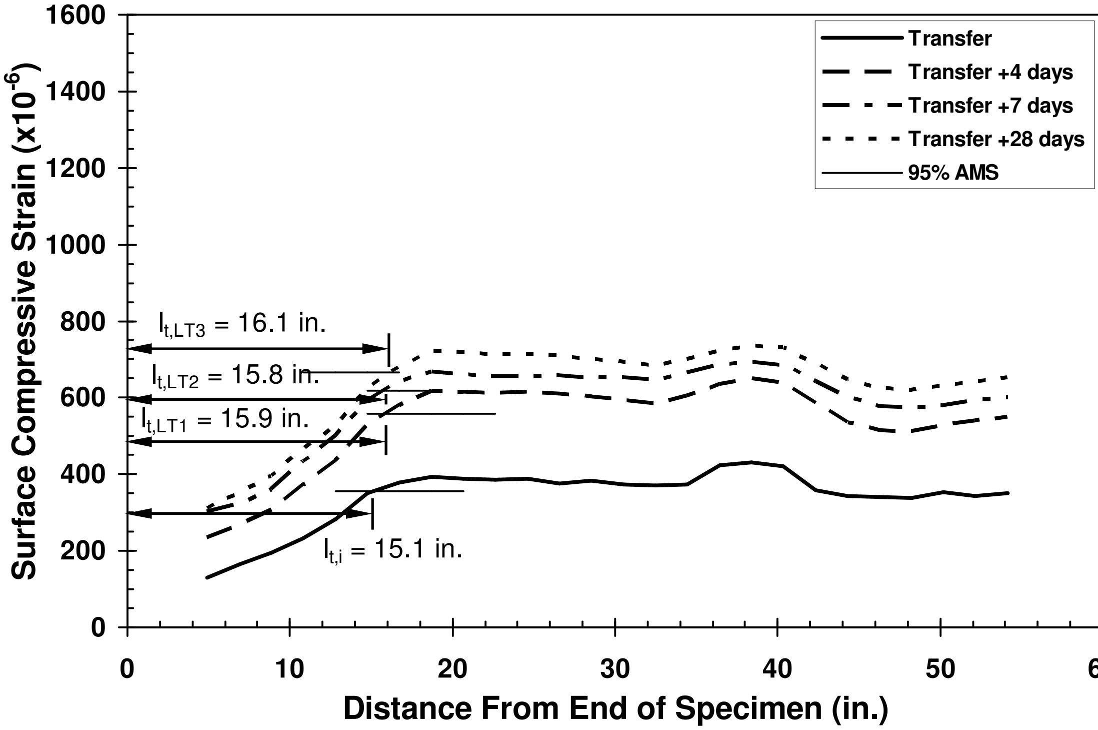

Figure D-62: Transfer Lengths at Various Ages for 13A-1-W

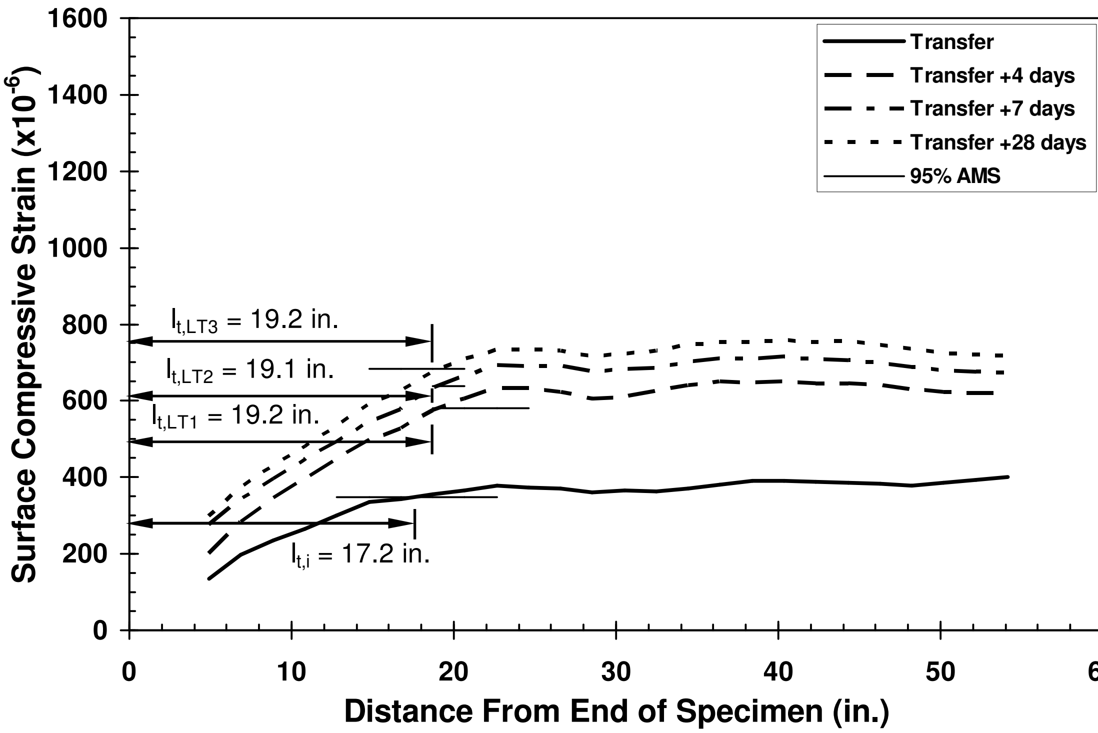

Figure D-63: Transfer Lengths at Various Ages for 13B-1-E

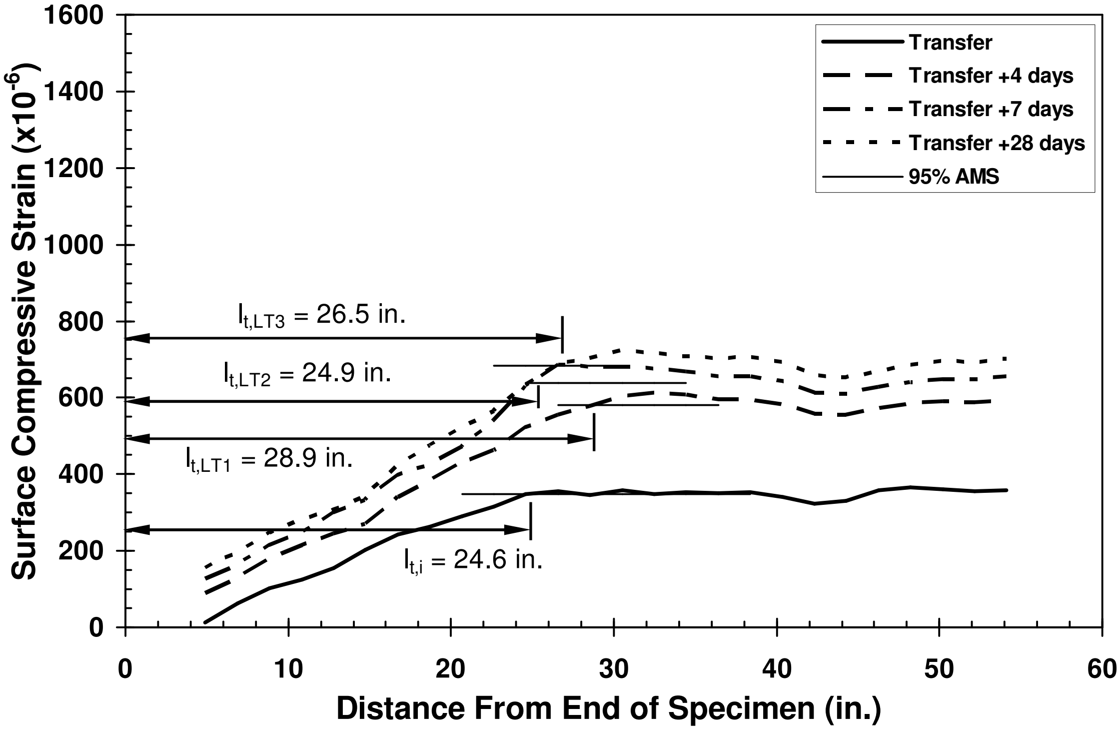

Figure D-64: Transfer Lengths at Various Ages for 13B-1-W

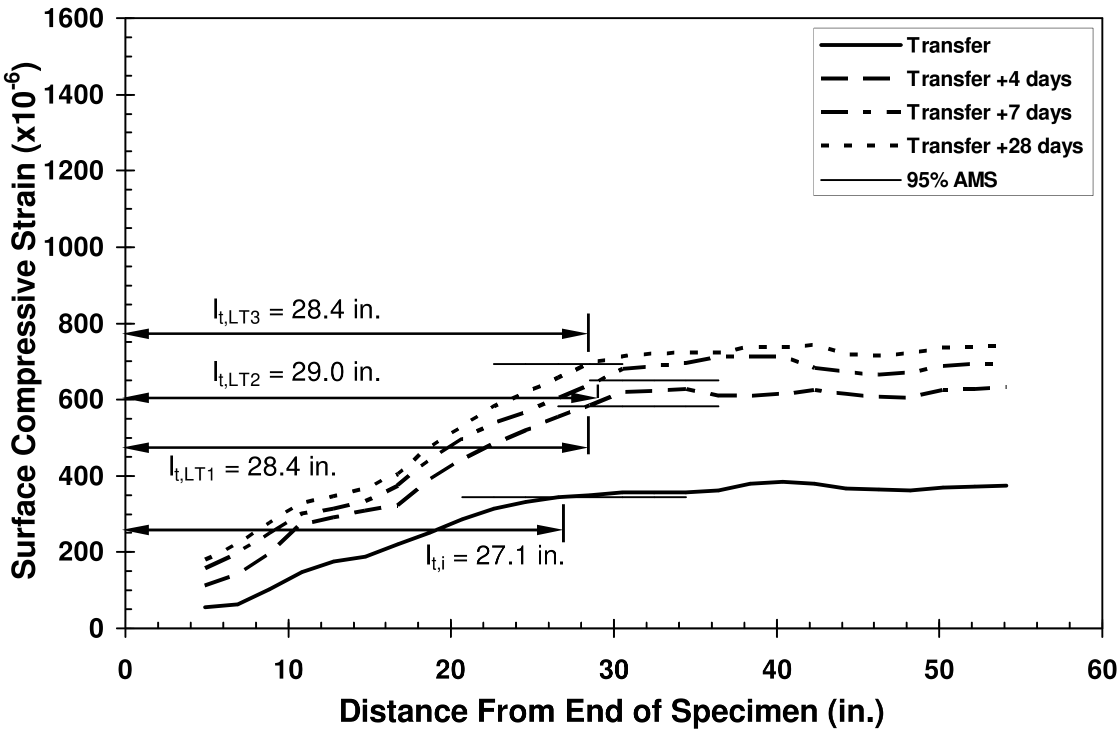

Figure D-65: Transfer Lengths at Various Ages for 13C-1-E

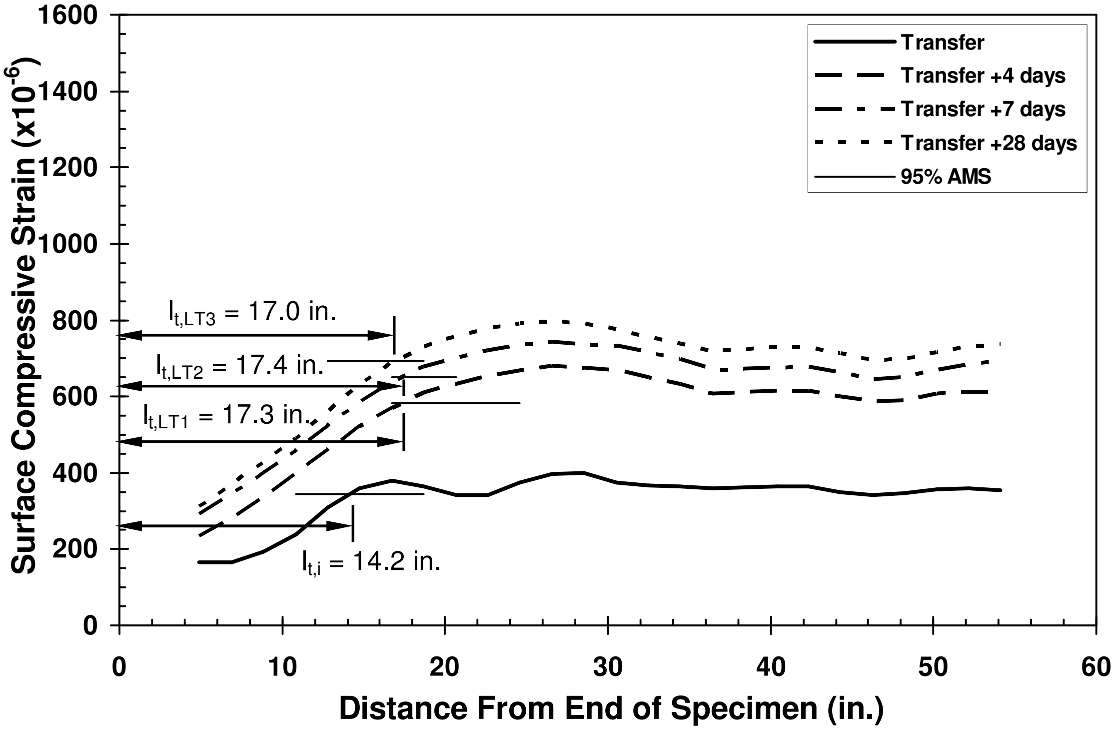

Figure D-66: Transfer Lengths at Various Ages for 13C-1-W

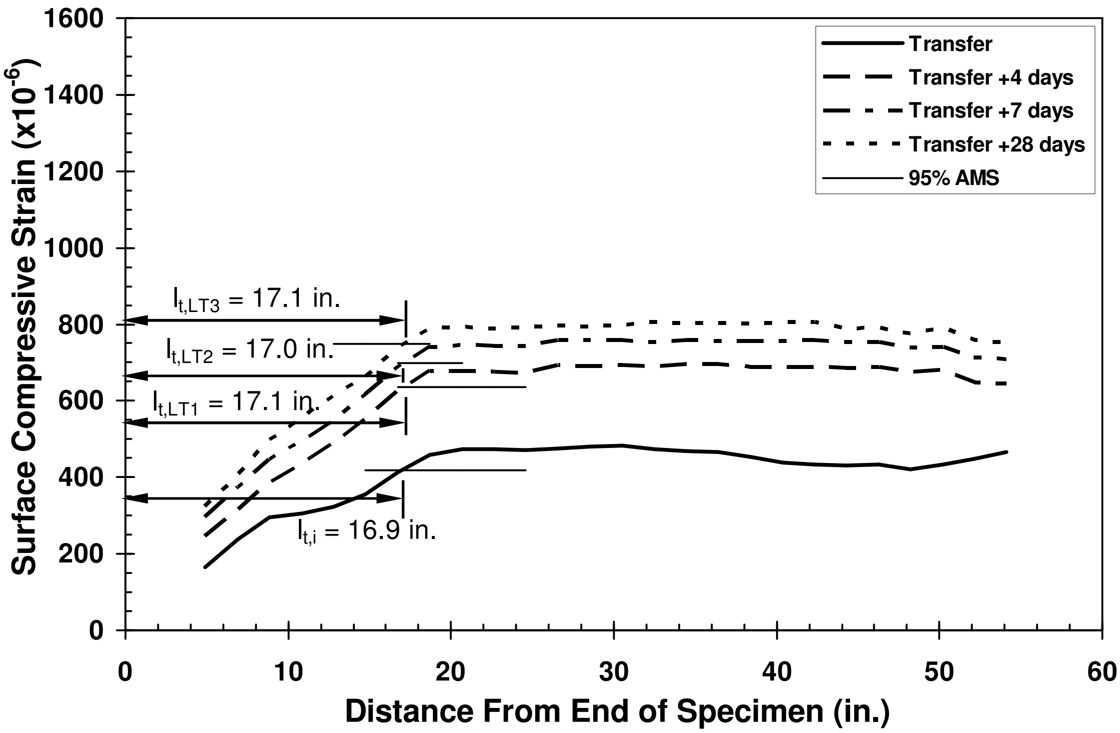

Figure D-67: Transfer Lengths at Various Ages for 13D-2-E

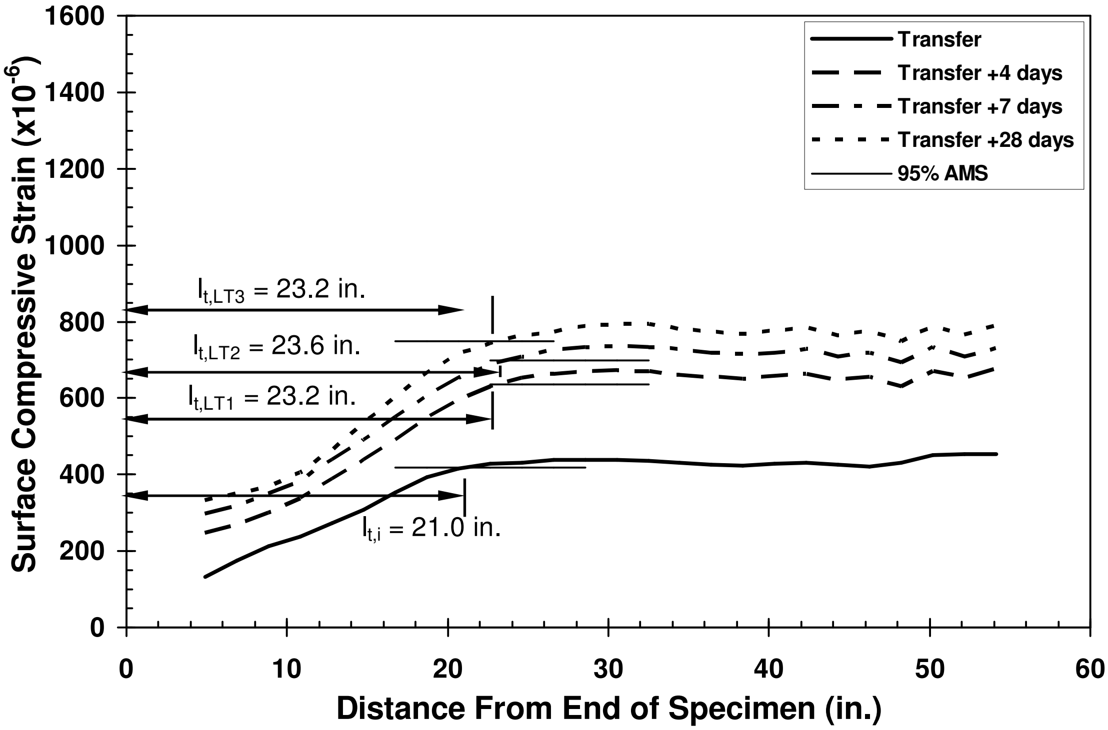

Figure D-68: Transfer Lengths at Various Ages for 13D-2-W

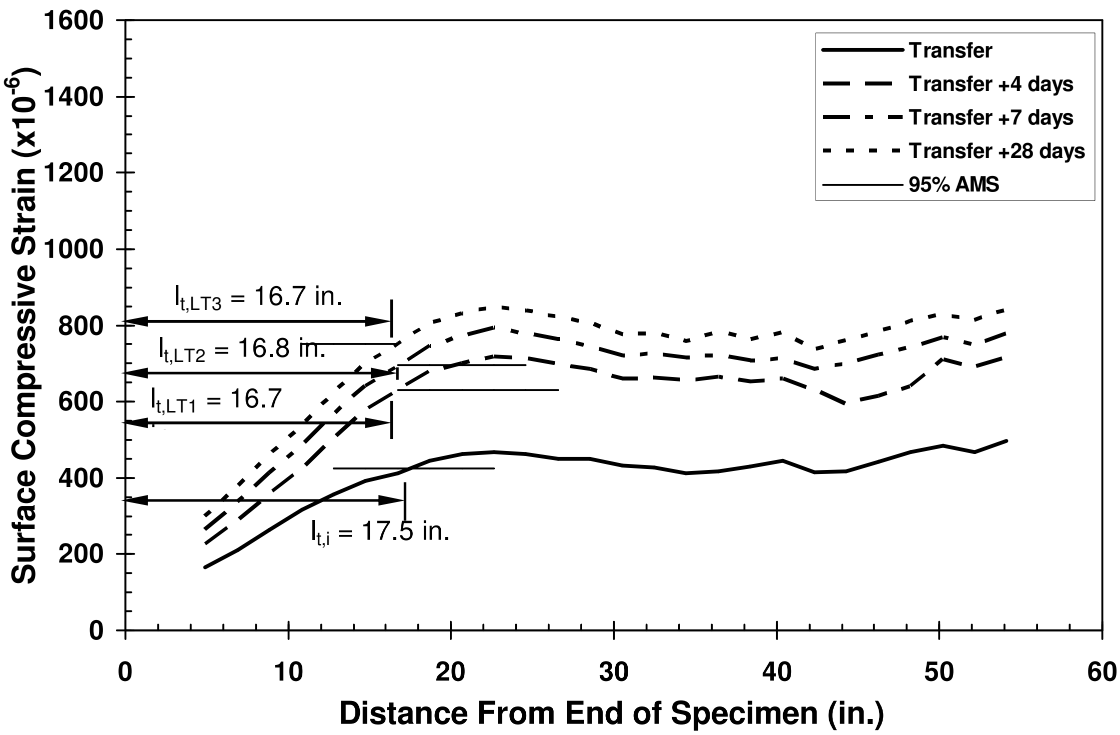

Figure D-69: Transfer Lengths at Various Ages for 13E-2-E

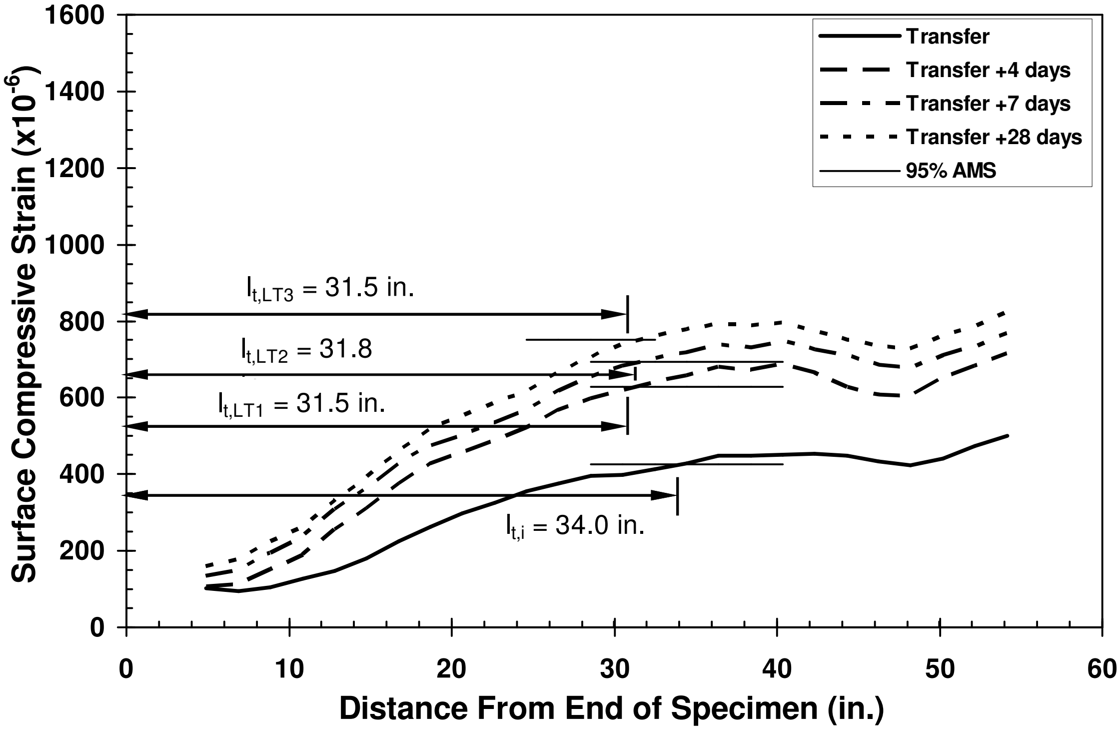

Figure D-70: Transfer Lengths at Various Ages for 13E-2-W

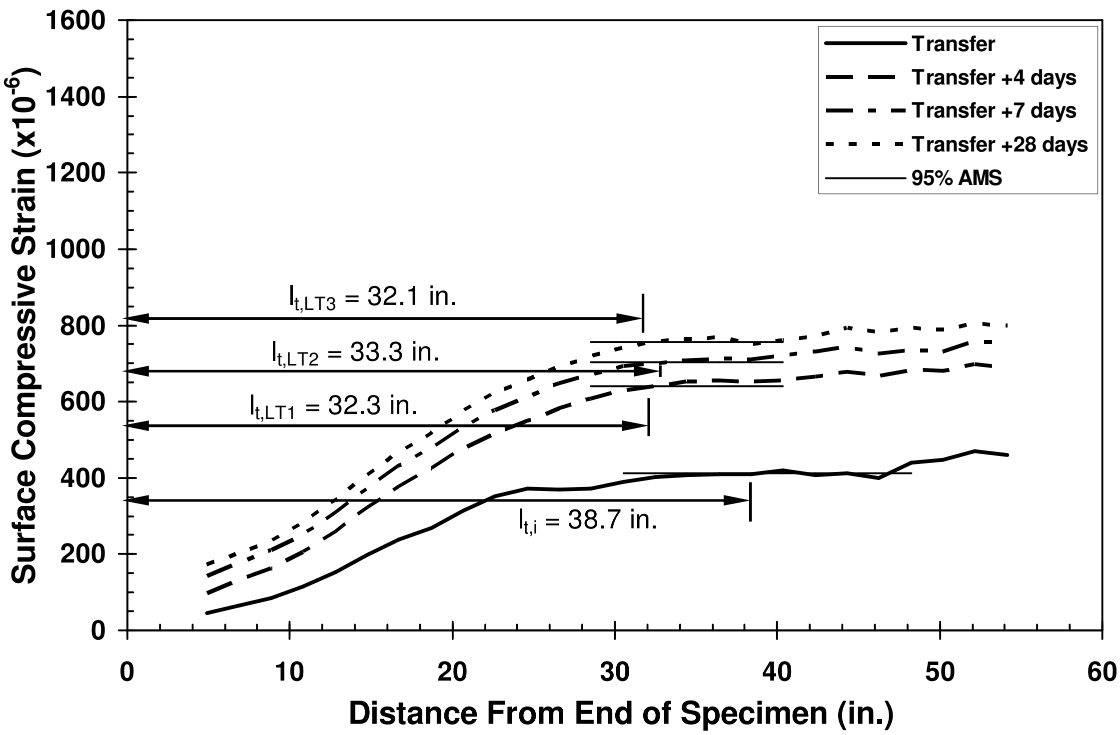

Figure D-71: Transfer Lengths at Various Ages for 13F-2-E

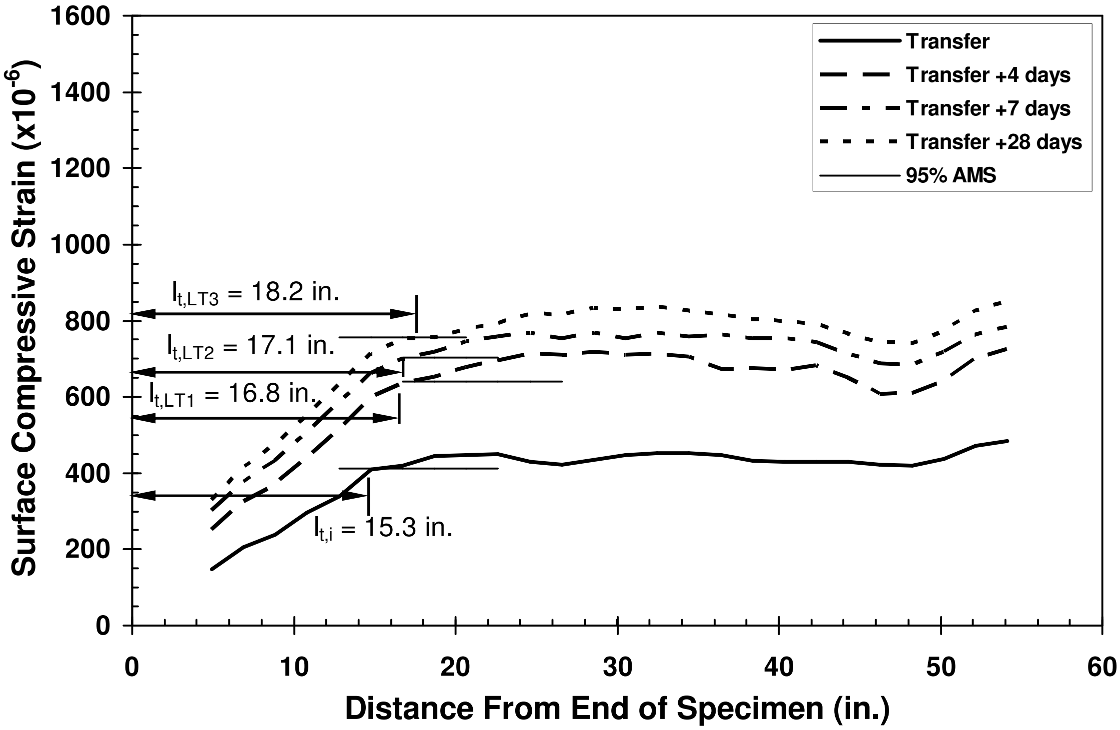

Figure D-72: Transfer Lengths at Various Ages for 13F-2-W

APPENDIX E

STRAND DRAW-IN RESULTS

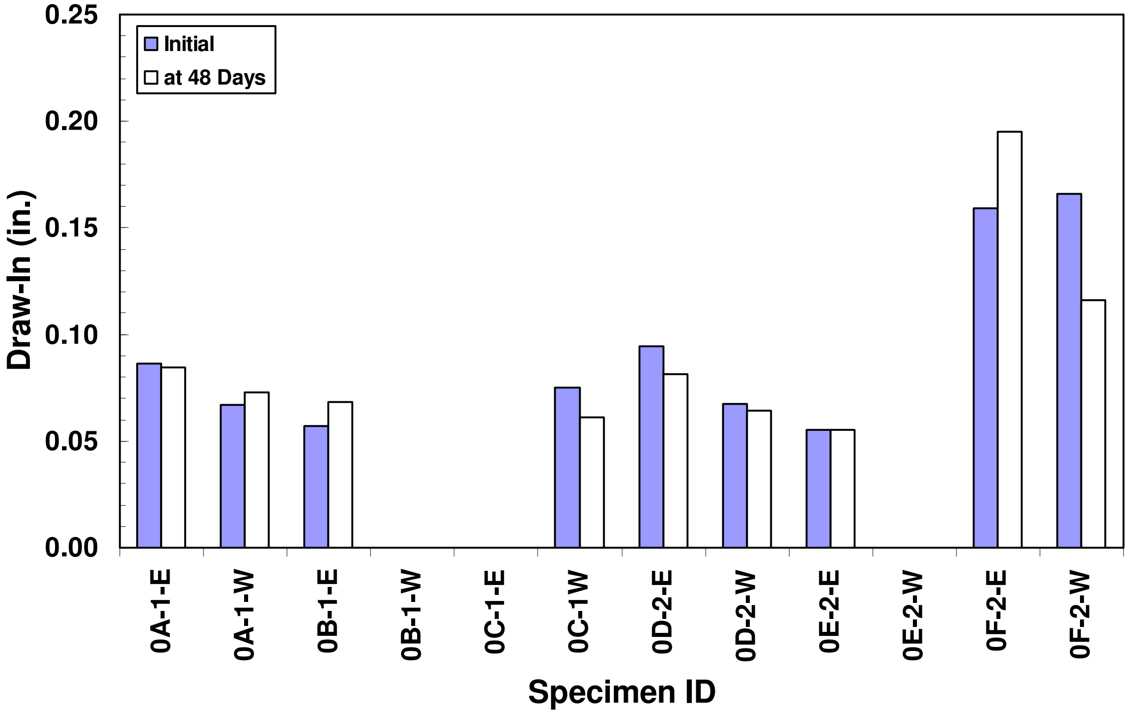

Figure E-1: Conventional Mixture 0 Strand Draw-In Results

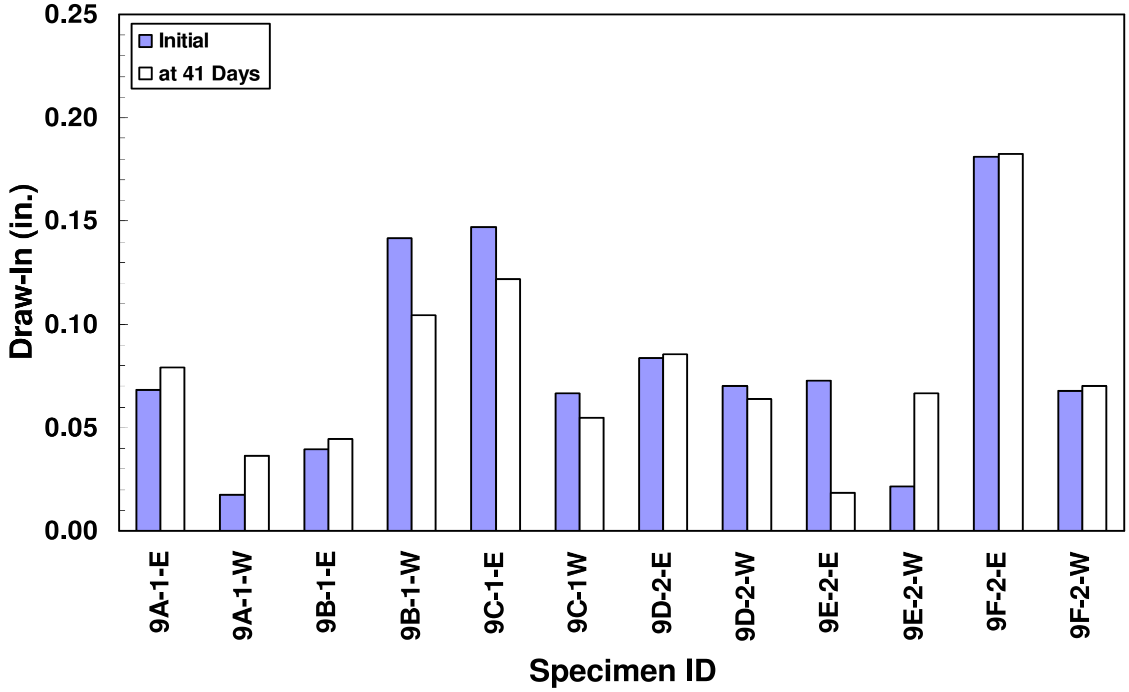

Figure E-2: SCC Mixture 9 Strand Draw-In Results

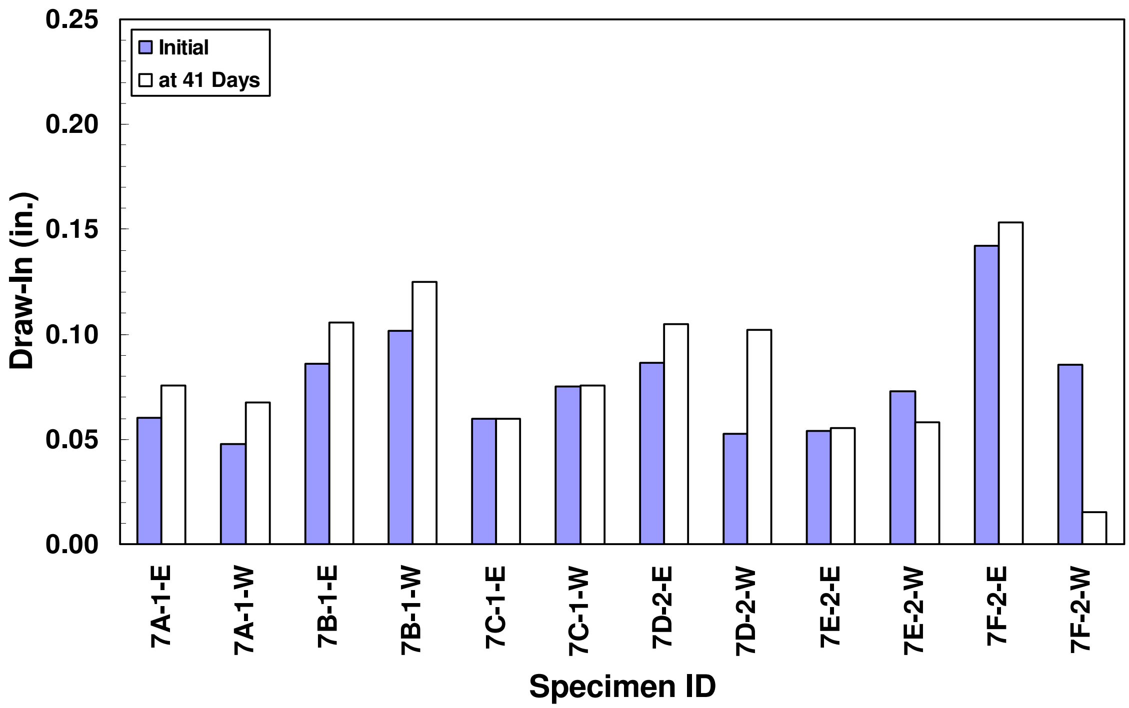

Figure E-3: SCC Mixture 7 Strand Draw-In Results

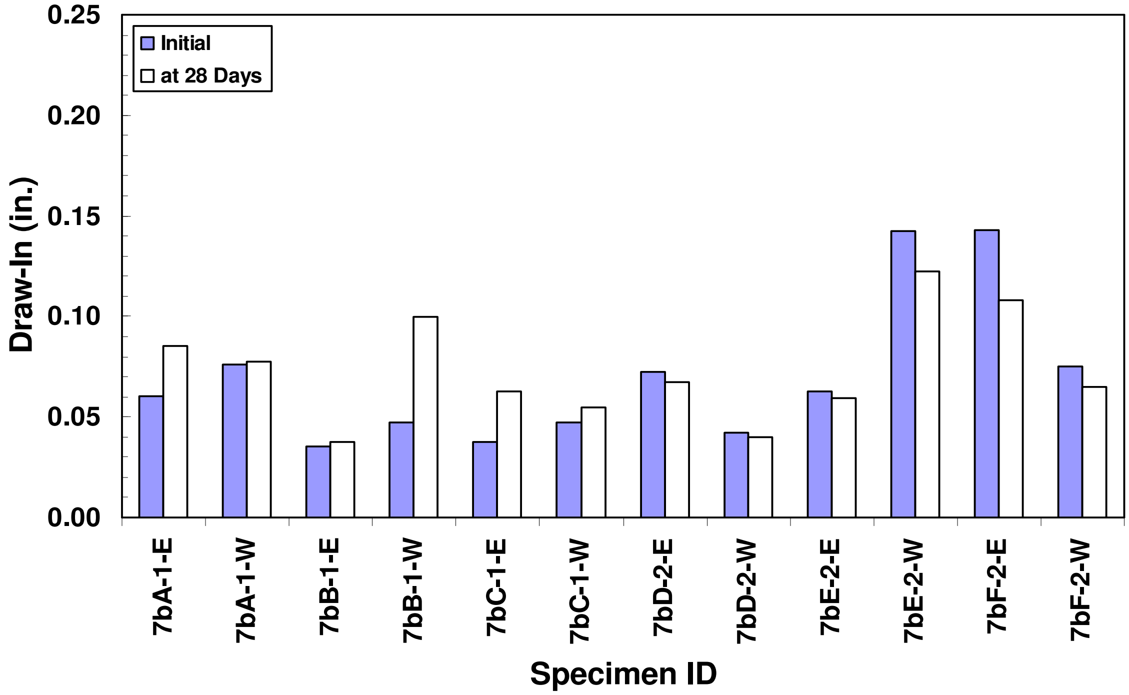

Figure E-4: SCC Mixture 7b Strand Draw-In Results

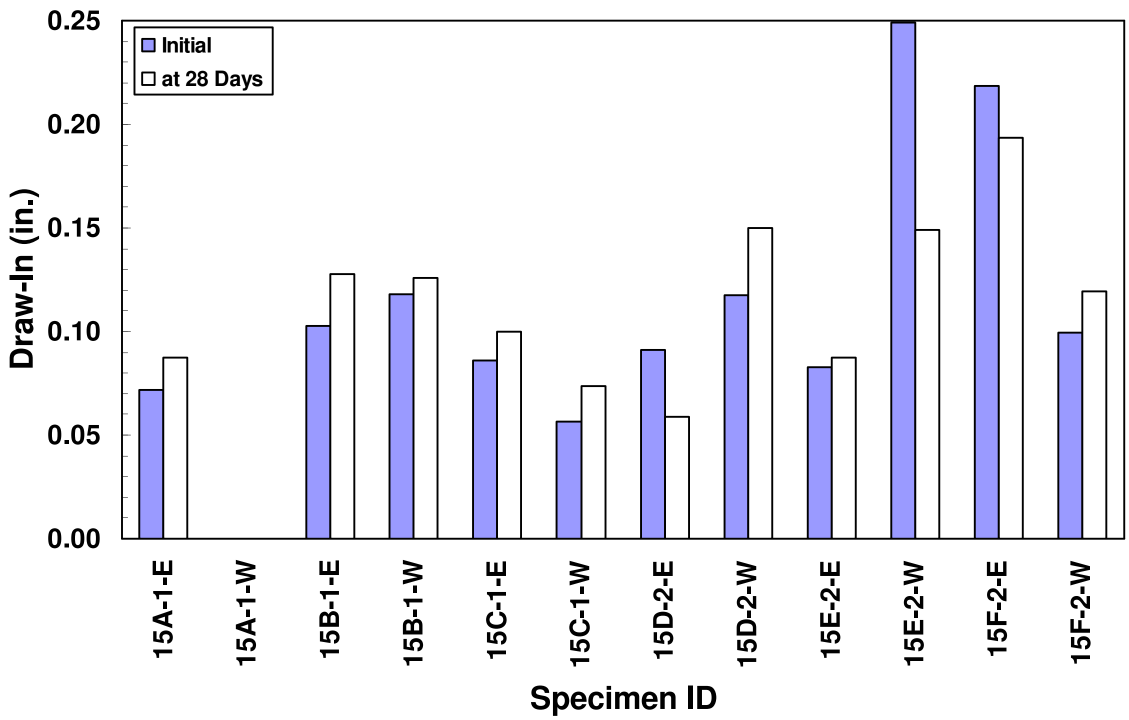

Figure E-5: SCC Mixture 15 Strand Draw-In Results

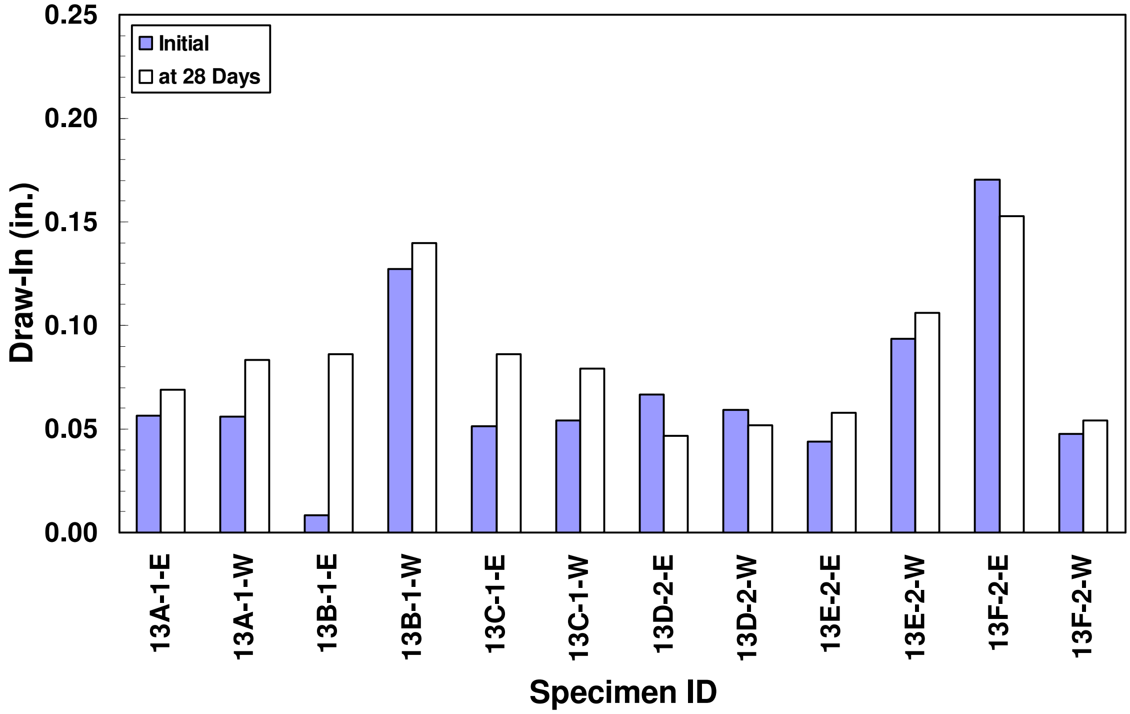

Figure E-6: SCC Mixture 13 Strand Draw-In Results

APPENDIX F

PROPORTIONALITY CONSTANTS FOR MODELS

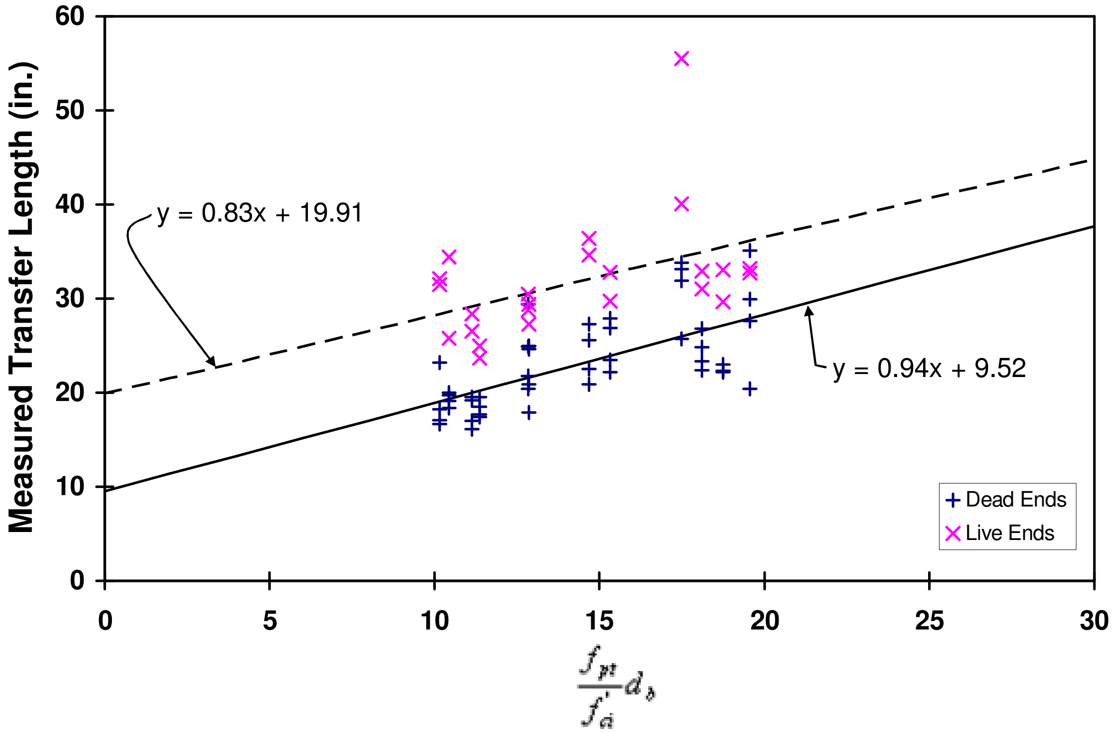

Figure F-1: Determination of Proportionality Constants for Zia and Mostafa (1978) Model

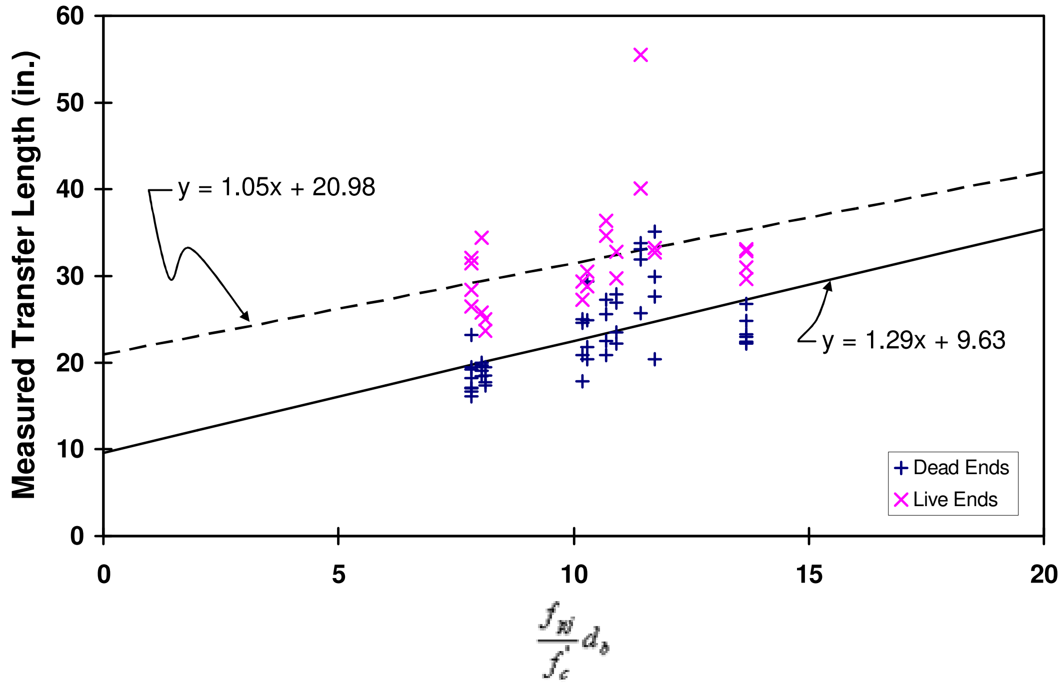

Figure F-2: Determination of Proportionality Constants for Lane (1998) Model

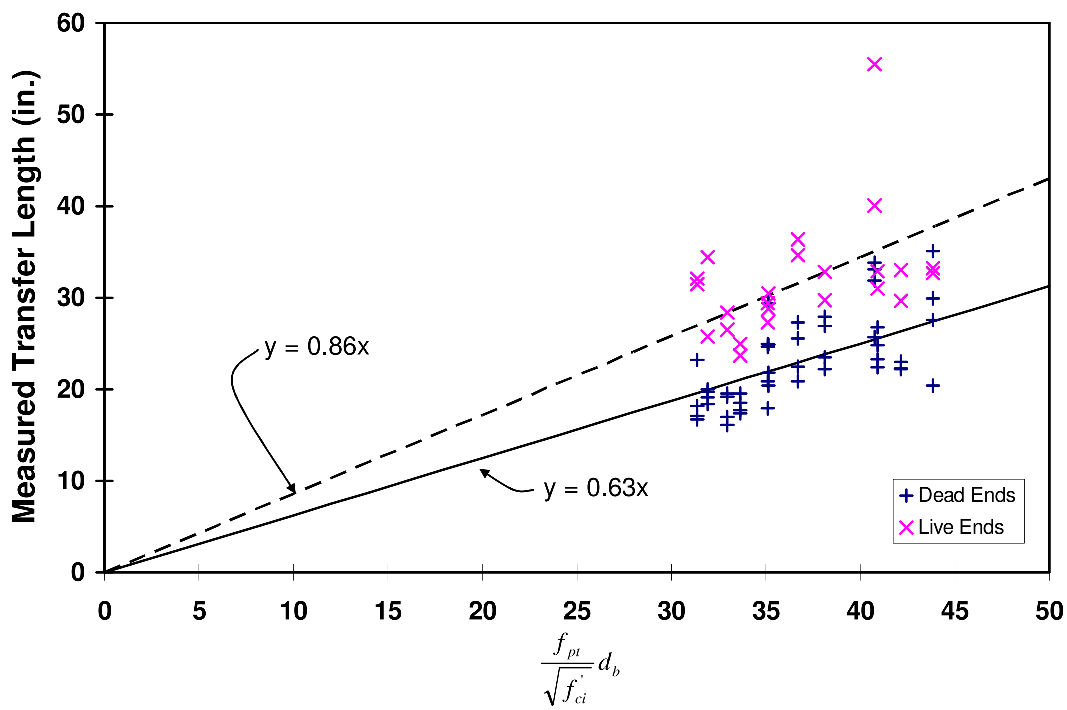

Figure F-3: Determination of Proportionality Constants for Barnes et al. (1999) Model

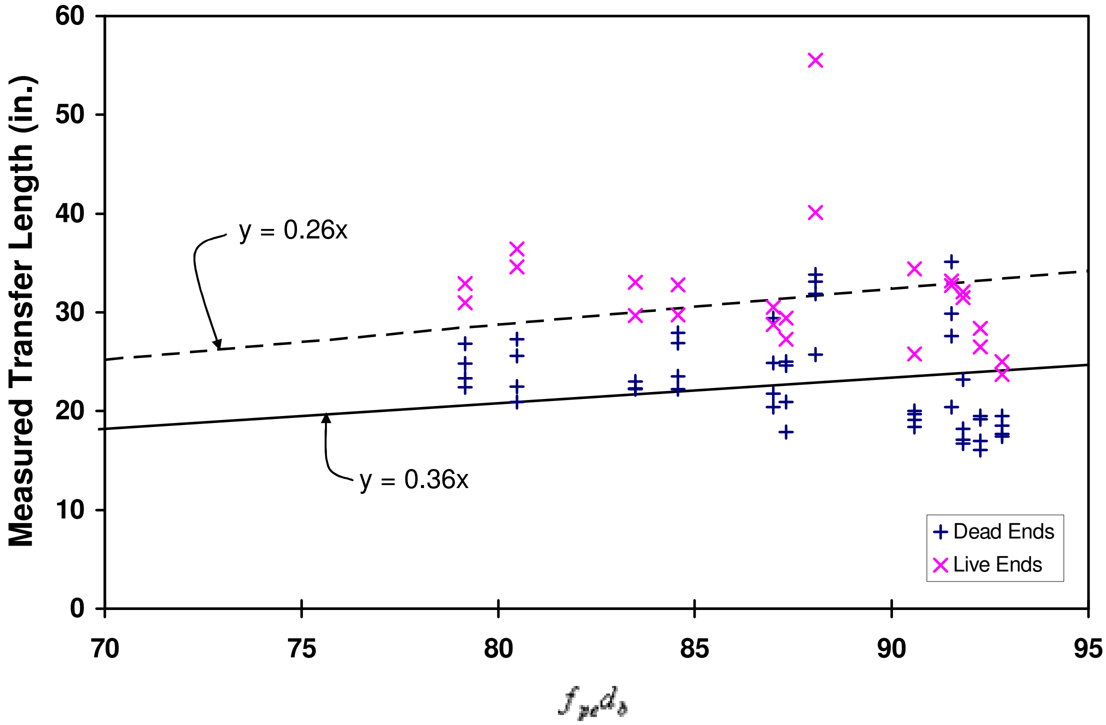

Figure F-4: Determination of Proportionality Constants for ACI 318-05 Model

APPENDIX G

NOTATION

Report (AASHTO LRFD)	AASHTO Standard	ACI 318-05	Description
A_{ps}	A_s*	A_{ps}	area of prestressing steel
d_b	D	d_b	nonminal diameter of reinforcement
E_p	—	—	modulus of elasticity of prestressing reinforcement
f'_c	f'_c	f'_c	specified compressive strength of concrete
f'_{ci}	f'_{ci}	f'_{ci}	specified compressive strength of concrete at transfer of prestress force
f_p	—	—	stress in prestressing reinforcement (not in AASHTO LRFD)
f_{pe}	f_{se}	f_{se}	effective stress in prestressed reinforcement after losses
f_{pj}	—	—	stress in prestressing force at jacking
f_{pbt}	—	—	stress in prestressing reinforcement immediately prior to transfer
f_{ps}	$f*_{su}$	f_{ps}	stress in prestressed reinforcement at nominal strength
f_{pt}	—	—	stress in prestressed reinforcement at immediately after transfer
f_{pu}	f'_s	f_{pu}	specified tensile strength of prestressing reinforcement
l_d	l_d	l_d	development length (only refers to nonprestressed reinforcement in AASHTO Standard and ACI 318)
l_t	—	—	transfer length (not in AASHTO LRFD)
l'_t	—	—	transfer length predicted from draw-in measurements (not in AASHTO LRFD)